UNIVERSITAT POLITÈCNICA DE CATALUNYA BARCELONATECH

Geometrically non-linear analysis with stiffness reduction for the in-plane stability design of stainless steel frames

Yanfei Shen

Geometrically Non-linear Analysis with stiffness reduction for the in-plane stability design of stainless steel frames.

DOCTORAL THESIS

Doctoral thesis by:
Yanfei Shen

Supervised by:
Rolando Chacón Flores

Doctoral programme:
Construction Engineering

Barcelona, October 2019

UNIVERSITAT POLITÈCNICA DE CATALUNYA
BARCELONATECH
Department of Civil and Environmental Engineering

Abstract

In AISC 360-16, the Direct Analysis Method (DM) has been set as the primary method for the stability design of frames. DM, considering initial global sway imperfection, is essentially Geometrically Non-linear Analysis (GNA) in which tangent modulus is used. The aim of this thesis is to provide stiffness reduction factor formulations for using GNA coupled with tangent modulus approach for the stability design of stainless steel frames. GNA with the proposed stiffness reduction factor is aligned to AISC 360-16 and it is aimed at facilitating greater and more efficient use of stainless steel. In accordance with current design standards, the ultimate limit state for this method is the formation of first plastic hinge, and the adequacy of the method is confirmed through member-based resistance checks.

The focus of the thesis is the development of flexural stiffness reduction factor formulation for the in-plane stability design of stainless steel elements and frames with cold-formed square hollow section (SHS) and rectangular hollow section (RHS). The proposed beam-column stiffness reduction factor (τ_{MN}) accounts for the deleterious influence of material non-linearity, residual stresses and member out-of-straightness. The use of a GNA coupled with the proposed τ_{MN} eliminates the need for member buckling strength checks and thus, only cross-sectional strength checks are required.

Two types of τ_{MN} formulations, applicable to compact SHS and RHS, are proposed: analytical and approximate. The analytical expression of τ_{MN} presumes knowing the maximum internal second order moment (M_{r2}) within a member. It is developed by means of extending the formulations for evaluating the elastic second order effects to the inelastic range. A GNA with τ_{MN} determined by the analytical expression for the design of stainless steel beam-columns proves accurate. Furthermore, since in practical design M_{r2} is not known in advance, an approximate expression of τ_{MN}, which is assumed to be a function of relevant variables, is proposed by fitting variables to the analytically determined expression. For the purpose of developing the approximate expression of τ_{MN}, column flexural stiffness reduction factor (τ_N) and beam flexural stiffness reduction factor (τ_M) are derived from stainless steel column strength curves and from the moment-curvature relationship, respectively.

The accuracy of the proposal is assessed in stability analysis of planar stainless steel frames with compact SHS and RHS. The applicability of GNA using a stiffness reduction factor equal to $0.8\tau_N$, which is similar to the DM provided in AISC 360-16 is also verified. For a series of frames, results determined by GNA-τ_{MN} as well as GNA-$0.8\tau_N$ are compared with those determined by Geometrically and Materially Non-linear Analysis with Imperfections (GMNIA).

In practical situations, many economical cold formed steel sections comprise slender thin-walled elements that are susceptible to local buckling. Thus, the approximate expression of flexural stiffness reduction factors (τ_N, τ_M, τ_{MN}) are extended to account for local buckling effects and initial localized imperfection (ω),

by means of reducing cross-section resistance. The reduction factor ρ, determined in accordance with the Direct Strength Method (DSM), depending on cross-sectional slenderness, is incorporated into the formulations. For elements with SHS and RHS, the accuracy of GNA with the extended stiffness reduction is verified against results determined by GMNIA. It is found that GNA with stiffness reduction (using beam element) generally achieves the accuracy of GMNIA (using shell element). Since thin-walled elements are sensitive to initial localized imperfections (ω), a new approach utilizing Fourier series to generate the three-dimensional (3D) models of members with random ω is proposed. Probabilistic studies based on the proposed 3D models are then carried out to evaluate the effect of uncertainty in ω on the accuracy of GNA coupled with the extended stiffness reduction factor.

Acknowledgements

The research presented in this thesis was carried out under the supervision of Associate Professor Rolando Chacón at the Department of Civil and Environmental Engineering at Universitat Politècnica de Catalunya (UPC). I would like to express my sincere gratitude to him for his patience and invaluable guidance throughout my doctoral studies. I also wish to thank Dr. Itsaso Arrayago, who is my second supervisor in the first year of my doctoral study. She always answered patiently to all my questions.

The financial support from China Scholarship Council is gratefully acknowledged.

I am grateful to Prof. Esther Real for her valuable advice. I would also like to express my sincere gratitude to Prof. Enrique Mirambell for his kindness and the help he provided.

The financial support received from the MINECO (Spain) under the Project BIA2016-75678-R is also acknowledged.

During my PhD studies in UPC, I had the opportunity to meet people with different backgrounds. I am thankful to the members from the steel structure research group and all my friends at UPC for their kind help.

Finally, I would like to express my heartfelt thankfulness to my parents for their unconditional love and continuous encouragement. I will always be grateful to them.

Principal notations

λ	Load factor
λ_c	Column slenderness
λ_l	Cross-sectional slenderness
ω	Initial localized imperfection
ω_{max}	The maximum initial localized imperfection
τ_b	Flexural stiffness reduction factor derived from the CRC column strength curve
τ_N	Flexural stiffness reduction factor derived from the AISC-based column strength curve
$\tau_{N-\rho}$	τ_N considers local buckling effects
τ_M	Flexural stiffness reduction factor for beams with compact sections
$\tau_{M-\rho}$	τ_M considers local buckling effects
τ_{MN}	Flexural stiffness reduction factor for beam-column with compact section
$\tau_{MN-\rho}$	τ_{MN} considers local buckling effects
$\tau_{M-shell}$	τ_M derived from the M-k curve determined by GMNIA-shell element
τ_{M-beam}	τ_M derived from the M-k curve determined by GMNIA-beam element
$\Delta_{2nd-order}/\Delta_{1st-order}$	The ratio of second-order to first-order story drifts
Δ/h	Out-of-plumbness
δ/L	Out-of-straightness
σ_{lb}	Through-thickness longitudinal bending residual stress
ρ	Reduction factor account for local buckling effects (determined by DSM)
μ	Mean value
COV	Coefficients of Variation
ε	$\varepsilon = M_{r2\text{-}GNA\text{-}\tau MN} / M_{r2\text{-}GMNIA}$ (Chapter 5)
ε_{av}	Average value of ε in the group (Chapter 5)
ε_{cov}	Coefficient of variation of ε in the group (Chapter 5)
$\varepsilon+$	Maximum value of ε in the group (Chapter 5)
$\varepsilon-$	Minimum value of ε in the group (Chapter 5)

$\lvert\varepsilon_{max}\rvert$	Maximum value of relative error for each set of 50 models (Chapter 8)
$\mu(M_{u\text{-}rand})$	The mean value of the $M_{u\text{-}rand}$ (Chapter 8)
$\frac{dM_{r1}}{d\kappa}$	The slope of the tangent at a given point on the M-k curve
ASOM	Approximate second-order elastic analysis method
B_1	Amplification factor accounts for P-δ effects provided in ASIC 360-16
B_2	Amplification factor accounts for P-Δ effects together with P-δ effects provided in ASIC 360-16
$B_{1\text{-}E}$	Amplification factor evaluates P-δ effects on elastic beam-columns
$B_{1\text{-}P}$	Amplification factor evaluates P-δ effects on inelastic beam-columns
$B_{2\text{-}E}$	Amplification factor evaluates P-Δ effects together with P-δ effects on elastic beam-columns
$B_{2\text{-}P}$	Amplification factor evaluates P-Δ effects together with P-δ effects on inelastic beam-columns
C_m	Equivalent uniform moment factor
DM	Direct Analysis Method provided in AISC 360-16
ELM	Effective length method
$(EI)_t$	Tangent flexural stiffness
LA	Linear Elastic Analysis
GMNIA	Geometrically and Materially Non-linear Analysis with Imperfections
GMNIA-shell	GMNIA using shell element (Chapter 7)
GMNIA-beam	GMNIA using beam element (Chapter 7)
GNA	Geometrically Non-linear Analysis
GNA-τ_{MN}	GNA coupled with τ_{MN}
GNA-τ_N	GNA coupled with τ_N
GNA-$\tau_{N\text{-}\rho}$	GNA coupled with $\tau_{N\text{-}\rho}$
K	Effective length factor of the column
K_b	Critical buckling factor for members

K_{sw} Second order sway effects factor provided in EN1993-1-1: 2015(E)

M_1 and M_2 Applied external end moments, $|M_1| \leq |M_2|$.

M_{crl} Elastic critical local buckling moment.

M_n Nominal flexural strength of a beam

M_{ne} Nominal global (lateral-torsional) buckling moment

M_{nl} Nominal local buckling moment

M_{nt} First order internal moment in sway-restrained (no lateral translation) frames

M_{lt} First order internal moment in sway-permitted (with lateral translation) frames

M_y Moment at yielding of the extreme fiber

M_P Moment at full cross-section yielding (not considering strain-hardening)

M_{r1} Maximum internal first order moment within the member

M_{r2} Maximum internal second order moment within the member

$M_{r2\text{-}E}$ Maximum internal second order elastic moment within the member

$M_{r2\text{-}P}$ Maximum internal second order inelastic moment within the member

$M_{r2\text{-}GMNIA}$ M_{r2} determined by GMNIA

$M_{r2\text{-}\tau MN}$ M_{r2} determined by GNA-τ_{MN}

$M_{r2\text{-}\tau N}$ M_{r2} determined by GNA-τ_N

$M_{r2\text{-}GMNIA\text{-}S}$ M_{r2} determined by GMNIA-shell (Chapter 7)

$M_{u\text{-}GMNIA}$ Ultimate external moment of the member determined by GMNIA

$M_{u\text{-}GMNIA\text{-}B}$ M_u determined by GMNIA-beam (Chapter 7)

$M_{u\text{-}GMNIA\text{-}S}$ M_u determined by GMNIA-shell (Chapter 7)

$M_{u\text{-}\tau MN\text{-}\rho}$ M_u determined by GNA-$\tau_{MN\text{-}\rho}$ (Chapter 7)

$M_{u\text{-}rand}$ Predicted ultimate external bending moment for each model with random ω (Chapter 8)

N Parameter in Ramberg-Osgood equation

P_e Elastic critical buckling strength of the member with effective length (KL)

P_{e1} Elastic critical buckling strength (non-sway mode) of the member with K=1

P_{es} Elastic critical buckling strength (sway mode) of the member with effective length (KL)

$P_{e\text{-}\tau N}$	Elastic critical buckling load determined by the reduced flexural stiffness: τ_N times EI
$P_{e\text{-}\tau N\rho}$	Elastic critical buckling load determined by the reduced flexural stiffness: $\tau_{N\text{-}\rho}$ times EI
P_{lt}	First order internal axial force in sway-permitted frames
P_{nt}	First order internal axial force in sway-restrained frames
P_n	Nominal compressive strength of a column
P_{ne}	Nominal global buckling strength in compression
P_{nl}	Nominal local buckling strength in compression
P_{story}	Total vertical load transferred by the story (from Linear Elastic Analysis)
$P_{e^*\text{-}story}$	Elastic critical buckling (sway mode) strength of the story (without including R_M)
P_{r1}	Maximum internal first order axial force within the member
P_{r2}	Maximum internal second order axial force within the member
$P_{r2\text{-}GMNIA}$	P_{r2} determined by GMNIA
$P_{r2\text{-}\tau MN}$	P_{r2} determined by GNA-τ_{MN}
$P_{r2\text{-}\tau N}$	P_{r2} determined by GNA-τ_N
P_u	Ultimate axial load of the member
$P_{u\text{-}GMNIA}$	P_u determined by GMNIA
$P_{u\text{-}\tau MN}$	P_u determined by GNA-τ_{MN}
$P_{u\text{-}\tau N\text{-}\rho}$	P_u determined by GNA-$\tau_{N\text{-}\rho}$
$P_{u\text{-}GMNIA\text{-}B}$	P_u determined by GMNIA-beam (Chapter 7)
$P_{u\text{-}GMNIA\text{-}S}$	P_u determined by GMNIA-shell (Chapter 7)
$P_{u\text{-}EXP}$	Ultimate compressive strength obtained from experiment (Chapter 8)
$P_{u\text{-}rand}$	Predicted ultimate compressive strength for each model with random ω (Chapter 8)
P_y	Cross-section yield strength
R_c	Demand-capacity ratio determined by interaction design equations provided in ASIC 360-16
$R_{c\text{-}GMNIA}$	R_c with second order axial force and moment determined by GMNIA
$R_{c\text{-}\tau MN}$	R_c with second order axial force and moment determined by GNA-τ_{MN}
$R_{c\text{-}\tau N}$	R_c with second order axial force and moment determined by GNA-τ_N

R_M	Factor accounts for P-δ effects on the global behavior of the structure
W_{el}	Elastic cross-section modulus
W_{pl}	Plastic cross-section modulus

Contents

1. Introduction

1.1 Background

1.1.1 Stainless steel

Stainless steel is a steel alloy that contains a minimum of 10.5% chromium (Cr) content by mass and a maximum of 1.2% carbon (C) by mass. Stainless steel is most notable for its corrosion resistance, which increases with the increasing chromium content. To suit the environment the alloy must endure, there is a wide range of stainless steels with varied levels of corrosion resistance and mechanical strength. So far, more than 200 standardized stainless steel grades have hitherto been developed (FCSA, 2008).

The basic alloying elements of stainless steel grades are chromium (Cr) and nickel (Ni), other alloying elements such as molybdenum (Mo), titanium (Ti) and manganese (Mn) are also included in stainless steels to improve their mechanical properties and corrosion resistance. According to Cr -Ni content by mass, stainless steels can be classified into five basic groups (Rossi, 2014). The five types are austenitic, ferritic, austenitic-ferritic (duplex), martensitic and precipitation hardening stainless steels, as shown in Fig 1.1. The first three types have a wide and diverse application in construction industry, such as building exteriors and facades, and pedestrian bridges (Baddoo, 2013). The last two types are for specialist applications. For instance, martensitic grades are commonly used for bearings and turbine blades, and precipitation hardening grades are mostly used in nuclear and aerospace industry (Baddoo, 2013).

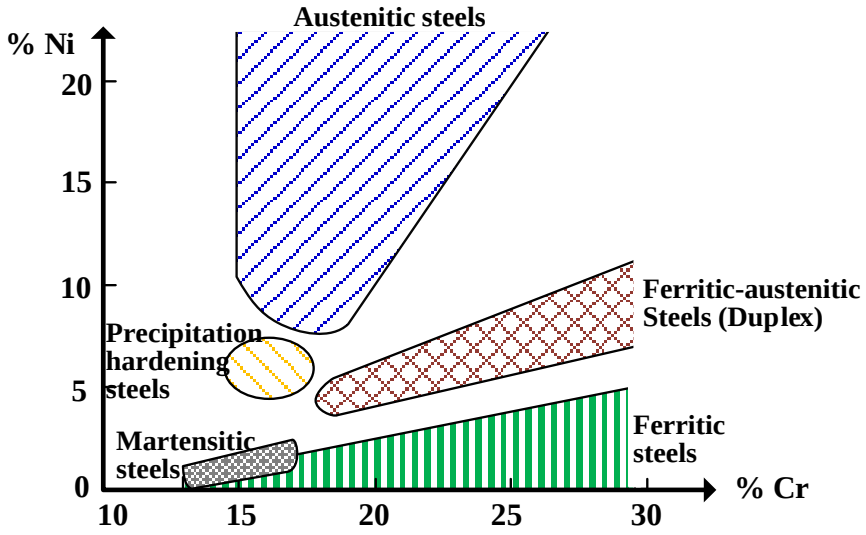

Fig.1.1. Classification of stainless steels groups based on the content of Cr and Ni

- Austenitic stainless steels

Austenitic stainless steels have favorable corrosion resistance and high ductility. They are easily cold-formed are readily weldable. The most widely used types of austenitic stainless steels have a Cr content of 17% to 18% and Ni content between 8% and 11%. Compared to carbon steels, austenitic stainless steels have significantly better toughness over a wide range of temperatures.

- Ferritic stainless steels

Compared to austenitic stainless steels, ferritic stainless steels are generally less ductile, less formable and less weldable. The most widely used ferritic stainless steels have a Cr content of 10.5% to 18%. The Ni content is either very small or not included in them.

- Duplex stainless steels

Duplex stainless steels have a mixed microstructure of austenite and ferrite. The most widely used types of duplex stainless steels contain 20% to 26% Cr, 1% to 8% Ni, 0.05 % to 5% Mo, and 0.05% to 0.3% N. Compared to austenitic stainless steels, they provide higher strength.

- Martensitic stainless steels

Martensitic stainless steels are similar to low alloy or carbon steels. Compared to austenitic and ferritic stainless steels, martensitic stainless steels have higher carbon content, and can be strengthened by heat treatment. They are generally used in a hardened and tempered condition.

- Precipitation hardening stainless steels.

Precipitation hardening steels have properties similar to a mix of martensitic and austenitic steels. They can be strengthened by heat treatment. Precipitation hardening steels are mostly used in the aerospace industry and are also used in other applications that require high strength and moderate corrosion resistance.

1.1.2 Application of cold-formed stainless steel RHS and SHS

Steel hollow sections are a versatile and efficient form for construction applications. Buildings that use steel hollow sections have high strength-to-weight ratios. The efficient use of steel hollow sections reduces material usage resulting in lightweight structures. It allows for large span, and thus is an alternative to achieve optimal economic benefits. Since stainless steels have excellent corrosion resistance properties,

considerable long-term durability, and good mechanical strength, the use of cold-formed stainless steel rectangular hollow section (RHS) and square hollow section (SHS) (shown in Fig. 1.2) in construction industry has attracted considerable attention.

Fig.1.2. Cold-formed stainless steel RHS and SHS

For construction applications, the most commonly used stainless steel hollow sections are made of austenitic grades EN1.4301, EN1.4307, EN1.4404 and EN1.4571. For example, these sections have been used in the facade of the building of Institute of Chemical and Bioengineering, ETH Zürich (Switzerland), shown in Fig. 1.3 (a), and the support frame of Marqués de Riscal Vineyard (Spain), shown in Fig. 1.3 (b), Also, they can be used for the main frame structure of residential buildings, as shown in Fig. 1.3 (c). Hollow sections made of austenitic steel grades EN1.4541, EN1.4318, EN1.4372, EN1.4432 and EN1.4539, ferritic steel grades EN1.4003 and EN1.4509, and duplex steel grades EN1.4162, EN1.4362 and EN1.4462, are mainly used for specialist applications.

(a)

(b)

(c)

Fig.1.3. Applications of stainless steel RHS and SHS in construction: (a) Facade of the building of Institute of Chemical and Bioengineering, ETH Zürich (Switzerland) (b) Support frame of Marqués de Riscal Vineyard (Spain) (c) Main frame structure of the private residential buildings (FCSA, 2008)

1.1.3 Manufacturing of cold-formed stainless steel RHS and SHS

Cold-formed hollow sections are manufactured by cold working and welding. There are two different forming methods for cold-formed stainless steel RHS and SHS, direct-forming and round to square forming. In direct forming (shown in Fig 1.4(a)), the steel strip is transformed into a square or rectangular hollow section by bending it through rollers, and welding the seam after that. In round to square forming (shown in Fig 1.4(b)), steel strip is first formed into a circular hollow section and then it is welded. After forming circular hollow section, square or rectangular shapes are created by using profiling rollers. The stages of a direct-forming line are shown in Fig.1.5.

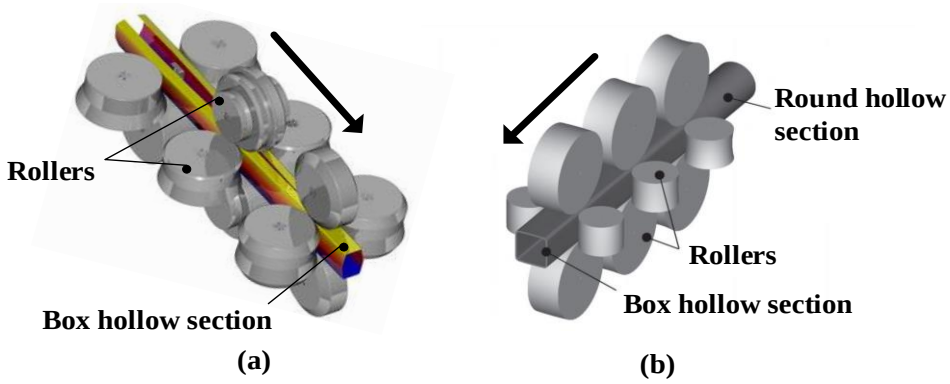

Fig.1.4. Two forming methods for cold-formed RHS and SHS (a) Direct forming (COPRA, 2014) (b) Round to square forming (Nagamachi et al., 2011)

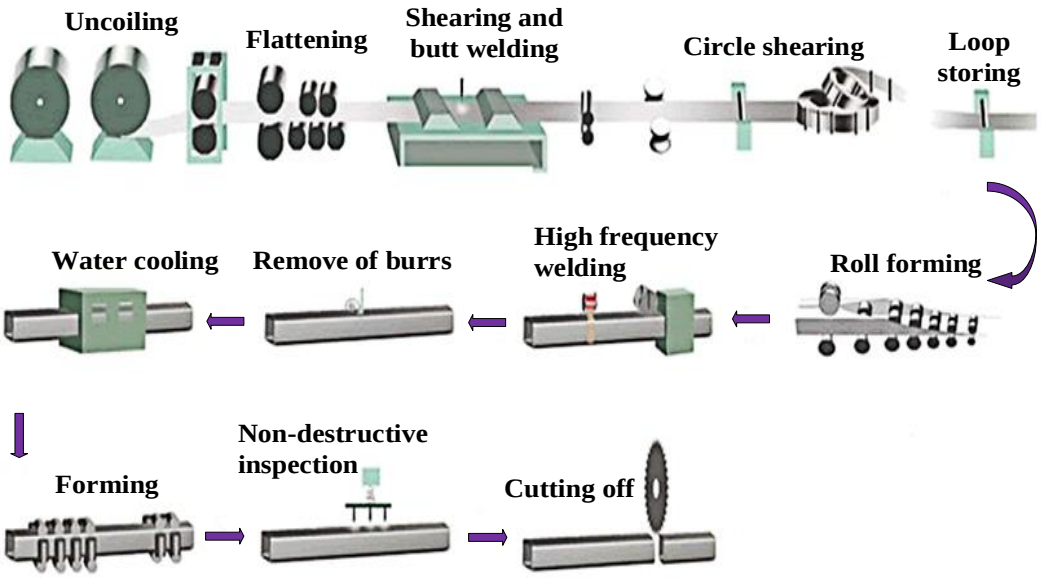

Fig.1.5. The stages of a direct-forming line (Sunny Steel)

Cold-forming process changes the mechanical properties of stainless steel, induces residual stresses and initial localized imperfection.

(1) Strength levels of stainless steels, especially the austenitic grades, are enhanced by cold working. A strength enhancement of about 50% is typical in the cold formed corners of cross sections (Design Manual for Structural Stainless steel, 2017); the strength of the material in the flat faces also increases. Accompanied with this enhancement is a reduction in ductility. The changes in mechanical properties depend on the forming method and dimensions of the hollow section, and the mechanical properties can be measured by testing coupons taken from the RHS and SHS.

(2) Plastic deformation produced in cold-working process such as uncoiling, leveling, and rolling to form a section, results in residual stresses. For cold formed steel box sections, the induced residual stresses are complicated, typically comprising bending residual stresses, membrane residual stresses, and layer residual stresses.

(3) The rolling and fabrication process produce initial localized imperfections. The induced localized imperfections have sufficient variability and have no definitive characterization. In practical situations, many economical cold-formed hollow sections, which contain slender thin-walled elements, are sensitive to initial localized imperfection. Initial localized imperfection, coupled with member imperfection and global sway imperfection that resulted from fabrication and erection process, should be considered in structural analysis.

1.2 Motivation

Current design methods are based on resistance checks at member levels and the design limit state is the formation of first plastic hinge. The internal forces and moments are evaluated using elastic structural analysis. For member-based design methods, using a Geometrically Nonlinear Analysis (GNA) coupled with stiffness reduction to determine internal forces and moments for ultimate limit state design checks has become a significant strategy. GNA with stiffness reduction can capture second order effects at system and member levels (P-Δ and P-δ), considers initial global sway imperfection, and adopts reduced stiffness to account for the influence of material non-linearity and residual stresses. For GNA with stiffness reduction, initial member out-of-straightness (δ/L) can be accounted for by four ways: (1) By geometrically modelling out-of-straightness directly (2) By applying equivalent horizontal loads appropriately (3) By reducing

stiffness implicitly using reduction factors (4) By checking bucking resistance of members. If member out-of-straightness is included in the stiffness reduction factors, there is no need for member buckling strength checks and only cross-sectional strength checks are required.

A representative example of GNA with stiffness reduction is the Direct Analysis Method (DM). DM first appeared in AISC 360-05 (2005) as an alternative to Effective Length Method (ELM) for frame stability design, was upgraded in AISC 360-10 (2010) and reorganized in AISC 360-16 (2016) as the primary method for frame stability design (ELM was moved to Appendix 7 of AISC 360-16). Compared with ELM, a significant advantage of GNA with stiffness reduction is that it eliminates the need of calculating of effective length of the column. The calculation of effective length factor (K) may be both difficult and inaccurate for geometrically irregular frames. Another main advantage is that it provides more accurate value of internal moment, which is a great concern for the design of connections. In most cases, compared to ELM, GNA with stiffness reduction gives an improved representation of internal moments.

The accuracy of GNA with stiffness reduction highly depends on the adopted stiffness reduction factor. The reduction in stiffness will produce more deformations, which will in turn result in increased internal forces and moments due to second order effects. Although calibration studies have shown that the flexural stiffness reduction factor provided in AISC 360-16 (2016) is appropriate to stability design of carbon steel beam-columns and frames, it may not be appropriate to the stainless steel counterparts. The reason is stainless steel is softer than carbon steel in the stress range of proportional limit and 0.2% proof strength, and member buckling curves of stainless steel differs from carbon steel. Therefore, when using GNA with stiffness reduction for the stability design of stainless steel elements and frames, appropriate stiffness reduction factors are needed.

1.3 Objectives

The primary objective of this thesis is to develop flexural stiffness reduction factor formulations that are applicable to the in-plane stability design of stainless steel elements and frames with cold-formed square hollow section (SHS) and rectangular hollow section (RHS). The proposed stiffness reduction factor formulations accounts for the deleterious influence of material non-linearity, residual stresses and member out-of-straightness. The specific generals are listed below:

(1) Developing column flexural stiffness reduction factor (τ_N), beam flexural stiffness reduction factor

(τ_M), and beam-column flexural stiffness reduction factor (τ_{MN}), which are applicable to compact sections.

(2) Assessing the accuracy of the GNA coupled with flexural stiffness reduction factors (τ_N, τ_M, τ_{MN}) in stability analysis of planar stainless steel elements and frames with compact SHS and RHS.

(3) Extending flexural stiffness reduction factors (τ_N, τ_M, τ_{MN}) that are applicable to compact sections to account for local buckling effects and initial localized imperfection (ω).

(4) Evaluating the effect of uncertainty in ω on the accuracy of GNA coupled with the extended stiffness reduction factor the sections that are susceptible to local buckling effects.

1.4 Research methodology

This thesis investigates the behavior of stainless steel structures made up of cold formed stainless steel RHS and SHS. The GNA coupled with stiffness reduction method is only applicable to the in-plane stability design of structures. The ultimate limit state for this method is the formation of first plastic hinge. Analytical and numerical studies are conducted to develop the beam-column flexural stiffness reduction factor (τ_{MN}) formulations. The accuracy of GNA coupled with stiffness reduction method is assessed through numerical studies. In-plane structural behavior of stainless steel elements and frames is studied using finite element (FE) software ABAQUS 6.13. MATLAB 2017b and MINITAB 18 are also employed in this study.

The adopted methodology is illustrated in Fig. 1.6. The details of the methodology are the following:

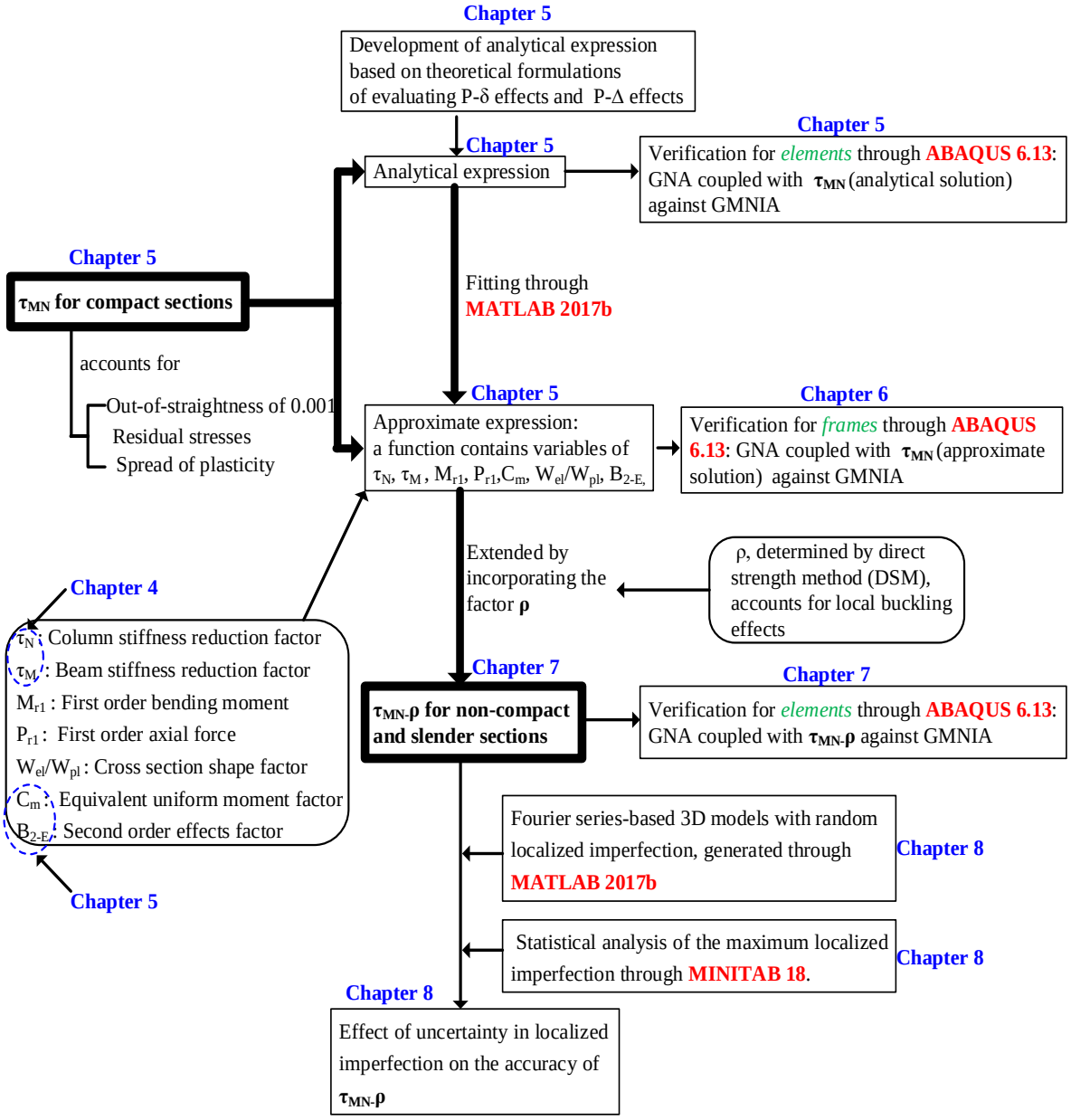

Fig 1.6. Illustration of the adopted methodology

- For compact sections that are not are not prone to local buckling reductions:

(1) Column flexural stiffness reduction factor (τ_N) is derived from AISC LRFD-based column flexural buckling strength curve. Beam flexural stiffness reduction factor (τ_M) is derived from moment-curvature relationship curve that based on Ramberg-Osgood equation.

(2) Two types of beam-column flexural stiffness reduction factor (τ_{MN}) formulations, applicable to compact SHS and RHS, are proposed: analytical and approximate. The analytical expression of τ_{MN} presumes knowing the maximum internal second order moment (M_{r2}) within a member. It is developed by means of

extending the formulations for evaluating the elastic second order effects to the inelastic range. The accuracy of the GNA coupled with τ_{MN} (determined by the analytical expression) is assessed in stability analysis of planar stainless steel elements and sub-assemblages. Since in practical design M_{r2} is not known in advance, an approximate expression of τ_{MN}, which is assumed to be a function of relevant variables, is proposed by fitting variables to the analytically determined expression.

(3) The accuracy of the GNA coupled with τ_{MN} (determined by the approximate expression) is assessed in stability analysis of planar stainless steel frames with compact SHS and RHS. The applicability of GNA using a stiffness reduction factor equal to $0.8\tau_N$, which is similar to the DM provided in AISC 360-16 is also verified. For a series of frames, results determined by GNA-τ_{MN} as well as GNA-$0.8\tau_N$ are compared with those determined by GMNIA. Comparisons of Demand-Capacity ratio and maximum internal second order moment within members are made.

- For non-compact and slender sections that are not are susceptible to local buckling reductions:

(1) The approximate expression of flexural stiffness reduction factors (τ_N, τ_M, τ_{MN}), applicable to compact sections, are extended to account for local buckling effects and initial localized imperfection (ω), by means of reducing cross-section resistance. The reduction factor ρ, determined in accordance with the Direct Strength Method (DSM), depending on cross-sectional slenderness, is incorporated into the formulations. For elements with SHS and RHS, the accuracy of GNA with the extended stiffness reduction is verified against results determined by GMNIA

(2) A Fourier series-based three-dimensional (3D) models for members with random ω is proposed. The proposed model is generated through MATLAB. Probabilistic studies based on the proposed 3D models are then carried out to evaluate the effect of uncertainty in ω on the accuracy of GNA coupled with the extended stiffness reduction factor.

1.5 Thesis outline

This thesis is structured as follows:

Chapter 2 provides a review of the various types of structural analysis methods as well as the assumptions implied within them, followed by discussion of the application and limitations of these structural analysis methods for evaluating frame and member stability. A brief summary and comparison of frame and beam-

column design provisions in different design standards are then presented. Finally, a review of the material response, initial geometric imperfections, and residual stresses considered in structural analysis is presented.

Chapter 3 describes the finite element (FE) modelling approach adopted in Chapter 4-6, to verify GNA coupled with stiffness reduction factor for the design of stainless steel elements and frames with compact cross-sections. The FE models are developed using the general-purpose package ABAQUS 6.13 (2013), and validated against experimental results from the literature.

Chapter 4 presents the development of column flexural stiffness reduction factor (τ_N) and beam flexural stiffness reduction factor (τ_M). The proposed τ_N and τ_M are applicable to stainless steel members with compact cold-formed RHS and SHS. τ_N is derived from stainless steel column strength curve provided in AISC design guide 27. τ_M is developed based on the moment-curvature relationship for stainless steel beams with cold formed RHS and SHS.

Chapter 5 focuses on the development of beam-column flexural stiffness reduction factor (τ_{MN}) formulation for the in-plane stability design of stainless steel beam-columns with compact cold-formed RHS and SHS. Two types of τ_{MN} formulations are proposed: analytical and approximate. The analytical expression of τ_{MN} presumes knowing the maximum internal second order moment (M_{r2}) within a member. It is developed by means of extending the formulations for evaluating the elastic second order effects to the inelastic range. A function (approximate expression) independent of $M_{r2\text{-}P}$, which matches analytical expression of τ_{MN}, is proposed. The approximate expression of τ_{MN} is developed by fitting variables to the analytically determined expressions.

Chapter 6 presents the verification of the accuracy of GNA with flexural stiffness reduction formulation (τ_{MN}) to in-plane stability design of stainless steel frames. The adopted τ_{MN} is determined by the approximate expression presented in the previous chapter. The applicability of GNA using a stiffness reduction factor equal to $0.8\tau_N$, which is similar to the Direct Analysis Method (DM) provided in AISC 360-16 is also verified. The study is focused on a series of stainless steel frames with different geometrical and loading configurations. The main objectives of verification study are the comparisons of Demand-Capacity ratio and comparisons of maximum internal second order moment within members determined by: GMNIA, GNA coupled with τ_{MN}, and GNA coupled with $0.8\tau_N$.

Chapter 7 presents the extension of flexural stiffness reduction factors (τ_N, τ_M, τ_{MN}), applicable to compact

sections, to account for local buckling effects and initial localized imperfection (ω). Local buckling reduction is taken into account by means of reducing cross-section resistance. The reduction factor ρ, determined in accordance with the Direct Strength Method (DSM), depending on cross-sectional slenderness, is incorporated into the formulations. For elements with SHS and RHS, the accuracy of GNA with the extended stiffness reduction is verified against results determined by GMNIA.

Chapter 8 presents the evaluation of the effect of uncertainty in ω on the ultimate capacity of stainless steel columns and the effect of uncertainty in ω on the accuracy of GNA with stiffness reduction for stainless steel beam-columns. For a series of tested stainless steel columns (susceptible to local buckling) reported in the literature, the statistical characteristics of the ultimate axial load, obtained from GMNIA in which ω is modelled randomly, are compared against the experimental results. Then, for the studied beam-columns presented in Chapter 7, the statistical characteristics of the ultimate capacity, obtained from GMNIA in which ω is modelled randomly, are compared against those determined by GNA-$\tau_{MN-\rho}$ as well as GMNIA in which ω is modelled as the lowest local buckling mode.

Chapter 9 draws conclusions about this research and provides recommendations for future research studies.

2. Literature review

2.1 Introduction

The chapter provides a review of the various types of structural analysis methods. A brief summary of frame and beam-column design provisions in different design standards is then presented, followed by a comparison of different design provisions. Finally, a review of the material response, initial geometric imperfections, and residual stresses considered in structural analysis is presented.

2.2 Structural analysis of steel structures

The structural analysis methods described in this chapter are distinguished according to whether or not geometric and material nonlinear behavior are considered in them. Geometric nonlinear behavior refers to equilibrium of internal forces and moments on the deformed geometry of the structure, while material nonlinear behavior refers to material yielding, or more specifically, spread of plasticity through the cross section and along the member length.

2.2.1 General analysis types

An overview of the structural analysis types for the design of frames is shown by the load-deflection curves in Fig. 2.1, where the load factor (λ) relates to the amplitude of the applied gravity and lateral loads. In general, the analysis types are classified into four groups:

- First-order Elastic Analysis
- Second-order Elastic Analysis
- First-order Elastic-Plastic Analysis
- Second-order Elastic-Plastic Analysis

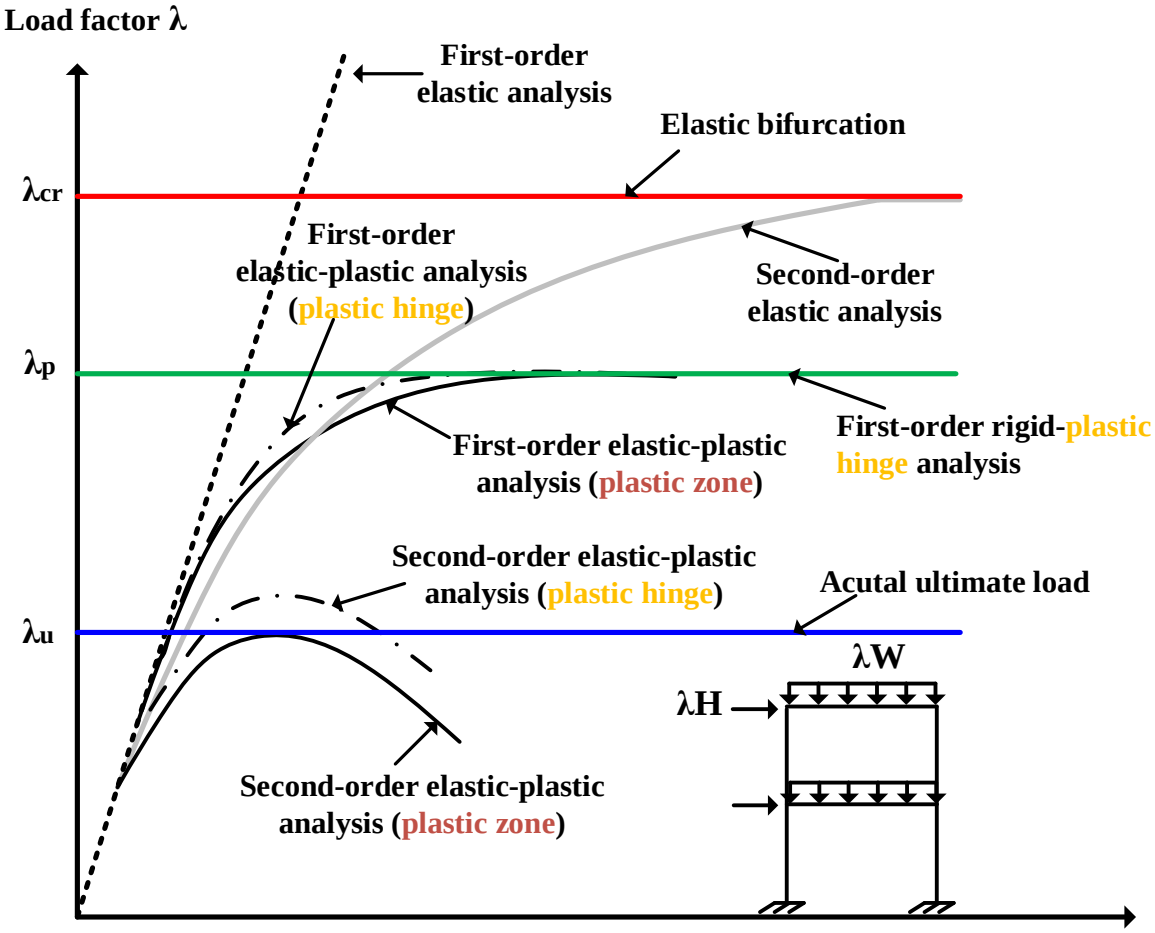

Fig. 2.1 Schematic illustration of structural analysis types by load-deflection curves

(1) First-order elastic analysis

First-order elastic analysis is the most basic type of structural analysis in which neither geometric non-linearity (P-Δ and P-δ effects) nor material non-linearity is considered. The material is modeled as linear-elastic and equilibrium of internal forces and moments are calculated based on the undeformed shape of the structure. Thus, the deformations of the structure are directly proportional to the applied loads throughout the analysis, and the principle of superposition which simplifies the analyses for different load combinations applies to first-order elastic analysis.

(2) Second-order elastic analysis

For a second order elastic analysis, the equilibrium of internal force is formulated on the deformed geometry of the structure, and the material is modeled as linear-elastic. The upper-bound solution for a second order analysis is the solution (eigenvalue λ_{cr}) obtained from bifurcation analysis, in which initial imperfection, pre-buckling deformation, and material non-linearity are ignored. The superposition that simplifies the

analyses for different load combinations does not apply to this type of analysis because the second-order response is nonlinear.

(3) First-order elastic-plastic analysis

A first-order elastic-plastic includes material non-linearity, but equilibrium of internal forces are formed based on the undeformed shape of the structure. When strain hardening is neglected, the load-defection response determined by a first-order inelastic analysis asymptotically approaches the plastic limit load (λ_p), which is determined by a first-order rigid-plastic hinge analysis. In the first-order rigid-plastic hinge analysis, spread of yielding along the member length and through the cross-section is concentrated in discrete regions.

(4) Second-order elastic-plastic analysis

A second-order inelastic analysis includes both geometric and material nonlinearity. It accounts for the reduction in stiffness caused by both member yielding and large deflections, and can accurately model inelastic force redistribution. The ultimate load determined by a second-order inelastic analysis is the most accurate representation of the actual ultimate load of the structure.

2.2.2 Inelastic analysis types

Based on how material nonlinearity is accounted for, elastic-plastic analysis types can be further divided into:

- Elastic-Plastic Hinge Analysis
- Refined-Plastic Hinge Analysis
- Reduced Tangent Modulus Analysis
- Plastic-Zone Analysis

(1) Elastic-plastic hinge analysis

In an elastic-plastic hinge analysis, spread of yielding along the member length is concentrated in discrete regions (zero length) where plastic hinges form. Fully yielded sections are modeled using plastic hinges that enforce a yield surface criterion and allow for elastic unloading. Plastic hinge methods rely on

simplified force interaction expressions to approximate the yield surface. It neglects residual stresses and typically one element is used to model each frame member. This analysis may be adequate for frames with slender members whose failure is governed by elastic instability (Chen, 2000; Chen and Lui, 2017). But it significantly overestimates the ultimate strength of multistory frames whose failure is governed by material yielding (White et al, 1991; White and Chen, 1993), since material yielding is concentrated in the zero-length plastic hinges and the associated instability are not considered.

(2) Refined-plastic hinge analysis

Based on modifications of the elastic-plastic hinge analysis, the refined-plastic hinge analysis captures partial yielding along member and across cross-section due to residual stresses and large axial force. The influence of spread of plasticity is accounted for by using a tangent modulus (E_t). It provides a more accurate estimate of member capacities in an inelastic analysis than a typical elastic-plastic hinge analysis (Ziemian, 2010). Great efforts have been contributed to this approach for the stability design of in-plane frames (Abdel-Ghaffar et al.,1991; Al-Mashary and Chen,1991; Clarke et al., 1992; King, et al.,1991; Liew and Chen,1991; Liew et al.,1993a,1993b; White,1993; Kim,1996; Kim and Chen,1996a, 1996b,1997,1998; Kim et al,2000; Ziemian and McGuire, 2002; Ziemian et al., 2008) and three-dimensional frames (Liew and Tang,1998; Kim et.al, 2001; Kim and Choi, 2001). Avery (1998) extended this approach to account for the effect of local buckling. A program (MASTAN2, 2000) that can perform refined-plastic hinge analysis, has been developed by Ziemian and McGuire (Ziemian and McGuire, 2000; McGuire et al., 2000). This program is based on MATLAB.

(3) Reduced tangent modulus analysis

This types of analysis captures the effects of spread-of plasticity by means of reducing the stiffness of members (Cheong-Siat-Moy,1977; Orbison et al., 1982; White and Chen, 1993; Ziemian et al., 1992a, 2008; Ziemian and McGuire, 2002, Surovek-Maleck and White, 2004a, 2004b; Zubydan, 2010; Kucukler et al., 2014, 2015a, 2015b, 2016; Kucukler and Gardner, 2018, 2019a,2019b; White et al., 2016). Some researchers use stiffness reduction factor derived from column flexural buckling curves to approximate stiffness reductions in steel members with high axial load (Ziemian et al., 1992a, 1992b; Ziemian and McGuire, 2002; White and Chen, 1993; Orbison et al., 1982). Since this tangent-modulus adjustment does not consider the combined action of axial compression and bending, it produces considerable errors for the

members whose plastification under combined axial compression and bending are significant (Ziemian 2010). To accurately capture plastification effects in a second-order analysis, the reduced stiffness must consider the combined effects of axial compression and bending, residual stresses, and shape factor for different cross-sections (Surovek-Maleck and White, 2004a, 2004b; Ziemian et al., 2008; White et al.,2016; Kucukler et al., 2014, 2016; Kucukler and Gardner, 2019a).

Surovek-Maleck and White (2004a, 2004b) proposed a general flexural stiffness reduction factor $0.9\tau_b$ for strong axis bending and $0.8\tau_b$ weak axis bending. The factor τ_b, derived from Column Research Council (CRC) column strength curve (Johnston, 1966), is intended to mainly account for the influence of partial yielding accentuated by the presence of residual stresses. The factor 0.8 or 0.9, accounts for additional stiffness reduction under combined axial loading and bending moment. The flexural stiffness reduction factor $0.8\tau_b$ has been adopted in the Direct Analysis Method (DM) for the design of steel frames provided in AISC 360-16 (2016). The definition for τ_b in AISC 360-16 (2016) has been modified to account for the effects of local buckling of slender elements in compression members.

Kucukler et al. (2014, 2016) developed a function of beam-column flexural stiffness reduction factor for the stability design of in-plane carbon steel beam-columns and frames with compact I sections (referred to as $\tau_{MN,Kucukler}$, note that the symbols presented in this section are not identical to their original symbols). The main variables of the function include first order maximum axial force, first order maximum bending moment, column flexural stiffness reduction factor (referred to as $\tau_{N,Kucukler}$), beam flexural stiffness reduction factor (referred to as $\tau_{M,\ Kucukler}$), and a moment gradient factor C_m. $\tau_{N,\ Kucukler}$ is derived from column buckling curves given in EN 1993-1-1 (2005), while $\tau_{M,\ Kucukler}$ for beams sufficiently restrained against lateral-torsional buckling (LTB) under pure bending, is developed using a similar empirical formulation to the one proposed by Zubydan (2010) for compact I and H cross-sections subjected to combined axial loading and bending moment. For the development of flexural stiffness reduction formulations in Kucukler et al. (2014, 2016) and Zubydan (2010), strain-hardening is not considered and residual stresses pattern recommended by the European Convention for Construction Steelwork (ECCS, 1984) is adopted.

Furthermore, White et al. (2016) proposed a simple interpolation equation to represent beam-column flexural stiffness reduction factor (referred to as $\tau_{MN,White}$) for using direct buckling analysis to the stability design of carbon steel members and frames with I-sections. The general expression of the interpolation

equation is $\tau_{MN,White} = \rho^*\tau_a(\theta/90^o)+ \tau_{M,AISC}(1-\theta/90^o)$, where the angle θ represents the position of the current force point within a normalized interaction plot of the axial and moment strength ratios for a given cross-section. For the interpolation equation, τ_a is derived from column buckling curves given in AISC 360-16 (2016) and ρ* accounts for local buckling effects, while $\tau_{M,AISC}$ is derived from lateral-torsional buckling (LTB) curve of beams given in AISC 360-16 (2016). For using second order refined plastic hinge method to frame stability design, Kim and Chen (1999) extended the column flexural stiffness reduction factor derived from Column Research Council (CRC) column strength curve, to be applicable to beam-columns with compact I cross-sections.

In addition, SEI/ASCE 8-02 (2002) provides the tangent modulus approach to determine the buckling strength of members. The flexural buckling stress (f_n) is determined by $f_n=(\pi^2 E_t)/(KL/r)^2$. The tangent modulus E_t is derived from the nonlinear stress–strain curve determined by the Ramberg–Osgood expression. E_t, shown in Fig.2.2, is given by

$$E_t = \frac{f_y E_0}{f_y + 0.002nE_0\left(\frac{f}{f_y}\right)^{n-1}} \tag{2.1}$$

Where n is Ramberg–Osgood parameter; f is the stress in the member; E_0 is initial elastic modulus (Young's Modulus); f_y is 0.2% proof stress.

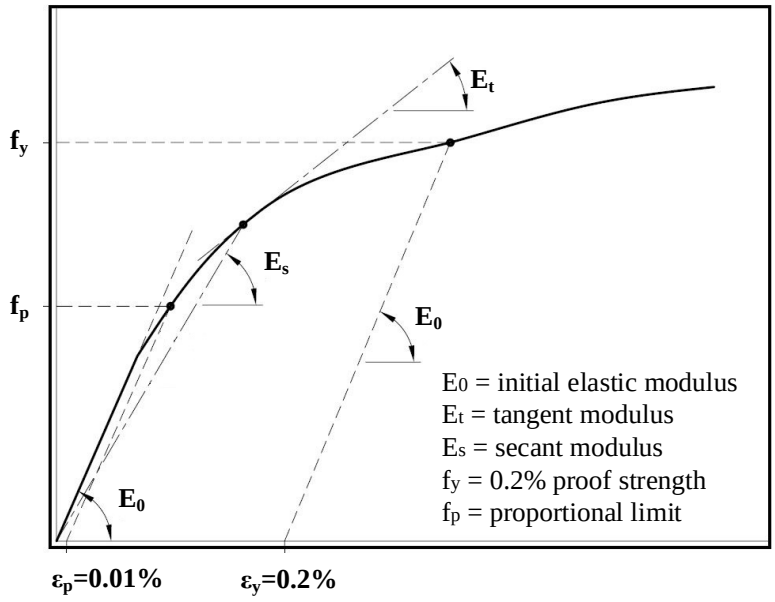

Fig.2.2 E_t derived from Ramberg-Osgood equation-based nonlinear stress–strain

However, it should be pointed out that E_t is not adopted in this paper and is not detailed further, due to the

reason that:

(1) Many studies have shown that, the single Ramberg-Osgood curve from which the tangent modulus E_t is derived, is generally incapable of accurately representing the full stress-strain curve of stainless steel (Mirambell and Real, 2000; Rasmussen, 2003; Gardner and Nethercot, 2004; Arrayago et al. 2015).

(2) The GNA coupled with stiffness reduction method proposed in this paper is aimed to align with AISC 360-16 (2016). Thus, the adopted column buckling strength curve, and beam-column interaction curve are based on AISC provisions, with modifications made where necessary to fit in with test results.

(4) Plastic-zone analysis

A plastic-zone analysis is typically taken as an "exact" solution and is used as a benchmark to verify other simplified analysis. The AISC-LRFD beam-column interaction equations were established based on "exact" beam-column strength curves from the plastic-zone analysis conducted by Kanchanalai (1977). In plastic-zone analysis, members are discretized into finite elements, and furthermore the cross-section of each finite element is subdivided into many fibers. The deflection at each division point along a member is obtained by numerical integration. Spread of plasticity and second-order effects are rigorously captured through the incremental load-deflection response at each loading step.

Over the past decades, the application of this type of analysis was limited to verifying the accuracy of simplified methods, since it was too intensive in computation (Alvarez and Birnstiel, 1967, King et al.,1992; Liew, 1992; Liew et al., 1993a, Clarke et al., 1992; White, 1993; Vogel, 1985; El-Zanaty et al., 1980; Wang, 1988; Chen and Atsuta, 1977). However, with the development computer technology, numerous finite element software, such as ANSYS v19.0 (2018), ABAQUS v2013 (2013), and LS-DYNA SMP R11.0.0 (2019), which can perform plastic-zone analysis, have been developed. These software facilitate the application of plastic-zone analysis in practical engineering.

2.3 Methodologies for evaluating frame stability provided in AISC 360-16

Chapter 3 of AISC 360-16 (2016) provides Direct Analysis Method (DM), which is the primary method for the stability design of steel frames. Appendix 7 and 8 of AISC 360-16 (2016) provide two alternative methods for the stability design of steel frames: Effective length method (ELM) and approximate second-order elastic analysis method.

2.3.1 Direct analysis method (DM)

DM first appeared in AISC 360-05 (2005) as an alternative to Effective Length Method (ELM) for frame stability design, was upgraded in AISC 360-10 (2010) and reorganized in AISC 360-16 (2016) as the primary method for frame stability design. DM has been further explored by the cold-formed steel industry (Sarawit and Pekoz, 2006) and was adopted in the AISI S100-16 (2016): North American Specification for the Design of Cold-Formed Steel Structural Members.

Compared with ELM, it eliminates the need of calculating of effective length of the column. The calculation of effective length factor (K) may be both difficult and inaccurate for geometrically irregular frames. Another main advantage is that it provides more accurate internal moment, which is a great concern for the design of connections. In most cases, DM gives an improved representation of internal moments, which is closer to the values obtained by more advanced analysis such as plastic-zone analysis at member-based ultimate strength limit state. For a frame example, the plots of normalized maximum internal moment (M_{r2}) and normalized axial force (P_{r2}) for a column in the frame determined by DM and GMNIA (plastic zone) are shown in Fig.2.3. P_n and M_n are nominal compressive strength and nominal bending strength, respectively. The P_{r2}/P_y versus M_{r2}/M_p curve determined by DM is softer than that determined by GMNIA, because the flexural stiffness of the frame is reduced (0.8EI) when implementing DM.

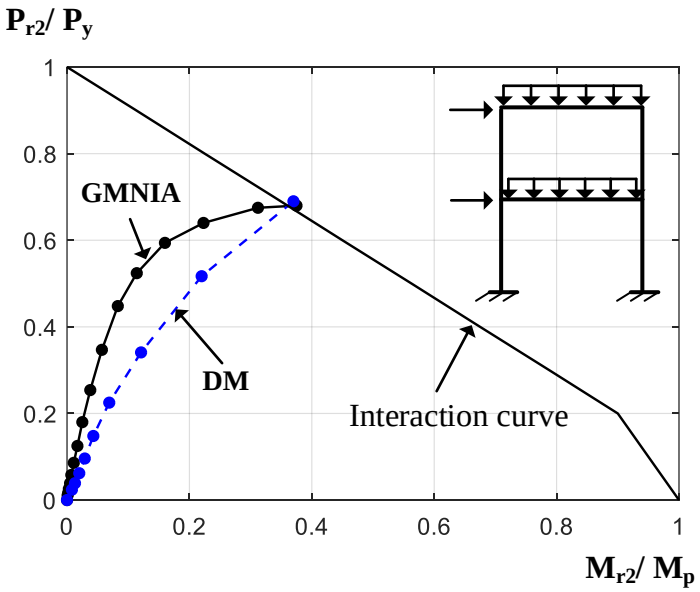

Fig.2.3 Plots of M_{r2}/M_p versus P_{r2}/P_y determined by DM and GMNIA

With heavy reliance on a rigorous second-order elastic analysis, DM takes into account initial geometric

imperfections and adopts adjusted (reduced) stiffness.

- Initial geometric imperfections

DM in AISC 360-16 (2016) conservatively adopts the maximum allowable initial imperfection values specified in AISC 303-16 (2016): out-of-plumbness (Δ/h) of 0.002 for frame and out-of-straightness (δ/L) of 0.001 for member. By employing a column buckling strength curve that accounts for member initial out-of-straightness, only the remaining initial out-of-plumbness needs to be incorporated within the analysis. In member buckling strength checks, the column length is taken as the length between braced points (K=1).

Initial imperfections may be accounted for through direct modeling or the applying horizontal notional loads of $Ni = 0.002Y_i$, where Y_i is the total factored gravity load applied at the i th level. When the ratio of second-order drift to first-order drift ($\Delta_{2nd\text{-}order}$ /$\Delta_{1st\text{-}order}$) or B_2 factor is not exceed 1.7, it is permitted to apply notional loads only in gravity load-only combinations and not in combination with other lateral loads (commentary in Section C2.2 of AISC 360-16).

- Stiffness adjustment

For frames with slender members, the axial load is typically not exceed $0.5P_y$ (τ_b is equal to 1). The limit state is governed by elastic stability. The $0.8\tau_b$ ($0.8\tau_b$=0.8*1=0.8) factor on stiffness results in a system available strength equal to 0.8 times the elastic stability limit. 0.8 is close to the resistance factor ϕ (ϕ=0.9) times 0.877, where 0.877 is the factor used within the AISC column buckling strength curve to modify the Euler buckling load to account for member out-of-straightness. The compressive strength of the slender member (governed by elastic stability) is $\phi P_n = 0.90(0.877P_e) = 0.79P_e$. The combination of axial load and partial yielding (accentuated by the presence of residual stresses) may has not considerable influence on bending stiffness.

For frames with intermediate or stocky columns, the $0.8\tau_b$ factor reduces the stiffness to account for inelastic softening prior to the members reaching their design strength. The bending stiffness of members with an axial load in excess of $0.5P_y$ is reduced by the stiffness reduction factor τ_b derived from CRC column strength curve, to account for the influence of partial yielding accentuated by the presence of residual stresses. τ_b also accounts for the effects of local buckling of slender elements in compression members. The 0.8 factor accounts for additional softening under combined axial compression and bending.

2.3.2 Effective length method (ELM)

2.3.2.1 ELM for the stability design of frames

The effective length method (ELM) has been used in various steel design codes and specifications. The current provisions for ELM in AISC 360-16 (2016) are essentially the same as those in Appendix 7 of the AISC 360-10 (2010). ELM utilizes the nominal geometry and the nominal elastic stiffness in the global analysis.

The column effective length factor K (K>1), accounts for the effects of initial out-of-plumbness and member stiffness reductions due to the spread of plasticity.

Some studies (Deierlein et al., 2002; White et al., 2006; Griffis and White, 2013; White and Hajjar, 1997; Surovek-Maleck and White, 2004a and 2004b) showed that the ELM could significantly overestimate the ultimate capacity of the symmetric framing systems with low redundancy and high gravity-to-horizontal load ratios. Particularly, the second-order internal moment was significantly underestimated since initial out-of-plumbness was not considered when modeling frames with nearly symmetrical geometry and loading patterns. As a consequence, AISC 360-16 (2016) stipulates two additional requirements for the use of the effective length method:

(1) The use of the ELM is restricted to cases where the second order sway effect amplification factor, $\Delta_{2nd\text{-}order}/\Delta_{1st\text{-}order}$ (the ratio of second-order to first-order story drifts), which can be taken as the B_2 multiplier, is less than or equal to 1.5.

(2) For gravity-only load cases (without lateral load component), a notional lateral load of $N_i = 0.002Y_i$ should be included, where Y_i is the total factored gravity load at the ith level.

For the stability design of frames, effective length method is combined with second order elastic analysis. The effective length, KL, is used to calculate the nominal compressive strength, P_n, through LRFD column strength curve (empirical) that accounts for initial member out-of-straightness and spread of plasticity (including the effects of residual stresses). The nominal compressive strength, P_n, is then combined with the nominal flexural strength, M_n, and second-order elastic axial force and moment (P_{r2} and M_{r2}), in the beam-column interaction equations. The beam-column interaction equations are determined by

$$\frac{P_{r2}}{\phi_c P_n} + \frac{8}{9}\frac{M_{r2}}{\phi_b M_n} \leq 1 \qquad \text{for } \frac{P_{r2}}{\phi_c P_n} \geq 0.2 \tag{2.2}$$

$$\frac{P_{r2}}{2\,\phi_c P_n} + \frac{M_{r2}}{\phi_b M_n} \leq 1 \qquad \text{for } \frac{P_{r2}}{\phi_c P_n} < 0.2 \tag{2.3}$$

where ϕ_c is resistance factor for compression and ϕ_b for bending; $\phi_c = \phi_b = 0.9$.

2.3.2.2 Calculation of the effective length factor K.

Over the past decades, a wide range of methods for determining the effective length K, ranging from simple solutions of idealized columns, to complicated solutions for frames with various loading and boundary conditions, has been proposed, such as the alignment chart approach (Kavanagh, 1962; Wood, 1974; Johnston, 1976), the storey buckling approach (LeMessurier, 1977) the system buckling approach (Ziemian, 1990; Liew et al.,1991), and the unified approach (White and Hajjar, 1997).

For practical design, the most commonly used method of calculating K is through the alignment charts (Kavanagh, 1962), as shown in Fig.2.4 for sway-restrained frames and Fig.2.5 for sway-permitted frames.

where

$$G = \frac{\sum(E_{col}I_{col}/L_{col})}{\sum(E_g I_g/L_g)} = \frac{\sum(EI/L)_{col}}{\sum(EI/L)_g} \tag{2.4}$$

The subscripts A and B represents the joints at the ends of the column being considered. The subscripts Col and g refer to the column and girder, respectively. E, I, and L are the elastic modulus, moment of inertia, and unsupported length.

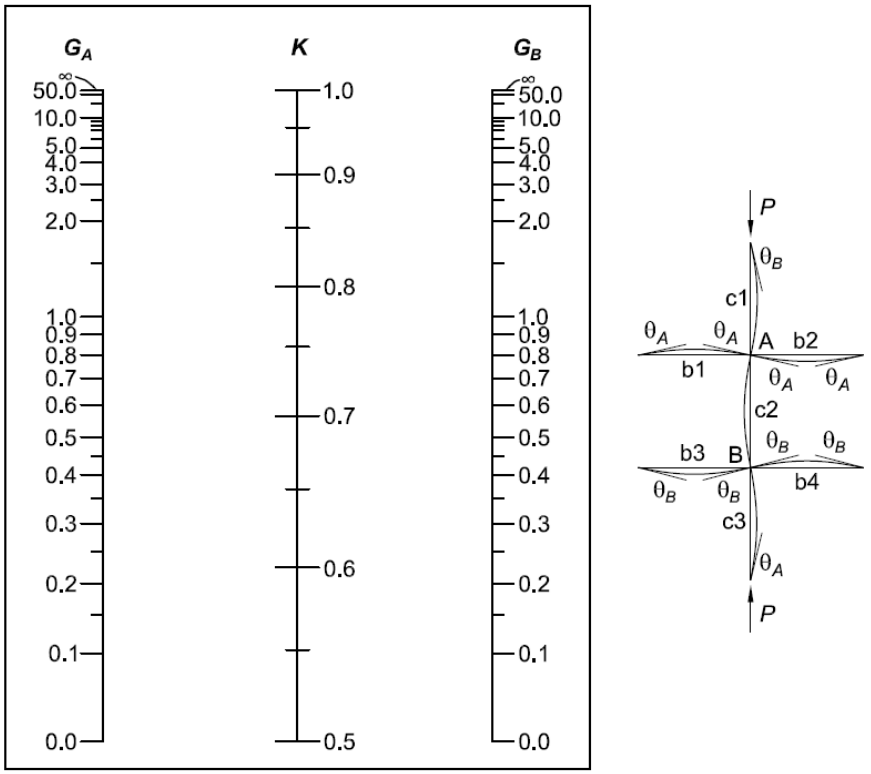

Fig. 2.4. Alignment chart—sway-restrained (braced frame).

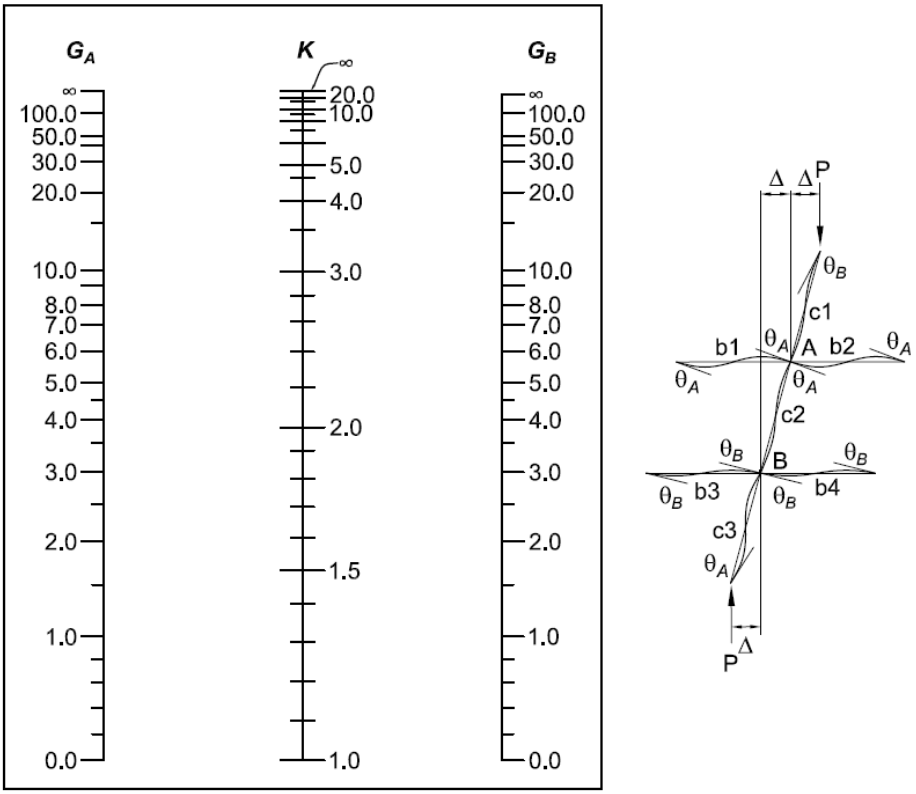

Fig.2.5. Alignment chart—sway-permitted (moment frame).

The alignment charts are developed based on the following assumptions, which are idealized and hardly satisfied in practical conditions.

(1) Behavior is purely elastic.

(2) All members have constant cross section.

(3) All joints are rigid.

(4) For sway-restrained frames, rotations at opposite end of beams are equal in magnitude, producing single curvature

(5) For sway-permitted frames, rotations at opposite ends of the restraining beams are equal in magnitude, producing reverse-curvature bending.

(6) The stiffness parameter of all columns is equal.

(7) Joint restraint is distributed to the column above and below the joint in proportion to I/L of the two columns.

(8) All columns buckle simultaneously.

(9) No significant axial compression force exists in the girders.

(10) Shear deformations are neglected.

For the calculation of K factor, AISC 360-16 (2016) additionally states that:

(1) For braced frames, the effective length factor, K, of components of the braced frame is normally taken as 1.0, unless a smaller value is justified by structural analysis.

(2) For moment frames, which rely primarily on the flexural stiffness of the connected beams and columns for stability, when $\Delta_{2nd\text{-}order}/\Delta_{1st\text{-}order}$ or $B_2 \leqslant 1.1$, it is permitted to use K = 1.0 in the design of all the columns in the storey. The study of White and Hajjar (1997a) showed that the simplification for stiffer structures results in a 6% maximum error in the in-plane beam-column strength checks)

2.3.3 Approximate second-order elastic analysis method (ASOM)

Approximate second-order elastic analysis (ASOM) is essentially amplified first order analysis. Different to explicit second order analysis, the approximate second-order elastic analysis apply amplification factors (B_1 and B_2) to first-order analysis results. It provides an approximate procedure to account for second-order effects in structures by amplifying the internal forces and moments determined by two first-order elastic

analyses, as expressed by

$$M_{r2} = B_1 M_{nt} + B_2 M_{lt} \quad (2.5)$$

$$P_{r2} = P_{nt} + B_2 P_{lt} \quad (2.6)$$

where M_{r2} and P_{r2} are second order internal axial force and moment, respectively. $B_1$is the multiplier factor accounts for P-δ effects, B_1 should be taken as 1.0 for members not subject to compression; B_2 accounts for P-Δ effects (P-δ effects on the overall response are indirectly considered through a factor R_M, (LeMessurier, 1977). B_2 is determined by an entire storey; M_{nt} and M_{lt} are first order internal moment in sway-restrained (no lateral translation) frames and sway-permitted frames (with lateral translation), respectively. P_{nt} and P_{lt} are first order internal axial force in sway-restrained frames and sway-permitted frames, respectively.

The main approximation in this technique is that it evaluates P-Δ and P-δ effects separately, through the two separate multipliers, B_2 and B_1, respectively. B_2 is applied to all members, while B_1 is only applied to compression members. To meet equilibrium requirement, other members at the joint should be multiplied by the same B_1 or the largest B_1 if there are more than one compression members at the joint. AISC 360-16 (2016) suggests that a more rigorous second-order elastic analysis should be performed if B_1 is larger than 1.2 in members that have a significant effect on the response of the overall structure.

It should be mentioned that B_1 and B_2 are used for developing the approximate expression of stainless steel beam-column stiffness reduction factor. Details on the determination of the two factors are shown in Chapter 5 of the thesis.

An illustration of amplifying first order moment for a sway permitted frame is shown in Fig.2.6. Although second order moments caused by P-δ or P-Δ effects may have different distribution to first order elastic moments (LeMessurier, 1977; Kanchanalai and Lu, 1979), one should keep in mind that member sizes are governed by the value of the maximum moment rather than the location of the maximum moment in practical design. Note that when performing a general second-order analysis, superposition of basic load cases is not appropriate since the second order effects are nonlinear

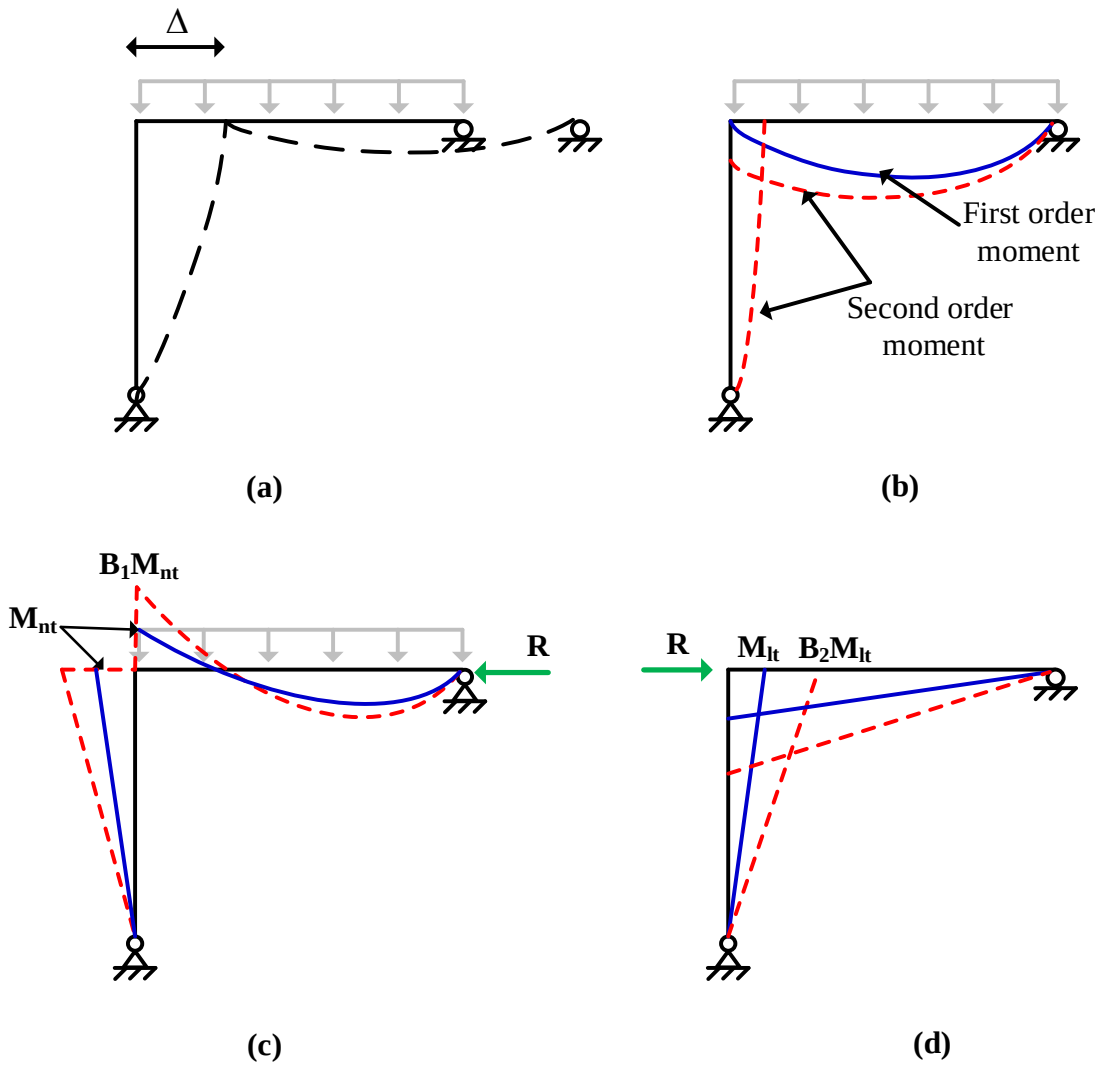

Fig.2.6 (a) Deflected shape (b) Actual bending moments (c) Moment amplification accounts for P-δ effects (d) Moment amplification accounts for P-Δ effects.

2.3.4 Comparison of DM, ELM and Approximate SOM

A comparison of DM, ELM and amplified first order analysis is shown in Table .2.1.

Note that for in-plane instabilities, the influence of geometric imperfections, partial yielding, and residual stresses are either (1) implicitly accounted for by using a column strength curve that is based on effective lengths in the AISC beam-column interaction equation or (2) explicitly accounted for by use of the direct analysis with column strength based on actual member length.

Table 2.1 Analysis method for ultimate limit state design checks provided in AISC 360-16

	DM	ELM	ASOM
Limitation	None	$\Delta_{2nd}/\Delta_{1st}$ (or B_2) $\leq$1.5 (for all stories)	$B_1 \leq 1.2$
Analysis to determine internal force and moment	Second order	Second order	First order
P-Δ effects	Structural analysis	Structural analysis	Amplification factor B_2
P-δ effects	Structural analysis	Member buckling resistance check with K>1(for P_n)	Amplification factor B_1
Initial out-of-plumbness	Notional load 0.002Yi or modelling directly	(1) K>1 (for P_n) (2)Notional load: for gravity-only load cases, 0.002Yi ; for other cases：not considered	K>1 (for P_n)
Initial out-of-straightness	Member buckling resistance check with K=1 (for P_n)	Member buckling resistance check with K>1 (for P_n)	Member buckling resistance check with K>1
Spread of plasticity (including residual stresses)	Reduced stiffness: 0.8EA and $0.8\tau_b$EI	K>1 (for P_n)	K>1 (for P_n)
Note:	(1) τ_b = 1.0 is permissible in all members if additional notional loads of 0.001Yi are applied. (2) Reduction of $0.8\tau_b$EI and 0.8EA to all members is recommended.	(1) For ELM provided in AISC, structural analysis commonly captures only P-Δ effects (2) Design using K = 1.0 is recommended, when K < 1.0 for columns in braced frames, or Δ2nd/Δ1st ≤1.1	B1 ≤1.2 is limited to compression members that have a significant influence on the response of the overall structure

The accuracy of ELM and Approximate second-order elastic analysis (ASOM) highly depend on K factors. For simple frames, K factors are easily calculated and thus effective length method or amplified first order analysis method may be a convenient tool for stability design. However, for most structures, the calculation of K factors is not straightforward, and even tedious. Therefore, the direct analysis method, is more efficient for the stability design of frames.

2.4 Methodologies for evaluating frame stability provided in and EN 1993-1-1:2015(E)

EN 1993-1-1 (2015 E), which is the next generation of EN 1993-1-1(2005), provides 6 methods of analysis for ultimate limit design checks of separated members, as summarized in Table. 2.2. The 6 methods, M0, M1, M2, M3, M4, and M5, are from less complex to more complex based on the type of second order effects and imperfections (including initial geometric imperfections and residual stresses) considered in global analysis. According to the global analysis types, second order effects (P-Δ and P-δ effects) are considered by:

- Entirely in the global analysis
- Partially by member buckling resistance checks and partially in the global analysis.

Table. 2.2 Analysis method for ultimate limit state design checks provided in EN 1993-1-1 (2015 E)

	M0	M1	M2	M3	M4	M5
Analysis to determine internal force and moment	First order	First order	First order	Second order	Second order	Second order
P-Δ effects	Neglected	Neglected	Neglected	Considered	Considered	Considered
P-δ effects	Neglected	Neglected	Considered	Considered	Considered	Considered
Initial out-of-plumbness	No need	No need	Considered	Considered	Considered	Considered
Initial out-of-straightness	No need	No need	Neglected	Neglected	Considered	Considered
Cross-sectional resistance check	Required	Required	Required	Required	Required	Required
Member buckling resistance check	No need	Out-of-plane	In-plane (K=1) and out-of-plane	In-plane (K=1) and out-of-plane	Out-of-plane	No need
Note:	(1) Geometric imperfections and residual stresses can be taken into account by equivalent geometric imperfections (2) Torsional effects are considered in M5					

The imperfections adopted in EN 1993-1-1 (2015 E) are the equivalent imperfections for some methods. For in-plane stability design, if the increase of internal forces and moments due to P-Δ effects is no more than 10% of the original internal forces and moments, first order analysis can be used for the determination of the internal forces and moments. This condition may be fulfilled if the second order sway effect factor

$\alpha_{cr,sw}$ is equal to or larger than 10. $\alpha_{cr,sw}$ is the ratio of $F_{cr,sw}/F_{Ed}$, where $F_{cr,sw}$ is the elastic critical flexural buckling load for a global sway buckling mode; F_{Ed} is the design load on the structure.

2.5 Comparison of the provisions in AISC 360-16 and EN 1993-1-1:2015(E)

Both EN 1993-1-1 (2015E) and AISC 360-16 (2016) rely on using global elastic analysis in conjunction with interaction equations to confirm frame and beam-column stability. Besides, they are similar in several key ways:

- The ultimate state is limited to the appearance of first plastic-hinge.
- Initial geometric imperfections are accounted for either by explicitly including them in the analysis model or by the use of equivalent notional loads;
- Resistance checks is on separated member-level through the use of interaction equations.

There are major differences in the two standards for frame stability and beam-column strength assessment, including:

- The resistance factors or partial safety factors for actions and resistances
- Column buckling strength curves, and beam buckling strength curves
- Whether or not stiffness reduction factors are used
- The number and shape of the interaction curves used for beam-column

For these difference, special focus is given on the interaction curves. AISC 360-16 (2016) employs a single interaction curve for or all types of cross sections, where cross sectional and member strength are not separate phenomena, since all beam-columns of finite length fail by some combination of inelastic bending and stability effects. The curve defines the lower-bound for compact wide-flange stub-columns bent about their major axis, and it is conservative for minor-axis bending. EN 1993-1-1 (2015E) provides separate interaction curves for cross-section strength, member in-plane buckling, and member lateral-torsional buckling. Based on classification of cross sections, different shape of interaction curves are used.

Beyond the differences listed above, there are many additional differences in the provisions of the two standards. Detailed comparisons of assessment of beam-column strength and frame stability are provided in Ziemian (2010), White and Clarke (1997a,1997b), Chen and Kim (1997), and Chen (1992, 2000).

2.6 Stainless steel design standards

Current stainless steel design standards, such as EN 1993-1-4 (2015), SEI/ASCE 8-02 (2002), and AS/NZS 4673 (2001), are developed based on assumed analogies with carbon steel behavior, with modifications made where necessary to fit in with test results. None of them allows the benefit of strain-hardening. A brief overview of the provisions for the stability design of frame systems and member buckling strength checks, given in these stainless steel design standards, are presented in this section. This overview is not intended to provide an in-depth explanation of the provisions, such as grades and mechanical properties covered by the each standard.

2.6.1 Frame stability

EN 1993-1-4 (2015) states that the provisions for structural analysis given in EN 1993-1-1 (2005) should be applied for stainless steels, with the exception that, plastic global analysis is not allowed unless there is sufficient experimental evidence to ensure that the assumptions made in the calculations are representative of the actual behavior of the structure. SEI/ASCE 8-02 (2002) and AS/NZS 4673 (2001) do not cover the design of frame systems. The two specifications apply to stainless steel structural members used for load-carrying purposes in buildings and other structures.

2.6.2 Member buckling resistance

EN 1993-1-4 (2015) provides similar formulations to EN 1993-1-1 (2005). The buckling curves (flexural, torsional, flexural-torsional buckling) of stainless steel columns, lateral-torsional buckling curves of stainless steel beams are essentially same to those of carbon steel, where slight differences exist in the selection of the imperfection parameter α and the limiting slenderness $\bar{\lambda}_0$. The two factors, α and $\bar{\lambda}_0$, effectively define the buckling curves' shape.

SEI/ASCE 8-02 (2002) provisions for the design of stainless steel members mainly follow the recommendations for carbon steel provided in AISI Specification (1986) for the design of cold-formed steel structural members. To take into account the nonlinear stress–strain behavior (determined by the Ramberg–Osgood expression), the tangent modulus is used to replace the initial elastic modulus in the buckling formulations. AS/NZS 4673 (2001) adopts the recommendations by SEI/ASCE 8-02 (2002) for the determination of the buckling strength of members. It also gives an additional method similar to the Europe

buckling curve approach for the design of columns.

2.6.2.1 Buckling strength of columns

(1) EN 1993-1-4 (2015)

In accordance with EN 1993-1-1 (2005), the flexural, torsional, and flexural-torsional buckling curves of stainless steel columns, are based on the Perry-Robertson buckling curves. Compared to carbon steel, different imperfection parameter α and the limiting slenderness $\bar{\lambda}_0$ for stainless steel is used, to account for the differences in mechanical properties and amplitudes of residual stresses.

(2) SEI/ASCE 8-02 (2002)

For doubly symmetric sections, closed cross-sections and any other sections that can be shown not to subject to torsional or flexural-torsional buckling, the flexural buckling stress (f_n) is determined by

$$f_n = \frac{\pi^2 E_t}{(KL/r)^2} \leq f_y \tag{2.7}$$

Where E_t is the tangent modulus in compression corresponding to the buckling stress; K is the effective length factor; L is the unbraced length of the member; r is the radius of gyration of the full, unreduced cross-section.

(3) AS/NZS 4673 (2001)

AS/NZS 4673 (2001) adopts the approach in SEI/ASCE 8-02 (2002), but additionally provides column buckling curves based on Perry-Robertson approach.

2.6.2.2 Lateral torsional buckling strength of unrestrained beams

(1) EN 1993-1-4 (2015)

Lateral torsional buckling curves for unrestrained beams bending about the major axis, provided in EN 1993-1-4 (2015), are based on the Perry-Robertson buckling curves, with different values of imperfection parameter α and the limiting slenderness $\bar{\lambda}_0$ to those applicable for flexural buckling.

(2) SEI/ASCE 8-02 (2002)

In ASCE 8-02 (2002), the lateral torsional buckling strength of unrestrained beams is calculated directly

from the expression for the elastic critical moment (for lateral torsional buckling). To account for the non-linear behavior of stainless steel in the inelastic stress range, the initial elastic modulus and initial shear modulus are replaced by the tangent modulus and tangent shear modulus.

(3) AS/NZS 4673 (2001)

AS/NZS 4673 (2001) adopts the approach in ASCE 8-02 (2002).

2.6.2.3 Interaction equation for beam-columns

(1) EN 1993-1-4 (2015)

EN 1993-1-4 (2015) adopts the approach taken for carbon steel in EN 1993-1-1 (2005). For in-plane beam-columns under bending and axial compression, the interaction equation provided is given by

$$\frac{N_{Ed}}{N_{b,Rd}} + \mathrm{k}\frac{M_{Ed}}{\frac{M_{b,Rd}}{\gamma_{M1}}} \leq 1 \tag{2.8}$$

N_{Ed} and M_{Ed} are the required axial force and moment (first order), respectively. $N_{b,Rd}$, and $M_{b,Rd}$ are column buckling resistance and beam bending resistance, respectively. γ_{M1} is partial factor, and γ_{M1}=1.1 is recommended.

The interaction factor k is determined by

$$1.2 \leq k = 1 + 2(\bar{\lambda} - 0.5)\frac{N_{Ed}}{N_{b,Rd}} \tag{2.9}$$

(2) SEI/ASCE 8-02 (2002)

SEI/ASCE 8-02 (2002) adopts the interaction equation in AISI Specification (1986) without modification. The AISI (1986) equation, given by Eq.(2.5) and (2.6), is based on the interaction equation recommended in the 1961 AISC specification (AISC,1961).

When $\frac{P_u}{\phi_c P_n} > 0.15$ $\qquad \frac{P_u}{\phi_c P_n} + \left(\frac{C_m}{1-\frac{P_u}{P_E}}\right)\frac{M_u}{\phi_b M_n} \leq 1$ (2.10)

When $\frac{P_u}{\phi_c P_n} \leq 0.15$ $\qquad \frac{P_u}{\phi_c P_n} + \frac{M_u}{\phi_b M_n} \leq 1$ (2.11)

The term $\frac{C_m}{1-\frac{P_u}{P_E}}$ accounts for P-δ effects together with the benefit of moment gradient. P_u and M_u are

required axial force and moment (first order), respectively. The resistance factor ϕ_c =0.85 for columns, ϕ_c =0.9 for beams. In the interaction equations, P-Δ effects are not accommodated.

(3) AS/NZS 4673 (2001)

AS/NZS 4673 (2001) adopts the approach in ASCE 8-02 (2002).

2.7 Consideration of material properties, geometric imperfections and residual stresses for frame stability design

2.7.1 Material properties

2.7.1.1 Stress-strain behavior of material

The most important difference between stainless and carbon steels is in the shape of the stress-strain curve. Carbon steel typically exhibits linear elastic behavior up to the yield stress and a plateau before strain hardening is encountered, while stainless steel has a more rounded response with no well-defined yield stress, as shown in Fig.2.7.

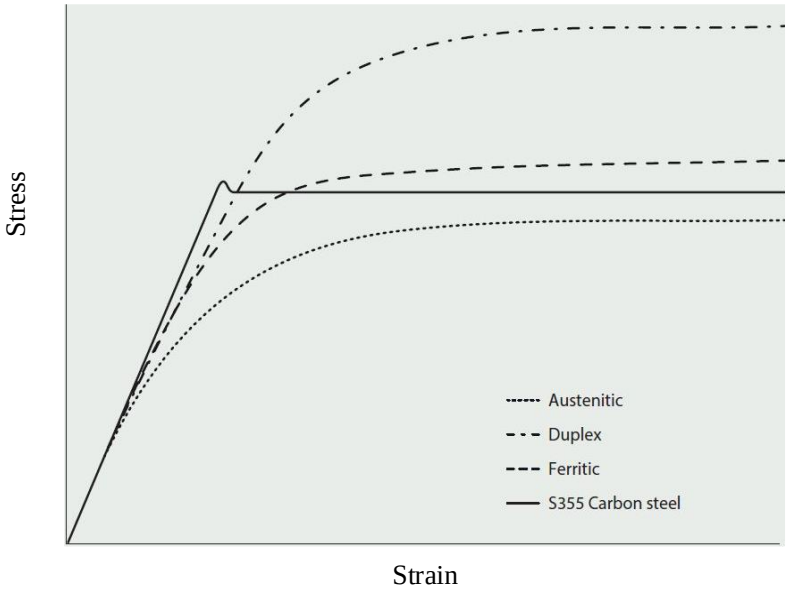

Fig.2.7 Stress-strain curves for stainless steel and carbon steel (Design Manual for Structural Stainless steel (2017))

For design and numerical simulation, many stress-strain models, based on the equation originally proposed

Ramberg and Osgood (1943) and modified by Hill (1944), have been developed. Mirambell and Real (2000) proposed a two-stage model based on the Ramberg-Osgood expression. In this proposed model, the basic Ramberg–Osgood expression was adopted up to the 0.2% proof stress. Beyond the 0.2% proof stress and up to ultimate stress, a second Ramberg–Osgood curve was used. Further work on this two-stage model was conducted by Rasmussen (2003) where the additional parameters required by the two-stage model were described. Gardner and Nethercot (2004) suggested that 1% proof stress should be used to replace the ultimate stress for the Mirambell-Real model. The accuracy of the modified model at low strains (less than approximately 10%) is improved and the modified model is applicable to describe the compressive stress-strain behavior. In addition, a comprehensive description of available stress-strain curves for stainless steels was reported by Arrayago te al. (2015).

2.7.1.2 Influence of the non-linear stress-strain response

Depending on the type of the structural element or system, the round nonlinear stress-strain behavior can lead to either a reduced or enhanced capacity compared to an equivalent component with idealized elastic-perfectly plastic stress-strain behavior.

(1) Frame systems

For stability governed frame systems, the early onset of stiffness degradation, which results in more deformation and in turn increased second order effects, may lead to reduced capacity.

(2) Members

For stainless steel members (columns and unrestrained beams)**,** their buckling behavior is broadly similar to that of carbon steel, even though stainless steels exhibit considerable nonlinear stress-strain behavior. The influence of the nonlinear stress-strain behavior on the ultimate strength (or stiffness) of a stainless steel member relies on the stress level in the member (Baddoo, 2013; Baddoo and Francis, 2014). Take columns for example, this can be explained in terms of slenderness:

(a) If the columns have very high slenderness (cross-sectional slenderness (λ_l) or member slenderness (λ_c)) so that they fail in the linear part of the stress-strain curve, the capacity of the columns are governed by the critical elastic local buckling strength or critical elastic global buckling strength. In this case, there may be little difference in the strength (stiffness) between the stainless steel and carbon steel columns, provided

that they have same initial geometric imperfections and residual stresses.

(b) For columns which have intermediate slenderness, the average stress lies in the range between proportional limit and 0.2% proof strength. The ultimate strength (stiffness) of stainless steel columns is lower than similar carbon steel columns, since stainless steel is softer than carbon steel in this stress-strain range.

(c) If the columns have relatively lower slenderness so that the average stress of the columns can exceed 0.2% proof strength, the ultimate strength (stiffness) of the stainless steel columns are expected to be higher than the similar carbon steel columns, due to the benefit of strain-hardening.

2.7.2 Initial geometric imperfections

Initial geometric imperfections of frame structures refer to member out-of-straightness (δ_0/L, member lever), out-of-plumbness (Δ_0/h, storey and frame level), and localized imperfection (ω_0, cross-sectional and member lever). Out-of-straightness and out-of-plumbness are resulted from fabrication and erection process. Localized imperfection is complicated and has sufficient variability. For cold-formed box sections, localized imperfection is mainly induced by cold forming process. The illustration of out-of-plumbness (storey-level) and out-of-straightness is shown in Fig.2.8.

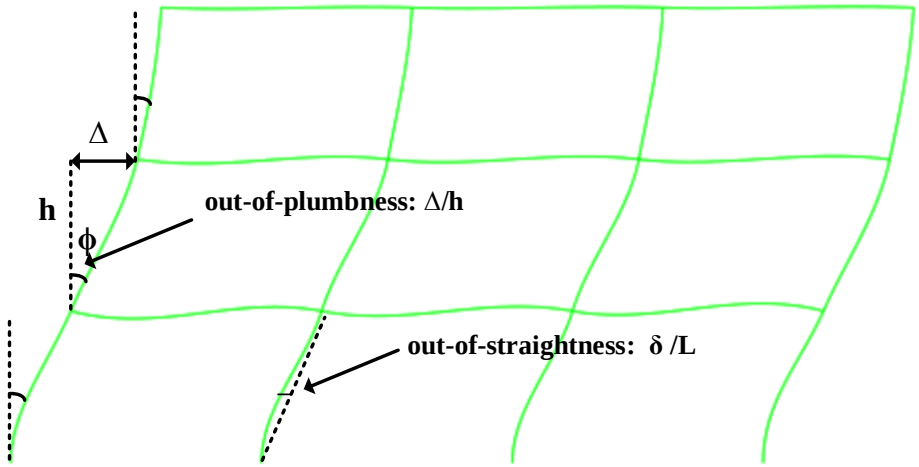

Fig.2.8 Illustration of out-of-plumbness (storey-level) and out-of-straightness

2.7.2.1 Out-of-plumbness and out-of-straightness

Out-of-straightness and out-of-plumbness of structures are commonly caused by the following factors

(Ziemian, 2010) :

(1) Actual column piece lengths and splice locations.

(2) Beam length and connection fit-up tolerances.

(3) Finite member size effects.

(4) Unavoidable eccentricities at foundations.

(5) Three-dimensional geometry.

(6) Imperfect load placement.

In the absence of more accurate information, the maximum allowable fabrication and erection tolerances specified in relevant design codes and specifications can be a reference for modelling geometric imperfections. The limits of out-of-straightness and out-of-plumbness specified in AISC 303-16 (2016): Code of Standard Practice for Steel Buildings and Bridges are:

- Member out-of-straightness: δ_0 /L < 1/1000, where L is the distance between brace points.
- Story out-of-plumbness: Δ_0/h < 1/500, where h is the story height.
- Maximum lack of verticality : the maximum value of Δ_0 should be less than 25 mm below the 20th floor, and less than 50 mm above the 20th floor.

EN1993-1-1: 2015(E) provides a specific formulation to determine the value of initial out-of-plumbness ($\phi=\Delta/h_{\text{-total}}$; $h_{\text{-total}}$ is the total height of the frame) that should be considered in the global analysis. The ϕ provided in EN1993-1-1: 2015(E) is based on the two reduction factors provided in ECCS (1984). ϕ is determined by

$$\phi = \phi_0 \alpha_h \alpha_m \tag{2.12}$$

where ϕ_0 is the basic value; ϕ_0 =1/400 for verification of elastic resistance; ϕ_0 =1/200 for verification of plastic resistance.

The two reduction factors, α_h and α_m, given by Eq.(2.13) and (2.14), are based on the number of columns in a story and the number of stories in the building (ECCS,1984).

$$\alpha_h = \frac{2}{\sqrt{h}} \qquad \text{but } \alpha_h \leq 1.0 \tag{2.13}$$

$$\alpha_m = \sqrt{0.5\left(1 + \frac{1}{m}\right)} \tag{2.14}$$

where h is the height of the structure in meters; m is the number of columns in a row including only those columns which carry a vertical load not less than 50% of the average value of all the columns in the vertical plane considered.

Note that the initial sway imperfection ϕ provided in this design code is uniform sway imperfection over the entire height of the frame, which is different isolated storey-level sway imperfection, as shown in Fig. 2.9. However, the study of Bridge and Bizzanelli (1987) showed that the imperfection values have no correlation to the number of columns in a story. Bridge and Bizzanelli's study is based on statistical data of actual imperfections of present in a 47 story office building. The conclusion is contradictory to the ECCS (1991) provisions.

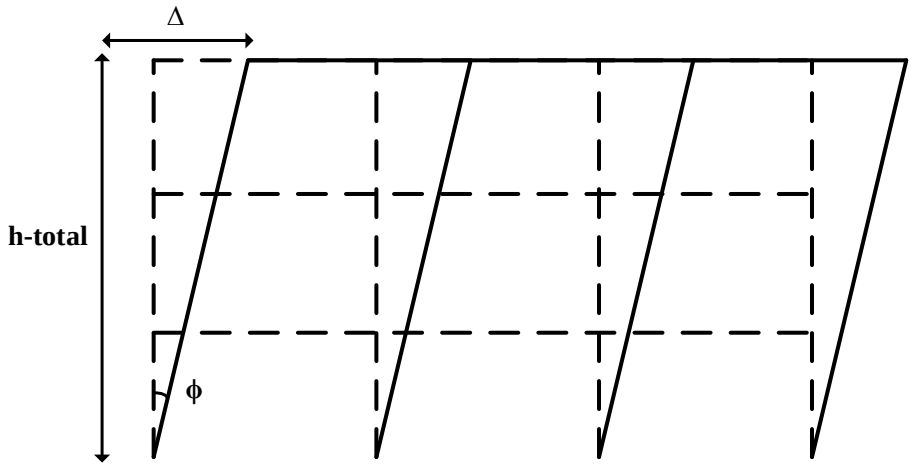

Fig.2.9 Uniform sway imperfection (frame-level)

According to the report of Clarke and Bridge (1992, 1996), using a uniform out-of-plumbness that equals to the maximum out-of-plumbness over the entire height of the frame, are generally conservative. Nevertheless, this method may be adopted in the design of taller buildings, for the purpose of simplicity in design. Clarke and Bridge (1996) indicates that, for multistory frames that are not extremely slender, assuming a uniform out-of-plumbness of 1/500 over the entire height of the frame is reasonable and not overtly conservative. For slender frames, a more accurate strategy is needed since a uniform out-of-plumbness applied over the height of the frame may generate unrealistically large overturning effects near the base of the frame.

The sensitivity of frames to imperfections cannot easily be correlated to a single parameter. It is not hard to identify frames for which imperfections can be neglected. Ziemian (2010) suggests that out-of-plumbness

should be accounted for in the global stability analysis for all frames subjected to gravity loads. The consideration of member out-of-straightness depends on:

- whether separated member buckling strength checks are conducted
- whether the member out-of-straightness has a considerable influence on the structural behavior of the frame.

Currently, member buckling strength checks are required in almost all the design codes and specifications. Thus, member out-of-straightness is not need to be included in the global analysis. If member buckling strength checks are not conducted, initial out-of-straightness should be taken into account unless its influence on the structural behavior of the frame can be neglected. The effect of out-of-straightness on frame behavior is based on:

- the relative magnitude of axial force and primary bending moment levels.
- whether the primary bending moments cause single or reverse curvature bending.
- the slenderness of the member.

Liew (1992) used the ratio of P_u/P_{e1} to evaluate the influence of member out-of-straightness, where P_u is the design value of compression load; P_{e1} is the critical buckling strength of the pinned member under compression (in-plane flexural buckling). Liew reported that effects due to member out-of-straightness are less than 5% for a wide range of section types when the ratio of P_u/P_{e1} is no more than 0.2. Later, White and Nukala (1997) suggest that a limit of $P_u/P_{e1} < 1/7$ is sufficient to restrict the reduction in strength due to out-of-straightness to less than 5%. EN1993-1-1: 2015(E) states that member out-of-straightness should be included in the global analysis for the frames that are sensitive to second order effects, where the following conditions are met: (1) at least one moment resistant joint at one member end, (2)$P_u/P_{e1} > 0.25$.

2.7.2.2 Localized imperfection

In practical situations, many economical cold-formed hollow sections, which comprise slender thin-walled elements, are sensitive to initial localized imperfection. Initial localized imperfection (ω) (shown in Fig.2.10) induced by rolling and fabrication process is inevitable. It has sufficient variability and has no

definitive characterization. The study of Wang et al. (2017) and Zhao et al. (2015, 2016) showed that both the shape and magnitude of ω varied randomly in longitudinal direction for cold-formed members with box section, as shown in Fig. 2.10 (a). The shape of ω in transverse direction (cross-sectional) was found to be convexity /concavity (Young and Lui, 2005; Lui et al., 2014), which can be modelled by a half-sine wave, as shown in Fig. 2.10(b). ω is typically modelled by local buckling mode (shown in Fig. 2.10(c)) obtained from linear perturbation buckle analysis. The local buckling mode gives idealized ω and neglects uncertainty in localized imperfection.

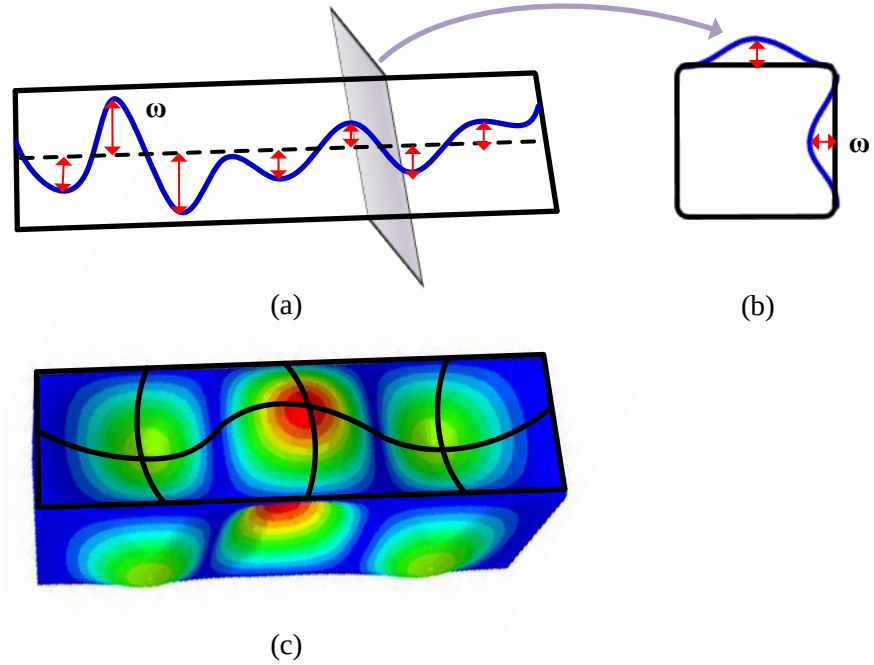

Fig. 2.10. Localized imperfection (ω): (a) Random ω along longitudinal centerline of the surface (b) ω in transverse direction (convexity /concavity) (c) Idealized ω obtained from Buckle Analysis

The distribution of ω in longitudinal direction for two tubes reported in (Zhao et al., 2016) are shown in Fig 2.11. It is observed that ω in longitudinal direction has a considerable variability and its characterization in a definite closed-form is not feasible.

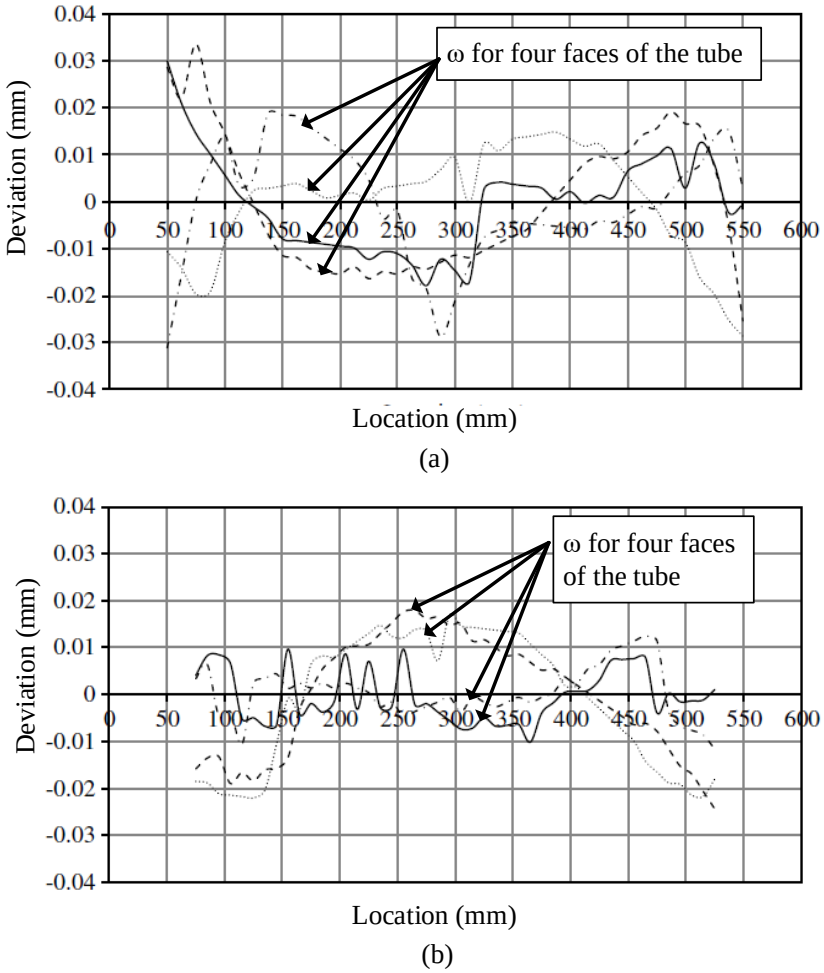

Fig 2.11. Distribution of ω in longitudinal direction for two tubes reported in (Zhao et al., 2016) (a) RHS 100 X 40 X 2 (b) SHS 60 X 60 X 3

Some standards provide the maximum allowable value of localized imperfection in transverse direction (EN 10219-2, 2019; JG/T 178, 2005). The tolerance for convexity /concavity of a cross-section specified in EN-10219-2 (2019) is min $\{\omega_{max}/b, 0.5mm\}$, where $\omega_{max}/b \leq 0.008$; b is the side (straight side of the cross-section) length; ω_{max} represents the maximum deviation from the straight side.

2.7.3 Residual stresses

Plastic deformation produced in cold-working process such as uncoiling, leveling, and rolling to form a section, results in residual stresses. Residual stresses of cold formed steel box sections comprise bending residual stresses, membrane residual stresses, and layer residual stresses (for the case of thick plates) (Key and Hancock,1993; Jandera and Gardner, 2008; Cruise and Gardner, 2008; Li et al., 2009; Tong et al., 2012; Ma et al., 2015; Somodi and Kövesdi, 2017). The distribution and magnitude of residual stresses of cold

formed stainless steel RHS and SHS were found to be comparable to those for cold formed carbon steel box sections, even though stainless steel shows different physical and thermal properties to carbon steel (Gardner and Cruise, 2009; Cruise and Gardner, 2008; Ma et al., 2015). A common conclusion from them is bending residual stresses (both longitudinal and transversal) in the corner area are smaller than those in the flat area. Bending residual were found significantly higher than membrane residual stresses in Key and Hancock (1993), Cruise and Gardner (2008) and Ma et al. (2015). Besides, for cold formed box sections comprised of thin steel plate, bending residual stresses typically vary linearly throughout the thickness while for those with thick steel plate, bending residual stresses throughout the thickness is nonlinear and there is a third component termed as layer residual stress (Key and Hancock, 1993; Gardner and Cruise, 2009; Liu et al., 2017).

The magnitude and distribution of tensile bending residual stresses in the out surface of cold formed stainless steel sections reported by Gardner and Cruise (2009) is shown in Fig.2.12. It can be seen that bending residual stresses are around 30% to 70% of the 0.2% proof stress (f_y), which is close to the proportional limit of stainless steels ($0.4f_y$ to $0.7f_y$) stated in Design Manual for Structural Stainless steel (2017). Characteristic values (representing the 95th percentile values based on a normal distribution) of bending residual stresses are $0.63f_y$ in the flat regions of the section and $0.37f_y$ in the corner regions. The bending residual stress pattern suggested in Gardner and Cruise (2009) is shown in Fig. 2.13, in which a rectangular block through thickness distribution is assumed.

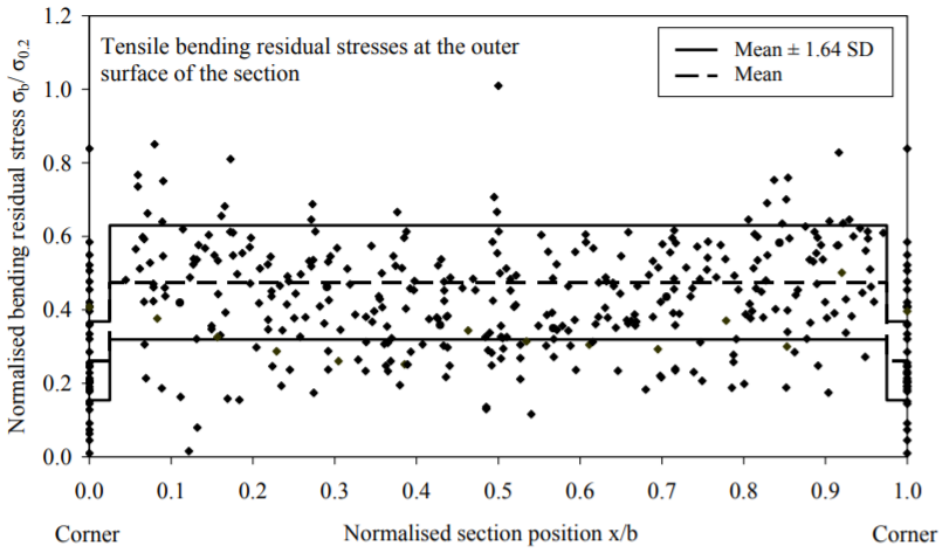

Fig.2.12. Normalized bending residual stresses in cold rolled boxes (Gardner and Cruise, 2009)

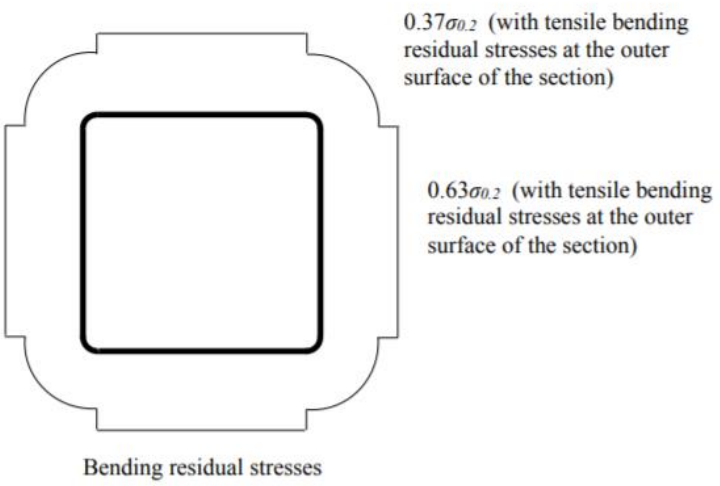

Fig 2.13. Bending residual stress pattern suggested in Gardner and Cruise (2009)

3. Numerical models and validation

3.1 Introduction

This chapter describes the finite element (FE) modelling approach adopted in Chapter 4-6, to verify GNA coupled with stiffness reduction factor for the design of stainless steel elements and frames with compact cross-sections. Compact sections in the current paper, which are in accordance with Baddoo N (2013), refer to sections that are not prone to local buckling reductions. These sections effectively cover Class 1 and 2 in the Eurocodes 3. The FE models are developed using the general-purpose package ABAQUS 6.13 (2013), and validated against experimental results from the literature. FE modelling approach for verifying GNA coupled with stiffness reduction factor that accounts for local buckling is presented in Chapter 7. FE modelling approach for probabilistic studies is presented in Chapter 8. In Chapter 4-6, only beam elements were employed, while both shell and beam elements were employed in Chapter 7-8.

3.2 Finite element models

3.2.1 Elements

Abaqus offers a wide range of beam elements with solid, thin-walled closed and thin-walled open sections (Abaqus User Manual, 2013). Among all beam elements, Euler-Bernoulli-type beams and Timoshenko-type beams are available.

(1) Euler-Bernoulli beams do not allow for transverse shear deformation, and thus plane sections, which are initially normal to the beam's axis, remain plane (if there is no warping) and are normal to the beam axis. They are typically used to model slender beams.

(2) Timoshenko beams allow for transverse shear deformation. They are applicable to model deep as well as slender beams. For beams made of uniform material, shear flexible beam theory provides accurate results for cross-sectional dimensions up to 1/8 of typical axial distances. Abaqus assumes that the transverse shear behavior of Timoshenko beams is linear elastic with a fixed modulus.

In this study, the 2-node linear Timoshenko-type beam element (B21) is employed for in-plane members and frames with compact cross-sections. Local buckling and lateral torsional buckling are not need to be considered. RHS and SHS are modelled using box section with sharp corners. A B21 box section has 5

default Simpson integration points in the two walls of the section, as shown in Fig.3.1. There are no default integration points in the top and bottom wall of the B21 box section, nor user defined integration points are allowed in the two walls.

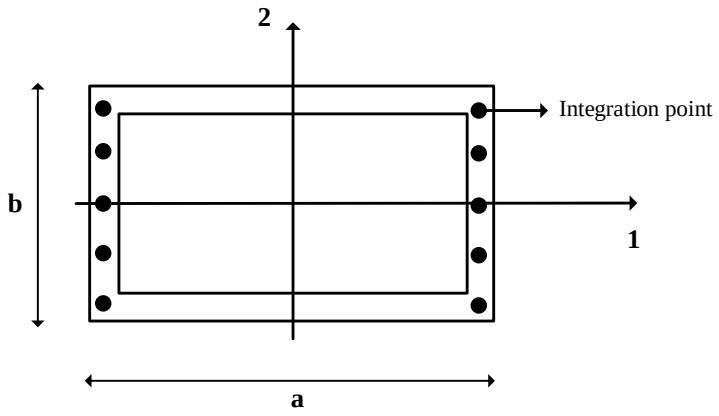

Fig.3.1 Default integration points in B21 box section

3.2.2 Iterative solution methods

In nonlinear analyses the total load applied in a step is broken into smaller increments so that the nonlinear solution path can be followed. At the end of each increment the structure is in (approximate) equilibrium. An iteration is an attempt at finding an equilibrium solution in an increment when solving with an implicit method. If the model is not in equilibrium at the end of the first iteration, further (second, third, ⋯) iterations will be conducted until the obtained solution is closer to equilibrium. Sometimes many iterations are needed to obtain an equilibrium solution. When an equilibrium solution has been obtained, the increment is complete.

ABAQUS/Standard (implicit solver) provides several numerical techniques to solve the nonlinear equilibrium equations:

- Load Control Newton-Raphson Method
- Displacement Control Method
- Arc-length Method

The load controlled Newton-Raphson method is the earliest method in this regard (Süli and Mayers, 2003). The conventional Newton-Raphson method (illustrated in Fig. 3.2(a)) updates the tangent stiffness matrix of the structure at each iteration, while the modified Newton-Raphson method (illustrated in Fig. 3.2(b)) only evaluates the stiffness relation at the start of the increment and the stiffness matrix is constant at each

iteration (within an increment). Both of the conventional and modified Newton-Raphson method fail near the limit point.

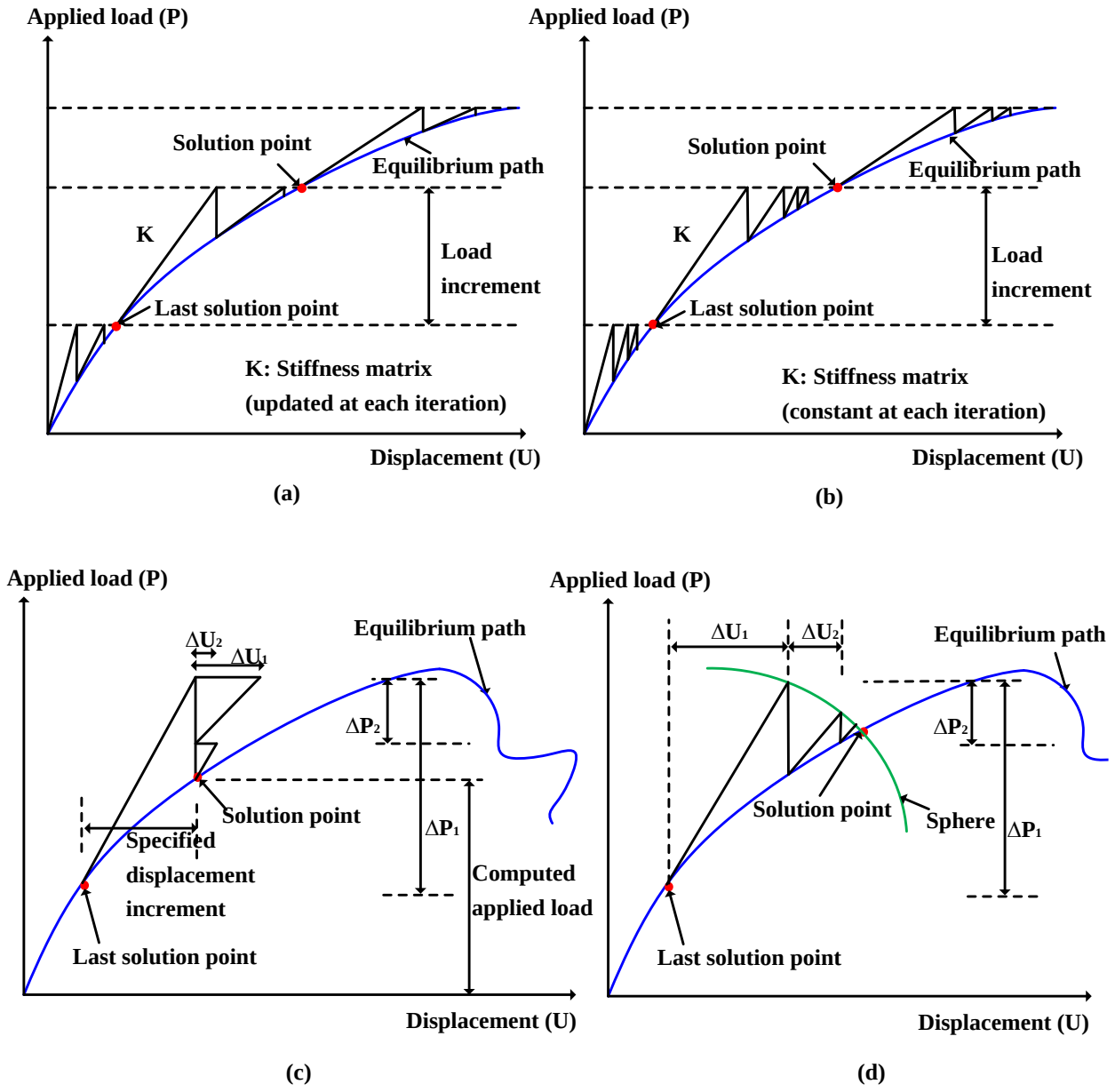

Fig .3.2 Numerical techniques for solving the nonlinear equilibrium equations (a) Conventional Newton-Raphson Method (b) Modified Newton-Raphson Method (c) Displacement Control Method (d) Arc-length Method

To overcome difficulties with limit points, Displacement Control Method (illustrated in Fig. 3.2(c)) was introduced (Argyris, 1965; Zienkiewicz, 1971; Sabir and Lock, 1972, Batoz and Dhatt, 1979). However, for structural systems exhibiting snap-through or snap-back behavior, this technique leads to error. To solve this problem and obtain a more general technique, the arc-length method (illustrated in Fig. 3.2(d)) for

structural analysis was developed by Wempner (1971), Riks (1972; 1979) and later modified by Ramm (1980).

In this study, Newton-Raphson method is adopted in first order elastic analysis and second order elastic analysis, where the applied load is known. The Arc-length Method is adopted in second order inelastic analysis, where the loading cases are proportional (unstable collapse and postbuckling analysis). ABAQUS/Standard, the Newton-Raphson method is available in *STATIC-GENERAL analysis type, while the arc-length method is available in *STATIC-RIKS analysis type.

3.2.3 Stress-strain curves

The material behavior of stainless steel is modelled based on the nonlinear two-stage stress-strain curve provided in EN 1993-1-4 (2015), given in Eq.(3.1) and (3.2) and shown in Fig.3.3, which is essentially the expression proposed by Ramberg-Osgood (1943).

$$\varepsilon = \frac{\sigma}{E} + 0.002\left(\frac{\sigma}{f_y}\right)^n \qquad \text{for } \sigma \le f_y \tag{3.1}$$

$$\varepsilon = 0.002 + \frac{f_y}{E} + \frac{\sigma - f_y}{E_y} + \varepsilon_u\left(\frac{\sigma - f_y}{f_u - f_y}\right)^m \qquad \text{for } f_y < \sigma \le f_u \tag{3.2}$$

where E is Young's Modulus; f_y is 0.2% proof stress; n is the first stage strain hardening exponent; E_y is the tangent modulus at the 0.2% proof stress; $E_y=E/(1+0.002nE/f_y)$; m is the second stage strain hardening exponent; ε_u is the ultimate strain; f_u is the ultimate stress.

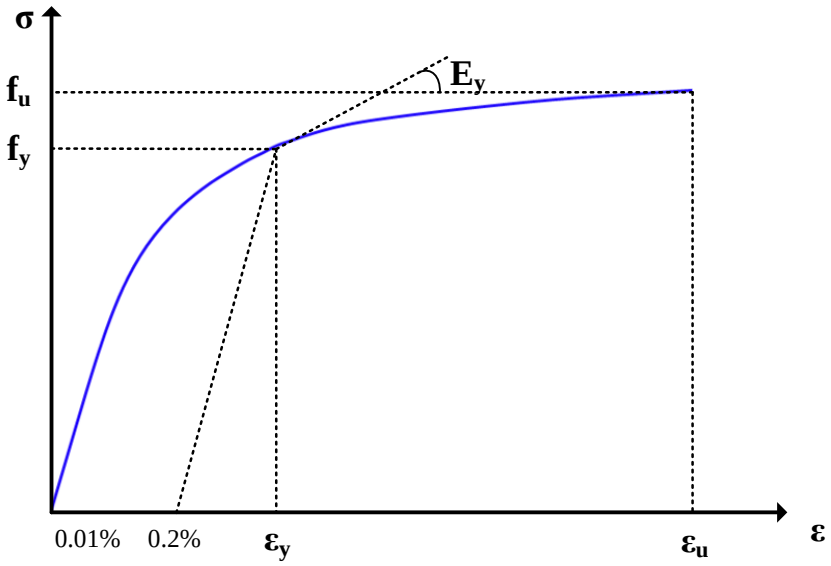

Fig.3.3 Stress-strain curve for stainless steel

The expression of the two-stage stress-strain curve involves three basic parameters (E, f_y, n) for $\sigma \leq f_y$ and three additional parameters (ε_u, f_u, m) for $\sigma > f_y$. The additional parameters can be determined in terms with E, f_y and n (Rasmussen,2003). Although the full stage Ramberg-Osgood curve was adopted in FE modeling, the ultimate strengths from FE analysis were limited to full plastic strength of the cross-section, and thus strain hardening that results in strengths greater than the full plastic strength of the cross-section is not considered in the study. Currently strain-hardening is not permitted to be considered in the stability design of stainless steel structures (EN 1993-1-4, 2015; ASCE 8-02, 2002; AS/NZS 4673, 2001), even though stainless steel has considerable strain-hardening behavior.

The weighted material property method proposed by Hradil and Talja (2013) is adopted to account for the enhanced material properties of the corner regions (including the extended area) in cold-formed stainless steel cross sections. In this method, the material parameters are weighted in accordance with the flat or corner area compared to the whole cross-section area, and the weighted average material properties are assigned to the whole cross-section. The study of Arrayago (2016) showed that the weighted average material property method provided excellent results for cold-formed stainless steel columns, beams, and beam-columns with cold formed RHS and SHS. For FE models described in this paper, the considered enhancement amplitude for yield strength and ultimate strength (if applicable) of the corner regions are based on the available test data reported in Arrayago (2016), Gardner and Nethercot (2004) and Afshan et al. (2013).

3.2.4 Modelling of initial geometric imperfections

Initial geometrical imperfections (out-of-plumbness and out-of-straightness) can be taken into account either by modifying them directly or by applying equivalent notional loads in combination with the gravity loads. It is generally acknowledged that geometrical imperfections should be modelled in the direction that produces the most destabilized effects.

In this study, both out-of-plumbness and out-of-straightness are considered for sway-permitted members and frames, while only out-of-straightness is considered for sway-restrained members and frames. In some studies, out-of-plumbness and out-of-straightness are treated as unified imperfection. The unified imperfection is typically modelled by means of introducing relevant buckling mode that obtained from Buckle Analysis. However, it is not straightforward to determine the amplitude of the unified imperfection,

since its shape is the combination of out-of-plumbness and out-of-straightness. In this study, the effects of out-of-plumbness and out-of-straightness are taken into account by applying horizontal notional loads. Out-of-plumbness is represented by concentrated notional loads and modelled in the direction of sway deformation. The notional loads are applied at all levels, as shown in Fig. 3.4. The magnitude (N_i) of the notional load is determined by

$$N_i = W_i \frac{\Delta_0}{h} \tag{3.3}$$

where *Wi* is gravity load applied at level *i*. The value of out-of-plumbness ($\frac{\Delta_0}{h}$) adopted in this study is the maximum allowable value 0.002 specified in AISC 303-16 (2016): Code of Standard Practice for Steel Buildings and Bridges.

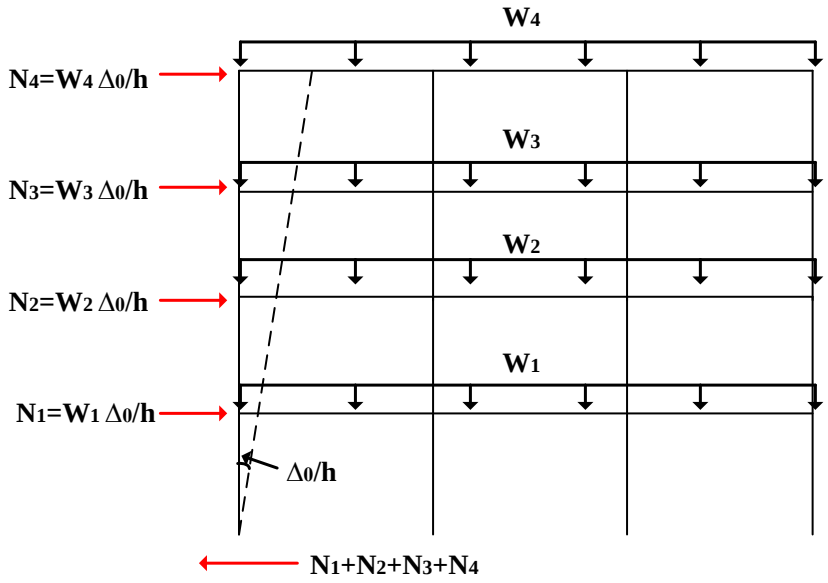

Fig. 3.4 Notional loads for modelling uniform out-of-plumbness over the height of the frame

To avoid additional shear force at the member or frame base due to notional loads, corresponding horizontal reaction forces, equal and opposite in direction to the sum of all notional loads, are applied.

Out-of-straightness is represented by concentrated notional loads and modelled in the direction that the members deforms in a preliminary Buckle Analysis through ABAQUS. Out-of-straightness could also be modelled using uniformly distributed loading instead of applying the concentrated load at the mid-height. Both modelling approaches should provide similar results. For the columns that have double curvatures, the concentrated notional loads are applied in the mostly deformed direction, as illustrated in Fig. 3.5.

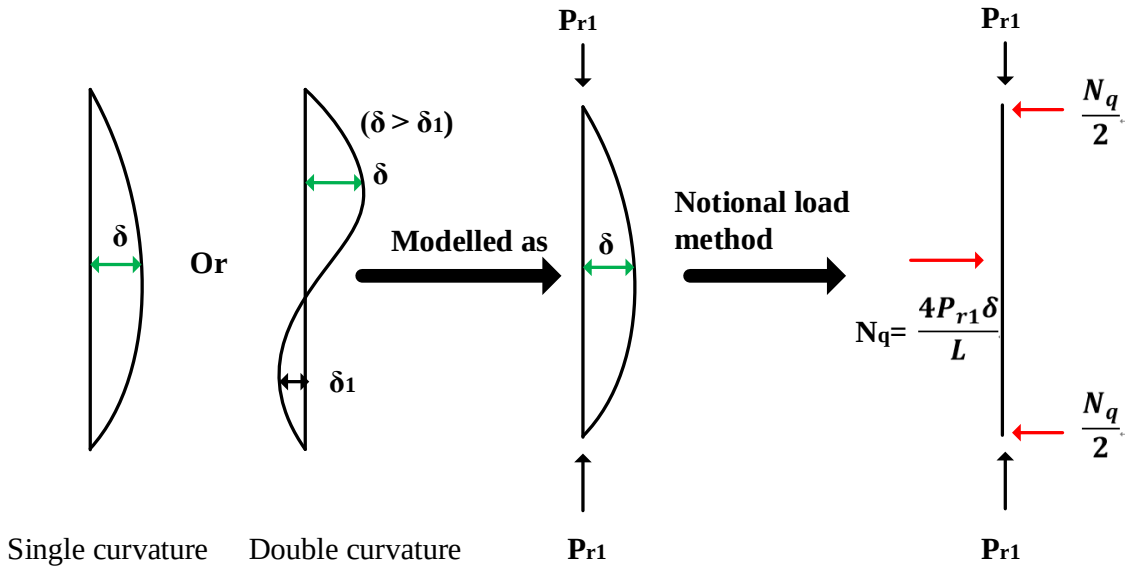

Fig. 3.5 Notional loads for modelling out-of-straightness of the member

The magnitude (N_q) of the notional load is determined by

$$N_q = \frac{4P_{r1}\delta}{L} \tag{3.4}$$

where P_{r1} is the maximum first order internal axial force within the member; L is the length between brace points; the adopted member out-of-straightness (δ/L) is 0.001.

Similarly, the horizontal reaction force of $\frac{N_q}{2}$ should be applied at both ends of the member to avoid additional fictitious shear forces.

3.2.5 Modelling of residual stresses

Due to the presence of residual stress, premature yielding may occur under external loading, and consequently loss of stiffness which results in a reduction in strength. The report of Jandera and Gardner (2008), Jandera and Machacek (2014) showed that for global behavior of stainless steel members with box sections, the effect of through-thickness longitudinal bending residual stresses is dominant and the effects of other residual stress components are negligible. Similar conclusion for carbon steel members with cold formed box sections has been reported in (Key and Hancock, 1993; Liu et al., 2017). Therefore, only longitudinal residual stresses are considered in this paper and they are accounted for by modifying the stress-strain curve. The procedure of modifying the stress-strain curve is in based on the study of Liu et al. (2017), and the amplitude of longitudinal residual stresses is based on the residual stress pattern for flat

zone of the cross section suggested in Gardner and Cruise (2009).

For shell elements, residual stresses are commonly incorporated into the FE models through integration points (using the SIGINI subroutine of ABAQUS). Nevertheless, residual stresses components considered here can not be introduced through integration points, since there is only one integration point through the thickness of beam element but the considered residual stresses varies linearly through the thickness of the section.

The modification of stress-strain curve is based on the assumption that the material properties of stainless satisfy von Mises yield criterion and Prandtl-Reuss flow rules.

According to von Mises yield criterion, for a plate in a plane stress state (shown in Fig. 3.6), yielding occurs when the equivalent stress (σ_{eq}) reaches the yield strength of the material, as given by

$$\sigma_{eq}{}^2 = \sigma_x{}^2 + \sigma_y{}^2 - \sigma_x\sigma_y + 3\tau_{xy}{}^2 \tag{3.5}$$

where σ_x and σ_y are the normal stresses in the longitudinal and transversal directions, respectively, and τ_{xy} is the shear stress.

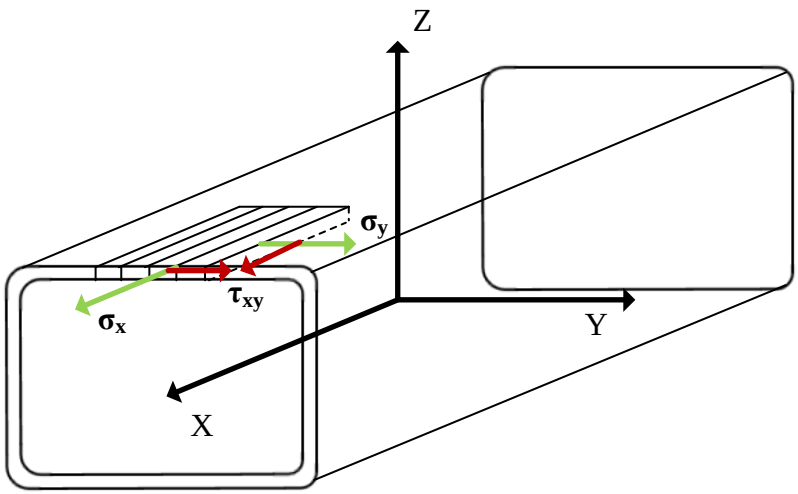

Fig.3.6 A plate in the state of plane stress

In the presence of both longitudinal and transverse residual stresses, σ_x , σ_y and τ_{xy} are given by

$$\sigma_x = \sigma + \sigma_l \tag{3.6}$$

$$\sigma_y = \sigma_t \tag{3.7}$$

$$\tau_{xy} = 0 \tag{3.8}$$

where σ is the applied stress in longitudinal direction; σ_l and σ_t are the residual stresses in the longitudinal and transversal directions, respectively.

Since the stress-strain curve of stainless steel differs to that of carbon steel, the procedure of modifying stress-strain curve is slightly differnt to the one present in Liu et al. (2017). It is carried out by the following steps.

1. Divide the section into different layers (shown in Fig.3.7 (a)) and monitor the stress at each node between the layers.

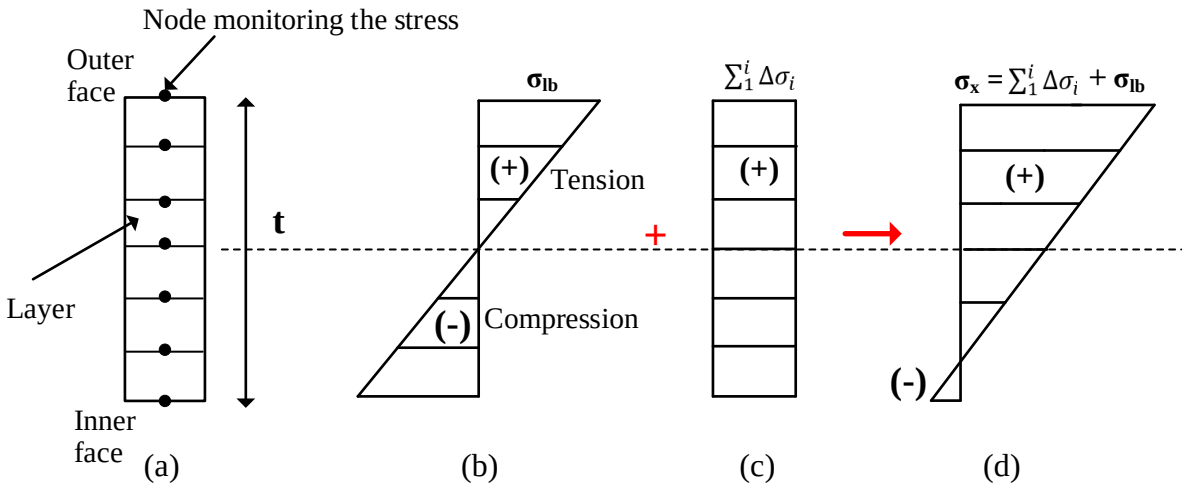

Fig.3.7 (a) layer through thickness (b) distribution of through-thickness longitudinal bending residual stress (σ_{lb}) (c) the applied tension stress (d) the total stress in longitudinal direction

2. Rewrite Eq.(3.1) that determines the stress-strain curves of stainless steel as

$$\varepsilon = \varphi(\sigma) \tag{3.9}$$

Then, it gives

$$\sigma = \varphi^{-1}(\varepsilon) \tag{3.10}$$

If strain-hardening is not considered, $\varphi^{-1}(\varepsilon)$ is the inverse function of one stage Ramberg-Osgood equation, while if strain-hardening is considered, $\varphi^{-1}(\varepsilon)$ is the inverse function of the two stage Ramberg-Osgood equations.

3. Assuming the applied initial strain ε_0 is zero, apply an increment of strain ($\Delta\varepsilon_i$) to the section

$$\Delta\varepsilon_i = \varepsilon_i - \varepsilon_{i-1} \qquad (i = 1,2,3\cdots) \tag{3.11}$$

The change in stress is

$$\Delta\sigma_i = \varphi^{-1}(\varepsilon_i) - \varphi^{-1}(\varepsilon_{i-1}) \tag{3.12}$$

4. Assume the applied initial stress is zero ($\varphi^{-1}(\varepsilon_0) = 0$) and only longitudinal bending residual stresses are considered. In the *i* (*i*=1,2,3……) step, the total stress in longitudinal direction is

$$\sigma_x = \sum_1^i \Delta\sigma_i + \sigma_{lb} \tag{3.13}$$

$$= \sum_1^i [\varphi^{-1}(\varepsilon_i) - \varphi^{-1}(\varepsilon_{i-1})] + \sigma_{lb} \tag{3.14}$$

$$= \varphi^{-1}(\varepsilon_i) - \varphi^{-1}(\varepsilon_0) + \sigma_{lb} \tag{3.15}$$

$$= \varphi^{-1}(\varepsilon_i) + \sigma_{lb} \tag{3.16}$$

where σ_{lb} is through-thickness longitudinal residual stress; σ_{lb}, $\sum_1^i \Delta\sigma_i$, and σ_x are shown in Fig.3.7 (b), (c) and (d), respectively.

5. Substituting Eq.(3.16) into Eq.(3.5), it gives

$${\sigma_{eq}}^2 = (\varphi^{-1}(\varepsilon_i) + \sigma_{lb})^2 \tag{3.17}$$

6. In the *i* step, if $\sigma_{eq} \leq f_y$, calculate the average applied stress on the cross section through integration for all the points as follows

$$\sigma_{av} = \frac{\int_t \sum_1^i [\varphi^{-1}(\varepsilon_i) - \varphi^{-1}(\varepsilon_{i-1})]dt}{t} = \frac{\int_t \varphi^{-1}(\varepsilon_i)dt}{t} \qquad (i = 1,2,3\cdots) \tag{3.18}$$

7. Else if $\sigma_{eq} > f_y$, define $\Delta\sigma_i$ in the *i* step as

$$\Delta\sigma_i = \alpha^*[\varphi^{-1}(\varepsilon_i) - \varphi^{-1}(\varepsilon_{i-1})] \tag{3.19}$$

8. Substituting Eq.(3.19) into Eq.(3.13), it gives

$$\sigma_x = \varphi^{-1}(\varepsilon_{i-1}) + \alpha[\varphi^{-1}(\varepsilon_i) - \varphi^{-1}(\varepsilon_{i-1})] + \sigma_{lb} \tag{3.20}$$

9. Calculate the solution of α*, so that

$$\sigma_{eq} = f_y \text{ (without strain hardening) } \ or \ \sigma_{eq} = f_u \text{ (with srain hardening)} \tag{3.21}$$

10. Calculate the average applied stress as follows

$$\sigma_{av} = \frac{\int_t \left[\varphi^{-1}(\varepsilon_{i-1}) + \alpha[\varphi^{-1}(\varepsilon_i) - \varphi^{-1}(\varepsilon_{i-1})]\right]dt}{t} \tag{3.22}$$

11. Repeat the above steps 1–10 to obtain a series of points of strain and stress ($\sum\Delta\varepsilon_i$, σ_{av}), where $\sum\Delta\varepsilon_i$ represents the total applied strain, and σ_{av} represents the corresponding stress. The curve of $\sum\Delta\varepsilon_i$ versus σ_{av}

is the modified stress-strain curve that accounts for longitudinal bending residual stresses.

For the example of stainless steel with E=200GPa, n=7 and f_y = 450MPa (without strain hardening), comparison of the modified stress-strain curve accounting for the influence of longitudinal bending residual stresses against the stress-strain curve without residual stresses is shown in Fig.3.8. In this example, longitudinal bending residual stresses (σ_{lb}) vary linearly throughout the thickness, and the amplitude of σ_{lb} in outer surface and inner surface of the wall is taken as $0.63f_y$.

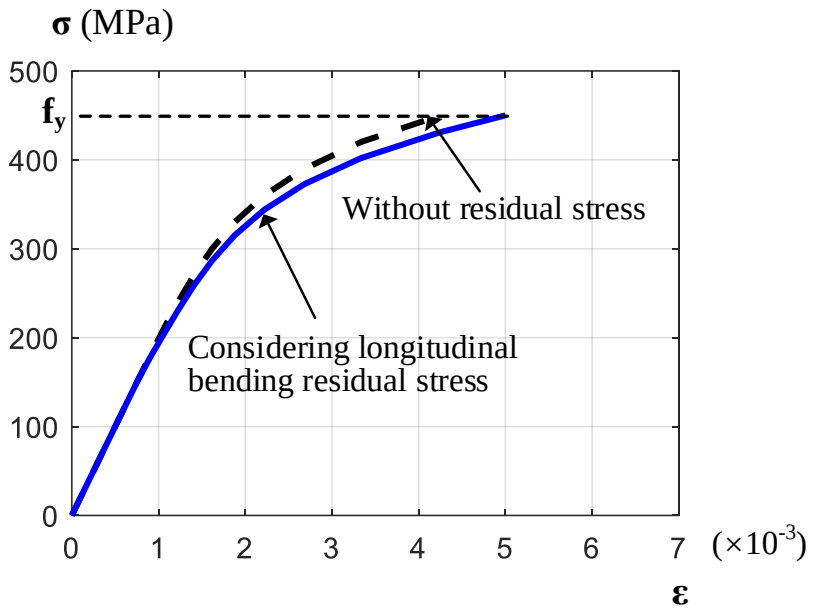

Fig. 3.8 Comparison of the stress-strain curves with and without residual stresses

It should be pointed out that, for numerical models using stress-strain curves obtained from tensile coupons test directly, there may be no need to reintroduce longitudinal bending residual stresses. This is due to the reason that the influence of through-thickness longitudinal bending residual stresses is approximately presented in the stress-strain curves obtained from tensile coupons test. It can be explained by the following. Due to releasing longitudinal bending residual stresses, coupons are typically curved after cutting from the member. Since the coupons will be straightened in the beginning of the test, the original through-thickness longitudinal residual stresses are approximately reintroduced again.

3.3 Validation of the finite element models

The developed FE models were validated against the test results on stainless steel beam-columns with cold-formed RHS reported in Arrayago et al. (2016), and validated against test results on carbon steel frames

comprising cold-formed RHS reported in Wilkinson and Hancock (1999). Both the beam-columns and frames considered for the validation study are not susceptible for local buckling (class 1 and 2 sections). For the validation study, initial geometric imperfections was modelled as explained in Section 3.2.3. The adopted imperfection value and the material properties were modelled as those reported in the literature. The longitudinal bending residual stresses were not modelled, since they are implicitly included in the stress-strain curves.

Comparison of numerical results against test results for the two beam-columns is shown in Fig. 3.9 (a). It can be seen that the numerical results are in very close agreement with experimental results. Fig. 3.9 (b) shows the comparison of the developed FE models against the tests results of two steel frames. The discrepancy between the predicted results and the test results may be attributed to the fact that the connections of the tested frames are not perfectly rigid. These differences were also observed in the FE models presented in Wilkinson and Hancock (1999). The close agreement between predicted results and the test results indicates that the developed FE models can accurately predict the in-plane response of steel frames.

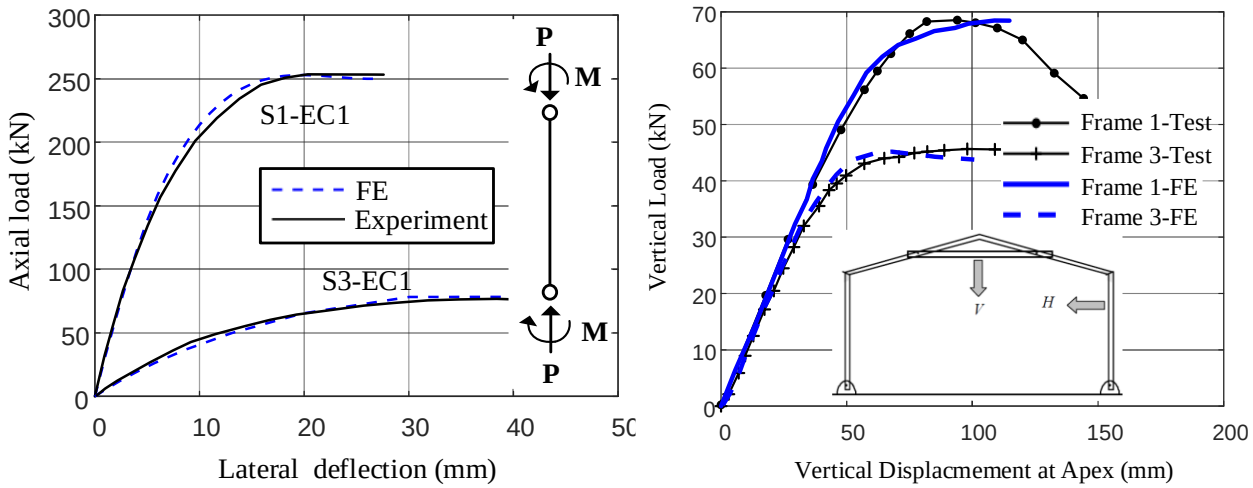

(a) (b)

Fig. 3.9 Validation of the developed FE models against the tests results for (a) beam-columns from Arrayago et al. (2016) (b) frames from Wilkinson and Hancock (1999).

3.4 Concluding remarks

The in-plane structural behavior of stainless steel elements and frames is studied through FE analysis. In

FE modelling, the influence of out-of-plumbness and out-of-straightness can be taken into account by applying equivalent notional loads. To avoid additional shear force at the member or frame base due to notional loads, corresponding horizontal reaction forces should be applied. For cold-formed RHS and SHS, only longitudinal bending residual stresses are considered in FE models and they are accounted for by modifying the stress-strain curve. For numerical models using stress-strain curves obtained from tensile coupons test directly, there is no need to model longitudinal bending residual stresses since they are approximately presented in the stress-strain curves obtained from tensile coupons test.

4. Flexural stiffness reduction factor for stainless steel columns and beams

4.1 Introduction

In this chapter, column flexural stiffness reduction factor (τ_N) and beam flexural stiffness reduction factor (τ_M) are derived from stainless steel column strength curve and moment-curvature curve, respectively. The accuracy of both τ_N and τ_M is subsequently verified.

The proposed τ_N and τ_M are applicable to stainless steel members with compact cold-formed RHS and SHS. The primary purpose of developing τ_N and τ_M is to develop the approximate expression of stainless steel beam-column stiffness reduction factor (τ_{MN}) formulation (presented in Chapter 5), since τ_N and τ_M are the main variables in the approximate expression.

- τ_N is derived from stainless steel column strength curve provided in AISC Design Guide 27. The stainless steel column strength curve is established by modifying relevant coefficient of AISC LRFD carbon steel column strength curve and calibrated against experimental data.
- τ_M is developed based on the moment-curvature relationship for stainless steel beams with cold formed RHS and SHS. The employed moment-curvature relationship considers material non-linearity and it is fitted by an analytical expression similar to the Ramberg-Osgood equation.

4.2 Derivation of flexural stiffness reduction factor for stainless steel columns

Carbon steel column flexural stiffness reduction factor τ_b is derived from Column Research Council (CRC) column strength curve. The CRC column strength curve is developed based on test results of columns with hot-rolled wide-flange I sections (Johnston,1976). The CRC curve (for compact sections) is given by:

When $\lambda_c \leq 1.414$ $\quad P_n = \left(1 - \frac{{\lambda_c}^2}{4}\right) P_y$ (4.1)

When $\lambda_c > 1.414$ $\quad P_n = P_e = \frac{P_y}{{\lambda_c}^2}$ (4.2)

where P_n is the nominal compressive strength of a column; P_n is equal to nominal global buckling strength (P_{ne}) for a column with compact section; λ_c is column slenderness; $\lambda_c = (P_y / P_e)^{\wedge}0.5$; P_e is the elastic critical

buckling strength of a column with effective length factor (K). Eq. (4.1) represents inelastic buckling whereas Eq. (4.2) represents elastic buckling. The plot of CRC column strength curve is shown in Fig. 4.1(a).

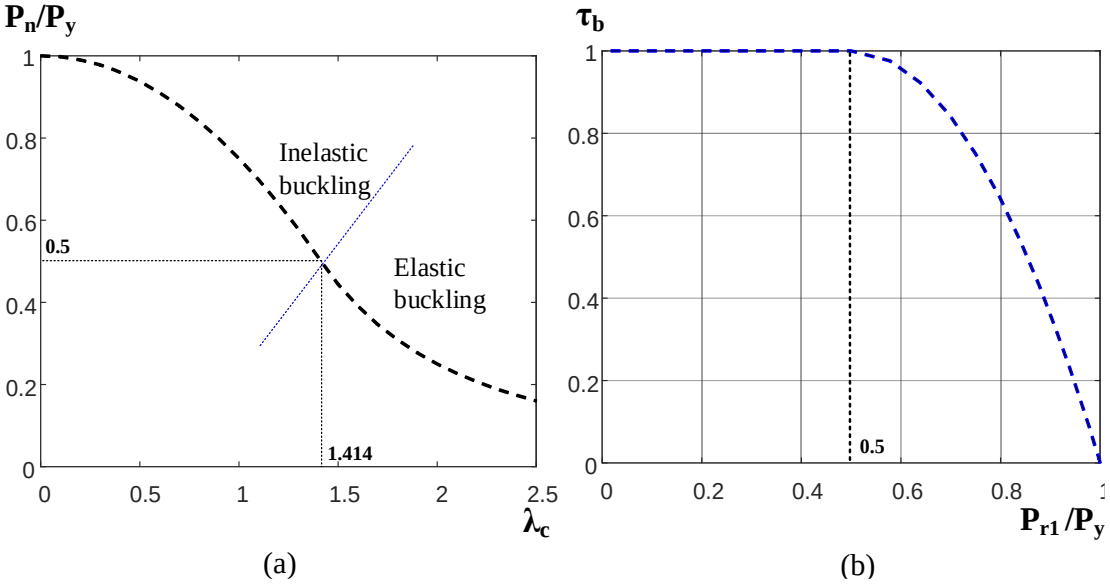

Fig.4.1. (a) CRC carbon steel column strength curve (b) A plot of τ_b against P_{r1}/P_y

τ_b is given by

$$\tau_b = 1 \qquad \text{for } \frac{P_{r1}}{P_y} \leq 0.5 \tag{4.3}$$

$$\tau_b = 4\frac{P_{r1}}{P_y}\left(1 - \frac{P_{r1}}{P_y}\right) \qquad \text{for } \frac{P_{r1}}{P_y} > 0.5 \tag{4.4}$$

where P_{r1} is maximum first order internal axial force; P_y is cross -section yield strength $P_y=Af_y$; A is cross-section area; f_y is 0.2% proof stress. A plot of τ_b curve is shown in Fig.4.1 (b).

τ_b is intended to mainly account for the influence of partial yielding accentuated by the presence of residual stresses, but it may not be applicable to cold-formed RHS and SHS. This is because the distribution and magnitude of residual stresses of cold-formed RHS and SHS differs from that of hot-rolled wide-flange I sections. Therefore, a new column stiffness reduction factor (τ_N) for cold-formed stainless steel with RHS is developed. τ_N is derived from stainless steel column strength curve provided in Section 5.3 of AISC Design Guide 27 (2013). This curve is established by modifying relevant coefficient of AISC LRFD carbon steel column strength curve and calibrated against experimental data. The AISC LRFD-based stainless steel column strength curve (for compact section) is given by:

When $\lambda_c \leq 1.2$ $\quad P_n = 0.5^{\lambda_c{}^2} P_y$ (4.5)

When $\lambda_c > 1.2$ $\quad P_n = 0.531 P_e = \frac{0.531}{\lambda_c{}^2} P_y$ (4.6)

where the nominal compressive strength P_n is equal to nominal global buckling strength for a column with compact section; Eq. (4.5) represents inelastic buckling while Eq. (4.6) represents elastic buckling. A plot of the AISC LRFD-based stainless steel column strength curve is shown in Fig 4.2 (a)

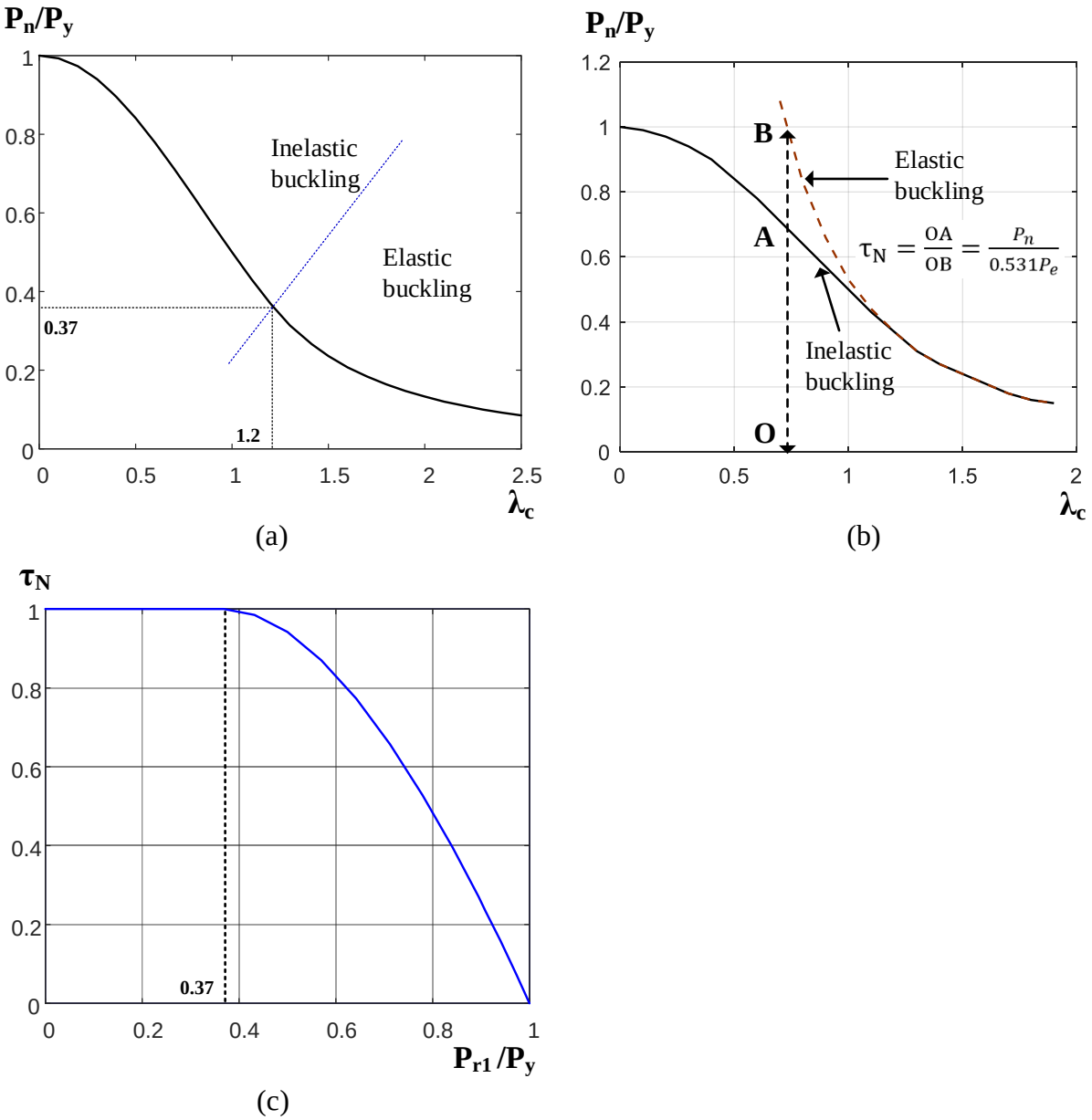

Fig. 4.2 (a) AISC-based stainless steel column strength curve (b) Illustration of deriving τ_N (c) A plot of τ_N

The derivation of column stiffness reduction formulation is based on Eq. (4.7), as illustrated in Fig.4.2 (b).

$$\tau_N = \frac{P_n}{0.531P_e} \tag{4.7}$$

For the elastic buckling case, τ_N=1. For the inelastic buckling case, τ_N is less than 1. Rewriting Eq. (4.7), the following equation for both elastic and inelastic buckling is obtained.

$$P_e = \frac{P_n}{0.531\tau_N} \tag{4.8}$$

Rewriting Eq. (4.5) gives

$$P_n = 0.5^{\frac{P_y}{P_e}} P_y \tag{4.9}$$

Substituting Eq.(4.8) into Eq.(4.9) gives

$$\frac{P_n}{P_y} = 0.5^{\frac{0.531\tau_N P_y}{Pn}} \tag{4.10}$$

$$\ln\frac{P_n}{P_y} = 0.531\tau_N \frac{P_y}{P_n} \ln 0.5 \tag{4.11}$$

$$\tau_N = -2.717\frac{P_n}{P_y} ln \frac{P_n}{P_y} \tag{4.12}$$

For $\lambda_c = 1.2,\ P_n/P_y = 0.37$. Thus,

when $\frac{P_n}{P_y} \leq 0.37\ (\lambda_c \geq 1.2)$ $\qquad \tau_N = 1$ (4.13)

when $\frac{P_n}{P_y} > 0.37\ (\lambda_c < 1.2)$ $\qquad \tau_N = -2.717\frac{P_n}{P_y} ln \frac{P_n}{P_y}$ (4.14)

A plot of τ_N is shown in Fig 4.2 (c). It should be noted that for the determination of τ_N under different axial load, the nominal compressive strength P_n should be replaced by maximum internal axial force P_{r1} under corresponding axial load. Thus, the expression of τ_N is given by

When $\frac{P_{r1}}{P_y} \leq 0.37$ $\qquad \tau_N = 1$ (4.15)

When $\frac{P_{r1}}{P_y} > 0.37$ $\qquad \tau_N = -2.717\frac{P_{r1}}{P_y} ln \frac{P_{r1}}{P_y}$ (4.16)

The above τ_N formulation accurately accounts for the effects of residual stress, member imperfection (out-of-straightness), and spread of plasticity on stainless steel columns. Comparison of τ_N and τ_b is shown in Fig.4.3. It can be observed that τ_N is lower than τ_b.

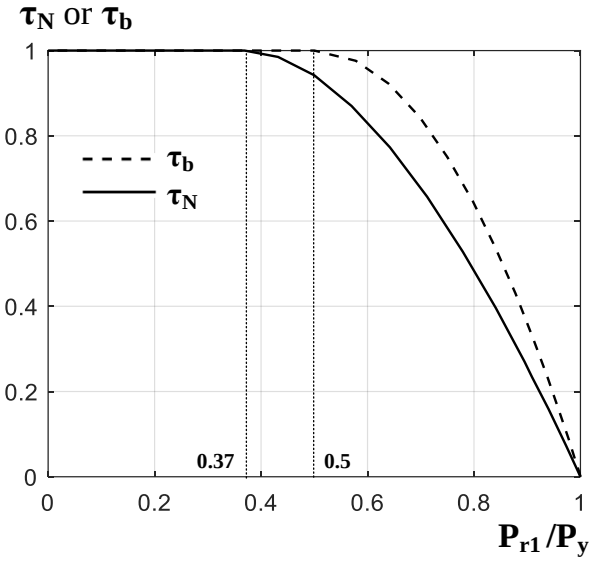

Fig 4.3 Comparison of τ_N and τ_b

4.3 Verification of column flexural stiffness reduction factor (τ_N)

The accuracy of column flexural stiffness reduction factor (τ_N) for predicting compressive strength of members subjected to axial load is assessed in this section. A total of 23 simply supported columns with section 120x80x6 (E=175 GPa, f_y=350MPa, n=6) subjected to axial loads are studied. The applied axial load is factored. The length of the columns varies from 50mm to 7000 mm. L= [50, 100, 200, 300, 350, 400, 450, 500, 600, 700, 1000, 1500, 2000, 2500, 3000, 3500, 4000, 4500, 5000, 5500, 6000, 6500, 7000]. For each column, GMNIA and GNA with τ_N (denoted by GNA-τ_N) are conducted.

The procedure of implementing GNA-τ_N is shown in Fig.4.4. Firstly, GMNIA is conducted to determine ultimate axial load (P_u) of the columns, where the introduced out-of-straightness is 0.001. In this figure, P_u predicted by GMNIA is denoted by $P_{u\text{-}GMNIA}$. Secondly, Linear Elastic Analysis (LA) is conducted to obtain maximum first order axial force, where the applied load is $P_{u\text{-}GMNIA}$. The introduced out-of-straightness is 0.001 in implementing LA. Maximum first order axial force obtained from LA is referred to as P_{r1}. For all the studied simply supported columns, P_{r1} is equal to $P_{u\text{-}GMNIA}$. τ_N is calculated according to Eq.(4.15) and (4.16). Lastly, GNA-τ_N is conducted to predict ultimate axial load of the columns. Ultimate axial load predicted by GNA-τ_N is denoted by $P_{u\text{-}\tau N}$. It should be mentioned that, an imperfection value much smaller than 0.001is introduced into the columns to ensure that these columns can buckle in GNA (columns without any imperfection would not buckle in GNA), even though τ_N includes out-of-straightness of 0.001. If the proposed τ_N

expression is "perfect", the failure load determined by GNA-τ_N should be equal to the failure load determined by GMNIA. The discrepancy between them shows the quality of τ_N.

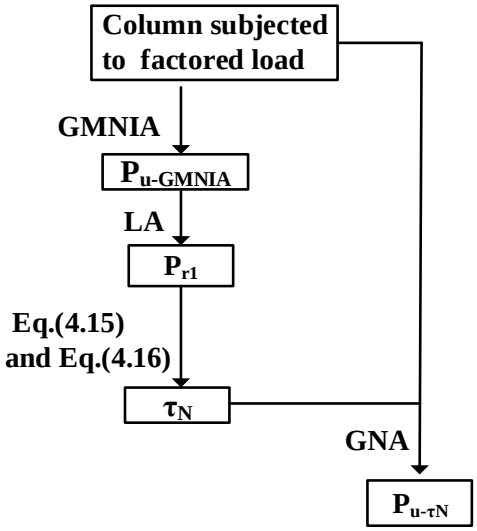

Fig.4.4 Procedure of implementing GNA-τ_N and GMNIA

It is found that, the ultimate load $P_{u\text{-}\tau N}$ (inelastic global buckling strength) of simply supported columns predicted by GNA-τ_N matches the bifurcation load (or elastic critical buckling load) $P_{e\text{-}\tau N}$ determined by reduced flexural stiffness (τ_N times EI), as shown in Fig.4.5. $P_{e\text{-}\tau N}$ is given by

$$P_{e-\tau N} = \frac{\pi^2(\tau_N EI)}{(L)^2} \tag{4.17}$$

where EI is initial flexural stiffness; L is unbraced length of the column.

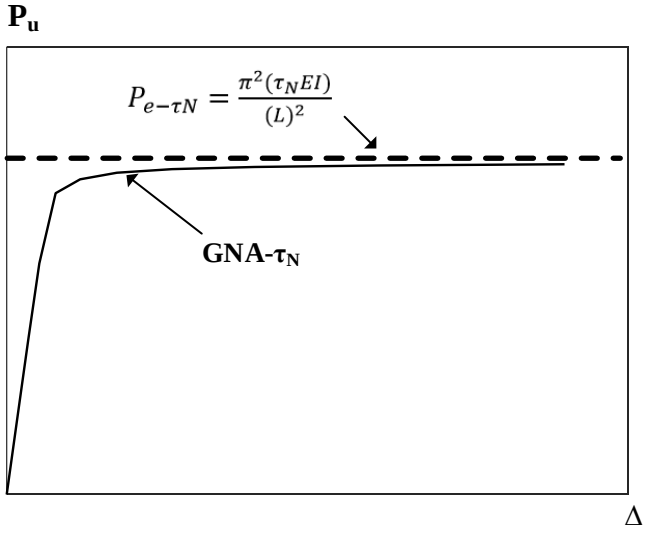

Fig.4.5 Illustration of ultimate axial load (P_u) determined by GNA-τ_N and elastic critical buckling load ($P_{e\text{-}\tau N}$) based on effective flexural stiffness (τ_NEI)

Comparison of predicted results from GNA-τ_N against those determined by GMNIA is shown in Fig.4.6, where ultimate axial load (P_u) predicted by different method is normalized by full cross-section yield strength (P_y). It is observed that the ultimate axial loads predicted by GNA-τ_N agree very well with those predicted by GMNIA. The discrepancy between $P_{u\text{-}\tau N}$ and $P_{u\text{-}GMNIA}$ relies on the ability of the adopted AISC LRFD-based stainless steel column strength curve to capture accurately the actual behavior of the studied columns. Since AISC LRFD-based stainless steel column strength curve provided in AISC design guide 27 (Baddoo, 2013) is calibrated against experimental data, further verification of column flexural stiffness reduction factor (τ_N) for other columns is not needed.

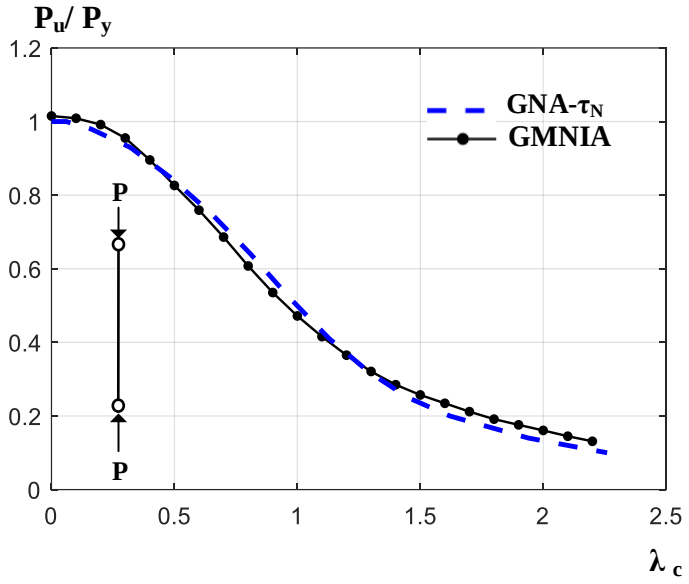

Fig.4.6 Normalized ultimate axial load (P_u/P_y) predicted by different methods against column slenderness (λ_c)

4.4 Derivation of flexural stiffness reduction factor for stainless steel beams

Bending stiffness reduction for in-plane beams refers to influence of spread of plasticity through cross-section and along the member. Bending stiffness reduction factor (τ_M) can be determined by the ratio of tangent flexural stiffness $(EI)_t$ to the initial flexural stiffness EI, given by:

$$\tau_M = \frac{(EI)_t}{EI} = \frac{\frac{dM_{r1}}{d\kappa}}{EI} \tag{4.18}$$

where $\frac{dM_{r1}}{d\kappa}$ is derived from a moment-curvature (M-κ) curve.

The adopted moment-curvature relationship prior to outer fibers yielding is based on the moment-curvature relationship for stainless steel beams with cold formed RHS and SHS, proposed by Real and Mirambell (2005). It considers material non-linearity and it is fitted by an analytical expression similar to the Ramberg-Osgood equation. The moment-curvature relationship is given by Eq.(19) (symbols are not identical to those employed in the original paper).

$$\kappa = \frac{M_{r1}}{EI} + \left[\frac{2}{D}\left(\frac{f_y}{E} + 0.002\right) - \frac{M_y}{EI}\right]\left(\frac{M_{r1}}{M_y}\right)^{n-1} \tag{4.19}$$

In Eq. (4.19), EI is the initial flexural stiffness; D is the height of the cross-section; f_y is 0.2% proof stress; n is the coefficient in the Ramberg–Osgood equation; M_y is moment at yielding of the extreme fiber; $M_y=W_{el}f_y$; W_{el} is elastic gross section modulus.It should be mentioned that the cross-section already undergoes plastic straining before internal moment reaches to M_y, due to the nonlinear stress-strain behavior of stainless steel.

Eq.(4.19) is an implicit equation. Differentiating with respect to κ on both sides of Eq. (4.19) gives

$$\frac{dM_{r1}}{d\kappa} = \left[\frac{1}{EI} + (n-1)\frac{1}{M_y}\left(\frac{2}{D}\left(\frac{f_y}{E} + 0.002\right) - \frac{M_y}{EI}\right)\left(\frac{M_{r1}}{M_y}\right)^{n-2}\right]^{-1} \tag{4.20}$$

Substituting Eq. (4. 20) into Eq. (4.18) gives

$$\tau_M = \left[1 + (n-1)\left(\frac{2}{D}\frac{1}{M_y}\left(f_y I + 0.002EI\right) - 1\right)\left(\frac{M_{r1}}{M_y}\right)^{n-2}\right]^{-1} \tag{4.21}$$

Substituting $\frac{2I}{D} = W_{el}$ into Eq. (4. 21) gives

$$\tau_M = \left[1 + (n-1)\left(\frac{W_{el}}{M_y}\left(f_y + 0.002E\right) - 1\right)\left(\frac{M_{r1}}{M_y}\right)^{n-2}\right]^{-1} \tag{4.22}$$

Substituting $W_{el}f_y = M_y$ into Eq. (4.22), the τ_M formulation is given by

$$\tau_M = \left[1 + (n-1)\frac{0.002E}{f_y}\left(\frac{M_{r1}}{M_y}\right)^{n-2}\right]^{-1} \tag{4.23}$$

Eq. (4.23) can be written in terms of the ratio of M_{r1}/M_p as follows:

$$\tau_M = \left[1 + (n-1)\frac{0.002E}{f_y}\left(\frac{M_{r1}}{M_p}\frac{W_{pl}}{w_{el}}\right)^{n-2}\right]^{-1} \quad (4.24)$$

where M_p is full plastic bending moment; $M_p=W_{pl}f_y$; W_{pl} is plastic gross section modulus.

4.5 Verification of beam flexural stiffness reduction factor (τ_M)

τ_M determined by Eq.(4.24) is assumed to be applicable to the deformation range when $M_y<M_{r1}\leq M_p$. To evaluate the ability of τ_M capturing spread of plasticity through cross-section and along member length, simply supported beams with a wide range of cross-sections and material properties subjected to varied load cases are studied. τ_M determined by Eq.(4.24) are compared against flexural stiffness reduction derived from M-k curves of GMNIA. The derivation of flexural stiffness reduction is based on Eq. (4.18), where $dM_{r1}/d\kappa$ is the slope of the tangent at a given point on the M-k curve. The calculation of tangent slope is conducted through MATLAB 2017b.

Two examples, a beam with cross-section 200x100x10 (E=175GPa, f_y=400MPa, n=6, W_{pl}/W_{el}=1.27, M_p=140.8 kN*m) subjected to a pair of identical end moments, and a beam with cross-section 120x80x6 (E=190GPa, f_y=370MPa, n=7, W_{pl}/W_{el}=1.23, M_p=33.2 kN*m) subjected to uniform distributed load, are shown in in Fig.8. For the two beams, the M-k curves determined by GMNIA are shown in Fig.4.7 (a) and (c). Comparison of flexural stiffness reduction derived from M-k curves of GMNIA (denoted by $\tau_{M\text{-}GMNIA}$) and τ_M determined by equations (denoted by $\tau_{M\text{-}Eq}$) is shown in Fig.4.7 (b) and (d).

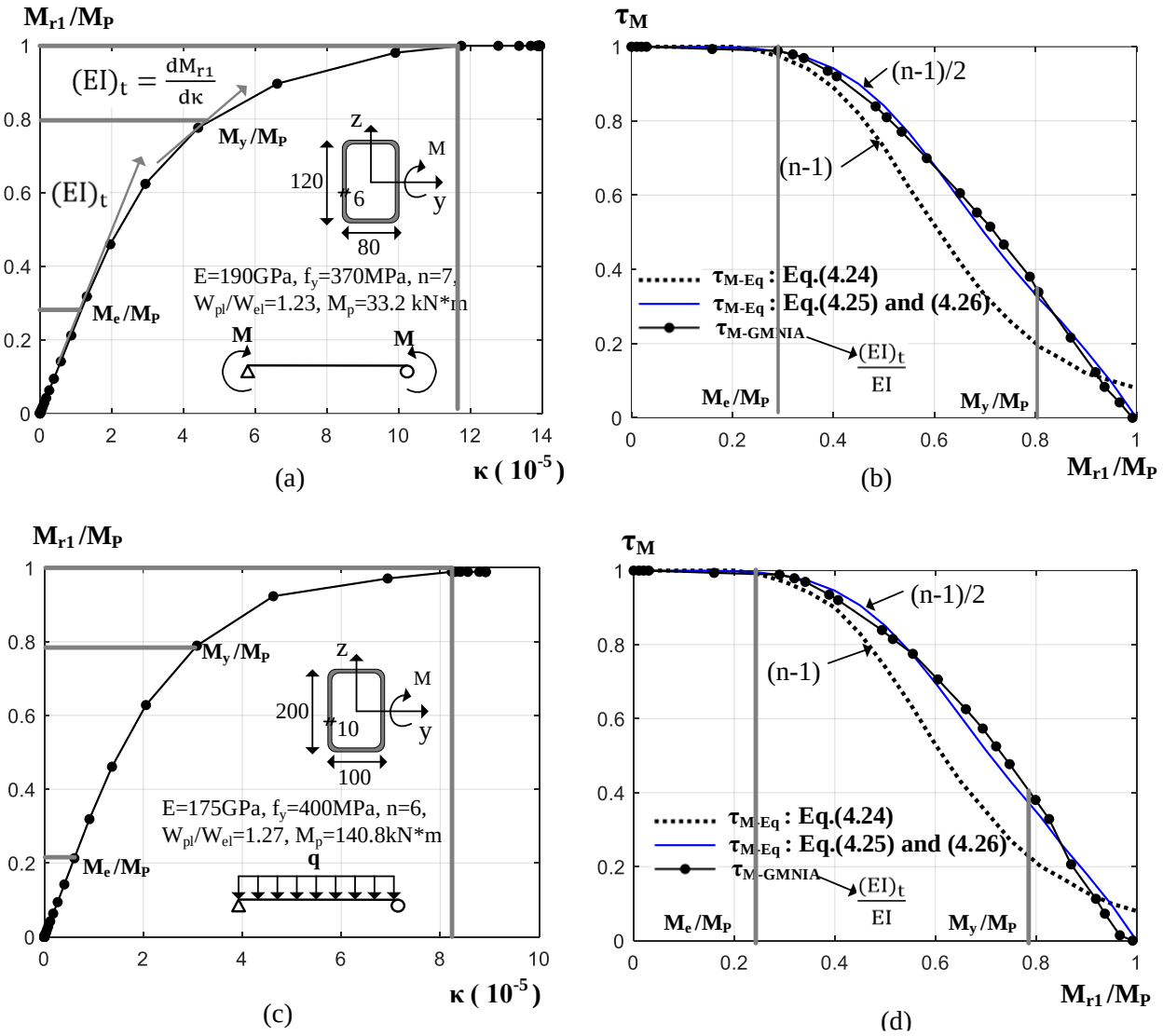

Fig.4.7 Two examples used to evaluate the accuracy of τ_M: (a) and (c) M-k relationship determined by GMNIA, (b) and (d) comparison of τ_M and flexural stiffness reduction derived from M-k relationship

It is observed that, $\tau_{M\text{-}Eq}$ determined using Eq. (4.24) underestimates the beam flexural stiffness reduction factor determined by GMNIA. Further analysis shows that, for the deformation range when $0 < M_{r1} \leq M_y$, replacing the term (n-1) by (n-1)/2 generates more accurate results. Thus, the modified τ_M formulation, given by Eq. (4.25), is adopted to predict flexural stiffness reduction before extreme fiber of the cross-section yields (Corresponding to M_y).

$$\tau_M = \left[1 + (n-1)\frac{0.002E}{2 \cdot f_y}\left(\frac{M_{r1}}{M_p}\frac{W_{pl}}{w_{el}}\right)^{n-2}\right]^{-1} \tag{4.25}$$

After yielding of the extreme fiber of the cross-section, plastic strain increases at a high rate, and results in rapid increase of plastic curvature (κ). For the deformation range when $M_y < M_{r1} \leq M_p$, the flexural stiffness

reduction factor, given by Eq. (4.26) is proposed in this paper. The development of Eq. (4.26) is based on the moment-curvature relationship (determined by GMNIA) of beams with a wide range of cross-sections and material properties.

$$\tau_M = \left[\left(1 - \frac{M_{r1}}{M_p}\right)\frac{1}{1-\frac{W_{el}}{W_{pl}}}\right]^{0.9}\left[1 + (n-1)\frac{0.002E}{2 \cdot f_y}\right]^{-1} \quad (4.26)$$

From Fig.4.7 (b) and (d), it is seen that $\tau_{M\text{-}Eq}$ determined Eq. (4.25) and (4.26) is in very close agreement with $\tau_{M\text{-}GMNIA}$, which shows that the adopted stiffness reduction formulations accurately captures spread of plasticity through cross-section and along member length. It should be mentioned that the discrepancy between $\tau_{M\text{-}Eq}$ (determined Eq. (4.25) and (4.26)) and $\tau_{M\text{-}GMNIA}$ is considered in the development of the approximate expression for beam-column stiffness reduction factor (τ_{MN}).

4.5 Concluding remarks

Column flexural stiffness reduction factor (τ_N) and beam flexural stiffness reduction factor (τ_M), applicable to stainless steel members with compact cold-formed RHS and SHS, are developed. The proposed τ_N depends on the maximum internal first order axial force within a member (P_{r1}). The proposed τ_M depends on the maximum internal first order moment within a member (M_{r1}) and material properties (E, f_y, and n).

The results of verification study show that GNA coupled with the developed stiffness reduction factor (τ_N and τ_M) reaches the accuracy of GMNIA. The slight discrepancy between the developed stiffness reduction factor (τ_N and τ_M) and the actual stiffness reduction factor will be considered in the development of the approximate expression of stainless steel beam-column stiffness reduction factor (τ_{MN}) expression.

5. Flexural stiffness reduction for stainless steel beam-columns

5.1 Introduction

This chapter focus on the development of beam-column flexural stiffness reduction factor (τ_{MN}) formulation for the in-plane stability design of stainless steel beam-columns with compact cold-formed RHS and SHS. Two types of τ_{MN} formulations are proposed: analytical and approximate. The analytical expression of τ_{MN} presumes knowing the maximum internal second order moment (M_{r2}) within a member. It is developed by means of extending the formulations for evaluating the elastic second order effects to the inelastic range.

The proposed τ_{MN} accounts for the deleterious influence of material non-linearity, residual stresses and member out-of-straightness. The use of a Geometrically Non-linear Analysis (GNA) with the proposed τ_{MN} eliminates the need for member buckling strength checks and thus, only cross-sectional strength checks are required.

To develop the analytical expression of τ_{MN}, formulations that determine maximum second order elastic moment ($M_{r2\text{-}E}$) within sway-restrained and sway-permitted beam-columns are first described. Then, based on these formulations, the analytical expression of stiffness reduction factor (τ_{MN}) for beam-columns (elastic and inelastic) is developed. The formulations that determine maximum second order elastic moments are assumed to be applicable to determining maximum second order inelastic moment ($M_{r2\text{-}P}$), if flexural stiffness reduction factor τ_{MN} is incorporated into the elastic critical buckling load. The soundness of this assumption as well as the accuracy of GNA with τ_{MN} (determined by the analytical expression) for stainless steel beam-columns are verified.

The aim of developing expression of τ_{MN} is to apply GNA with stiffness reduction to stability design of frames. Nevertheless, τ_{MN} determined by the analytical expression cannot be applied directly to the design of frames, since the maximum internal second order inelastic moment ($M_{r2\text{-}P}$) in the analytical expression is unknown. Therefore, a function (approximate expression) independent of $M_{r2\text{-}P}$, which matches analytical expression of τ_{MN}, is proposed. The approximate expression of τ_{MN} is developed by fitting variables to the analytically determined expressions.

5.2 Maximum second order elastic moment within sway-restrained beam-columns

For elastic beam-columns with no relative lateral displacement between member ends (sway-restrained), maximum second order elastic moment ($M_{r2\text{-}E}$) within the member can be calculated by amplification of maximum first order moment (M_{r1}), as shown in Eq.(5.1).

$$\frac{M_{r2-E}}{M_{r1}} \approx \frac{C_m}{1-\frac{P_{r1}}{P_{e1}}} = B_{1-E} \geq 1 \tag{5.1}$$

$$P_{e1} = \frac{\pi^2 EI}{l^2} \tag{5.2}$$

where the amplification factor $B_{1\text{-}E}$ evaluates P-δ the effects on maximum second order elastic moment ($M_{r2\text{-}E}$). $B_{1\text{-}E}$ has the same definition as the amplification factor B_1 provided in Appendix 8 of AISC 360-16 (2016). P_{e1} (K=1) is elastic critical buckling strength of the member with unbraced length. Equivalent uniform moment factor C_m accounts for the beneficial effects of moment gradient for beam-columns.

Eq. (5.1) is developed based on differential equations governing the in-plane behavior of the elastic beam-column. For an elastic beam-column (sway-restrained and without transverse loadings) subjected to varied end moments, shown in Fig. 5.1 (a), the maximum moment within the member is given by Eq. (5.3). Detailed differential equations is provided in Chapter 2 of Chen and Lui (2017).

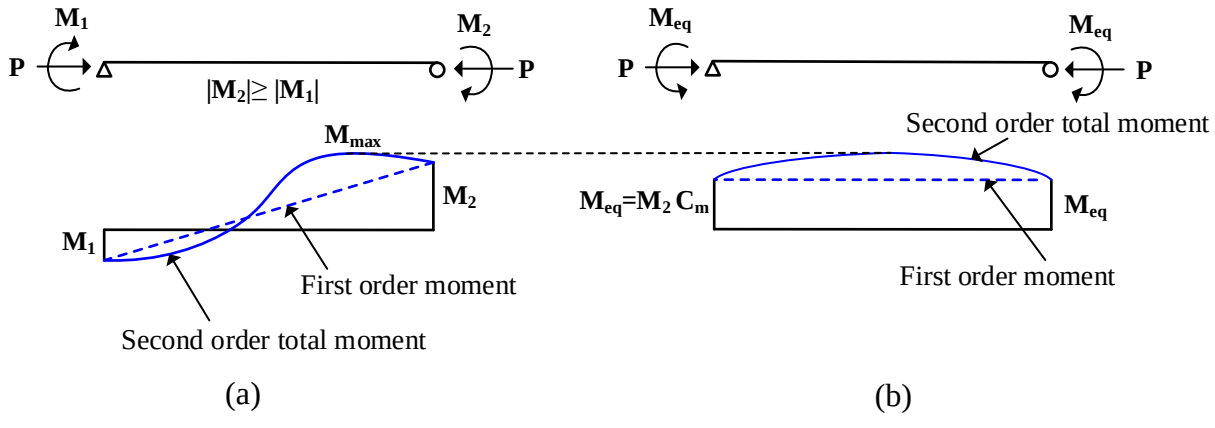

Fig. 5.1. Illustration of equivalent moment (a) Moment of beam-column subjected to varied end moments (b) Moment of beam-column subjected to a pair of equal and opposite end moments

$$M_{max} = M_2 \left[\frac{\sqrt{(M_1/M_2)^2+2(M_1/M_2)cosk l+1}}{sinkl}\right] \tag{5.3}$$

where $= \sqrt{\frac{P}{EI}}$; $|M_2| \geq |M_1|$; l is the length of the beam-column.

For the same elastic beam-column subjected to a pair of equal and opposite end moments, shown in Fig. 5.1 (b), the maximum moment within the member is given by

$$M_{max} = M_{eq}\left[\frac{\sqrt{2(1-coskl)}}{sinkl}\right] \tag{5.4}$$

Setting Eq. (5.3) equal to Eq. (5.4), it gives

$$M_{eq} = M_2\left[\frac{\sqrt{(M_1/M_2)^2+2(M_1/M_2)coskl+1}}{2(1-coskl)}\right] \tag{5.5}$$

The expression in brackets is regarded as equivalent uniform moment factor (C_m)

$$\frac{\sqrt{(M_1/M_2)^2+2(M_1/M_2)coskl+1}}{2(1-coskl)} = C_m \tag{5.6}$$

$$M_{eq} = M_2 C_m \tag{5.7}$$

Substituting Eq. (5.7) back into Eq. (5.4), it gives

$$M_{max} = M_2 C_m\left[\frac{\sqrt{2(1-coskl)}}{sinkl}\right] \tag{5.8}$$

Substituting $k = \sqrt{\frac{P}{EI}}$ back into the expression in brackets, it gives

$$\frac{\sqrt{2(1-coskl)}}{sinkl} = \frac{\sqrt{2(1-cos(\pi\sqrt{P/P_e}))}}{sin(\pi\sqrt{P/P_e})} = \sec\left(\frac{\pi}{2}\sqrt{P/P_e}\right) \approx \frac{1}{1-\frac{P}{P_e}} \tag{5.9}$$

Therefore, Eq. (5.8) can be approximately expressed by

$$\frac{M_{max}}{M_2} \approx \frac{C_m}{1-\frac{P}{P_e}} \tag{5.10}$$

Note that M_{max} , M_2, and P correspondents to $M_{r2\text{-}E}$, M_{r1} and P_{r1} in Eq.(5.1), respectively.

Since the theoretical expression of C_m is impracticable for engineering design, a simplified linear expression for C_m has been proposed by Austin (1961), given by

$$C_m = 0.6\text{-}0.4(M_1/M_2) \tag{5.11}$$

where M_1 and M_2 are applied external end moments, $|M_1| \leq |M_2|$.

For sway-restrained beam-columns with transverse loadings, the Austin equation is adopted. It does not

consider material non-linearity, however, according to the research findings of Chen (Chapter 2 of Chen and Lui (2017)), the derived C_m considering material non-linearity is always lower than the solutions of Austin equation, which means C_m determined by Eq.(5.11) is conservative and safe for design. For sway-restrained beam-columns with transverse loadings between member ends, C_m is determined by equation C-A-8-4 provided in Commentary to Appendix 8 of AISC 360-16 (2016).

5.3 Maximum second order elastic moment within sway-permitted beam-columns

For sway-permitted elastic beam-columns, maximum internal elastic moment (for a storey) within different columns caused by P-Δ effects and together with P-δ effects may be determined by amplifying maximum first order moment (M_{r1}) through the factor $B_{2\text{-}E}$, given by Eq.(5.12). It is essentially the expression of evaluating P-Δ effects provided in Cheong-Siat-Moy (1977). The amplification factor $B_{2\text{-}E}$ in this paper is based on a similar definition of factor B_2 provided in Appendix 8 of AISC 360-16 (2016) for frames with lateral displacement between stories, where the influence of P-δ effects on the global behavior of the frame (including isolated beam-column) is considered indirectly through the factor R_M given by Eq. (5.14).

$$\frac{M_{r2-E}}{M_{r1}} \approx \frac{1}{1-\frac{P_{story}}{R_M P_{e*-story}}} = B_{2-E} \geq 1 \tag{5.12}$$

$$P_{e*-story} = \frac{F_H h}{\Delta} \tag{5.13}$$

$$R_M = 1 - 0.15\frac{P_{mf}}{P_{story}} \tag{5.14}$$

where P_{story} is total vertical load transferred by the story ($P_{story} = \sum P_{r1}$); $P_{e*\text{-}story}$ is elastic critical buckling (sway mode) strength of the story; $P_{e*\text{-}story}$ can be determined by side-sway buckling analysis or Eq.(5.13); F_H and Δ are first order total story shear force and relative story drift due to F_H, respectively; h is storey height; the factor R_M, accounts for P-δ effects on the overall response of the structure, $0.85 \leq R_M \leq 1$; P_{mf} is total vertical load in columns of the story that are part of moment frames. For isolated sway-permitted elastic beam-column, P_{story} is P_{r1} of the member; $P_{e*\text{-}story}$ is equal to P_{es}; $P_{es} = (\pi^{\wedge 2}\, EI)/(KL)^{\wedge 2}$; R_M=0.85.

It should be mentioned that $P_{e*\text{-}story}/P_{story}$ corresponds to the definition of $\alpha_{cr,sw}$ provided in EN1993-1-1: 2015(E); If R_M is taken as 1, $B_{2\text{-}E}$ then corresponds to second order sway effects factor K_{sw} provided in EN1993-1-1: 2015(E).

$$K_{sw} = \frac{1}{1-\frac{1}{\alpha_{cr,sw}}} \tag{5.15}$$

5.4 Development of analytical expression of τ_{MN}

Analytical expressions of stiffness reduction factor τ_{MN} for beam-columns are developed through extending the formulations (Eq.(5.1) and Eq.(5.12)) that evaluate second order effects for elastic beam-columns to inelastic range. These formulations are assumed to be applicable to determine maximum second order inelastic moment ($M_{r2\text{-}P}$) of beam-columns provided that flexural stiffness reduction factor τ_{MN} is incorporated into elastic critical buckling load. After $M_{r2\text{-}P}$ for studied beam-columns are obtained, τ_{MN} determined by the analytical expression is subsequently calculated.

For sway-restrained beam-columns including material non-linearity, through incorporating τ_{MN} into Eq.(5.1), it is obtained:

$$\frac{M_{r2-P}}{M_{r1}} \approx \frac{C_m}{1-\frac{P_{r1}}{P_{e-\tau MN}}} = B_{1-P} \geq 1 \tag{5.16}$$

where

$$P_{e-\tau MN} = \tau_{MN} P_{e1} = \frac{\pi^2(\tau_{MN} EI)}{l^2} \tag{5.17}$$

The amplification factor $B_{1\text{-}P}$ evaluates P-δ effects on maximum second order inelastic moment ($M_{r2\text{-}P}$).

Rewriting Eq.(5.16), the analytical solution of τ_{MN} can be expressed by

$$\tau_{MN} \approx \frac{P_{r1}}{(1-C_m\frac{M_{r1}}{M_{r2-P}})(P_{e1})} \tag{5.18}$$

Similarly, for sway-permitted beam-columns including material non-linearity, through incorporating τ_{MN} into Eq.(5.12), it gives

$$\frac{M_{r2-P}}{M_{r1}} \approx \frac{1}{1-\frac{P_{story}}{P_{e*-story-\tau MN}}} = B_{2-P} \geq 1 \tag{5.19}$$

where

$$P_{e*-story-\tau MN} = \tau_{MN} R_M P_{e*-story} \tag{5.20}$$

In Eq.(5.19), the amplification factor $B_{2\text{-}P}$ evaluates P-Δ effects and together with P-δ effects on $M_{r2\text{-}P}$; $M_{r2\text{-}P}$ (for a storey) is maximum internal second order moment within different columns in a storey.

Rewriting Eq.(5.19), τ_{MN} for sway-permitted inelastic beam-columns can be expressed by

$$\tau_{MN} \approx \frac{P_{story}}{(1-\frac{M_{r1}}{M_{r2-P}})(R_M P_{e-story})} \tag{5.21}$$

τ_{MN} determined by Eq.(5.18) and Eq.(5.21) accounts for influence of member out-of-straightness, residual stresses and spread of plasticity, provided that maximum second order inelastic moment ($M_{r2\text{-}P}$) in these equations are obtained from an analysis that includes corresponding out-of-straightness, residual stresses and material non-linearity.

Note that Eq.(5.21) is essentially the same as Eq.(5.18). The equivalent uniform moment factor C_m is implicitly included in Eq.(5.21) whereas it is explicitly used in Eq.(5.18). It should be stressed that, the concept of C_m is, by amplifying maximum first-order moment of pinned beam-column subjected to a pair of equal and opposite end moments, to obtain maximum total second order moment of beam-columns with different loading conditions (varied moment distribution along member) and different boundary conditions, as illustrated in Fig. 5.1. In Eq.(5.21), the influence of different loading conditions (moment distribution) and different boundary conditions is implicitly included in the ratio of $P_{story}/P_{e^*\text{-}story}$ (or P_{r1}/P_{es}), where the accuracy of $P_{e^*\text{-}story}$ (or P_{es}) depends on the column effective length (K) that amplifies the length of pinned column.

It is worth noting that although second order moments caused by P-δ or P-Δ effects may have different distribution to first order elastic moments (altering the location of maxima), one should keep in mind that member sizes are governed by the value of the maximum moment rather than the location of the maximum moment in practical design.

5.5 Verification of GNA with analytically determined τ_{MN}

This section verifies the accuracy of GNA with τ_{MN} determined by the proposed analytical expressions and demonstrates the soundness of the above-described assumption. A series of beam-columns including simply supported beam-columns, cantilever beam-columns, and beam-columns in structural sub-assemblages, are studied. All members bend about major axis.

Maximum second order moment within a member obtained from GMNIA and that obtained from GNA with τ_{MN} are denoted by $M_{r2\text{-}GMNIA}$ and $M_{r2\text{-}GNA\text{-}\tau MN}$, respectively. The target of verification study in this section is that $M_{r2\text{-}GNA\text{-}\tau MN}$ provided by GNA with τ_{MN}, where the value of τ_{MN} is determined by analytical

expressions, should tend towards, or close to $M_{r2\text{-}GMNIA}$ provided by GMNIA.

5.5.1 Steps for verification

Verification study for sway-restrained beam-columns and sway-permitted beam-columns are carried out through the following steps, illustrated in Fig.5.2.

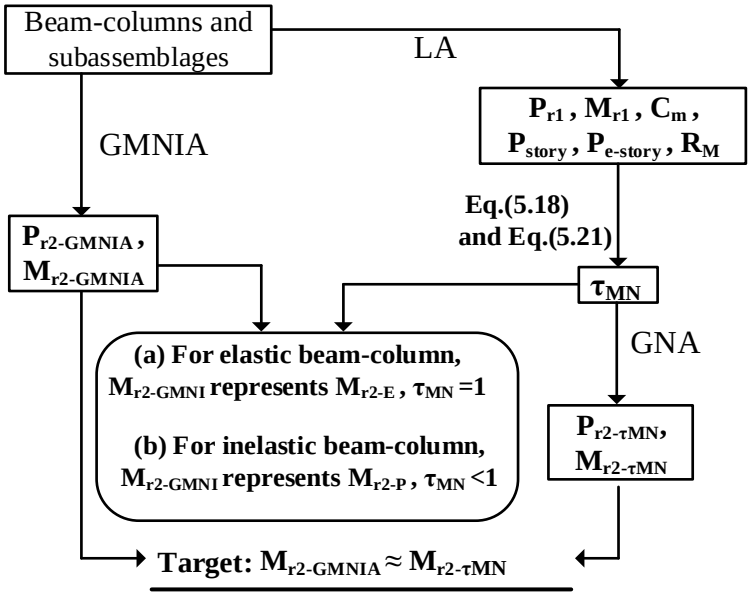

Fig.5.2 Procedure of verification study for beam-columns

Firstly, GMNIA analysis for beam-columns subjected to factored loading is conducted. Out-of-straightness of 0.001 is introduced to simply supported beam-columns and sway-restrained sub-assemblages while out-of-plumbness of 0.002 and out-of-straightness of 0.001 are introduced to cantilever beam-columns and sway-permitted sub-assemblages. Maximum second order moment and axial force within a member determined by GMNIA are denoted by $M_{r2\text{-}GMNIA}$ and $P_{r2\text{-}GMNIA}$, respectively. Secondly, Linear Elastic Analysis (LA) is conducted, where the applied loads are same to those in GMNIA. P_{r1}, M_{r1}, C_m, P_{story} , $P_{e^*\text{-}story}$ and R_M are obtained. Thirdly, analytical solutions of τ_{MN} for sway-restrained and sway-permitted beam-columns that experience inelastic stage are calculated according to Eq. (5.18) and Eq. (5.21). In such calculation, $M_{r2\text{-}P}$ is taken as $M_{r2\text{-}GMNIA}$. Note that for beam-columns in elastic stage, analytical solution of τ_{MN} is equal to unity. Fourthly, under the same load applied in GMNIA, GNA with τ_{MN} (denoted by GNA-τ_{MN}) is conducted. Maximum second order moment and axial force within a member obtained from GNA-τ_{MN} are denoted by $M_{r2\text{-}\tau MN}$ and $P_{r2\text{-}\tau MN}$, respectively. Out-of-straightness is not introduced in GNA-τ_{MN}, since the influence of out-of-straightness of 0.001 is intended to be included in the above τ_{MN}. Thus, when

conducting GNA-τ_{MN}, only out-of-plumbness of 0.002 is considered for cantilever beam-columns and sway-permitted sub-assemblages, while no geometric imperfection is considered for sway-restrained beam-columns. The material stress-strain curve for GNA-τ_{MN} does not include the effect of residual stress, because the influence of residual stresses is included in τ_{MN}. Lastly, $M_{r2\text{-}\tau MN}$ are verified against $M_{r2\text{-}GMNIA}$.

$M_{r2\text{-}GMNIA}$ contains both maximum second order elastic moment and maximum second order inelastic moment. In the elastic range, $M_{r2\text{-}GMNIA}$ refers to $M_{r2\text{-}E}$ of the member and the analytical solution of τ_{MN} is actually equal to 1, since both internal axial force and moments are small. With P_{r1} and M_{r1} increasing, the beam-column reaches to inelastic range, and consequently $M_{r2\text{-}GMNIA}$ represents $M_{r2\text{-}P}$ of the member.

5.5.2 Verification study for simply supported beam-columns and cantilever beam-columns

Firstly, simply supported beam-columns (shown in Fig. 5.3.) with cross-section 120x80x6 (E=175GPa, f_y=350MPa, n=7, and λ_c=0.65) are studied. The beam-columns are subjected to a combination of axial load (P) and moments (M_1, M_2) at the ends. P is a continuously factored load; M_2=e*P; "e" ranges from 5 to 150 (e= [5,10,20,30,50,100,150]) and the unit of e is mm; M_1=s*M_2; the non-dimensional factor s ranges from -1 to 1(s= [-1,-0.5,0, 0.5, 1]) ; $|M_2| \geq |M_1|$. For the simply supported beam-columns, one focus is whether the influence of non-uniform bending moments (moment gradient) on inelastic maximum second order moments is well captured by τ_{MN}. Non-uniform bending moments are produced by applying varied end moments. End moment variation is controlled by the non-dimensional factor s.

The normalized strength curves ($M_{u\text{-}GMNIA}/M_p$ versus $P_{u\text{-}GMNIA}/P_y$) provided by GMNIA are shown in Fig. 5.3 (a), where $P_{u\text{-}GMNIA}$ is the ultimate axial load for a given factor *e* and *s*, and the corresponding ultimate external moment (denoted by $M_{u\text{-}GMNIA}$) is equal to M_2. By varying "s", it can be observed that the benefit of moment gradient is considerable for the studied beam-columns.

Comparison of $M_{r2\text{-}GMNIA}$ against $M_{r2\text{-}\tau MN}$ for this cross-section is shown in Fig.5.3. (b). In this figure, $M_{r2\text{-}GMNIA}$ and $M_{r2\text{-}\tau MN}$ are normalized by maximum first order internal bending moment M_{r1} obtained from Linear Elastic Analysis (LA). Similarly maximum second order internal axial force $P_{r2\text{-}GMNIA}$ and $P_{r2\text{-}\tau MN}$ are normalized by cross-section yield strength (P_y). It is observed that for the case of uniform bending (s= -1), $M_{r2\text{-}\tau MN}$ values are in very close agreement with $M_{r2\text{-}GMNIA}$. For the cases of non-uniform bending moment

(s ≠-1), a slight discrepancy between $M_{r2\text{-}GMNIA}$ and $M_{r2\text{-}\tau MN}$ occurs in the inelastic range. For the studied simply supported beams, it can be concluded that GNA coupled with τ_{MN} determined by Eq.(5.18) gives accurate predictions. It indicates the above-described assumption for sway-restrained beam-columns is sound, and the influence of moment gradient on maximum second order inelastic moment is well captured by the analytical expression of τ_{MN}.

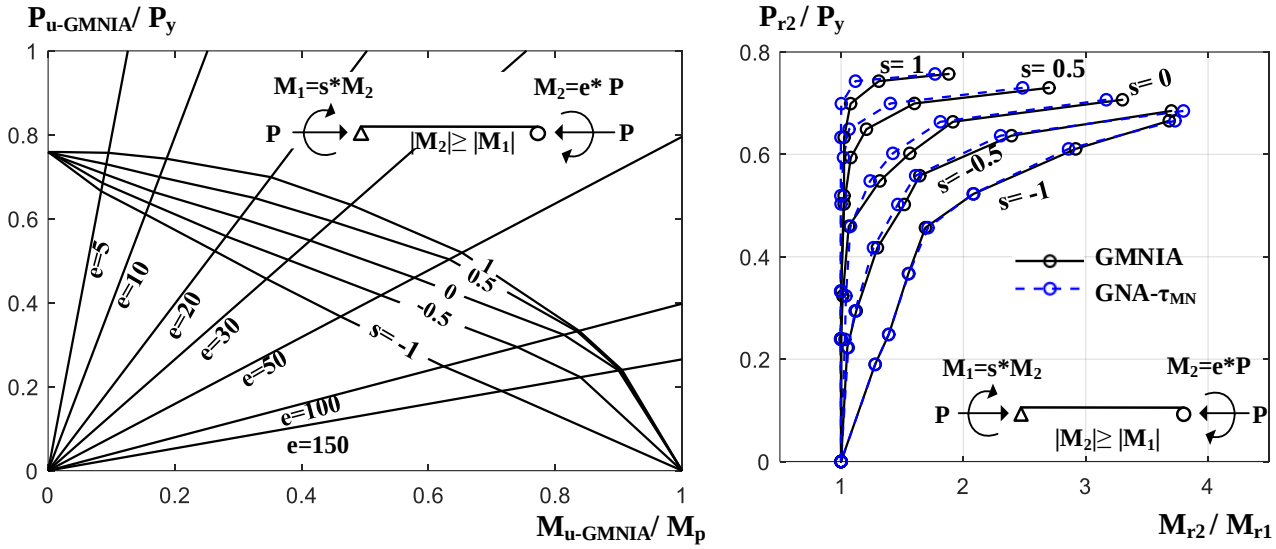

Fig.5.3 Predicted results for simply supported stainless steel beam-column (a) Strength curve under moment gradient obtained from GMNIA, (b) Comparison of maximum second order moment (M_{r2}) predicted by GMNIA and GNA-τ_{MN}

Secondly, cantilever beam-columns (shown in Fig.5.4) with cross-section 100x100x5 (E=180 GPa, fy=370MPa, and n=6), subjected to a combination of axial (P) and transverse (0.1P) loads at the cantilever end, are studied. The applied load P is discretely factored, where $P=i\ P_{u\text{-}GMNIA}$; i is less than 1 and it has 7 different values for each cantilever beam-column; $P_{u\text{-}GMNIA}$ is the ultimate axial load of a cantilever beam-column under the combined loading determined by GMNIA. The cantilever beam-columns have different column slenderness (λ_c): 0.73, 0.95, 1.1, 1.25, and 1.47.

Comparison of $M_{r2\text{-}GMNIA}$ and $M_{r2\text{-}\tau MN}$ is shown in Fig. 5.4. $M_{r2\text{-}GMNIA}$ and $M_{r2\text{-}\tau MN}$ are also normalized to M_{r1} and $P_{r2\text{-}GMNIA}$ and $P_{r2\text{-}GNA\text{-}\tau MN}$ are normalized by cross-section yield strength (P_y). Compared to P_y, the ultimate axial load of the studied cantilever beam-columns is relatively small, and consequently the ratio of P_{r2} to P_y is small, as observed. For cantilever beam-columns with varied column slenderness (λ_c), maximum second moments obtained from GNA-τ_{MN} agree well with those obtained from GMNIA. As the

applied axial load P increases, a slight discrepancy between $M_{r2\text{-}GMNIA}$ and $M_{r2\text{-}\tau MN}$ occurs in the inelastic range. For the studied cantilever beam-columns, it can be concluded that GAN with τ_{MN} determined by Eq.(5.21) gives accurate predictions. It demonstrates that the above assumption for sway-permitted beam-columns is reasonable and the analytically determined expression for τ_{MN} is accurate.

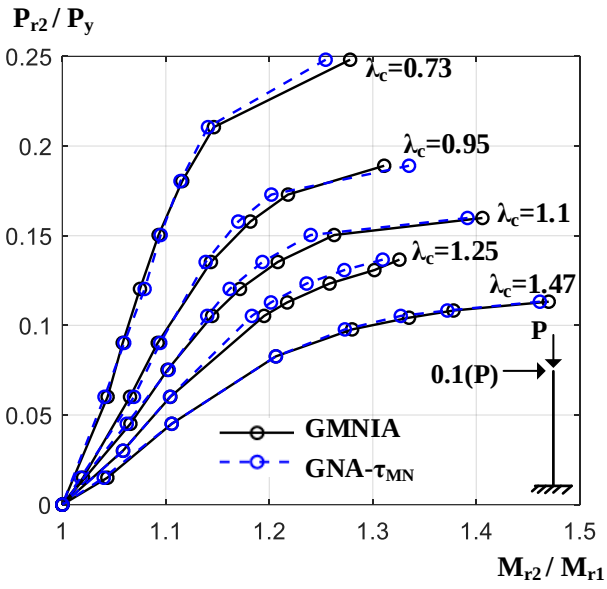

Fig. 5.4. Comparison of maximum second order moment predicted by GMNIA and GNA-τ_{MN} for cantilever beam-columns

Lastly, a series of simply supported and cantilever beam-columns with varied cross-sections and material properties, (shown in Table. 5.1) are studied. 3 different column slenderness (λ_c), where $0.5 \leq \lambda_c \leq 1.5$, are considered for each cross-section. The loading cases are shown in Fig. 5.5, where the applied axial load is factored load for all the cases, and the unit of the *e* is mm for the simply supported beam-columns. The accuracy of GNA-τ_{MN} is assessed using the newly defined parameter *ε*. $\varepsilon = M_{r2\text{-}GNA\text{-}\tau MN} / M_{r2\text{-}GMNIA}$. The predicted results are shown in Table. 5.1, where N_ε is the total number of ε for a particular group; ε_{av} and ε_{cov} indicate average values of ε and the coefficient of variation (COV). ε+ and ε- are the maximum and minimum value of ε in the group.

Table.5.1 Details of simply supported and cantilever beam-columns with varied cross-sections and material properties, and evaluation of predicted results of ε

Beam-column	Cross-section	Load case	E (GPa)	f_y (MPa)	n	W_{el}/W_{pl}	N_ε	ε_{av}	ε_{cov}	$\varepsilon+$	$\varepsilon-$
Simply supported	80x80x4	SL	200	300	6	0.85	105	0.99	0.008	1.03	0.97
	150x100x8		175	350	7	0.85	105	1.01	0.010	1.03	0.96
	160x80x8	SL-T	190	450	5	0.84	48	0.97	0.017	1.07	0.93
	150x150x8		190	400	7	0.79	48	1.05	0.021	1.08	0.95
Cantilever	80x60x4	CL	175	350	5	0.85	63	0.98	0.013	1.05	0.94
	200x200x10		175	450	7	0.82	63	1.03	0.010	1.06	0.95
	150x120x10		190	400	6	0.82	63	0.99	0.019	1.05	0.94

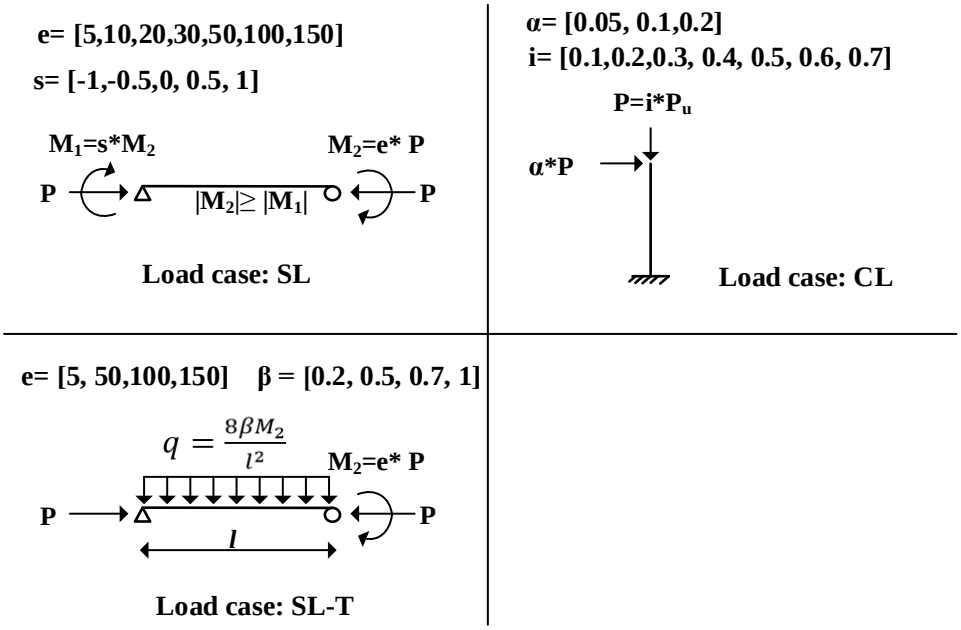

Fig.5.5 Load cases for studied beam-columns

It can be seen that, the COVs for the 60 beam-columns are about 0.008-0.021, which indicates a small scatter of the ratio of $M_{r2\text{-}\tau MN}$ / $M_{r2\text{-}GMNIA}$. The ε_{av} for all the beam-columns are about 0.97–1.05, which demonstrates that maximum internal second order moment determined by GNA-τ_{MN} are in very close agreement with those determined by GMNIA. The maximum $\varepsilon+$ and $\varepsilon-$ are 1.08 and 0.93, respectively. From the perspective of practical design, the maximum error of overestimation and underestimation of $M_{r2\text{-}GMNIA}$ are in acceptable range. From Table.5.1, it confirms again that GNA with τ_{MN} determined by the two analytical expressions gives accurate predictions and indicates that the above-described assumption for sway-restrained and sway-permitted beam-columns is sound.

5.5.3 Verification study for beam-columns in structural sub-assemblages

Further verification study is conducted for beam-columns in structural sub-assemblages. The studied beam-columns present double curvature in sway-restrained sub-assemblages (C1, shown in Fig. 5.6 (a)), beam-column with single curvature in sway-restrained sub-assemblages (C2, shown in Fig. 5.6 (b)), and beam-column with double curvature in sway-permitted sub-assemblages (C3, shown in Fig. 5.6 (c)).

Details of cross-section and material properties are shown in Table .5.2. Geometry and boundary conditions are shown in Fig. 5.6. Factored uniformly distributed loads (q) are applied on beams, concentrated loads (P) and bending moment (M) are applied on top and bottom of the columns, where P=qL; M=100mm*P; L is the length of the beam.

Table 5.2 Cross-section and material properties for the studied sub-assemblages

Sub-assemblage	Beam-column	Curvature	Cross-section	E (GPa)	f_y (MPa)	n	W_{pl}/W_{el}
Sway-restrained (a)	C1	double	120x80x6	200	300	6	1.23
		double	120x80x6	200	350	6	1.23
Sway-restrained (b)	C2	single	200x100x10	190	350	7	1.27
		single	200x100x10	175	455	7	1.27
Sway-permitted (c)	C3	double	150x100x10	190	400	7	1.25
		double	150x100x10	200	450	7	1.25

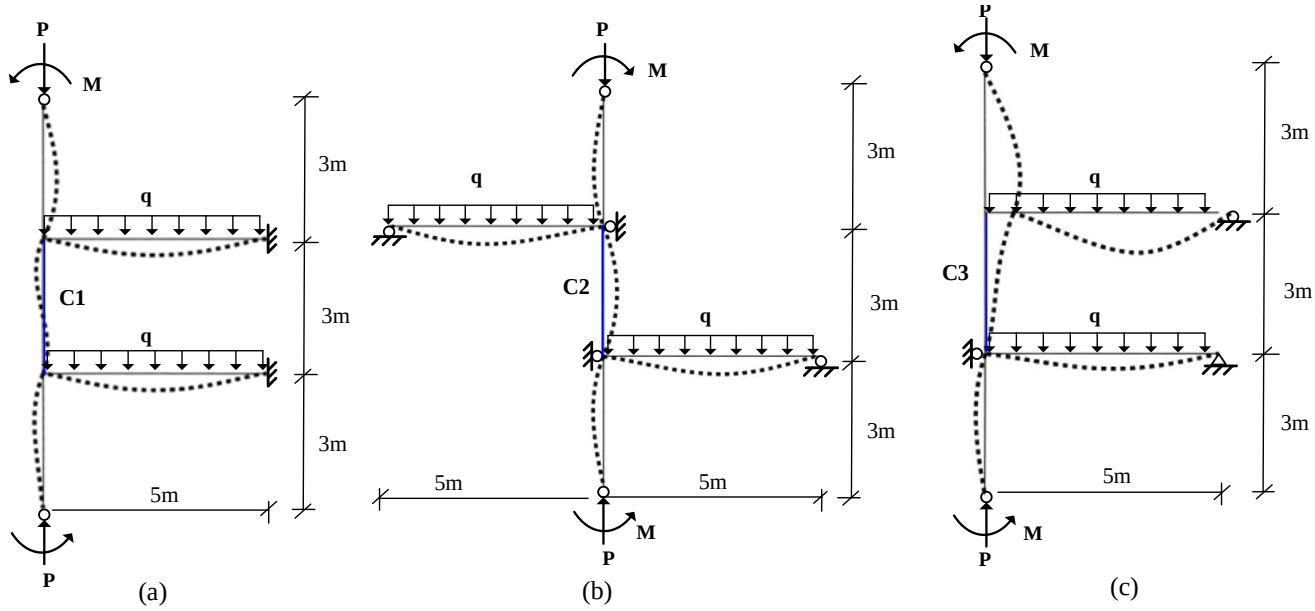

Fig. 5.6 (a) beam-column with double curvature (sway-restrained) (b) beam-column with single curvature (sway-restrained) (c) beam-column with double curvature (sway-permitted)

Comparison of $M_{r2\text{-}GMNIA}$ against $M_{r2\text{-}\tau MN}$ for studied beam-columns in all structural sub-assemblages is shown in Fig.5.7. In this figure, the vertical axis represents selected load ratios (λ). $M_{r2\text{-}GMNIA}$ and $M_{r2\text{-}\tau MN}$ are normalized by M_{r1} (determined by LA). It is observed that for all the cases, maximum second moments obtained from GNA-τ_{MN} is in close agreement with those obtained from GMNIA in both elastic and inelastic ranges. For beam-column C2, it seems that the discrepancy between $M_{r2\text{-}\tau MN}$ and $M_{r2\text{-}GMNIA}$ increases as the load ratio (λ) increases. However, it can be seen that the maximum error is within 5%. It can be concluded that GNA coupled with τ_{MN} determined by the above-described two analytical expressions provides accurate predictions for the studied beam-columns in structural sub-assemblages. It further demonstrates the extension of formulations for evaluating elastic second order effects to determine inelastic maximum second order moment is sound, provided that τ_{MN} is incorporated into elastic critical buckling load.

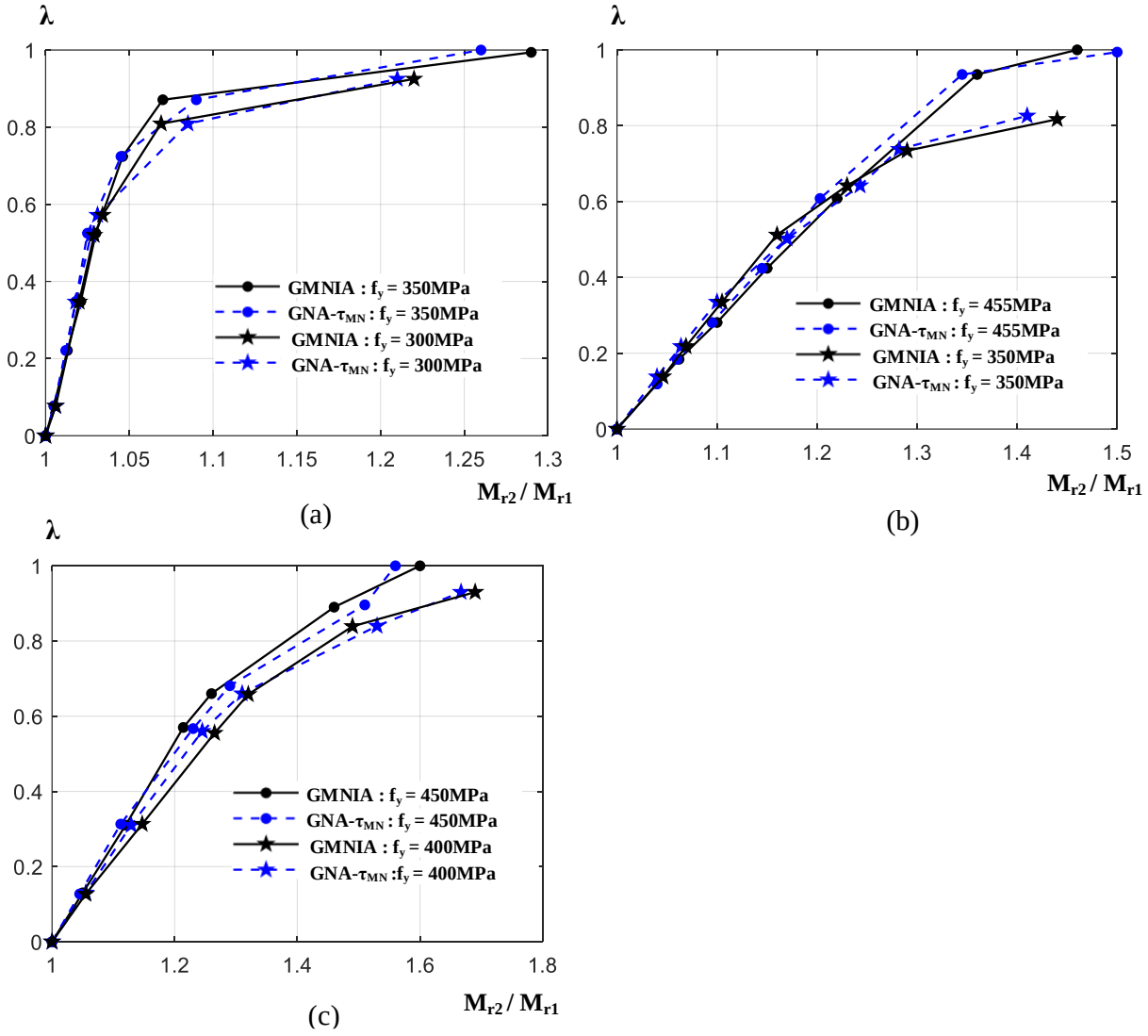

Fig.5.7 Comparison of the maximum second order moments predicted by GMNIA and GNA-τ_{MN} for the studied beam-columns in structural sub-assemblages (a) C1 (b) C2 (c) C3

5.6 Development of an approximate expression of τ_{MN}

Since the maximum second order internal moment ($M_{r2\text{-}P}$) is unknown in the actual design cases, the analytically determined τ_{MN} can not be applied directly. The aim of proposing the analytically determined τ_{MN} is to develop an approximate expression for τ_{MN} (has no relationship with $M_{r2\text{-}P}$) which can be applied in practice.

As flexural stiffness reduction factor of carbon steel beam-columns can be determined by a function that includes relevant variables without $M_{r2\text{-}P}$ (Kucukler et al., 2014, 2016, 2019; White et al., 2016), a function (approximate expression) independent of $M_{r2\text{-}P}$, which matches analytical expression of τ_{MN}, is proposed. The variables in the proposed approximate expression are: first order maximum axial force (P_{r1}), first order maximum bending moment (M_{r1}), equivalent uniform moment factor (C_m), cross-section shape factor (W_{el}/W_{pl}), second order effects factor ($B_{2\text{-}E}$), column flexural stiffness reduction factor τ_N (τ_N depends on the independent variable P_{r1}), beam flexural stiffness reduction factor τ_M (τ_M depends on the independent variable M_{r1} and material properties (E, f_y, and n)).

The approximate expression of τ_{MN} is developed by fitting variables to the analytical expressions determined by Eq.(18) and Eq.(21), as illustrated in Fig. 5.8. The fitting process is carried out through running codes in MATLAB (2017b). Since analytical solution of τ_{MN} accounts for member out-of-straightness of 0.001, residual stresses and spread of plasticity, these factors are consequently included in the approximate expression of τ_{MN}.

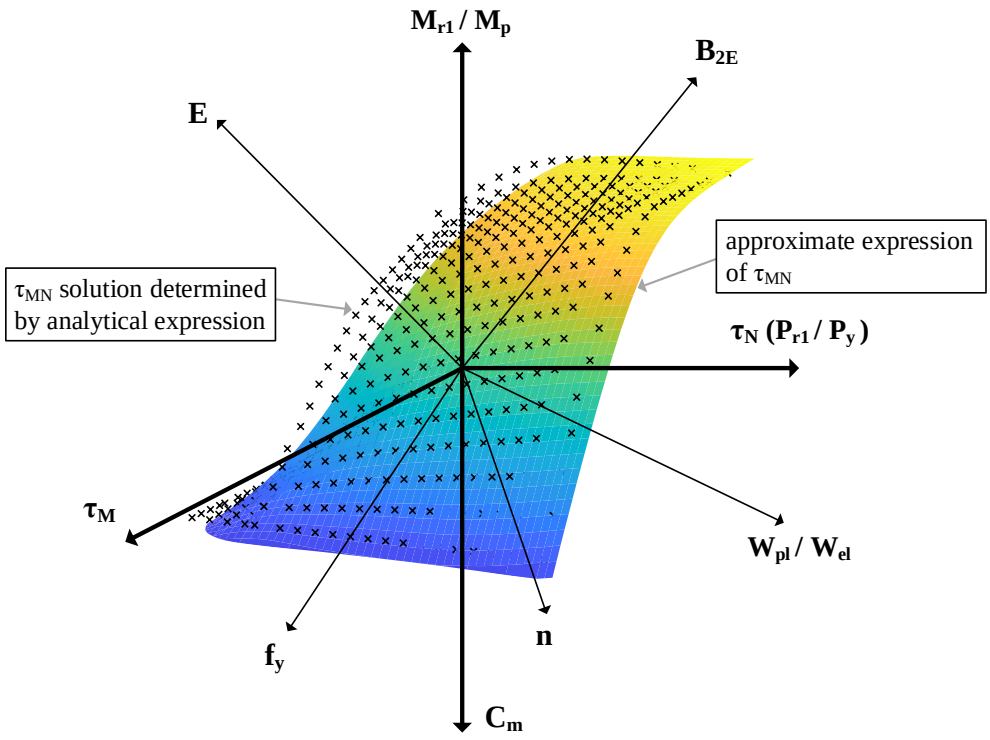

Fig. 5.8. Illustration of the development of the approximate expression of τ_{MN}

The approximate expression of τ_{MN} is given by Eq.(5.22). It is based on the numerical study of stainless steel beam-columns with a wide range of cross-sections, length, material properties, and boundary conditions. Uncertainty in material strength and stiffness is not considered here, since it is intended to be accounted through resistance factor ϕ_c and ϕ_b in beam-column interaction design equation.

$$\tau_{MN} = \gamma \Omega_M \tau_N \tau_M \left[1 - \left(\frac{P_{r1}}{P_y}\right)^{0.9} \left(C_m \frac{M_{r1}}{M_p}\right)^{\frac{W_{el}}{W_{pl}}}\right] \tag{5.22}$$

$$0.8 \leq \gamma = 2(B_{2-E} - 0.6) < 1 \quad \text{for } 1 \leq B_{2\text{-}E} < 1.1 \tag{5.23}$$

$$\gamma = 1 \quad \text{for } 1.1 \leq B_{2\text{-}E} \tag{5.24}$$

$$\Omega_M = 1 \quad \text{for } 0 \leq \frac{M_{r1}}{M_p} < 0.4 \tag{5.25}$$

$$\Omega_M = \left(0.6 + \frac{M_{r1}}{M_p}\right)^{1.4} \quad \text{for } 0.4 \leq \frac{M_{r1}}{M_p} \leq 1 \tag{5.26}$$

It should be noted that, for sway-restrained beam-columns, the factor $B_{2\text{-}E}$ is taken as 1. The proposed equation is affected by $B_{2\text{-}E}$ factor ($B_{2\text{-}E} \geq 1$). $B_{2\text{-}E} < 1.1$ means the increase of internal forces and moments due to P-Δ effects and together with P-δ effects can not be greater than 10%.

For the cases of $1 \leq B_{2\text{-}E} < 1.1$, when M_{r1} and P_{r1} are close to 0, the upper bound for τ_{MN} would be $\gamma \cdot \tau_N$ and $\gamma \cdot \tau_M$, respectively. For the cases of $1.1 \leq B_{2\text{-}E}$, when M_{r1} and P_{r1} are close to 0, the asymptotic upper bound of τ_{MN} is τ_N and τ_M, respectively. When $\gamma=1$ and $M_{r1}/M_p \leq 0.4$, Eq.(5.22) has the similar formation to beam-column stiffness reduction expression proposed by Kucukler et.al (2014).

A three-dimensional (3D) plot of τ_{MN} determined by Eq. (5.22) for beam-columns with two typical cross-sections is shown in Fig.5.9. For the beam-column with cross-section 150x100x8 (n=6, f_y=350MPa, E=200GPa), $B_{2\text{-}E}$ is assumed to be equal to 1.0 (sway-restrained, γ =0.8) and moment gradient factor C_m is assumed to be equal to 1.0 (subjected to a pair of equal but opposite end moments). For the beam-column with cross-section 150x150x10 (n=7, f_y=450MPa, E=190GPa), $B_{2\text{-}E}$ is assumed to be larger than 1.1 (sway-permitted, γ =1) and C_m is assumed to be equal to 0.6 (subjected to only one end moment).

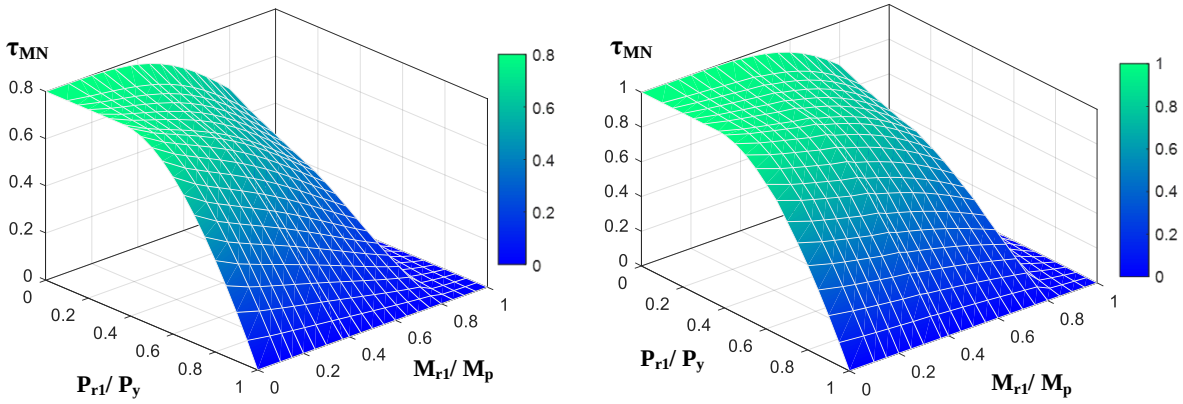

(a) (b)

Fig.5.9 3D plot of τ_{MN} for beam-columns (a) cross-section 150x100x8 (b) cross-section 150x150x10

A two dimensional (2D) plot of Eq.(5.22) for the case of sway-permitted beam-column with cross-section 120x80x6 (f_y = 350 MPa, E=200GPa, W_{el}/W_{pl}=0.798, and n=6) is shown in Fig. 5.10. In Fig. 5.10 (a), $B_{2\text{-}E}$ is assumed to be equal to 1.05 (γ =0.9) and equivalent uniform moment factor C_m is assumed to be equal to 1.0 (subjected to a pair of equal but opposite end moments). In Fig. 5.10 (b), $B_{2\text{-}E}$ is assumed to be higher than 1.1 (γ =1) and C_m =1.0. It can be observed that, when M_{r1} is close to 0, the asymptotic upper bound of τ_{MN} is $0.9\tau_N$ in Fig. 5.10 (a) and τ_N in Fig. 5.10 (b). The lower bound of τ_{MN} for different ratio of M_{r1}/M_p correspondents to cross-sectional Demand-Capacity ratio (R_c) being equal to unity , where R_c is determined by AISC-based beam-column design interaction equations (note that required axial force and moment here are taken as P_{r1} and M_{r1}). In the two figures, the dash line represents flexural stiffness reduction factor $0.8\tau_b$ for carbon steel provided in AISC 360-16 (2016).

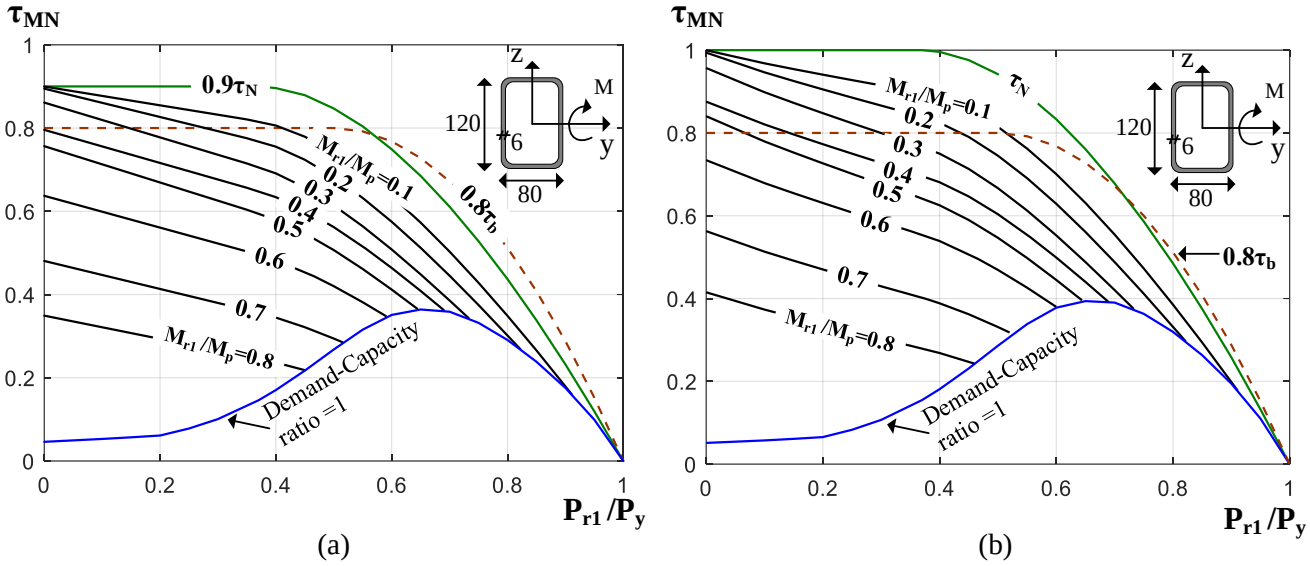

Fig.5.10. A 2D plot of the proposed stiffness reduction factor: (a) $B_{2\text{-}E}$ =1.05, C_m=1 (b) $B_{2\text{-}E}$ >1.1, C_m=1

5.7 Concluding remarks

In this chapter, the flexural stiffness reduction formulation for applying Geometrically Non-linear Analysis (GNA) to in-plane stability design of stainless steel beam-columns is proposed through analytical and numerical study. The proposed beam-column flexural stiffness reduction factor (τ_{MN}) accounts for deleterious influence of spread of plasticity, residual stresses and member out-of-straightness of 0.001. Two main aspects of developing τ_{MN} are: (1) Develop analytical expression of τ_{MN} through extending formulations that evaluate second order effects of beam-columns. These formulations are extended to determine maximum second order inelastic moment of beam-columns by incorporating τ_{MN} into elastic critical buckling load. (2) Based on numerical study of beam-columns, the approximate expression of τ_{MN} is developed by fitting relevant variables to analytically determined expression.

The soundness and accuracy of τ_{MN} determined by analytical expression are verified through comparison of maximum bending moments within members determined through GNA-τ_{MN} against those obtained from GMNIA. It is observed that predicted results from GNA-τ_{MN} are in very close agreement with those provided by GMNIA. Besides developing flexural stiffness reduction factor (τ_N, τ_M , τ_{MN}) formulations that are applicable to stainless steel members. Moreover, it is worth pointing out that the formulations of evaluating second order elastic effects are extended to determine inelastic maximum second order moment within beam-columns, through incorporating τ_{MN} into elastic critical buckling load.

6. Verification of GNA with τ_{MN} for stainless steel frames with compact sections

6.1 Introduction

In this chapter, the accuracy of GNA with flexural stiffness reduction formulation (τ_{MN}) to in-plane stability design of stainless steel frames is verified. The adopted τ_{MN} is determined by the approximate expression presented in the previous chapter. It accounts for the deleterious influence of spread of plasticity, residual stresses and member out-of-straightness of 0.001. The applicability of GNA using a stiffness reduction factor equal to $0.8\tau_N$, which is similar to the Direct Analysis Method (DM) provided in AISC 360-16 is also verified.

The study is focused on a series of stainless steel frames with different geometrical and loading configurations. Comparisons between GMNIA (full nonlinear analysis) and GNA coupled with stiffness reduction are provided. The main objectives of verification study are the comparisons of Demand-Capacity ratio and comparisons of maximum internal second order moment within members determined by:

- Geometrically and materially nonlinear analysis with imperfections: GMNIA
- Geometrically nonlinear analysis with stiffness reduction based on τ_{MN}: GNA-τ_{MN}
- Geometrically nonlinear analysis with stiffness reduction based on $0.8\cdot\tau_N$: GNA-τ_N

6.2 Description of the conducted analysis

GMNIA, GNA-τ_{MN} and GNA-τ_N are conducted. Details of the three methods are shown in Table.6.1. For GNA-τ_{MN}, since the influence of out-of-straightness of 0.001 and residual stresses are included in τ_{MN}, only out-of-plumbness of 0.002 is introduced to the frame models. Similarly, for GNA-τ_N, the influence of out-of-straightness and residual stresses are included in τ_N, only out-of-plumbness of 0.002 is introduced. It should be noted that out-of-straightness considered by τ_N is taken as 0.001, since τ_N is derived from the AISC LRFD-based column strength curve, where sinusoidal out-of-straightness of 0.001 is considered. In the implementation of GMNIA, out-of-plumbness of 0.002 and out-of-straightnes of 0.001 are introduced, and residual stress is considered through modified stress-strain curves. There is no need to conduct member

buckling strength check for internal forces and moments determined by the three methods since second order effects (P-Δ and P-δ) as well as initial geometric imperfections (out-of-plumbness, out-of-straightness) are accounted for.

Table 6.1 Details of GNA-τ_{MN} , GNA-τ_N and GMNIA

Analysis	P-Δ and P-δ effects	Material nonlinearity	Geometric imperfection		Residual stresses
			Out-of-plumbness	Out-of-straightness	
GMNIA	Captured	Captured	by notional load	by notional load	Considered in stress-strain curve
GNA-τ_{MN}	Captured	Implicitly included in τ_{MN}	by notional load	Considered in τ_{MN}	Considered in τ_{MN}
GNA-τ_N	Captured	Implicitly included in $0.8\tau_N$	by notional load	Considered in τ_N	Considered in τ_N

It should be mentioned that instead of direct modelling geometric imperfection, the effects of out-of-plumbness (Δ/h) and out-of-straightness (δ/L) are accounted for by means of applying notional loads (equivalent horizontal loads). Notional loads are applied to the directions that produce most destabilizing effects. Out-of-straightness is represented by concentrated notional loads and modelled in the direction that the members deforms in a preliminary Buckle Analysis through ABAQUS. For the columns that have double curvatures, the notional loads are applied in the mostly deformed direction. Out-of-plumbness is represented by concentrated notional loads and modelled in the direction of sway deformation. To avoid additional shear force at the frame base due to notional loads, corresponding horizontal reaction forces are applied.

6.3 Geometries and loads of the studied stainless steel frames

Two-bay two-storey frames with pinned end, three-bay three-storey frames with fixed end, and a two-bay five-storey frame with fixed end, are studied. All beam-to-column joints of the studied frames are rigid. The geometry of the studied frames are shown in Fig.6.1. The frames shown in Fig.6.1 (a), (b), and (c) are referred to as Frame-2X2, Frame-3X3 and Frame-2X5, respectively, and the presented load case is combination of wind load and gravity load. Members of Frame-2X2 have varied cross-sections, as shown in Fig.6.1, while all members of Frame-3X3 have same cross-section 200x100x10, and all members of

Frame-2X5 have same cross-section 250x150x10. The use of the same cross-section for all members in a frame is intended to obtain widely dispersed flexural stiffness reduction τ_{MN}. All beams and columns for the studied frames bend about major axis. Information related to design load combinations as well as to material properties are provided in Table. 6.2.

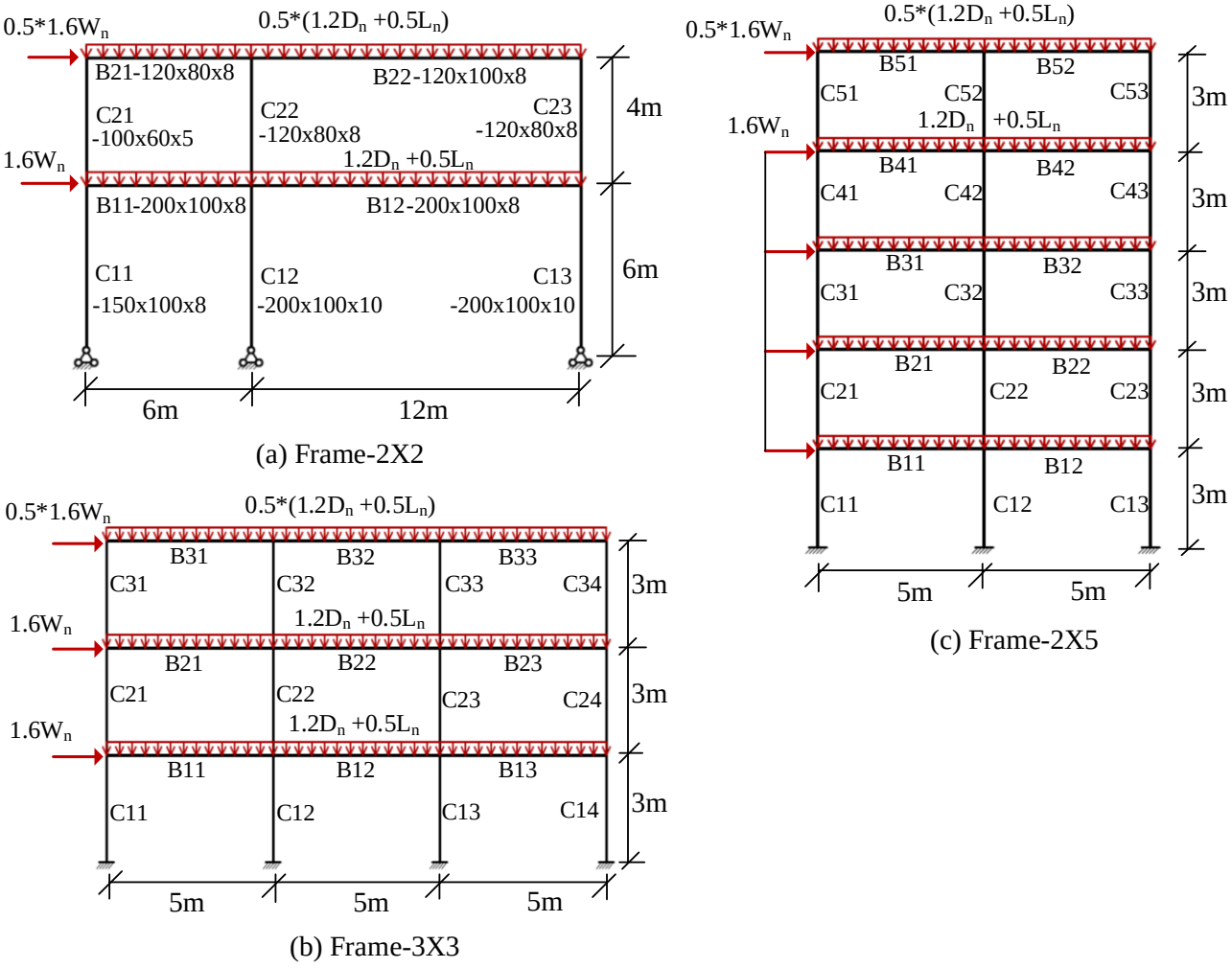

Fig.6.1 Studied stainless steel frame: (a) two bay-two storey frame, (b) three bay-three storey frame (c) two bay-five storey frame

Table. 6.2 Details of the studied frames

Frame	Load combination	Cross-section	E(GPa)	f_y (MPa)	n
Frame-2X2-G	$1.2D_n$ +$1.6L_n$	Varied	200	400	7
Frame-2X2-GW	$1.2D_n$+$0.5L_n$+$1.6W_n$	Varied	200	400	7
Frame-3X3-G	$1.2D_n$ +$1.6L_n$	200x100x10	175	450	6
Frame-3X3-GW	$1.2D_n$+$0.5L_n$+$1.6W_n$	200x100x10	175	450	6
Frame-2X5-GW	$1.2D_n$+$0.5L_n$+$1.6W_n$	250x150x10	190	450	7

For the 2x2 and 3x3 cases, two types of load combination provided in ASCE/SEI 7-16 (2016) are considered:

Gravity load combination $1.2D_n + 1.6L_n$, in which D_n and L_n denote nominal dead (gravity) load and nominal live (gravity) load, respectively, and the typical nominal live-to-dead load ratio $L_n/D_n = 1.5$. Combination of wind load and gravity load 1.2Dn+0.5Ln+1.6Wn, in which Wn denotes nominal wind load; live-to-dead load ratio Ln/Dn= 1.0, and wind-to-gravity load ratio Wn /(Ln+Dn)=0.1. For the 2x5 frame, one load case (wind load and gravity load 1.2Dn+0.5Ln+1.6Wn) is considered. Besides, for all the frames, the combined load applied on the top-storey is half of that applied on other storeys.

It should be mentioned that Frame-3X3-G, Frame-3X3-GW, and Frame-2X5-GW represent frames that have considerable load redistribution capacity after occurrence of first plastic hinge, where λ_u = 1.13, 1.20, and 1.21 for Frame-3X3-G, Frame-3X3-GW, and Frame-2X5-GW, respectively. λ_u is the ultimate load factor of the frame system, shown in the following section.

6.4 Procedure of implementing GNA-τ_{MN}, GNA-τ_N and GMNIA

The procedure of implementing GNA-τ_{MN}, GNA-τ_N and GMNIA is illustrated in Fig.6.2. Firstly, for the studied frames subjected to the assumed factored load, a GMNIA analysis is conducted. The applied load is defined as a design load for the Demand-Capacity ratio (R_c) of the critical member equal to 1.0. R_c is defined as the value of $\frac{P_{r2}}{\phi_c P_n} + \frac{8}{9}\frac{M_{r2}}{\phi_b M_n}$ or $\frac{P_{r2}}{2\,\phi_c P_n} + \frac{M_{r2}}{\phi_b M_n}$. Maximum internal second order moment within a member (M_{r2}), maximum internal second order axial force within a member (P_{r2}), and Demand-capacity ratio (R_c), determined by GMNIA, are denoted by $M_{r2\text{-}GMNIA}$, $P_{r2\text{-}GMNIA}$, and $R_{c\text{-}GMNIA}$ and thus defined as benchmark solutions. Secondly, under this design load, GMNIA is continued to obtain ultimate load factor (λ_u) of the frame system. Thirdly, a Linear Elastic Analysis (LA) under the design load is conducted to obtain P_{r1}, M_{r1}, P_{story}, $P_{e^*\text{-}story}$. Then τ_N, τ_M, C_m, R_M, $B_{2\text{-}E}$ are calculated according to relevant equations. τ_{MN} determined by Eq.(5.22) is subsequently calculated. Finally, under the design load, GNA-τ_{MN} and GNA-τ_N are conducted to obtain relevant maximum internal forces and moments, and Demand-Capacity ratios.

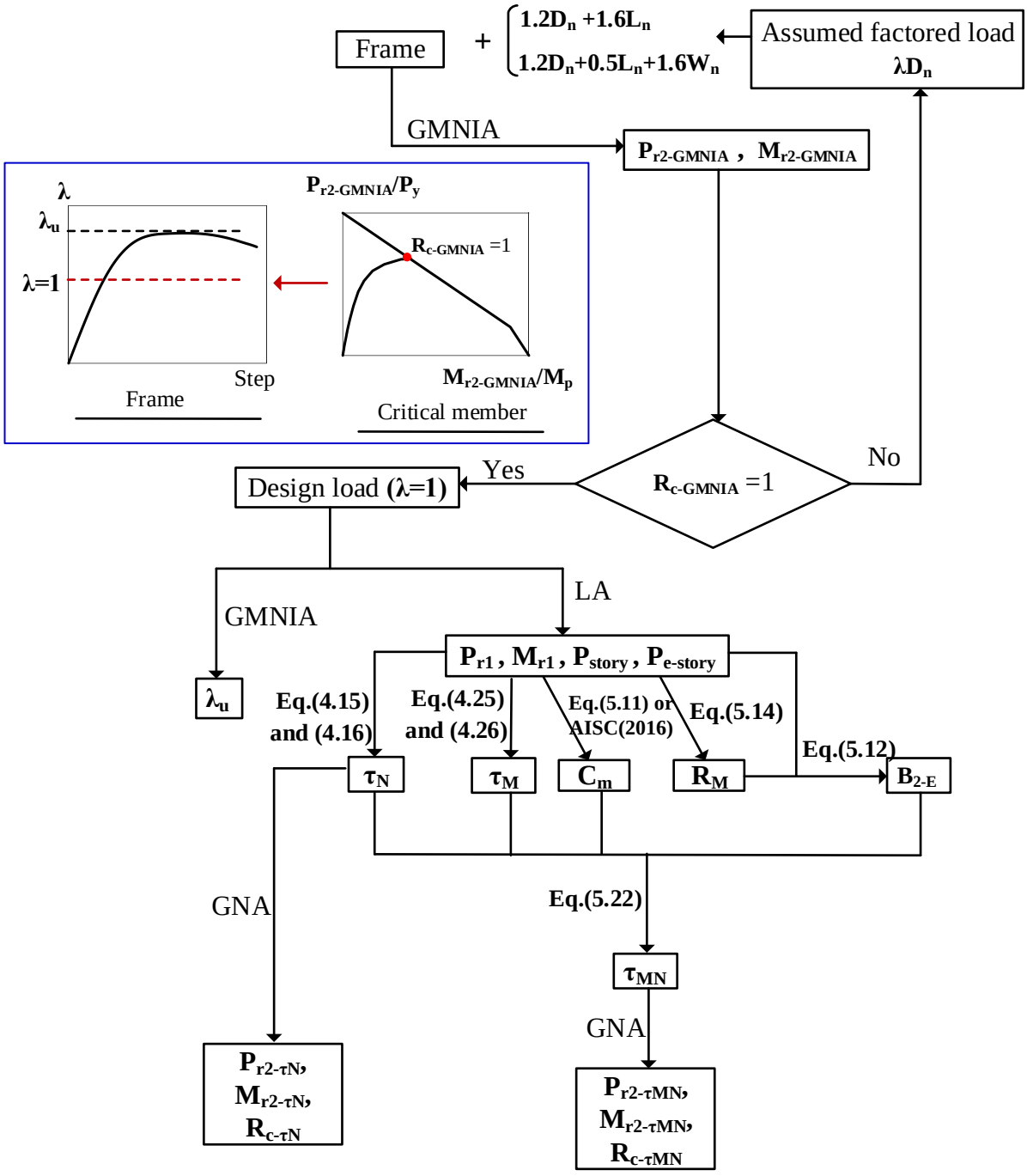

Fig.6.2 Procedure of conducting GNA-τ_{MN}, GNA-τ_N and GMNIA for studied frames

6.5 Predicted results from GNA-τ_{MN}, GNA-τ_N and GMNIA

Firstly, the relationship between the ratio of $M_{r2\text{-}GMNIA}/M_{r1}$ and the factors ($B_{2\text{-}E}$ and $B_{2\text{-}P}$) that evaluate second order effects is studied. Secondly, the accuracy of GNA-τ_{MN}, GNA-τ_N is assessed. Comparison of predicted results from different methods is mainly focused on Demand-capacity ratio (R_c) and Maximum internal second order moment (M_{r2}).

6.5.1 Relationship of $M_{r2\text{-}GMNIA}/M_{r1}$ and $B_{2\text{-}P}$ ($B_{2\text{-}E}$)

Predicted results of $M_{r2\text{-}GMNIA}/M_{r1}$, $B_{2\text{-}P}$ and $B_{2\text{-}E}$ for the studied frames are shown in Fig.6.3. In this figure, the horizontal axis represents specific member in the frame (for example, 1 correspondents to C11 and 10 correspondents to B22 for Frame-2X2).

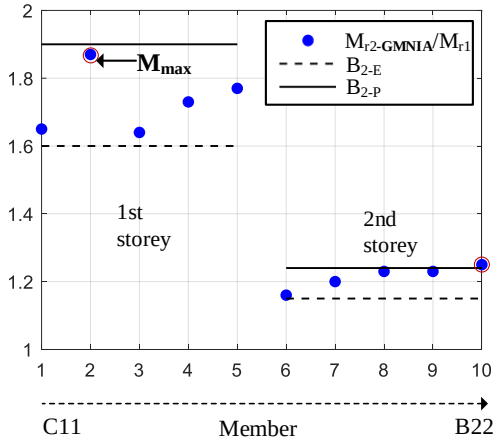

(a) Frame-2X2-G

C11	1
C12	2
C13	3
B11	4
B12	5
C21	6
C22	7
C23	8
B21	9
B22	10

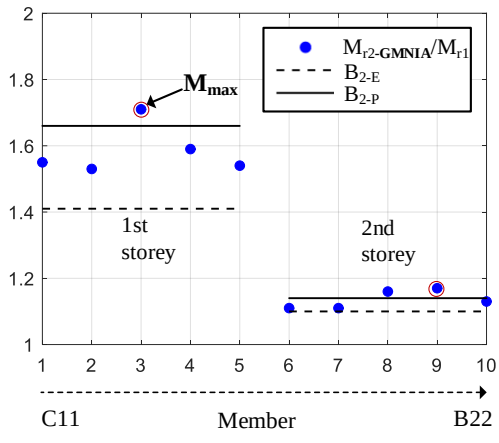

(b) Frame-2X2-GW

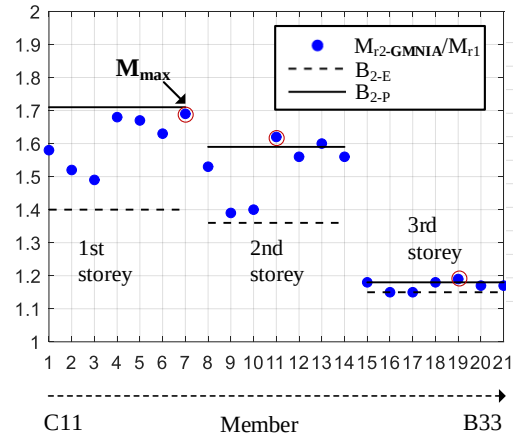

C11	1	B21	12
C12	2	B22	13
C13	3	B23	14
C14	4	C31	15
B11	5	C32	16
B12	6	C33	17
B13	7	C34	18
C21	8	B31	19
C22	9	B32	20
C23	10	B33	21
C24	11		

(c) Frame-3X3-G

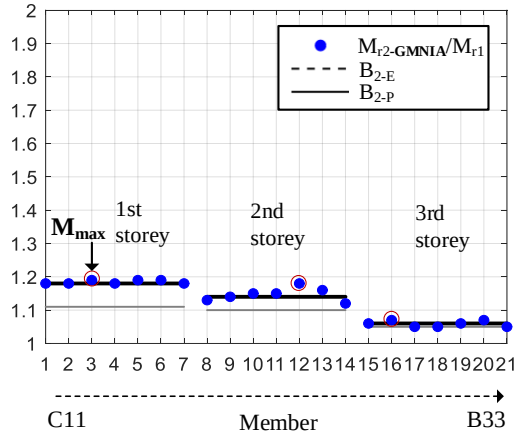

(d) Frame-3X3-GW

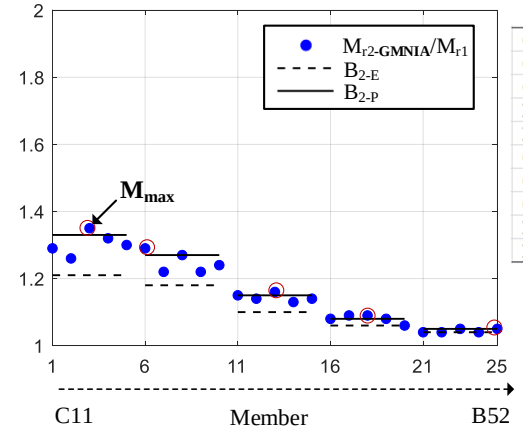

C11	1	C31	11	C51	21
C12	2	C32	12	C52	22
C13	3	C33	13	C53	23
B11	4	B31	14	B51	24
B12	5	B32	15	B52	25
C21	6	C41	16		
C22	7	C42	17		
C23	8	C43	18		
B21	9	B41	19		
B22	10	B42	20		

(e) Frame-2X5-GW

Fig.6.3 Predicted results of $M_{r2\text{-}GMNIA}/M_{r1}$, $B_{2\text{-}P}$ and $B_{2\text{-}E}$: (a) Frame-2X2-G (b) Frame-2X2-GW (c) Frame-3X3-G (d) Frame-3X3-GW (e) Frame-2X5-GW

Both $B_{2\text{-}E}$ and $B_{2\text{-}P}$ are calculated at storey levels. For the calculation of $B_{2\text{-}P}$, τ_{MN} from the member with the maximum ratio of $M_{r2\text{-}\mathbf{GMNIA}}/M_{r1}$ (denoted by $(M_{r2\text{-}\mathbf{GMNIA}}/M_{r1})_{max}$) within a storey is employed. If the $B_{2\text{-}E}$ factor of a storey is larger than 1.1, the increase of internal moments due to P-Δ effects and together with P-δ effects may be more than 10%, and the whole storey is regarded as sensitive to second order effects.

From Fig. 6.3, it is found that, for those storeys with high sensitivity to second order effects, such as the 1st storey of Frame-2X2-G which has a $B_{2\text{-}E}$ equal to 1.60, the $B_{2\text{-}P}$ factor is significantly higher than the $B_{2\text{-}E}$, compared to those storeys with lower sensitivity to second order effects. The discrepancy between $B_{2\text{-}E}$ and $B_{2\text{-}P}$ is resulted from additional second order effects due to material non-linearity, as illustrated in Fig. 6.4. After equilibrium is established, applying more load produces more deflections. Load combined with deformed (initial geometric imperfection) shape produces second order effects (P-Δ and P-δ effects). With load increasing, material yielding occurs through cross-section and along member. Material yielding leads to loss in flexural stiffness, results in increased deflections, and in turn produces additional second order effects. Equilibrium can be achieved until the structure becomes instable.

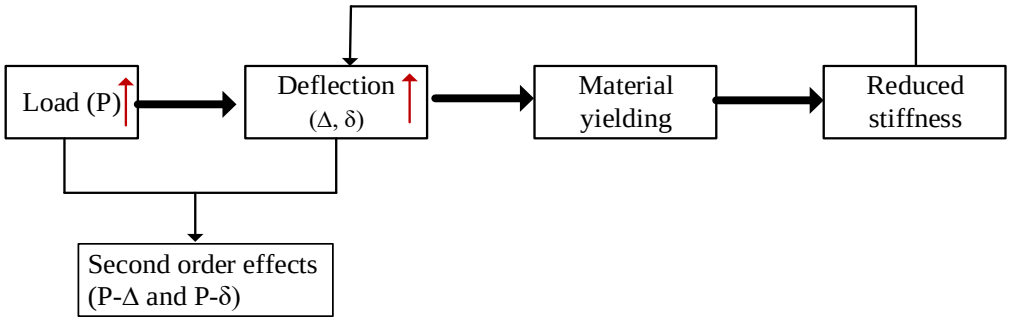

Fig. 6.4 Illustration of additional second order effects resulted from material non-linearity

From Fig. 6.3, it is observed that, for each storey of these frames, $(M_{r2\text{-}\mathbf{GMNIA}}/M_{r1})_{max}$ within different members in a storey is in very close agreement with $B_{2\text{-}P}$. There are considerable discrepancy between the ratio of $M_{r2\text{-}\mathbf{GMNIA}}/M_{r1}$ and $B_{2\text{-}P}$ for other members in a storey, especially for the storeys with a large $B_{2\text{-}E}$. This may be explained that $B_{2\text{-}P}$ is calculated based on storey-level, while $M_{r2\text{-}\mathbf{GMNIA}}/M_{r1}$ is calculated on member-level. Besides, the discrepancy between $M_{r2\text{-}GMNIA}/M_{r1}$ and $B_{2\text{-}P}$ also relies on the accuracy of the employed τ_{MN}. For the storeys with $B_{2\text{-}E}$ close to or less than 1.1, the ratio of $M_{r2\text{-}\mathbf{GMNIA}}/M_{r1}$of different members within a storey are close to $B_{2\text{-}E}$.

A plot of $B_{2\text{-}E}$ and $(M_{r2\text{-}\mathbf{GMNIA}}/M_{r1})_{max}$ for the five frames is shown in Fig.6.5. From this figure, the higher the $B_{2\text{-}E}$ factor is, the larger the discrepancy between $(M_{r2\text{-}\mathbf{GMNIA}}/M_{r1})_{max}$ and $B_{2\text{-}E}$ becomes. It indicates that

for the stability design of the frames with a large $B_{2\text{-}E}$ factor, the increase of internal second order moments caused by additional second order effects due to material nonlinearity is considerable and should be taken into consideration. Similar remarks have been reported in Walport et al. (2019).

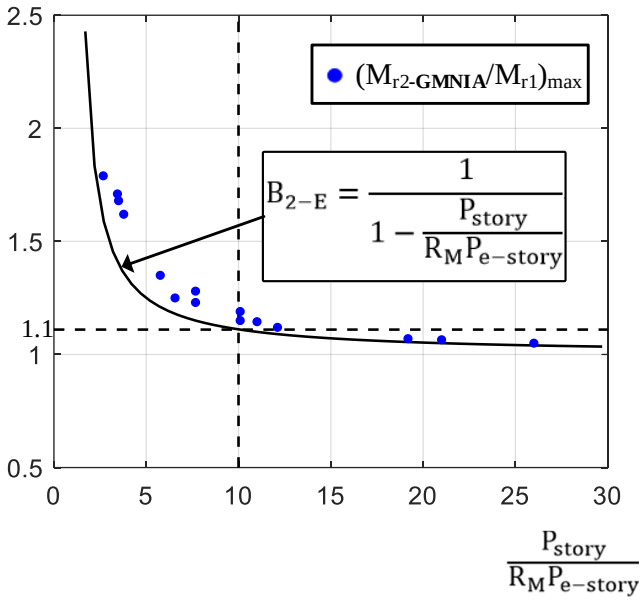

Fig. 6.5 A plot of $(M_{r2\text{-}GMNIA}/M_{r1})_{max}$ and $B_{2\text{-}E}$ against $P_{story}/R_M P_{e\text{-}story}$

6.5.2 Comparison of predicted results. 2X2-G and 2X2-GW

For 2X2-G and 2X2-GW, the ratio of axial force to cross-section yield strength of all the members is very small, and the Demand-Capacity ratio (R_c) of these members is very close to the ratio of maximum second moment to plastic moment (M_{r2}/M_P). Therefore, comparison of predicted results from different methods is focused on the ratio of $R_{c\text{-}\tau MN}$ /$R_{c\text{-}GMNIA}$ and $R_{c\text{-}\tau N}$ /$R_{c\text{-}GMNIA}$, where $R_{c\text{-}GMNIA}$, $R_{c\text{-}\tau MN}$ and $R_{c\text{-}\tau N}$ represent R_c determined by GMNIA, GNA-τ_{MN} and GNA-τ_N, respectively, as shown in Table. 6.3. In this table, μ represents mean value and COV represents coefficient of variation.

Table. 6.3: Predicted results for two-bay two-storey frames (members have varied cross-sections)

Member	Frame-2X2-G					Frame-2X2-GW				
	GMNIA	GNA-τ_{MN}		GNA-τ_N		GMNIA	GNA-τ_{MN}		GNA-τ_N	
	$R_{c\text{-}GMNIA}$	τ_{MN}	$R_{c\text{-}\tau MN}$ / $R_{c\text{-}GMNIA}$	$0.8\tau_N$	$R_{c\text{-}\tau N}$ / $R_{c\text{-}GMNIA}$	$R_{c\text{-}GMNIA}$	τ_{MN}	$R_{c\text{-}\tau MN}$ / $R_{c\text{-}GMNIA}$	$0.8\tau_N$	$R_{c\text{-}\tau N}$ / $R_{c\text{-}GMNIA}$
C11	0.24	0.81	1.11	0.80	1.03	0.88	0.72	1.05	0.80	0.99
C12	0.42	0.79	1.04	0.80	0.82	0.87	0.76	1.16	0.80	1.00
C13	0.27	0.72	1.18	0.80	0.89	0.90	0.68	0.99	0.80	1.03
B11	0.33	0.79	0.98	0.80	1.02	0.96	0.76	1.12	0.80	0.96
B12	0.87	0.76	1.07	0.80	0.97	1.00	0.64	1.04	0.80	0.99
C21	0.49	0.84	1.09	0.80	1.03	0.32	0.90	1.00	0.80	0.93
C22	0.68	0.77	1.16	0.80	0.99	0.16	0.90	0.99	0.80	0.86
C23	0.96	0.67	0.96	0.80	0.93	0.78	0.67	1.00	0.80	1.02
B21	0.50	0.7	1.09	0.80	1.01	0.64	0.69	1.12	0.80	0.99
B22	1.00	0.66	1.06	0.80	0.96	0.67	0.63	1.00	0.80	1.02
μ			1.07		0.97			1.05		0.98
COV			0.07		0.06			0.06		0.05
Max			1.18		1.03			1.16		1.03
Min			0.96		0.82			0.99		0.86

In Table 6.3, the value of τ_{MN} (determined by Eq.(5.22)) for different members is mainly dominated by the ratio of maximum first order moment to plastic moment (M_{r1}/M_P) and τ_M, since the ratio of axial force to cross-section yield strength of all the members is very small (τ_N =1) . For all members, the value of $0.8\tau_N$ is equal to 0.8. The critical members of both frames are beams whose failure is governed by the formation of first-plastic hinge (no elastic global buckling occurs in advance).

It is observed that both $R_{c\text{-}\tau MN}$ and $R_{c\text{-}\tau N}$ are in close agreement with $R_{c\text{-}GMNIA}$ for the two frames. Nevertheless, $R_{c\text{-}\tau N}$ underestimates $R_{c\text{-}GMNIA}$ for most members, which means that GNA-τ_N provides unsafe predictions for these members. It should be pointed out that, under the same design load, safe prediction and unsafe prediction refer to overestimating $R_{c\text{-}GMNIA}$ and underestimating $R_{c\text{-}GMNIA}$, respectively. If $R_{c\text{-}\tau MN}$ or $R_{c\text{-}\tau N}$ are larger than $R_{c\text{-}GMNIA}$, it means that the predicted internal moments or axial forces are overestimated compared against those predicted by GMNIA. For the critical members (B22 of Frame-2X2-G and B12 of Frame-2X2-GW), GNA-τ_{MN} gives accurate and safe predictions, while GNA-τ_N underestimates $R_{c\text{-}GMNIA}$ of the critical members to some extent (within 5%).

The difference in the predicted results may be explained as follows. Since the two frames are very sensitive to second order effects, where the maximum value of $B_{2\text{-}E}$ is 1.60 and 1.41 for Frame-2X2-G and Frame-2X2-GW, respectively, the increase of internal forces and moments resulted from additional second order effects are considerable. For GNA-τ_{MN}, the influence of additional second order effects due to material nonlinearity is well captured by the flexural stiffness reduction factor τ_{MN}, and therefore GNA-τ_{MN} gives improved predictions. From Table 6.3, τ_{MN} is smaller than $0.8\tau_N$ for most members and τ_{MN} for different members is not widely dispersed. It indicates that, for the two frames that are very sensitive to second order effects, a reduced flexural stiffness factor smaller than $0.8\tau_N$ should be adopted when using GNA-τ_N.

6.5.3 Comparison of predicted results. 3X3-G and 3X3-GW

Predicted results for the three-bay three-story rigid frame under gravity load combination (Frame-3X3-G) and under combination of wind load and gravity load (Frame-3X3-GW) are shown in Table 6.4 and Table 6.5, respectively. In table 6.4, $P_{r2\text{-}GMNIA}$, $P_{r2\text{-}\tau MN}$ and $P_{r2\text{-}\tau N}$ represent P_{r2} determined by GMNIA, GNA-τ_{MN} and GNA-τ_N, respectively; $P_{r2\text{-}\mathbf{GMNIA}}$ and $M_{r2\text{-}\mathbf{GMNIA}}$ are normalized by cross-section yield strength (P_y) and major axis plastic bending moment resistance (M_p), respectively. For Frame-3X3-GW, P_{r2} determined by different methods is not shown in Table 6.5, since the ratio of $P_{r2\text{-}\mathbf{GMNIA}}/P_y$ is small for all the members of the frame.

As expected, τ_{MN} for the two frames are widely dispersed, due to the reason that all members have the same cross-section but the distribution of first order axial forces and moments is varied within different members. Columns C12 and C13 of Frame-3X3-G are axially loaded to a high extent. The value of $0.8\tau_N$ for the two columns is 0.75. For all other members of the two frames, the value of $0.8\tau_N$ is equal to 0.8. For Frame-3X3-G, there are two critical members (B13 and B22).

Table 6.4: Predicted results for Frame-3X3-G

Member	GMNIA			GNA-τ_{MN}				GNA-τ_N			
	$P_{r2-GMNIA}/P_y$	$M_{r2-GMNIA}/M_P$	$R_{c-GMNIA}$	τ_{MN}	$P_{r2-\tau MN}/P_{r2-GMNIA}$	$M_{r2-\tau MN}/M_{r2-GMNIA}$	$R_{c-\tau MN}/R_{c-GMNIA}$	$0.8\tau_N$	$P_{r2-\tau N}/P_{r2-GMNIA}$	$M_{r2-\tau N}/M_{r2-GMNIA}$	$R_{c2-\tau N}/R_{c-GMNIA}$
C11	0.245	0.59	0.77	0.72	0.99	0.98	0.98	0.80	0.97	0.94	0.95
C12	0.505	0.17	0.66	0.78	1.00	0.95	0.99	0.75	1.01	0.99	1.01
C13	0.503	0.19	0.67	0.79	1.01	1.09	1.03	0.75	1.02	1.06	1.03
C14	0.249	0.62	0.80	0.72	0.98	0.99	0.99	0.80	0.96	0.97	0.97
B11	0.013	0.87	0.87	0.66	1.14	1.10	1.10	0.80	0.99	1.01	1.01
B12	0.011	0.97	0.97	0.61	1.15	1.03	1.03	0.80	1.06	0.93	0.93
B13	0.012	0.99	1.00	0.69	1.12	1.12	1.12	0.80	0.96	1.07	1.07
C21	0.146	0.43	0.50	0.76	1.00	1.14	1.12	0.80	0.98	1.02	1.01
C22	0.303	0.11	0.40	0.9	1.01	0.97	0.99	0.80	1.01	0.91	0.99
C23	0.302	0.13	0.42	0.93	1.01	1.09	1.03	0.80	1.01	1.01	1.01
C24	0.149	0.48	0.55	0.71	0.99	1.08	1.07	0.80	0.97	0.99	0.99
B21	0.007	0.98	0.98	0.68	0.97	1.11	1.11	0.80	0.98	1.00	1.00
B22	0.007	0.99	0.99	0.74	1.07	1.05	1.05	0.80	1.11	1.09	1.09
B23	0.007	0.98	0.98	0.74	1.12	1.08	1.08	0.80	0.88	0.98	0.98
C31	0.047	0.47	0.49	0.86	1.02	1.02	1.02	0.80	1.01	0.93	0.93
C32	0.102	0.09	0.14	1.00	0.99	1.10	1.06	0.80	1.00	1.11	1.07
C33	0.102	0.05	0.10	1.00	1.00	1.05	1.02	0.80	0.97	1.04	1.00
C34	0.049	0.44	0.46	0.86	0.99	1.08	1.08	0.80	1.01	0.94	0.94
B31	0.013	0.63	0.63	0.88	1.07	0.99	0.99	0.80	0.97	0.98	0.98
B32	0.012	0.61	0.61	0.89	1.07	0.98	0.98	0.80	0.93	1.01	1.01
B33	0.012	0.48	0.48	0.92	1.08	1.14	1.14	0.80	0.97	0.91	0.91
μ					1.04	1.05	1.05		0.99	0.99	0.99
COV					0.06	0.06	0.05		0.04	0.06	0.05
Max					1.15	1.14	1.14		1.11	1.11	1.09
Min					0.97	0.95	0.98		0.88	0.91	0.91

Table 6.5: Predicted results for Frame-3X3-GW

Member	GMNIA		GNA-τ_{MN}			GNA-τ_N		
	$M_{r2\text{-}GMNIA}/M_P$	$R_{c\text{-}GMNIA}$	τ_{MN}	$M_{r2\text{-}\tau MN}/M_{r2\text{-}GMNIA}$	$R_{c\text{-}\tau MN}/R_{c\text{-}GMNIA}$	$0.8\tau_N$	$M_{r2\text{-}\tau N}/M_{r2\text{-}GMNIA}$	$R_{c\text{-}\tau N}/R_{c\text{-}GMNIA}$
C11	0.73	0.76	0.66	1.09	1.08	0.80	0.95	0.95
C12	0.80	0.89	0.65	1.01	1.01	0.80	0.99	0.99
C13	0.79	0.88	0.62	1.03	1.03	0.80	1.04	1.03
C14	0.80	0.85	0.65	1.03	1.03	0.80	1.02	1.02
B11	0.97	0.99	0.59	1.10	1.10	0.80	1.07	1.06
B12	0.85	0.86	0.61	1.05	1.05	0.80	0.98	0.98
B13	0.88	0.88	0.66	1.04	1.04	0.80	1.04	1.04
C21	0.19	0.20	0.82	1.07	1.08	0.80	0.96	1.01
C22	0.55	0.60	0.69	1.10	1.09	0.80	1.00	1.01
C23	0.53	0.59	0.70	1.08	1.07	0.80	0.98	0.97
C24	0.56	0.59	0.68	1.09	1.09	0.80	1.00	1.00
B21	0.74	0.75	0.64	1.01	1.02	0.80	1.03	1.04
B22	0.71	0.71	0.59	1.06	1.06	0.80	0.99	0.99
B23	0.69	0.69	0.61	1.10	1.10	0.80	1.01	1.02
C31	0.18	0.19	0.91	1.07	1.06	0.80	1.03	1.01
C32	0.25	0.27	0.89	1.06	1.05	0.80	0.98	0.97
C33	0.22	0.24	0.89	1.05	1.05	0.80	0.97	0.96
C34	0.31	0.32	0.87	1.03	1.03	0.80	0.98	0.98
B31	0.34	0.34	0.85	1.05	1.05	0.80	1.02	1.03
B32	0.31	0.31	0.87	1.10	1.10	0.80	0.99	0.99
B33	0.29	0.29	0.88	1.02	1.02	0.80	0.99	1.01
μ				1.06	1.06		1.00	1.00
COV				0.03	0.03		0.03	0.03
Max				1.10	1.10		1.07	1.06
Min				1.01	1.01		0.95	0.95

From Table 6.4 and 6.5, it is observed that predicted results from both GNA-τ_{MN} and GNA-τ_N are in close agreement with those determined by GMNIA. For the critical members, both GNA-τ_{MN} and GNA-τ_N give safe predictions, where the maximum error of overestimating $R_{c\text{-}GMNIA}$ is 12% for GNA-τ_{MN} and 9% for GNA-τ_N. It should be noted that, GNA-τ_N gives safe predictions for Frame-3X3-G that is also very sensitive to second order effects. It is contrary to the predicted results of the 2X2 frames. One possible explanation is, besides the influence of additional second order effects, the increase of internal forces and moments is affected by distribution of internal force and moment, which may be related to the configuration of a structure. Note that the distribution of internal force and moment here is different to redistribution of internal force and moment after the formation of first plastic hinge for statically indeterminate structures.

The Coefficient of Variation (COV), absolute value of maximum error caused by underestimation and maximum error caused by overestimation, for $P_{r2,}$ M_{r2} and R_c predicted by GNA-τ_{MN}, are generally smaller than those predicted by GNA-τ_N. It shows that the predicted results of GNA-τ_{MN} have lower deviation from predicted results of GMNIA, and indicates that GNA-τ_{MN} provides improved estimation of internal forces, moments and Demand-capacity ratios for the studied frames. This is due to the reason that τ_{MN} can more accurately capture stiffness reduction caused by spread of plasticity through cross-sections and along members. The accurate stiffness reduction for different members leads to reasonable distribution of internal force and moment and well captures additional second order effects due to material non-linearity. It should be mentioned that GNA-τ_N, with COV ranging from 0.03 to 0.06, and μ around 1.0, also predicts results with acceptable errors for the studied frames.

Compared to the predicted results for the frames that are sensitive to second order effects (Frame-2X2-G, Frame-2X2-GW, Frame-3X3-G), both GNA-τ_{MN} and GNA-τ_N give more accurate predictions for Frame-3X3-GW that is not sensitive to second order effects. One possible explanation is additional second order effects caused by spread of plasticity are not considerable. Consequently, the increase of internal forces and moments is not dominated by material nonlinearity whose influence is accounted for through the flexural stiffness reduction factor (τ_{MN} or $0.8\tau_N$).

6.5.4 Comparison of predicted results. 2X5-GW

Predicted results for Frame-2X5-GW are shown in Fig. 6.6. In this figure, the horizontal axis represents specific member in the frame (for example, 1 correspondents to C11, and 25 correspondents to B52); P_{r2}, M_{r2} and R_c determined by GNA-τ_{MN} and GNA-τ_N are compared against those determined by GMNIA.

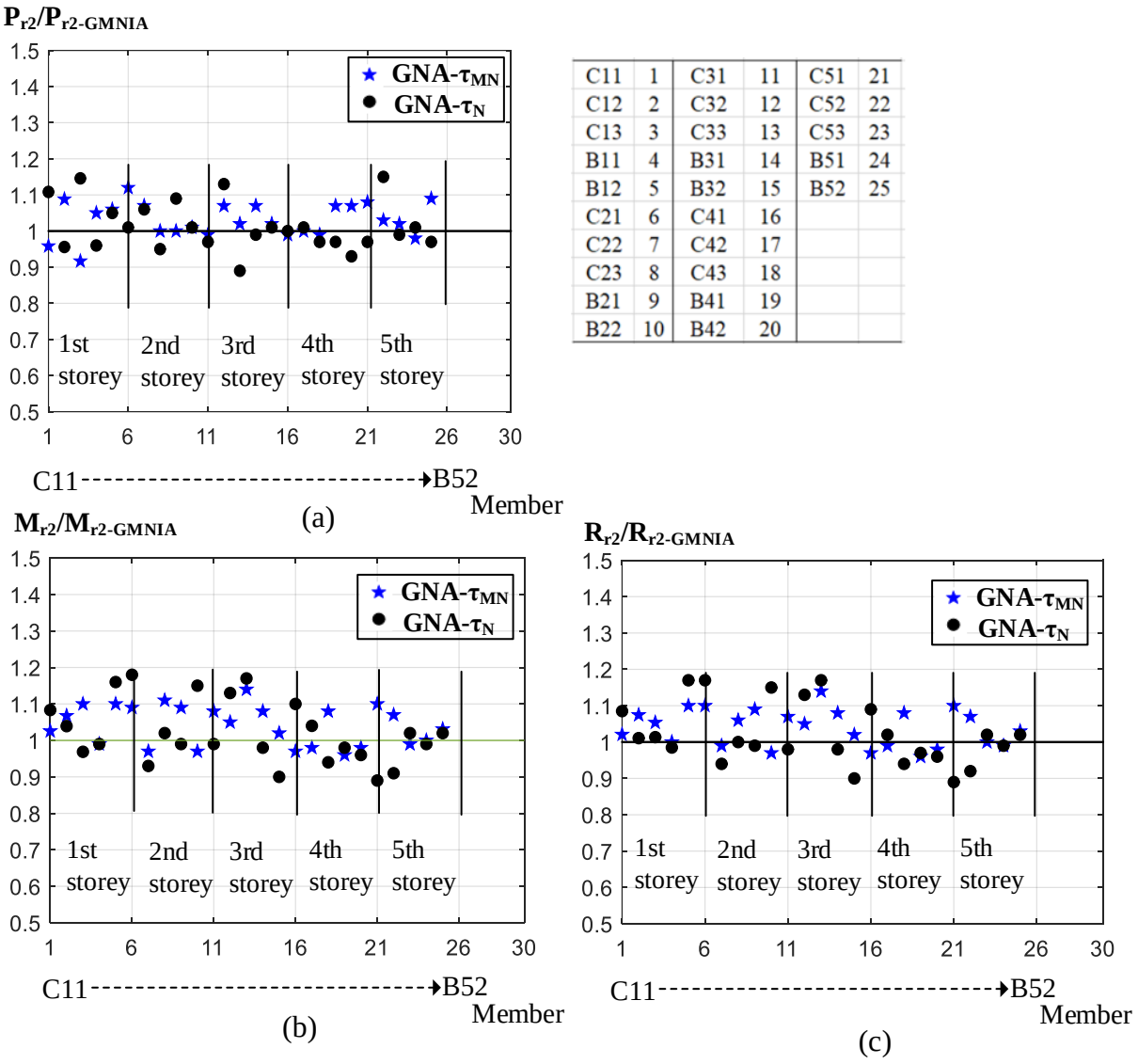

C11	1	C31	11	C51	21
C12	2	C32	12	C52	22
C13	3	C33	13	C53	23
B11	4	B31	14	B51	24
B12	5	B32	15	B52	25
C21	6	C41	16		
C22	7	C42	17		
C23	8	C43	18		
B21	9	B41	19		
B22	10	B42	20		

Fig. 6.6 Comparison of the predicted results determined by GNA with stiffness reduction against those determined by GMNIA for Frame-2X5-GW (a) P_{r2} of different members (b) M_{r2} of different members (b) R_c of different members

The studied Frame-2X5-GW is not sensitive to second order effects. It is seen that, from the 3rd storey up to the top storey, the distribution of R_{c}-τ_{MN}/ $R_{c\text{-}GMNIA}$ (or R_{c}-τ_N/ $R_{c\text{-}GMNIA}$) is in very close agreement with the distribution of M_{r2}-τ_{MN}/ $M_{r2\text{-}GMNIA}$ (or M_{r2}-τ_N/ $M_{r2\text{-}GMNIA}$). This is due to the reason that, for the columns in these storeys, the ratio of axial force to cross-section yield strength is small, and thus R_c is dominated by M_{r2}.

It is observed that, for the critical member (C12), both GNA-τ_{MN} and GNA-τ_N provide accurate and safe predictions. GNA-τ_{MN} gives a maximum error of overestimation (safe) of $R_{c\text{-}GMNIA}$ within 13% for other

members, where slight error of underestimation of $R_{c\text{-}GMNIA}$ is found for few members. GNA-τ_N gives predictions with acceptable errors for most members, but it produces large errors for few members, for example, overestimation of $M_{r2\text{-}GMNIA}$ nearly 20% for B11. Compared to GNA-τ_N, GNA-τ_{MN} gives improved predictions.

It is found that, M_{r2} and R_c determined by GNA-τ_{MN} are generally higher than those determined by GMNIA. This may be explained that τ_{MN} determined by the approximate expression is conservative. The conservative stiffness reduction produces more deformations, which in turn results in increased second order effects (P-Δ and P-δ) and subsequently increased internal bending moment and Demand-capacity ratio.

6.6 Concluding remarks

The accuracy of GNA coupled with flexural stiffness reduction factor to in-plane stability design of stainless steel frames is verified. The maximum bending moment and Demand-Capacity ratio within a member determined by GNA-τ_{MN} and GNA-τ_N are compared against those determined by GMNIA. It is found that predicted results of GNA-τ_{MN} are in close agreement with those provided by GMNIA. In some cases, GNA-τ_N gives unsafe predictions for the frames that are very sensitive to second order effects, one possible explanation is the adopted stiffness reduction factor $0.8\tau_N$ underestimates actual reduced stiffness, and therefore underestimates additional second order effects resulted from material non-linearity. Both GNA-τ_{MN} and GNA-τ_N are safe for predicting the ultimate capacity (member-based) of the studied frames that are not sensitive to second order effects. Compared to GNA-τ_N, GNA-τ_{MN} with lower deviation from predicted results of GMNIA, provides improved estimation of internal moments and Demand-Capacity ratios for most members. This is due to the reason that τ_{MN} can accurately capture stiffness reduction caused by spread of plasticity through cross-section and along members. As a consequence, GNA-τ_{MN} produces more reasonable distribution of internal force and moment, and well captures additional second order effects due to material non-linearity.

7. Flexural stiffness reduction factor accounting for local buckling effects

7.1 Introduction

In this chapter, for stainless steel elements with non-compact and slender sections, the stiffness reduction formulations presented previously are extended using a similar approach to the one adopted in AISC 360-16 (2016). For the determination of column flexural stiffness reduction factor (τ_N), beam flexural stiffness reduction factor (τ_M), beam-column flexural stiffness reduction factor (τ_{MN}), the cross-sectional resistance is reduced by an additional coefficient that accounts for local buckling effects.

Non-compact section here refers to cross-section that is able to reach the yield stress (0.2% proof stress) in its compression elements before inelastic local buckling occurs, but is unable to develop fully plastic stress distribution due to local buckling. Slender section here refers to cross-section in which inelastic local buckling will occur in the range between proportional limit (0.01% proof stress) and yield stress (0.2% proof stress). According to Design Manual for Structural Stainless steel (2017), the proportional limit of stainless steels ranges from 40% to 70% of the 0.2% proof strength. Cross-sections in which elastic local buckling occurs below proportional limit are not considered in this paper. The studied cross-sections are cold-formed rectangular hollow section (RHS) and square hollow section (SHS). Due to the nonlinear stress-strain characteristics of stainless steel, the limiting width-to-thickness ratios for stainless steel given in AISC Design Guide 27: Structural Stainless Steel (2013) differ from those given for carbon steel in AISC 360-16 (2016).

7.2 Reduction factors for considering local buckling effects

In general, reduction factors accounting for local buckling effects for compression elements can be determined by two approaches, the Effective Width Method (EWM) and Direct Strength Method (DSM). EWM, which is firstly proposed by von Karman (1932), extended and improved by Winter (1970), has been adopted in many design codes and specifications worldwide. The reduction factor formulations based on EWM may vary slightly in different design codes and specifications. DSM, which is originally proposed by Schafer (2000, 2019), has already been adopted in AISI S100-16 (2016) and AS/NZS4600 (2005). The reduction factor determined by DSM is hereafter referred to as ρ, while the reduction factor implicitly

provided in AISC 360-16 (2016) is referred to as ρ*.

It should be pointed out that, since the reduction factor formulations determined by EWM and DSM were calibrated against experimental results, the influence of initial localized imperfection are implicitly included in the reduction factor.

7.2.1 Reduction factor determined by DSM

(1) ρ for members in compression

For members in compression, ρ is given by Eq.(7.1) and (7.2), shown in Fig.7.1. The reduction factor ρ considers interaction between global and local buckling.

when $\lambda_l \leq 0.776$ $\quad \frac{P_{nl}}{P_{ne}} = \rho = 1$ (7.1)

when $\lambda_l > 0.776$ $\quad \frac{P_{nl}}{P_{ne}} = \rho = {\lambda_l}^{-0.8} - 0.15{\lambda_l}^{-1.6}$ (7.2)

where $\lambda_l = \sqrt{\frac{P_{ne}}{P_{crl}}}$; P_{nl} is the nominal local buckling strength in compression; P_{nl} is equal to the nominal compressive strength (P_n) of a column (without distortional buckling); P_{ne} is the nominal global buckling strength in compression; P_{crl} is the elastic critical local buckling strength.

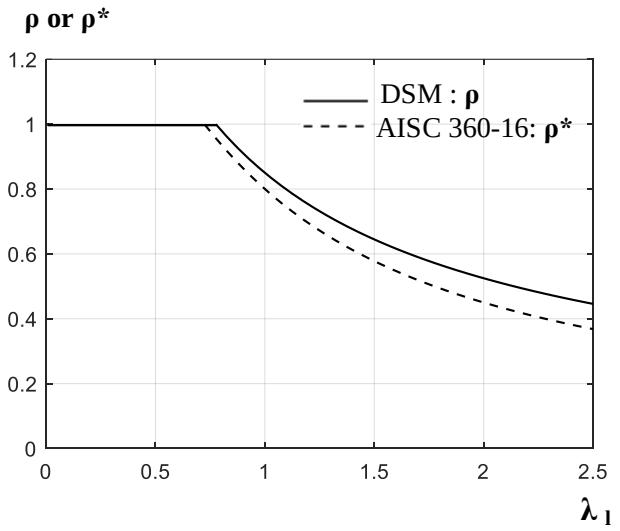

Fig.7.1 Reduction factor versus cross-section slenderness (λ_l)

(2) ρ for members in bending

Eq. (7.1) and (7.2) are applicable to members subjected to bending, provided that inelastic reserve strength resulted from partial plastification of the cross-section under bending is not considered (AISI S100-16: 2016).The reduction factor for members in bending is given by

when $\lambda_l \leq 0.776$ $\quad \frac{M_{nl}}{M_{ne}} = \rho = 1$ (7.3)

when $\lambda_l > 0.776$ $\quad \frac{M_{nl}}{M_{ne}} = \rho = {\lambda_l}^{-0.8} - 0.15{\lambda_l}^{-1.6}$ (7.4)

where $\lambda_l = \sqrt{\frac{M_{ne}}{M_{crl}}}$; M_{nl} is the nominal local buckling moment; without distortional buckling, M_{nl} is equal to the nominal flexural strength (M_n) of a beam; M_{ne} is the nominal global (lateral-torsional) buckling moment; M_{crl} is elastic critical local buckling moment.

7.2.2 Reduction factor implicitly provided in AISC 360-16

For members with RHS and SHS in compression, the reduction factor ρ* is implicitly included in the two equations (E7-2 and E7-3 provided in ASIC 360-16) that determine the nominal compressive strength (P_n) of a member comprising slender-elements. The two equations are given by

When $b/t \leq \lambda_r \sqrt{f_y/f_{ne}}$ $\quad \frac{A_e}{A} = \rho^* = 1$ (7.5)

When $b/t > \lambda_r \sqrt{f_y/f_{ne}}$ $\quad \frac{A_e}{A} = \rho^* = (1 - c_1\sqrt{\frac{f_{crl}}{f_{ne}}})\sqrt{\frac{f_{crl}}{f_{ne}}}$ (7.6)

where A_e is effective section area; A is gross section area; b is the width of flat element, t element thickness; λ_r is the limiting width-to-thickness ratio; f_{crl} is critical local buckling stress, $f_{crl} = [c_2\lambda_r/(b/t)]^2$; f_{ne} is global buckling stress, $f_{ne} = P_{ne}/A$; c_1 and c_2 are effective width imperfection adjustment factor.

Eq. (7.5) and (7.6) can be written in terms of cross-section slenderness (λ_l) through the following procedure.

For RHS and SHS

$\lambda_r = 1.4\sqrt{E/f_y}$ (7.7)

c_1=0.2 and c_2=1.38, and thus gives

$f_{crl} = 3.73E/(b/t)^2$ (7.8)

Substituting Eq.(7.7) and (7.8) back into Eq.(7.5) and (7.6), gives

When $\frac{f_{ne}}{f_{crl}} \leq 0.5256$ $\quad \frac{A_e}{A} = \rho^* = 1$ (7.9)

When $\frac{f_{ne}}{f_{crl}} > 0.5256$ $\quad \frac{A_e}{A} = \rho^* = (1 - 0.2\sqrt{\frac{f_{crl}}{f_{ne}}})\sqrt{\frac{f_{crl}}{f_{ne}}}$ (7.10)

Members with RHS and SHS are not subject to distortional buckling, and thus the nominal compressive strength P_n is equal to the nominal local buckling strength (P_{nl}). Substituting $\lambda_l = \sqrt{\frac{P_{ne}}{P_{crl}}} = \sqrt{\frac{f_{ne}}{f_{crl}}}$ into Eq. (7.9) and (7.10) and replacing $\frac{A_e}{A}$ by $\frac{P_{nl}}{P_{ne}}$, gives

when $\lambda_l \leq 0.725$ $\quad \frac{P_{nl}}{P_{ne}} = \rho^* = 1$ (7.11)

when $\lambda_l > 0.725$ $\quad \frac{P_{nl}}{P_{ne}} = \rho^* = {\lambda_l}^{-1} - 0.2{\lambda_l}^{-2}$ (7.12)

A plot of ρ* versus λ_l is shown in Fig.7.1. It can be seen that the ρ* curve is under the ρ curve determined by DSM. It should be noted that the ρ* curve determined by Eq.(7.11) and (7.12) does not apply to members subjected to bending.

7.2.3 Reduction factor for stainless steel

Although the ρ curve determined by DSM is developed based on experimental results of cold formed carbon steel members with C and Z sections Schafer (2000, 2019), it is also applicable to cold formed stainless steel members with RHS and SHS (Arrayago et al., 2017a, 2017b) . The reduction factor ρ determined by DSM gives accurate prediction for stainless steel SHS and RHS members. Thus, the reduction factor ρ determined by DSM is adopted in this paper.

It should be pointed out that, for stainless steel members with RHS and SHS, initial localized imperfection (ω) considered in the ρ factor is unknown. In the current paper, the value of ω considered in the ρ factor is conservatively taken as the mean value of the maximum localized imperfection (ω_{max}) collected from reported tests, since the results determined by the ρ curve agree well with the reported experimental results of stainless steel SHS and RHS members.

For the calculation of ρ, the nominal buckling strength and moment (P_{ne}, P_{crl}, M_{ne}, and M_{crl}) are determined in accordance with rules that are applicable to stainless steels, as follows:

(1) The nominal global buckling strength P_{ne}, given by Eq. (7.13) and (7.14), is determined in accordance

with AISC Design Guide 27: Structural Stainless Steel (2013).

When $\lambda_c \leq 1.2$ $\quad P_{ne} = 0.5^{\lambda_c{}^2} P_y$ (7.13)

When $\lambda_c > 1.2$ $\quad P_{ne} = 0.531 P_e = \frac{0.531}{\lambda_c{}^2} P_y$ (7.14)

where λ_c is member slenderness; $\lambda_c = \sqrt{\frac{P_y}{P_{cre}}}$; P_y is full cross -section yield strength; $P_y = Af_y$; f_y is 0.2% proof stress; A is gross section area; $P_{cre} = \frac{\pi^2 EI}{(Kl)^2}$; E is Young's Modulus, I moment of inertia, K effective length factor, *l* length of the member.

(2) The elastic critical local buckling strength P_{crl} is given by

$$P_{crl} = f_{crl} A \tag{7.15}$$

where f_{crl} is the elastic critical local buckling stress. f_{crl} can be determined by the following equation or determined by the software CUFSM (Schafer, 2019).

$$f_{crl} = \frac{k\pi^2 E t^2}{12(1-\nu)^2 b^2} \tag{7.16}$$

where t is plate thickness; ν is Poisson's ratio; b is width of the slender element; K_b is the buckling factor.

The buckling factor K_b for members with RHS (SHS) under uniform compression can be conservatively taken as 4 or be determined by the formulation provided in BS 5950-1(2000), given by

$$K_b \approx 7 - \frac{2\beta}{0.11+\beta} - 1.2\beta^3 \tag{7.17}$$

where $\beta = b_2/b_1$; b_1 and b_2 are the length and breadth of the rectangular hollow section, respectively. A plot of Eq.(7.17) is shown in Fig.7.2.

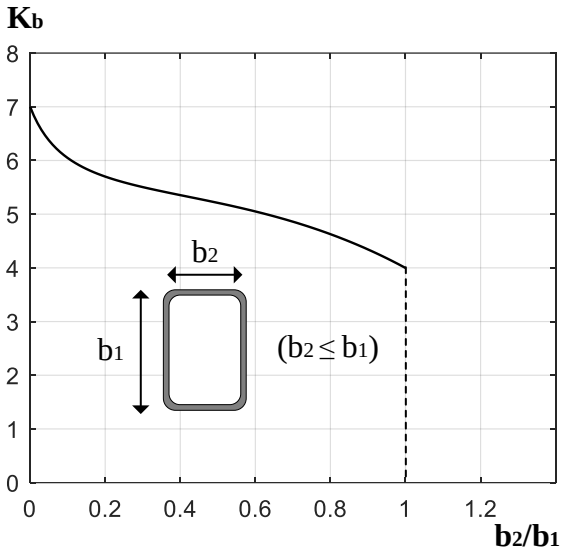

Fig.7.2 The buckling factor K_b for box section subjected to compression

(3) The nominal global (lateral-torsional) buckling moment M_{ne} is determined based on AISC Design Guide 27: Structural Stainless Steel (2013). Since global lateral-torsional buckling is not considered in this paper, M_{ne} is taken as M_p for beams with non-compact sections while M_{ne} is taken as M_y for beams with slender sections.

(4) The elastic critical local buckling moment M_{crl} is given by

$$M_{crl} = W_{el} f_{crl} \tag{7.18}$$

where W_{el} is elastic gross section modulus; f_{crl} can be determined by the software CUFSM (https://www.ce.jhu.edu/bschafer/cufsm/), or determined by Eq.(7.17) but with the buckling factor K for slender plates subjected to bending (AISI S100-16).

7.3 Numerical modelling

7.3.1 Elements, material models and residual stresses

In-plane structural behavior of stainless steel elements susceptible to local buckling is studied using finite element (FE) software Abaqus 6.13. Two types of finite elements are employed: one-dimensional beam elements (B21) and three-dimensional shell elements (S4R). In conducting GNA with stiffness reduction, beam elements are employed, while both beam and shell element are employed in implementing Geometrically and Materially Non-linear Analysis with Imperfections (GMNIA). The cross-section

(without rounder corner) is defined as box section for beam element. To make the results determined by beam element and those determined by shell element comparable, the same box section is used for shell element. The stress-strain curves and the longitudinal bending residual stresses were modelled as those presented in Chapter 3. Spread of plasticity through cross-section and along member length is traced by distributed plasticity approach.

7.3.2 Initial geometric imperfections

For sway-restrained members, out-of-straightness (δ/L) and localized imperfection (ω) are considered and modelled directly. Out-of-straightness and localized imperfection are combined together by means of linear superposition of relevant modes (local buckling mode and global buckling mode). These modes are obtained from preliminary Buckle Analysis through ABAQUS. The deterministic value for out-of-straightness is taken as 0.001. The deterministic value for localized imperfection (ω), is taken as the mean value (0.185) of the maximum ω collected from the reported tests results. For linear superposition, the global buckling mode is multiplied by 0.001, while local buckling mode is multiplied by the mean value (0.185) of the maximum ω.

For sway-permitted members, out-of-plumbness (Δ/h), out-of-straightness (δ/L) and localized imperfection (ω) are considered. Localized imperfection (ω) is directly modelled through local buckling mode times the mean value of the maximum ω. Out-of-plumbness (Δ/h) is taken as 0.002 and out-of-straightness is taken as 0.001. The effects of out-of-plumbness and out-of-straightness are accounted for by means of applying notional loads (equivalent horizontal loads). Notional loads are applied to the directions that produce most destabilizing effects. The procedure of applying notional load is similar to the one present in [42].To avoid additional shear force at the member base due to notional loads, corresponding horizontal reaction forces are applied.

7.3.3. FE model validation

A validation of the developed FE models against experimental results reported in Arrayago et al. (2016) is shown in Fig.7.3. For the validation study, initial geometric imperfections was modelled as explained in Chapter 3. The material properties were modelled as those reported in Arrayago et al. (2016). The longitudinal bending residual stresses were not modelled, since they are implicitly included in the stress-

strain curves. In Fig. 7.3, the FE model using beam element is validated against the beam-column with compact cross-section, while the FE model using shell element is validated against the beam-column prone to local buckling reduction. It is seen that the numerical results are in very close agreement with experimental results.

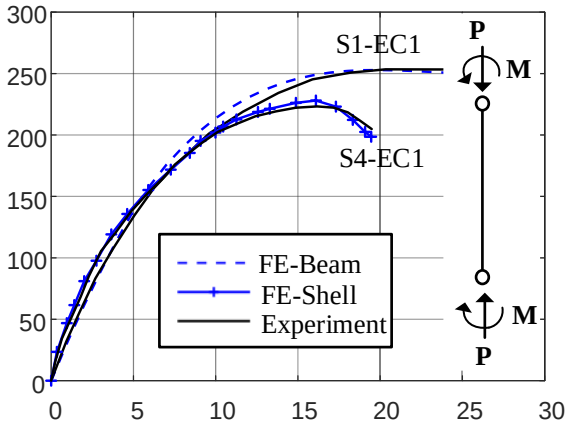

Fig.7.3. Validation of the developed FE models using shell element against experimental results reported in Arrayago et al. (2016).

7.4 Flexural stiffness reduction accounting for local buckling effects and localized imperfection

7.4.1 Introduction

In this section, stiffness reduction formulations, presented in Chapter 4 and 5, are extended to account for local buckling effects and initial localized imperfection (ω) by means of incorporating the reduction factor (ρ) to reduce the resistance of the gross section. Verification studies for GNA with extended stiffness reduction are then carried out numerically. Predicted results by GNA with extended stiffness reduction (using beam element) are compared against those determined by GMNIA using shell element. To evaluate local buckling effects and influence of initial localized imperfection (ω), predicted results by GMNIA using shell element are compared against those obtained from GMNIA using beam element.

7.4.2 Extended column flexural stiffness reduction factor

Stiffness reduction caused by local buckling and initial localized imperfection (ω) is accounted for by reducing the resistance of the gross section through incorporating the reduction factor ρ (ρ≤1) determined

by DSM. The extended column flexural stiffness reduction factor ($\tau_{N-\rho}$) formulation is given by

$$\tau_{N-\rho} = 1 \qquad \text{for } \frac{P_{r1}}{\rho P_y} \leq 0.37 \tag{7.19}$$

$$\tau_{N-\rho} = -2.717 \frac{P_{r1}}{\rho P_y} ln \frac{P_{r1}}{\rho P_y} \qquad \text{for } \frac{P_{r1}}{\rho P_y} > 0.37 \tag{7.20}$$

A plot of the extended column stiffness reduction factor ($\tau_{N-\rho}$) against $P_{r1}/\rho P_y$ is shown in Fig.7.4 (a). Regardless of the reduction factor ρ, the curve of $\tau_{N-\rho}$ versus $P_{r1}/\rho P_y$ is same to the curve of τ_N versus P_{r1}/P_y (compact sections). To exhibit the influence of ρ on column stiffness reduction, cross-section slenderness (λ_l) is assumed to be varied from 0 to 2, as shown in Fig.7.4 (b). In the figure, the curve with $\lambda_l \leq 0.776$ (ρ=1) represents stiffness reduction for columns with compact cross-sections.

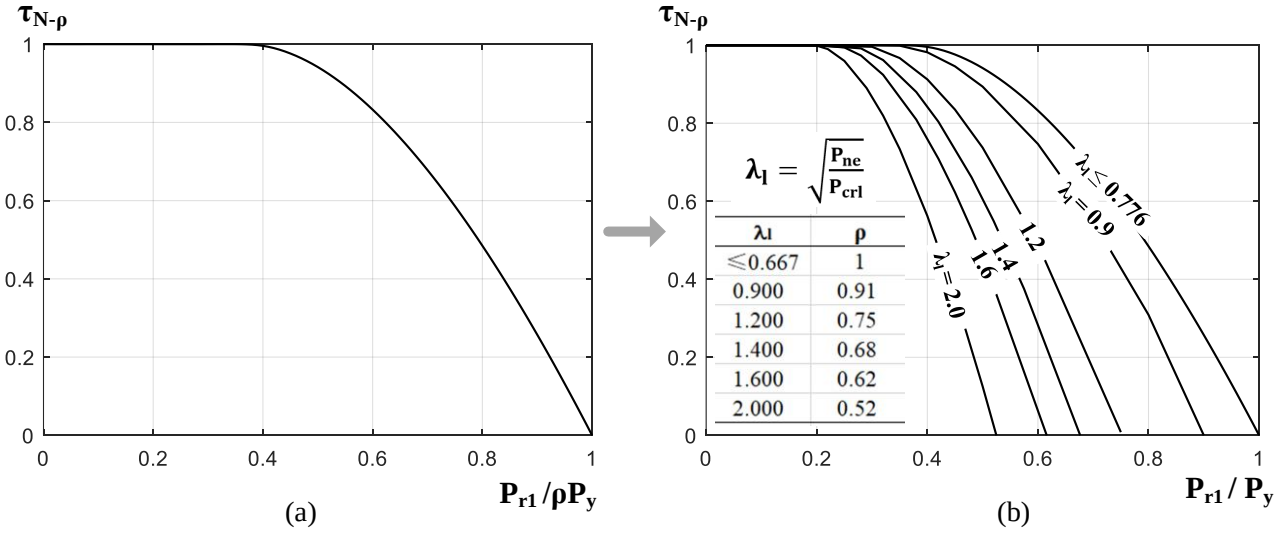

Fig.7.4 Column stiffness reduction ($\tau_{N-\rho}$) accounts for local buckling effects and initial localized imperfection: (a) $\tau_{N-\rho}$ versus $P_{r1}/\rho P_y$ (b) $\tau_{N-\rho}$ versus P_{r1}/P_y

7.4.3 Verification of the extended column flexural stiffness reduction factor

The accuracy of the extended column stiffness reduction factor ($\tau_{N-\rho}$) for stainless steel members susceptible to local buckling effects subjected to axial load is assessed. Simply supported columns with cross-section 120x80x2.5 (E=200GPa, f_y=350MPa, n=6) subjected to axial loads are studied. The length of the columns varies from 100mm to 7000 mm. The applied axial load is factored load. For each column, GMNIA using shell element (denoted by GMNIA-shell), GMNIA using beam element (denoted by GMNIA-beam), and GNA with $\tau_{N-\rho}$ (denoted by GNA-$\tau_{N-\rho}$) are conducted.

The procedure of implementing GMNIA-beam, GMNIA-shell and GNA-$\tau_{N-\rho}$, shown in Fig.7.5, is illustrated by the following.

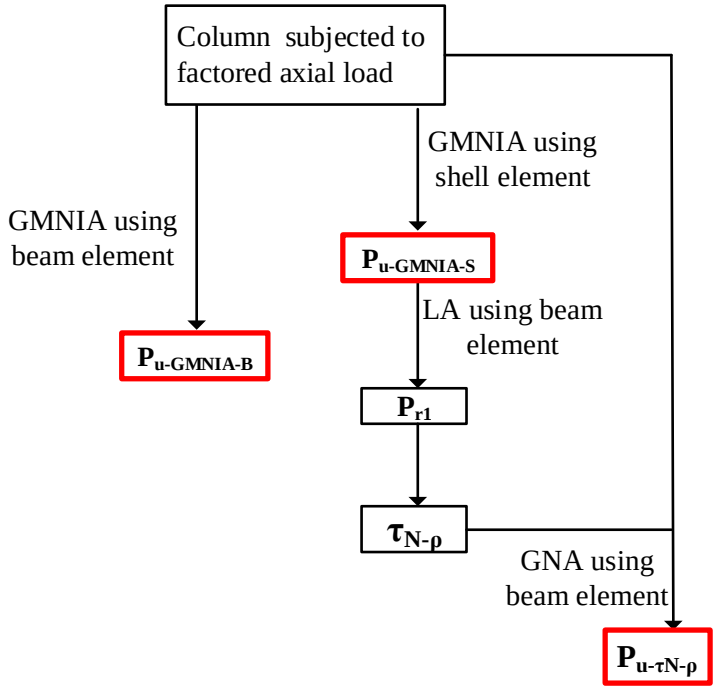

Fig.7.5. Procedure of implementing GNA-$\tau_{N-\rho}$, GMNIA-shell and GMNIA-beam

(1) Perform GMNIA-shell and GMNIA-beam analysis to obtain the ultimate axial load (P_u) of the columns.

The introduced out-of-straightness is 0.001 and the amplitude of maximum localized imperfection (ω_{max}) is 0.185. The value of 0.185 is the mean value of ω_{max} for stainless steel RHS and SHS members collected from reported test results. P_u predicted by GMNIA-beam is denoted by $P_{u\text{-}GMNIA\text{-}B}$, while P_u predicted by GMNIA-shell is denoted by $P_{u\text{-}GMNIA\text{-}S}$.

(2) Perform Linear Elastic Analysis (LA, using beam element) to obtain maximum first order axial force.

The applied load is $P_{u\text{-}GMNIA\text{-}S}$. Maximum first order axial force obtained from LA is referred to as P_{r1}. For all the studied simply supported columns, P_{r1} is equal to $P_{u\text{-}GMNIA\text{-}S}$.

(3) Calculate the ρ factor and the extended column flexural stiffness reduction factor $\tau_{N-\rho}$.

The ρ factor is calculated according to Eq. (7.1) and (7.2). $\tau_{N-\rho}$ is determined according to Eq.(7.19) and (7.20).

(4) Perform GNA-$\tau_{N-\rho}$ (using beam element) analysis to predict the ultimate axial load of the columns.

Ultimate axial load predicted by GNA-$\tau_{N-\rho}$ is denoted by $P_{u-\tau N-\rho}$.

As expected, the ultimate load (P_u) of the simply supported columns predicted by GNA-$\tau_{N-\rho}$ matches the bifurcation load (or elastic critical buckling load) $P_{e-\tau N\rho}$ determined by the reduced flexural stiffness ($\tau_{N-\rho}$ times EI), shown in Fig.7.6. $P_{e-\tau N\rho}$ is given by

$$P_{e-\tau N\rho} = \frac{\pi^2(\tau_{N-\rho}EI)}{(L)^2} \tag{7.21}$$

where EI is initial flexural stiffness; L is unbraced length of the column.

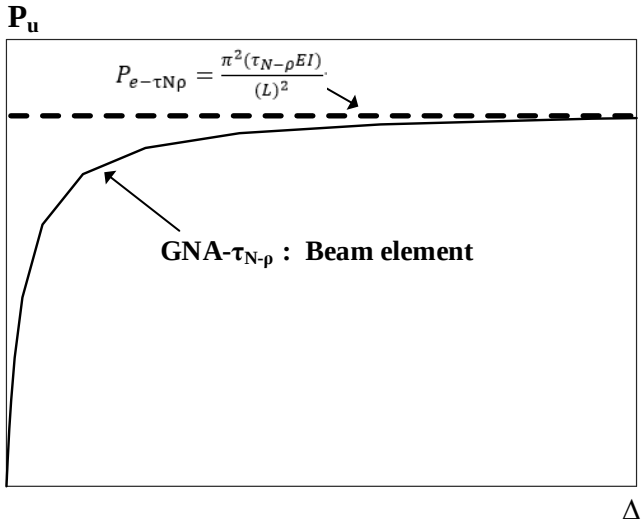

Fig.7.6. Comparison of the ultimate axial load (P_u) determined by GNA-$\tau_{N-\rho}$ and the elastic critical buckling strength ($P_{e-\tau N\rho}$) based on effective flexural stiffness ($\tau_{N-\rho}$EI)

Comparison of the results determined by GNA-$\tau_{N-\rho}$, GMNIA-shell and GMNIA-beam is shown in Fig.7.7, where the ultimate axial load (P_u) predicted by different method is normalized by full cross-section yield strength (P_y). The difference between the curve of GMNIA-beam and the curve of GMNIA-shell is mainly resulted from local buckling effects. It is observed that the smaller the column slenderness (λ_c) is, the more significant the difference is. This can be explained by the following. For a given cross-section, since elastic critical local buckling strength (P_{crl}) is constant, the cross-sectional slenderness λ_l ($\lambda_l = \sqrt{\frac{P_{ne}}{P_{crl}}}$)) is governed by P_{ne}. According to Eq. (7.13) and (7.14), P_{ne} increases with λ_c decreasing. It means the smaller λ_c is, the larger λ_l . As a consequence, the difference between the two curves due to the influence of local buckling becomes more considerable.

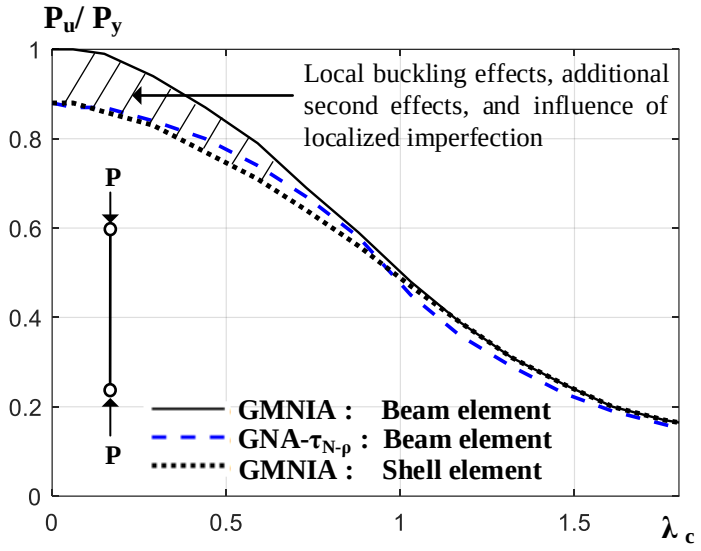

Fig.7.7. Normalized ultimate axial load (P_u) determined by different methods against column slenderness (λ_c)

It is observed that the ultimate axial loads predicted by GNA-$\tau_{N-\rho}$ using beam element are in very close agreement with those predicted by GMNIA-shell. For columns with low member slenderness (λ_c), GNA-$\tau_{N-\rho}$ slightly overestimates the ultimate axial load. One possible explanation is that the incorporated reduction factor ρ somewhat underestimates local buckling effects, which results in a higher $\tau_{N-\rho}$ than the actual stiffness reduction factor. Since the ultimate load predicted by GNA-$\tau_{N-\rho}$ is equal to the bifurcation load determined by Eq.(7.21), in which the bifurcation load is directly proportional to $\tau_{N-\rho}$, a higher $\tau_{N-\rho}$ leads to overestimated ultimate axial load. Note that the discrepancy between the predicted results of GNA-$\tau_{N-\rho}$ and those determined by GMNIA may also be caused by the introduced initial localized imperfection (ω), since the actual localized imperfection (ω) considered in the ρ factor is unknown.

7.4.4 Extended beam flexural stiffness reduction factor.

For beams with non-compact and slender sections, local buckling effects and the influence of initial localized imperfection are accounted for by means of incorporating the reduction factor (ρ) to reduce the resistance of the gross section (M_y for slender section, M_p for non-compact section).

The extended beam flexural stiffness reduction factor ($\tau_{M-\rho}$) formulation for slender section is given by

When $0 < M_{r1} \leq \rho M_y$ $$\tau_{M-\rho} = \left[1 + (n-1)\frac{0.001E}{f_y}\left(\frac{M_{r1}}{\rho M_y}\right)^{n-2}\right]^{-1} \quad (7.22)$$

The extended beam flexural stiffness reduction factor ($\tau_{M-\rho}$) formulation for non-compact section is given by

When $0 < M_{r1} \leq \rho M_y$ $$\tau_{M-\rho} = \left[1 + (n-1)\frac{0.001E}{f_y}\left(\frac{M_{r1}}{\rho M_p}\frac{W_{pl}}{w_{el}}\right)^{n-2}\right]^{-1} \quad (7.23)$$

When $\rho M_y < M_{r1} \leq \rho M_p$ $$\tau_{M-\rho} = \left[\left(1 - \frac{M_{r1}}{\rho M_p}\right)\frac{1}{1-\frac{W_{el}}{W_{pl}}}\right]^{0.9}\left[1 + (n-1)\frac{0.001E}{f_y}\right]^{-1} \quad (7.24)$$

For a non-compact cross-section (f_y = 430MPa, E=200GPa, and n=6, W_{el}/W_{pl}=0.82), a plot of the extended beam stiffness reduction ($\tau_{M-\rho}$) determined by Eq.(23) and (24) against $M_{r1}/\rho M_y$ is shown in Fig.7.8 (a). To exhibit the influence of ρ on beam flexural stiffness reduction, cross-section slenderness (λ_l) is assumed to be varied from 0 to 1.1, as shown in Fig.7.8 (b). The figure shows the decreasing trend of $\tau_{M-\rho}$ as the assumed cross-section slenderness (λ_l) increases.

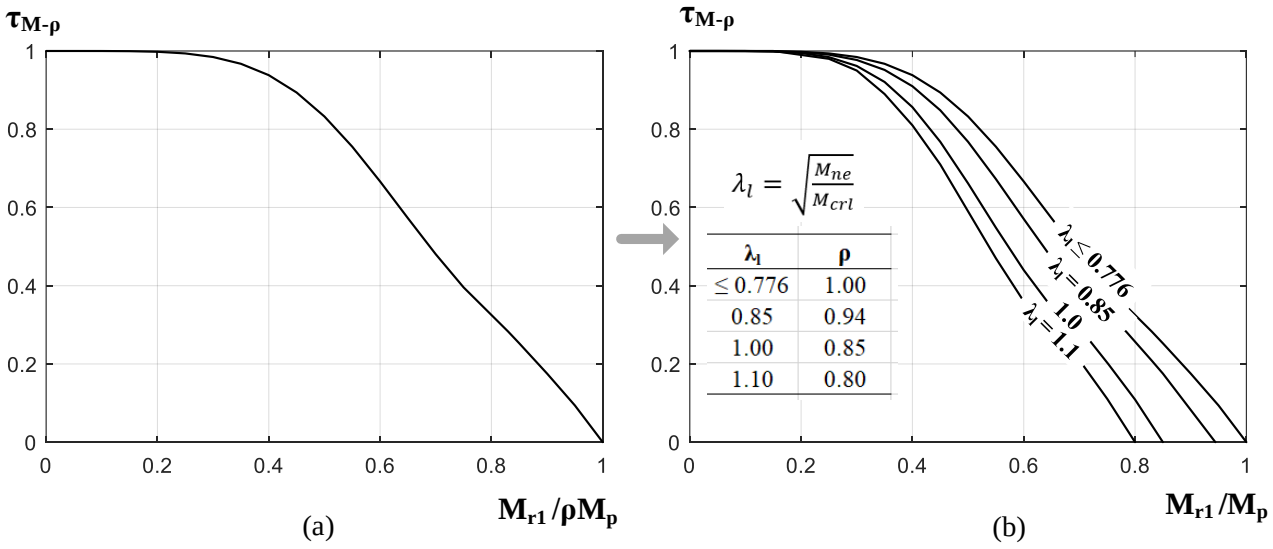

Fig.7.8 A plot of beam flexural stiffness reduction (a) $\tau_{M-\rho}$ versus $M_{r1}/\rho M_P$ (b) $\tau_{M-\rho}$ versus M_{r1}/M_P

7.4.5 Verification of the extended beam flexural stiffness reduction factor

The ability of $\tau_{M-\rho}$ capturing the effects of local buckling and spread of plasticity through cross-section and along member length is verified. It should be noted that, due to the non-linear stress-strain behavior (beyond proportional limit) of stainless steel, the cross-section already undergoes plastic straining before internal moment reaches to M_y.

Simply supported beams with slender cross-section 120x80x2 (E=200GPa, f_y=350MPa, n=7,

M_y=9.53kN*m, ρ=0.97, M_u =9.24kN*m, M_u is the maximum bending moment predicted by GMNIA-shell) and non-compact cross-section 250x150x5 (E=190GPa, f_y=450MPa, n=7,W_{pl}/W_{el}=1.204, M_p=147.49 kN*m, ρ=0.95, M_u =9.24kN*m) are studied. The beam with slender cross-section is subjected to a pair of identical end moments, while the beam with non-compact cross-section is subjected to uniformly distributed loads. GMNIA-shell element and GMNIA-beam element are conducted to obtain M-k curves, where the introduced out-of-straightness is 0.001 and the amplitude of the maximum localized imperfection (ω_{max}) is 0.185 in implementing GMNIA-shell.

$\tau_{M-\rho}$ determined by Eq. (7.22), (7.23) and (7.24) are compared against flexural stiffness reduction derived from M-k curves provided by GMNIA-shell element. Stiffness reduction derived from M-k curve of GMNIA-shell element is denoted by $\tau_{M\text{-shell}}$, and that derived from M-k curve of GMNIA-beam element is denoted by $\tau_{M\text{-beam}}$.

The derivation of flexural stiffness reduction is based on

$$\tau_{M-shell}(or\ \tau_{M-beam}) = \frac{(EI)_t}{EI} = \frac{\frac{dM_{r1}}{d\kappa}}{EI} \tag{7.25}$$

where $\frac{dM_{r1}}{d\kappa}$ is the slope of the tangent at a given point on the M-k curve. The procedure of calculating tangent slope is conducted through MATLAB 2017b.

Comparison of $\tau_{M-\rho}$ against $\tau_{M\text{-shell}}$ and $\tau_{M\text{-beam}}$ is shown in Fig.7.9. In the figure, the difference between $\tau_{M\text{-beam}}$ and $\tau_{M\text{-shell}}$ is mainly attributed to the influence of local buckling. Compared to the curve of $\tau_{M\text{-beam}}$, the curve of $\tau_{M\text{-shell}}$ decreases at a high rate after local buckling occurs in the inelastic range. It is observed that the $\tau_{M-\rho}$ curves generally agree well with $\tau_{M\text{-shell}}$ curves. The discrepancy between $\tau_{M-\rho}$ and $\tau_{M\text{-shell}}$ may be attributed to the incorporated reduction factor ρ or introduced initial localized imperfection. It should be pointed out that, besides the influence of the factor ρ and initial localized imperfection, the discrepancy between $\tau_{M-\rho}$ and $\tau_{M\text{-shell}}$ also relies on the accuracy of the beam flexural stiffness reduction τ_M applicable to compact sections to capture the spread of plasticity of the beams.

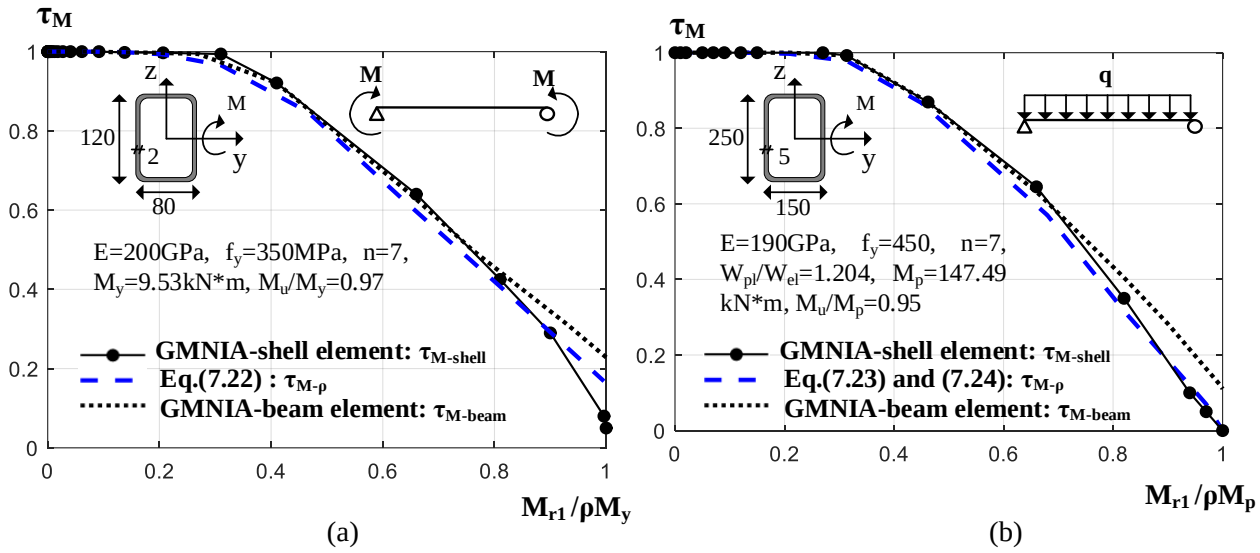

Fig.7.9 Comparison of $\tau_{M\text{-}\rho}$ against $\tau_{M\text{-shell}}$ and $\tau_{M\text{-beam}}$ (a) slender section (b) non-compact section

7.4.6 Extended beam-column flexural stiffness reduction factor

Similar to the above approach, local buckling effects and the influence of initial localized imperfection on beam-columns are taken into consideration by reducing the resistance of the gross section through the factor ρ. It should be pointed out that ρ is taken as min {ρ-column, ρ-beam}. ρ-column is calculated according to Eq. (7.1) and (7.2), while and ρ-beam is calculated according to Eq. (7.3) and (7.4).

The extended $\tau_{MN\text{-}\rho}$ formulation is given by

$$\tau_{MN-\rho} = \gamma \Omega_M \tau_{N-\rho} \tau_{M-\rho} \left[1 - \left(\frac{P_{r1}}{\rho P_y}\right)^{0.9} \left(C_m \frac{M_{r1}}{\rho M_p}\right)^{\frac{W_{el}}{W_{pl}}}\right] \tag{7.26}$$

$$0.8 \leq \gamma = 2(B_{2-E} - 0.6) < 1 \quad \text{for } 1 \leq B_{2\text{-}E} < 1.1 \tag{7.27}$$

$$\gamma = 1 \quad \text{for } 1.1 \leq B_{2\text{-}E} \tag{7.28}$$

$$\Omega_M = 1 \quad \text{for } 0 \leq \frac{M_{r1}}{\rho M_p} < 0.4 \tag{7.29}$$

$$\Omega_M = \left(0.6 + \frac{M_{r1}}{\rho M_p}\right)^{1.4} \quad \text{for } 0.4 \leq \frac{M_{r1}}{\rho M_p} \leq 1 \tag{7.30}$$

The factor $B_{2\text{-}E}$ evaluates P-Δ effects and together with P-δ effects on sway-permitted elastic beam-columns. For sway-restrained beam-columns, $B_{2\text{-}E}$ is equal to 1. For sway-permitted isolated beam-column, $B_{2\text{-}E}$ is given by

$$B_{2-E} = \frac{1}{1-\frac{P_{r1}}{0.85\,P_{es}}} \geq 1 \quad (31)$$

where the factor 0.85 accounts for the influence of P-δ effects on the global behavior of a sway-permitted member; $P_{es}=(F_H L)/\Delta$; F_H is first order shear force; Δ is relative drift between member ends due to F_H; L is length of the member.

Note that Eq.(7.26) is not applicable to slender cross-sections, since inelastic reserve strength is considered in this equation. For beam-columns with slender sections, Eq. (7.26) is slightly modified, where plastic bending moment (M_p) is replaced by M_y, and W_{el}/W_{pl} is replaced by the factor 0.7. The factor 0.7 is based on the results of numerical studies.

7.4.7 Verification of the extended beam-column flexural stiffness reduction factor

The accuracy of the extended beam-column stiffness reduction factor ($\tau_{MN-\rho}$) for in-plane stainless steel beam-columns with non-compact and slender sections are evaluated. Simply supported beam-columns and cantilever beam-columns are studied.

Simply supported beam-columns, with different cross-sections and material properties (shown in Table.1), are subjected to combined axial load (P) and varied moments (M_1, M_2) at the member ends. The applied P is factored load, M_2=e*P; e ranges from 1 to 150 (e= [0,10,30,50,80,100,150]) and the unit of e is mm; $|M_2|\geq|M_1|$. The applied end moments are varied for different cross-sections: a pair of equal but opposite end moments for cross-section 120x80x2, one end moment for cross-section 200x100x3, and a pair of identical end moments for cross-section 250x150x5.

Cantilever beam-columns, with different cross-sections and material properties (shown in Table.7.1), are subjected to combined axial load (P) and horizontal load (iP) at the cantilever end, where the applied load P is factored load, and i=[0, 0.05, 0.1, 0.15, 0.2, 0.25, 0.3].

Table.7.1 Details of studied beam-columns

Beam-column		Cross-section	L(mm)	E(GPa)	f_y(MPa)	n	W_{pl}/W_{el}
Simply supported	a	120x80x2	2000	200	350	6	1.19
	b	200x100x3	2500	175	400	8	1.22
	c	250x150x5	3000	190	450	7	1.20
Cantilever	a	120x80x1.5	2000	200	350	6	1.19
	b	200x100x3	2500	175	400	7	1.22

Verification study for the studied beam-columns are conducted through the following steps, as illustrated in Fig.7.10.

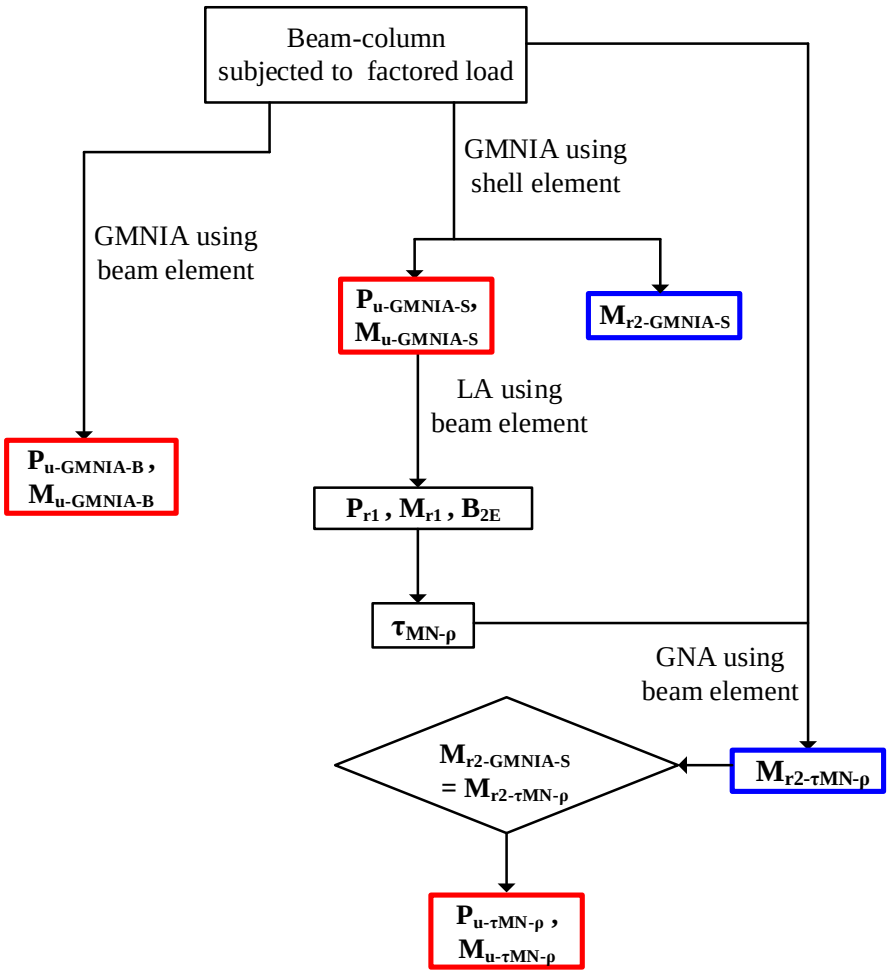

Fig.7.10 Procedure of implementing GNA-$\tau_{MN\text{-}\rho}$, GMNIA-shell and GMNIA-beam analysis.

(1) Perform GMNIA-shell and GMNIA-beam to obtain the ultimate axial load and moment (P_u and M_u) of the beam-columns.

The introduced maximum localized imperfection (ω_{max}) is 0.185 for all beam-columns. Out-of-straightness of 0.001 is introduced to simply supported beam-columns, while out-of-straightness of 0.001 and out-of

plumbness of 0.002 are introduced to cantilever beam-columns. For simply supported beam-columns, M_u is the end moment M_2, and it is equal to e*P_u. For cantilever beam-columns, M_u is equal to horizontal load (iP_u) multiplied by member length (L). P_u and M_u determined by GMNIA-beam are denoted by $P_{u\text{-}GMNIA\text{-}B}$ and $M_{u\text{-}GMNIA\text{-}B}$, respectively, while P_u and M_u determined by GMNIA-shell are denoted by $P_{u\text{-}GMNIA\text{-}S}$ and $M_{u\text{-}GMNIA\text{-}B}$, respectively. For GMNIA-shell analysis, maximum internal second order moment (denoted by $M_{r2\text{-}GMNIA\text{-}S}$) within the beam-column, corresponding to $P_{u\text{-}GMNIA\text{-}S}$ and $M_{u\text{-}GMNIA\text{-}S}$, are obtained.

(2) Perform Linear Elastic Analysis (LA, using beam element) to obtain maximum first order internal axial force (P_{r1}) and moment (M_{r1})

The applied axial load and end moment are $P_{u\text{-}GMNIA\text{-}S}$ and $M_{u\text{-}GMNIA\text{-}S}$, respectively. For cantilever beam-columns, the applied horizontal load multiplied by member length is treated as end moment. The factor $B_{2\text{-}E}$ is calculated according to Eq. (7.31).

(3) Calculate the ρ factor and the extended beam-column flexural stiffness reduction factor $\tau_{MN\text{-}\rho}$.

The reduction factor ρ is taken as min {ρ-column, ρ-beam}. ρ-column is calculated according to Eq. (7.1) and (7.2), while and ρ-beam is calculated according to Eq. (7.3) and (7.4). For the calculation of the ρ factor, the nominal local buckling strength (P_{nl}) is taken as $P_{u\text{-}GMNIA\text{-}S}$ for the column case, while the nominal local buckling moment (M_{nl}) is taken as $M_{u\text{-}GMNIA\text{-}S}$ for the beam case. $\tau_{MN\text{-}\rho}$ is determined according to Eq.(7.26).

(4) Perform GNA-$\tau_{MN\text{-}\rho}$ using beam element to predict the maximum internal second order moment (M_{r2}).

M_{r2} determined by GNA-$\tau_{MN\text{-}\rho}$ is denoted by $M_{r2\text{-}\tau MN\text{-}\rho}$. For GNA-$\tau_{MN\text{-}\rho}$, the ultimate axial load ($P_{u\text{-}\tau MN\text{-}\rho}$) and end moment ($M_{u\text{-}\tau MN\text{-}\rho}$) of the beam-columns are achieved when $M_{r2\text{-}\tau MN\text{-}\rho}$ is equal to $M_{r2\text{-}GMNIA\text{-}S}$.

Comparison of the predicted results for simply supported beam-columns and cantilever beam-columns is shown in Fig.7.11 and 7.12, respectively. In the two figures, P_n and M_n are the nominal compressive strength of the column and nominal flexural strength of the beam, respectively; P_n and M_n determined by equations provided in Section 7.2.3 are very close to P_u (column case) and M_u (beam case) determined by GMNIA-shell element, respectively; P_u and M_u predicted by different method are normalized by P_n and M_n, respectively. It should be mentioned that for all the beam cases, $M_{u\text{-}\tau MN\text{-}\rho}$ is taken as the ultimate end moment determined by GMNIA-shell element.

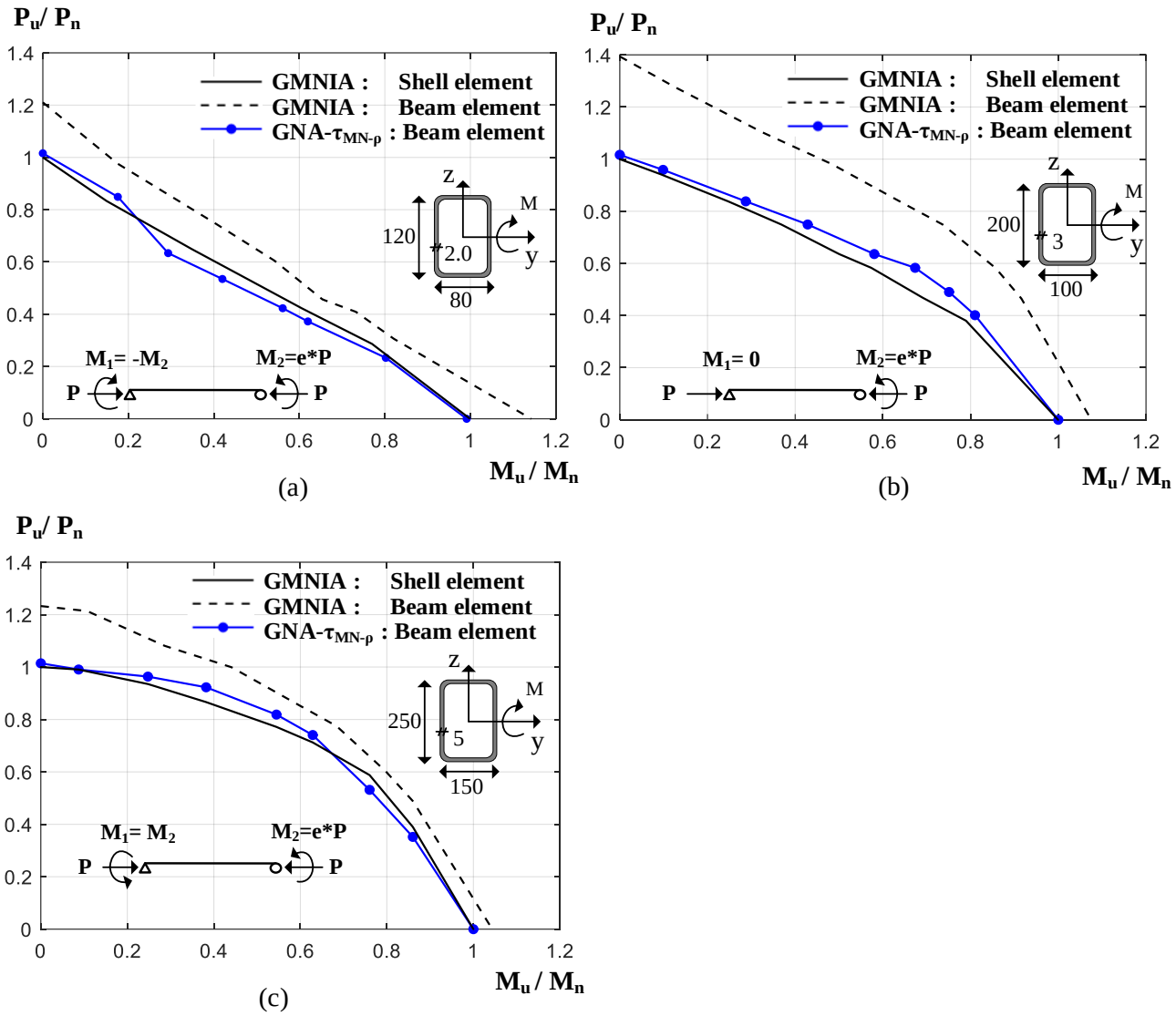

Fig.7.11 Comparison of predicted results for simply supported beam-columns

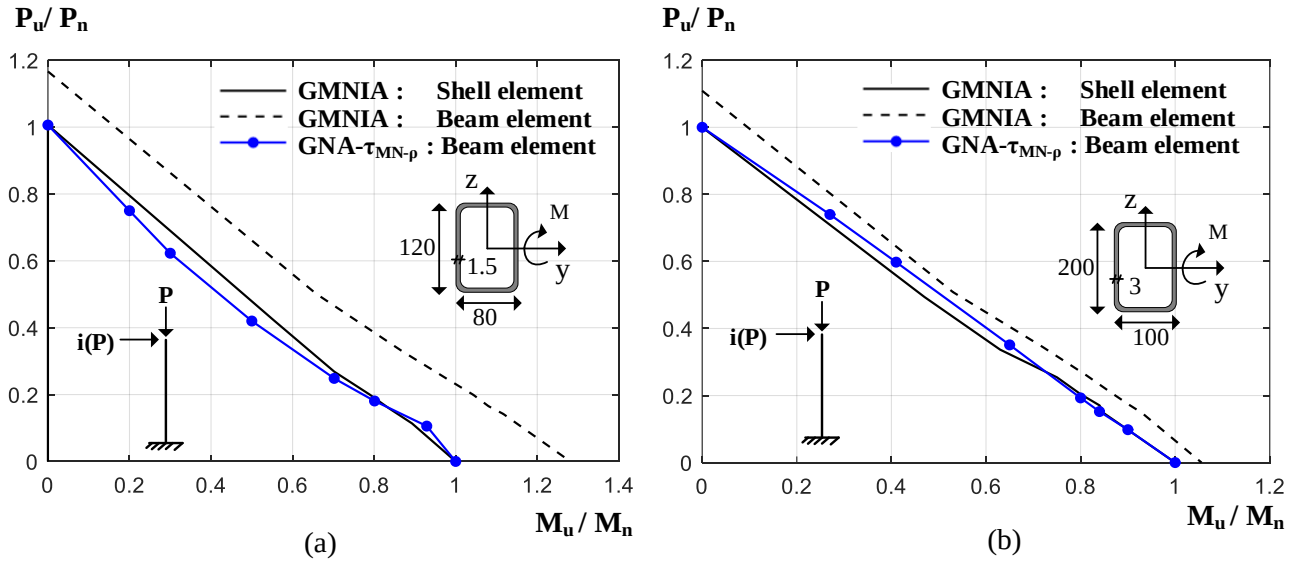

Fig.7.12 Comparison of predicted results for cantilever beam-columns

In the two figures, the considerable discrepancy between the curve of GMNIA-beam element and the curve of GMNIA-shell element is attributed to local buckling effects and the influence of initial localized imperfection (ω). It is observed that the results predicted by GNA-$\tau_{MN-\rho}$ are in close agreement with those determined by GMNIA-shell element. For the studied beam-columns, the discrepancy between the predicted results of GNA-$\tau_{MN-\rho}$ and those provided by GMNIA-shell mainly occurs in the intermediate part of the interaction curves (P_u/P_n versus M_u/M_n). It may be resulted from the incorporated reduction factor ρ or the amplitude of introduced maximum initial localized imperfection (ω_{max}) in implementing GMNIA-shell analysis. From the Fig.7.11 and Fig.7.12, it is concluded that, besides capturing the influence of spread of plasticity, the extended stiffness reduction $\tau_{MN-\rho}$ can well capture local buckling effects.

It should be noted that, for design check of non-compact and slender cross-sections, full cross-section resistance have to be reduced by the ρ factor to account for local buckling effects. For member-based ultimate limit design checks using internal axial forces and moments determined by GNA-$\tau_{MN-\rho}$ or GMNIA-shell in this paper, only cross-section strength check is needed and member buckling strength check is eliminated. This is because second order effects (P-Δ and P-δ) and all initial geometric imperfections (out-of-plumbness, out-of-straightness, and localized imperfection) are considered in both GNA-$\tau_{MN-\rho}$ and GMNIA.

7.5 Concluding remarks

In this chapter, the stiffness reduction formulations, applicable to stainless steel elements and frames with compact sections, are extended to account for local buckling effects and initial localized imperfection (ω). Local buckling effects and influence of initial localized imperfection are accounted for by means of reducing the gross section resistance using a factor ρ. The factor ρ, determined by the Direct Analysis Method, depending on cross-section slenderness, is adopted. The accuracy of GNA with extended stiffness reduction factor for in-plane stability design of stainless steel elements (columns, beams and beam-columns) with non-compact and slender sections is verified. Predicted results by GNA with stiffness reduction (using shell element) are in close agreement with those determined by GMNIA using shell element.

8. Effect of uncertainty in localized imperfection on members susceptible to local buckling

8.1 Introduction

The structural behavior of members with non-compact and slender sections are sensitive to initial localized imperfection (ω). In this chapter, probabilistic studies based on the proposed 3D model with random ω (presented in Chapter 3) are conducted to

(1) evaluate the effect of uncertainty in ω on the ultimate capacity of stainless steel columns.

(2) evaluate the effect of uncertainty in ω on the accuracy of GNA coupled with stiffness reduction for stainless steel beam-columns. It is indirectly assessed through evaluating the effect of uncertainty in ω on the ultimate capacity of stainless steel beam-columns.

Firstly, a statistical analysis of experimental results of the ω_{max} from the literature is carried out. The studied samples refer to the stainless steel grades commonly used in construction.

Secondly, a new approach utilizing Fourier series to generate the three-dimensional (3D) model of elements with random localized imperfection (ω) is presented. The proposed 3D models are used to conduct probabilistic studies of stainless steel elements that are susceptible to local buckling.

Thirdly, for a series of tested stainless steel columns (susceptible to local buckling) reported in the literature, the statistical characteristics of the ultimate axial load, obtained from GMNIA in which ω is modelled randomly, are compared against the experimental results.

Lastly, for the studied beam-columns presented in Section 7.4, the statistical characteristics of the ultimate capacity, obtained from GMNIA in which ω is modelled randomly, are compared against those determined by GNA-$\tau_{MN-\rho}$ as well as GMNIA in which ω is modelled as the lowest local buckling mode (obtained from Buckle Analysis) times a deterministic value . Through probabilistic studies, the influence of uncertainty in ω on the accuracy of GNA-$\tau_{MN-\rho}$ is indirectly evaluated.

Parts of the research presented in this chapter have also been reported by Shen and Chacón (2019).

8.2 Statistical analysis of the maximum localized imperfection (ω)

Although there is a considerable uncertainty when characterizing localized imperfection (ω) in cold-formed hollow sections, experimental data on the maximum localized imperfection (ω_{max}) are available for the particular case of RHS and SHS stainless steel specimens. A statistical analysis of experimental results of the ω_{max} from the literature is carried out in this section. A total of 161 cold-formed stainless steel RHS and SHS samples are collected. A summary of the samples is shown in Table 8.1. The studied samples refer to the stainless steel grades commonly used in construction. In these references, some studies (Young and Lui, 2005; Lui et al., 2014) provided the pattern of ω in transverse direction (cross-sectional), in which all the reported patterns are very close to a half-sine wave. Few of them reported the variation of localized imperfection in longitudinal direction.

Table.8.1 Summary of the samples collected from the literature

Reference	Stainless steel groups	Grade	No. of samples with measured ω
B.F. Zheng et al., 2016	Austenitic	EN1.4301	4
I. Arrayago. et al., 2016	Ferritic	EN1.4003	12
B. Young and W.M. Lui, 2005	Duplex	EN1.4162	5
O. Zhao et al.,2015	Austenitic	EN1.4301	10
	Austenitic	EN1.4571	6
	Austenitic	EN1.4307	6
	Austenitic	EN1.4404	6
	Duplex	EN1.4162	6
M.Theofanous and L.Gardner, 2009	Duplex	EN1.4162	8
W.M. Lui et al., 2014	Duplex	EN1.4462	10
Y. Huang and B.Young, 2013	Duplex	EN1.4162	22
S.Afshan and L.Gardner,2013	Ferritic	EN1.4003	6
	Ferritic	EN1.4509	2
M. Bock et al., 2015	Ferritic	EN1.4003	8
I. Arrayago and E. Real, 2015	Ferritic	EN1.4003	26
O. Zhao et al.,2016	Ferritic	EN1.4003	24
			Total :161

The probability distribution for ω_{max} among the samples collected in the literature was identified by statistical distribution tests (Anderson–Darling method) as well as from probability plots. Both distribution tests and probability plots were performed by using the statistical software Minitab 18 (2018).

For the case of distribution tests, Anderson-Darling statistics (AD) and P-values measure how well specified distributions fit to the data. For a given sample data and distribution, the smaller the AD is, the better the distribution fits to the data. Higher p-values indicate a better fit, and p-values less than 0.05 typically indicate that the data do not follow the specified distribution. The indicator LRT P is for 3-parameter distributions only. A lower LRT P indicates that the related 2-parameter distribution can be significantly improved by a third parameter. Goodness of fit test results for 16 different distribution tests is shown in Fig 8.1(a). The Box-Cox transformation and the Johnson transformation are disregarded since the target is to identify probability distribution rather than to perform any transformation. It is found that, the log-normal distribution (AD=1.016, P-value = 0.011) represents the best fit for the data of ω_{max}.

Probability plots is another efficient way to determine whether the specified distribution fits the sample data. The closer the data to the middle straight line, the better the distribution fits the data. The probability plot of the sample data is shown in Fig 8.1(b). It is observed that the data points are in close agreement with the center straight line. It again demonstrates that the sample data follow the log-normal distribution. The histogram of ω_{max} is shown in Fig 8.1(c). The log-normal distribution is fitted to the histogram. Comparison of the cumulative probability (CDF) curve against the log-normal distribution is shown in Fig 8.1(d), in which CDF determines the probability that an observation will be less than or equal to a certain value.

Distribution	AD	P	LRT P
Normal	9.172	<0.005	
Box-Cox Transformation	1.016	0.011	
Lognormal	1.016	0.011	
3-Parameter Lognormal	0.910	*	0.540
Exponential	15.137	<0.003	
2-Parameter Exponential	9.523	<0.010	0.000
Weibull	4.287	<0.010	
3-Parameter Weibull	2.994	<0.005	0.000
Smallest Extreme Value	16.361	<0.010	
Largest Extreme Value	2.873	<0.010	
Gamma	2.718	<0.005	
3-Parameter Gamma	2.053	*	0.014
Logistic	7.914	<0.005	
Loglogistic	1.810	0.014	
3-Parameter Loglogistic	1.628	*	0.176
Johnson Transformation	0.542	0.162	

(a)

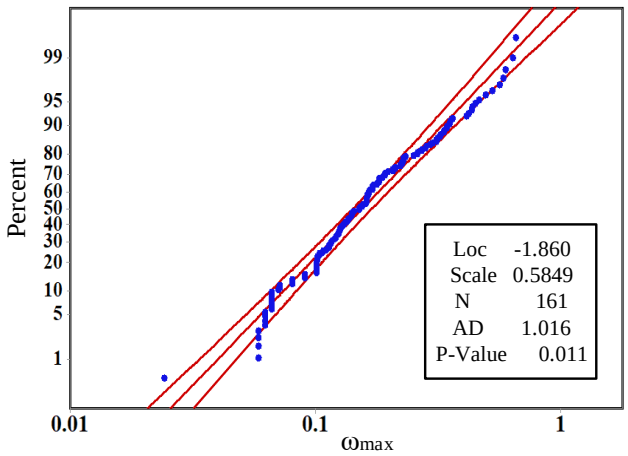

(b)

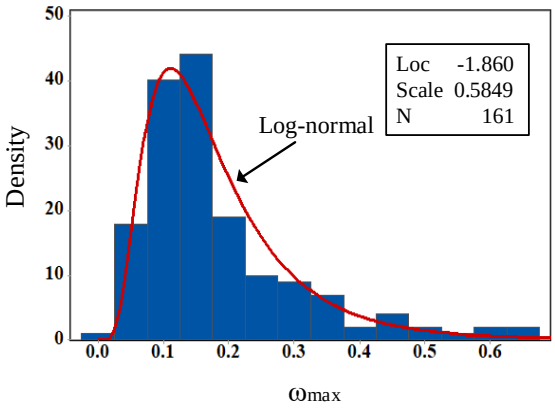

(c)

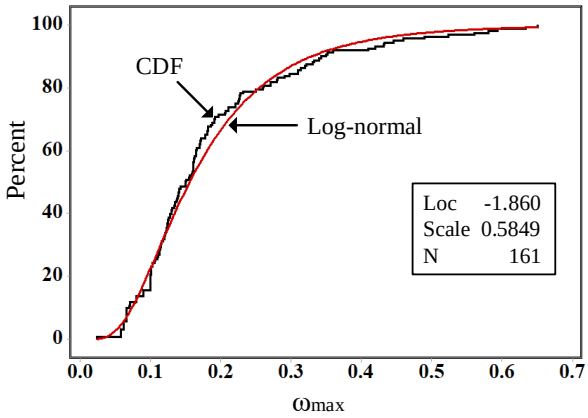

(d)

Fig 8.1. Identifying probability distribution for ω_{max} (a) Goodness of fit test results for 16 different distribution tests (b) Probability plot of ω_{max} (c) histogram of ω_{max} (d) Comparison of cumulative probability (CDF) curve against the log-normal distribution

8.3 Fourier series-based 3D models

Cross-sections comprising slender elements are widely used in construction engineering to pursue economic benefits. These sections undergo local buckling reduction in advance of failure, and their ultimate capacity may be significantly influenced by the uncertainty in localized imperfection, which has been described in Chapter 2. For this purpose, a new approach utilizing Fourier series to generate the 3D models of members with random ω is proposed. The proposed 3D model is employed for probabilistic studies presented in Chapter 8.

The proposed 3D model with random localized imperfection (ω) is based on superposition of Fourier series

expansion of different functions. Fourier series technique has been widely used for 3D surface modeling (Davis, 1973; Higgins, 1996). For a function f(x) that is periodic on an interval [−L, L], it can be expressed as Fourier series, given by

$$\mathrm{f}(x) = \frac{a_0}{2} + \sum_{k=1}^{\infty} [\mathrm{a}_k \cos\left(\frac{\mathrm{k}\pi x}{L}\right) + \mathrm{b}_k \sin\left(\frac{\mathrm{k}\pi x}{L}\right)] \qquad (8.1)$$

where

$$a_0 = \frac{1}{L}\int_{-L}^{L} f(x)\,dx \qquad (8.2)$$

$$a_k = \frac{1}{L}\int_{-L}^{L} f(x)\cos\left(\frac{\mathrm{k}\pi x}{L}\right)dx \quad (\mathrm{k} = 0, 1, 2, 3, \cdots) \qquad (8.3)$$

$$b_k = \frac{1}{L}\int_{-L}^{L} f(x)\sin\left(\frac{\mathrm{k}\pi x}{L}\right)dx \quad (\mathrm{k} = 1, 2, 3, \cdots) \qquad (8.4)$$

Assume a surface consists of $n \times m$ points in a 3D coordinate system, where X coordinate represents longitudinal (length) direction, Y represents transverse (width) direction, and Z represents deviation from the flat surface parallel to XY plane. For a point (x_i, y_j, z_{ij}) (i=1, 2, ···, m; j=1, 2, ···, n) on the surface, z_{ij} governs localized imperfection (ω). All $\boldsymbol{z_{ij}}$ elements comprise $n \times m$ matrix **[Z]** which can be determined by

$$[\mathbf{Z}] = [\mathbf{F_1}] + ([\mathbf{F_2}] - [\mathbf{F_1}])[\mathbf{S}] \qquad (8.5)$$

$$[\mathrm{F1}] = \begin{bmatrix} \mathrm{f}_1(\mathrm{x}_1) & \mathrm{f}_1(\mathrm{x}_2) & \cdots & \mathrm{f}_1(\mathrm{x}_i) & \cdots & \mathrm{f}_1(\mathrm{x}_m) \\ \mathrm{f}_1(\mathrm{x}_1) & \mathrm{f}_1(\mathrm{x}_2) & \cdots & \mathrm{f}_1(\mathrm{x}_i) & \cdots & \mathrm{f}_1(\mathrm{x}_m) \\ \vdots & \vdots & \vdots & \vdots & \vdots & \vdots \\ \mathrm{f}_1(\mathrm{x}_1) & \mathrm{f}_1(\mathrm{x}_2) & \cdots & \mathrm{f}_1(\mathrm{x}_i) & \cdots & \mathrm{f}_1(\mathrm{x}_m) \end{bmatrix}_{n\times m} \qquad (8.6)$$

$$\mathbf{[F_2]} = \begin{bmatrix} \mathrm{f}_2(\mathrm{x}_1) & \mathrm{f}_2(\mathrm{x}_2) & \cdots & \mathrm{f}_2(\mathrm{x}_i) & \cdots & \mathrm{f}_2(\mathrm{x}_m) \\ \mathrm{f}_2(\mathrm{x}_1) & \mathrm{f}_2(\mathrm{x}_2) & \cdots & \mathrm{f}_2(\mathrm{x}_i) & \cdots & \mathrm{f}_2(\mathrm{x}_m) \\ \vdots & \vdots & \vdots & \vdots & \vdots & \vdots \\ \mathrm{f}_2(\mathrm{x}_1) & \mathrm{f}_2(\mathrm{x}_2) & \cdots & \mathrm{f}_2(\mathrm{x}_i) & \cdots & \mathrm{f}_2(\mathrm{x}_m) \end{bmatrix}_{n\times m} \qquad (8.7)$$

Where $\mathrm{f}_1(\mathrm{x}_i)$ and $\mathrm{f}_2(\mathrm{x}_i)$ are functions that are decomposed into Fourier series.

[**S**] is m×m diagonal matrix

$$[\mathbf{S}] = \begin{bmatrix} \sin(\pi \mathrm{y}_j/\mathrm{B}) & 0 & \cdots & 0 \\ 0 & \sin(\pi \mathrm{y}_j/\mathrm{B}) & \cdots & 0 \\ \vdots & \vdots & \ddots & \vdots \\ 0 & 0 & \cdots & \sin(\pi \mathrm{y}_j/\mathrm{B}) \end{bmatrix}_{m\times m} \qquad (8.8)$$

$([\mathbf{F_2}] - [\mathbf{F_1}])[\mathbf{S}] =$

$$\begin{bmatrix} [f_2(x_1)-f_1(x_1)]\sin(\frac{\pi y_1}{B}) & \cdots & [f_2(x_i)-f_1(x_i)]\sin(\frac{\pi y_1}{B}) & \cdots & [f_2(x_m)-f_1(x_m)]\sin(\frac{\pi y_1}{B}) \\ [f_2(x_1)-f_1(x_1)]\sin(\frac{\pi y_2}{B}) & \cdots & [f_2(x_i)-f_1(x_i)]\sin(\frac{\pi y_2}{B}) & \cdots & [f_2(x_m)-f_1(x_m)]\sin(\frac{\pi y_2}{B}) \\ \vdots & \vdots & \vdots & \vdots & \vdots \\ [f_2(x_1)-f_1(x_1)]\sin(\frac{\pi y_n}{B}) & \cdots & [f_2(x_i)-f_1(x_i)]\sin(\frac{\pi y_n}{B}) & \cdots & [f_2(x_m)-f_1(x_m)]\sin(\frac{\pi y_n}{B}) \end{bmatrix} \quad (8.9)$$

The fundamental principles of generating 3D surfaces with random ω are illustrated by the following. $f_1(x_i)$ and $f_2(x_i)$ are two functions that are decomposed into Fourier series with random coefficients. **[F_1]** and **[F_2]** governs two curved surfaces, as shown in Fig 8.2(a), where L and B are the length and width of the surface, respectively. Localized imperfection (ω) is determined by matrix **([F_2]-[F_1])[S]**. It comprises two components: transverse variation and longitudinal variation, as shown in Fig. 8.2 (b). The shape and magnitude of ω in the longitudinal direction depends on the curve along longitudinal centerline. It is determined by the function $[f_2(x_i) - f_1(x_i)] \sin(\pi/2)$.The shape of ω in the transverse direction is modelled by a half-sine-wave, since its shape in transverse direction reported in most literatures is convexity /concavity. The half-sine-wave is determined by the function $[f_2(x_i) - f_1(x_i)] \sin(\pi y_j/B)$, as shown in Fig 8.2 (b), where the two half-sine waves correspond to (x_a, y_j) and (x_b, y_j) (j= 0, 1, ···, m). The generated surface with random ω is determined by **[F_1] + ([F_2]-[F_1])[S]**, as shown in Fig 8.2 (c).

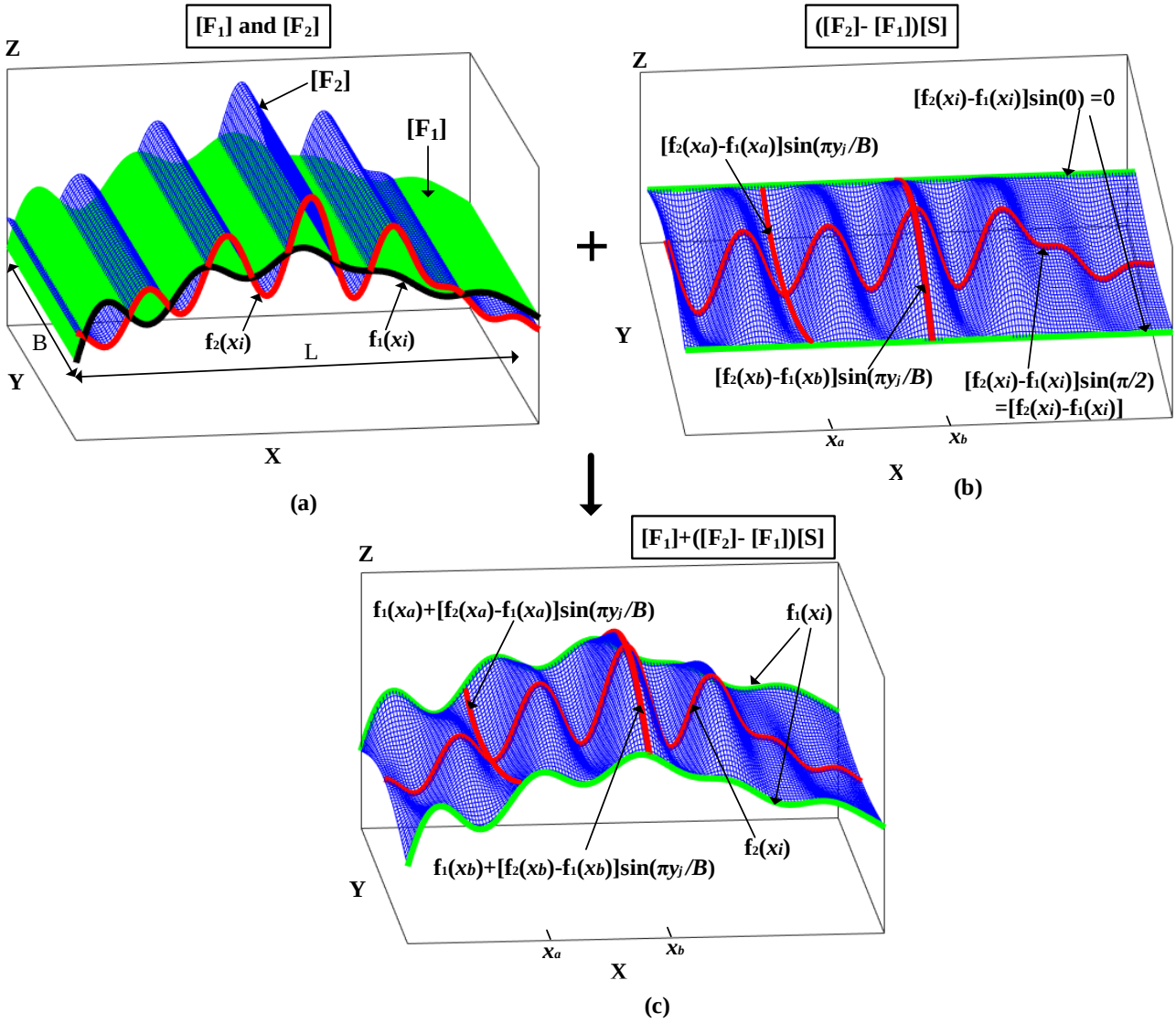

Fig. 8.2. Development of 3D surface with random ω (a) Two surfaces determined by $[F_1]$ and $[F_2]$ (b) Surface determined by $([F_2]-[F_1])[S]$ (c) Surface determined by $[F_1] + ([F_2]-[F_1])[S]$

Fig 8.3 shows the generated 3D model for a typical surface with random ω and half-sine edges. The 3D model of a member is finally assembled by four surfaces. It should be mentioned that in order to fit the four faces together, relevant coordinate transformation should be conducted. Coordinate transformation depends on assembling order and the position of the surface in a 3D space. For developing 3D model of RHS and SHS with round corners, additional curved surfaces representing round corners should be modelled. The generated 3D model for member with random ω and straight edges is shown in Fig. 8.4 (a). The 3D model of a member with random ω and half-sine-wave edges is shown in Fig.8.4 (b). Fig. 8.4 (c) shows the 3D model of a member with random ω and complex edges. For developing 3D model of RHS and SHS with round corners, additional curved surfaces representing round corners should be modelled and assembled.

Fig. 8.4 (d) shows the generated 3D model with round corner, random localized imperfection and half-sine-wave edges.

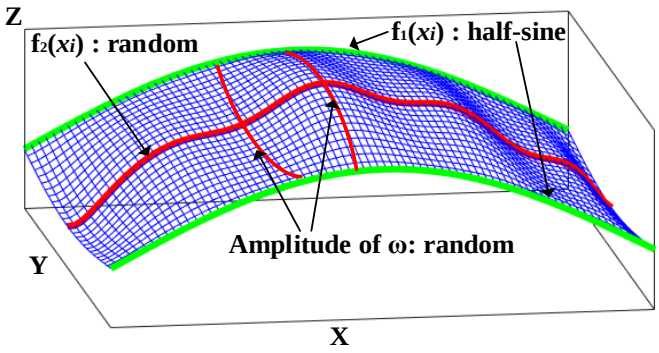

Fig 8.3 A typical surface with random ω and half-sine edges

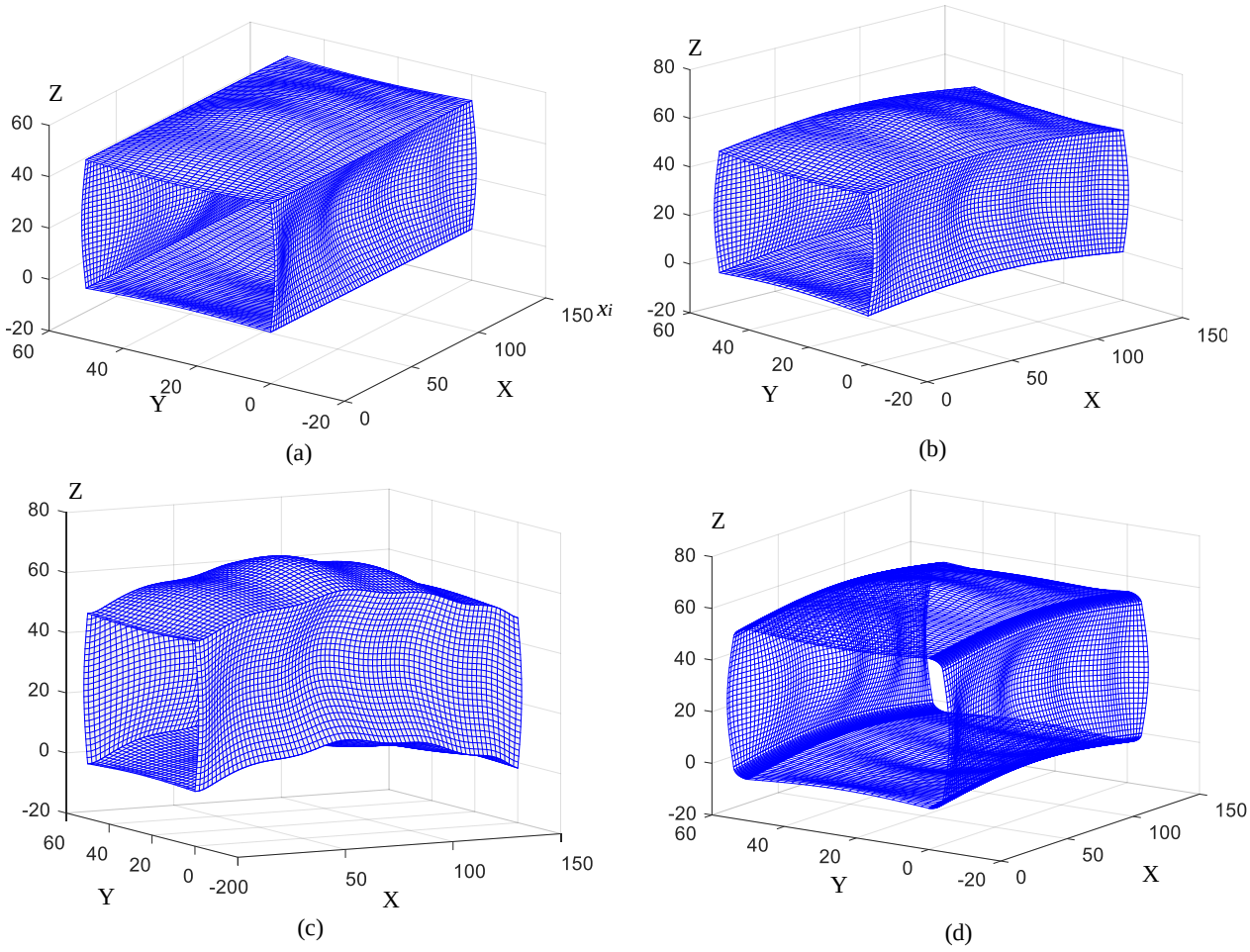

Fig. 8.4. Generated 3D models with random localized imperfection (a) member with straight edges (b) member with half-sine-wave edges (c) member with complex edges (d) member with round corners and

half-sine-wave edges

8.4 Effect of uncertainty in ω on the capacity of columns susceptible to local buckling

8.4.1 Columns for probabilistic studies

A series of stainless steel columns with cold-formed RHS and SHS are selected among the tested specimens reported in the literature. The studied columns have cross-sectional slenderness (λ_l) higher than 0.776. This is to ensure that the columns undergo cross-sectional local buckling reduction before they reach the ultimate compressive strength.

Table 8.2. Details of the selected stainless steel columns for probabilistic studies

Reference	Specimen	D (mm)	W (mm)	t (mm)	R (mm)	L (mm)	λ_c	λ_l	ω_g
Young and Lui, 2006	SHS2L300	50.1	50.3	1.58	2.8	300	0.14	0.8	-
	RHS1L3000	140.1	79.9	3.01	10.0	3000	0.71	0.9	0.927
Huang and Young, 2013	C5L200	100.1	50.1	2.5	3.7	200	0.18	1.0	-
	C6L200	150.0	50.1	2.5	4.3	200	0.18	1.5	-
	C6L550	150.1	50.2	2.49	4.5	550	0.48	1.4	0.5
	C5L900R	100.1	50.4	2.49	3.5	900	0.79	0.8	0.857
	C6L900	150.4	50.3	2.47	4.7	900	0.79	1.3	0.857
	C6L1200	149.9	50.5	2.46	4.5	1200	1.04	1.2	1.143
	C6L1550	150.5	50.3	2.49	4.5	1550	1.35	1.0	1.476
Afshan and Gardner, 2013	RHS 120x80x3-SC2	120.0	80.0	2.83	6.7	362	0.16	0.82	-
	RHS 120x80x3-1077	120.0	79.9	2.87	6.8	1077	0.35	0.8	0.95
	RHS 120x80x3-1577	120.0	79.9	2.81	6.4	1577	0.51	0.8	0.96
Young and Liu, 2003	R1L1200	120.1	40.1	1.94	5.0	1199	0.48	1.1	0.254
	R1L2000	120.2	40.0	1.95	5.1	2000	0.80	1.0	0.444
	R3L2000	120.0	80.0	2.80	6.7	2000	0.44	0.8	0.381
Gardner and Nethercot,2004	SHS100x100x2-LC-2m	99.8	99.9	1.86	3.2	2000	0.73	1.0	0.1
	RHS100x50x2-LCJ-2m	99.8	49.8	1.83	3.7	2000	0.80	0.9	0.6
	RHS100x50x2-LC-1m	99.8	50.0	1.82	3.6	1000	0.69	1.0	0.1
	RHS120x80x3-LC-1m	120.0	80.2	2.86	5.7	1001	0.45	0.8	1
Young and Lui, 2005	160x80x3	160.1	80.8	2.87	9.0	600	0.09	1.2	-
	200x110x4	196.2	108.5	4.01	13.0	600	0.07	1.1	-

The Details of the studied columns are shown in Table 8.2. Namely, D, W and t are the depth, width and thickness of the hollow cross-section, respectively; R is external radius of the round corner; L is the length

of the column; λ_c and λ_l are member slenderness and cross-sectional slenderness, respectively; ω_g is the amplitude of global member imperfection (out-of-straightness). ω_g is not reported for some cases of stub columns ($\lambda_c \leq 0.2$), while the shape of ωg is adopted as a half-sine wave for other columns.

8.4.2. Generation of 3D models and FE analysis

The structural behavior of stainless steel columns with random ω was studied using finite element (FE) software Abaqus 6.13. The Fourier series-based 3D model of the columns with random ω was generated by Matlab 2017b. Then the generated models were then imported into Abaqus to conduct FE analysis. Input file of ABAQUS is generated by MATLAB script.

8.4.2.1 Generation of 3D model with random ω using MATLAB

The development of the coefficient of Fourier series terms of function $f_2(x)$ and $f_2(x)$ was performed in Matlab. For the stub columns ($\lambda_c \leqslant 0.2$), Fourier series expansion of function $f_1(x)$ generated a straight line. For other columns, $f_1(x)$ generated half-sine-waves, where the magnitude of half-sine wave was taken as the corresponding ω_g shown in the above Table 8.2. For all columns, coefficients of Fourier series terms of function $f_2(x)$ were defined as random. The maximum amplitude of the modelled ω for each column was limited to min{0.008b, 0.5}. For each column, 50 models with random values of localized imperfection **ω** were produced. The developed Matlab program automatically created a Python script associated with an Input file operated in Abaqus. It is worth pointing out that the distribution of the generated random ω_{max} followed a log-normal distribution as the experimental data of ω_{max}. This was explicitly set in the developed Matlab program.

8.4.2.2 FE analysis using ABAQUS

To accurately predict the response of the studied columns, the adopted stress-strain curve for each column is obtained from tensile coupons test. Details of the stress-strain curves are reported in the literature. In the FE analysis, only longitudinal bending residual stresses are considered and they are implicitly included in the stress-strain curves obtained from tensile coupons test. For each model of the column with random ω,

Abaqus/Standard (implicit solver) was employed for FE analysis. A 4-nodes shell element with reduced integration (S4R) was used. It allows transverse shear deformation, and accounts for finite membrane

strains and arbitrarily large rotations. The number of integration points through the thickness is five (Simpson's rule). The load-displacement response was predicted using an incremental procedure based on arc-length methods. The modified Riks method (1979), which is available in Abaqus, was used. Based on a mesh convergence study, at least ten elements across the plate widths were used. Stainless steels have considerable non-linear stress-strain response. To accurately predict the structural behavior of the studied columns, the adopted material property for each column was obtained from corresponding uniaxial tensile stress-strain coupon test. Details of the parameters that describe the stress-strain curves can be found in the literature. For all the models, edge elements at both ends (top and bottom) were kinematically coupled and connected to two control points where the relevant degrees of freedom were constrained.

Spread of plasticity through cross-section and along member length was traced by distributed plasticity approach. In FE analysis, residual stresses have to be considered as they may have negative effects on the ultimate capacity of a structure. Since the effect of through-thickness longitudinal bending residual stresses on the global behavior of stainless steel members with box sections are dominant (Jandera and Machacek, 2014), only longitudinal bending residual stresses were considered and they were implicitly included in the stress-strain curves obtained from tensile coupons test. For each model of the column with random ω_{max}, GMNIA was carried out to determine the ultimate compressive strength of the column.

8.4.3. Predicted results of the statistical characteristics of the ultimate compressive load

The experimental results and predicted results of the columns with random localized imperfection and are shown in Table 8.3. Namely, $P_{u\text{-}EXP}$ is the ultimate compressive strength obtained from experiment; $P_{u\text{-}rand}$ is the predicted ultimate compressive strength for each model (each column have 50 models); μ and COV are the mean value and Coefficients of Variation, respectively; $|\varepsilon_{max}|$ is the maximum value of relative error for each set of 50 models.

Table 8.3 Experimental results and predicted results for the studied columns

Specimen	λ_l	$P_{u\text{-}EXP}$ (kN)	$\mu(P_{u\text{-}rand})$ (kN)	$\mu(P_{u\text{-}rand})$ / $P_{u\text{-}EXP}$	COV($P_{u\text{-}rand}$)	$\lvert\varepsilon_{max}\rvert$
SHS2L300	0.84	175.7	177.8	0.985	0.086	0.043
RHS1L3000	0.88	513.5	454.7	0.980	0.073	0.077
C5L200	0.95	370.1	387.5	1.103	0.036	0.065
C6L200	1.47	404.1	413.2	0.931	0.175	0.171
C6L550	1.41	353.2	388.1	1.026	0.212	0.175
C5L900R	0.84	336.0	326.0	1.007	0.055	0.029
C6L900	1.32	333.5	345.2	0.988	0.139	0.098
C6L1200	1.20	284.5	300.7	1.142	0.108	0.185
C6L1550	1.02	230.0	249.2	1.008	0.095	0.102
RHS 120x80x3-SC2	0.82	441.0	434.2	1.072	0.093	0.086
RHS 120x80x3-1077	0.79	463.0	432.1	1.018	0.109	0.075
RHS 120x80x3-1577	0.79	382.0	401.5	0.973	0.045	0.058
R1L1200	1.07	167.0	153.5	1.02	0.129	0.115
R1L2000	0.97	141.3	137.9	0.999	0.088	0.055
R3L2000	0.79	394.0	355.7	1.071	0.071	0.047
SHS100x100x2-LC-2m	1.04	176.0	183.0	1.066	0.162	0.096
RHS100x50x2-LCJ-2m	0.92	157.0	145.3	1.041	0.085	0.117
RHS100x50x2-LC-1m	0.96	163.0	151.4	1.090	0.133	0.102
RHS120x80x3-LC-1m	0.79	448.0	415.5	1.053	0.079	0.086
160x80x3	1.24	537.3	505.0	0.939	0.158	0.139
200x110x4	1.07	957.0	928.0	0.958	0.081	0.070

For all the studied columns, $\mu(P_{u\text{-}rand}) / P_{u\text{-}EXP}$ and COV ($P_{u\text{-}rand}$) versus λ_l are plotted in Fig 8.5(a) and 8.5(b), respectively. A plot of $|\varepsilon_{max}|$ against λ_l is shown in Fig 8.5(c). It is observed that the value of $\mu(P_{u\text{-}rand}) / P_{u\text{-}EXP}$ range between 0.931-1.103 for all the columns except the column with λ_l =1.20. Compared to $P_{u\text{-}EXP}$, the value of $\mu(P_{u\text{-}rand})$ for most columns with relatively lower cross-sectional slenderness (λ_l < 1.0) is overestimated, while the value of $\mu(P_{u\text{-}rand})$ for columns with higher cross-sectional slenderness seems to be underestimated. For the column with λ_l =1.20, the value of $\mu(P_{u\text{-}rand}) / P_{u\text{-}EXP}$ is 1.142. It indicates that most predicted results (from the 50 models with random ω) significantly overestimate the experimental result. This may be due to the reason that the value of actual maximum localized imperfection for this column, which is not reported in the literature, is relatively larger compared to the modelled ω whose maximum value is min{0.008b, 0.5}.

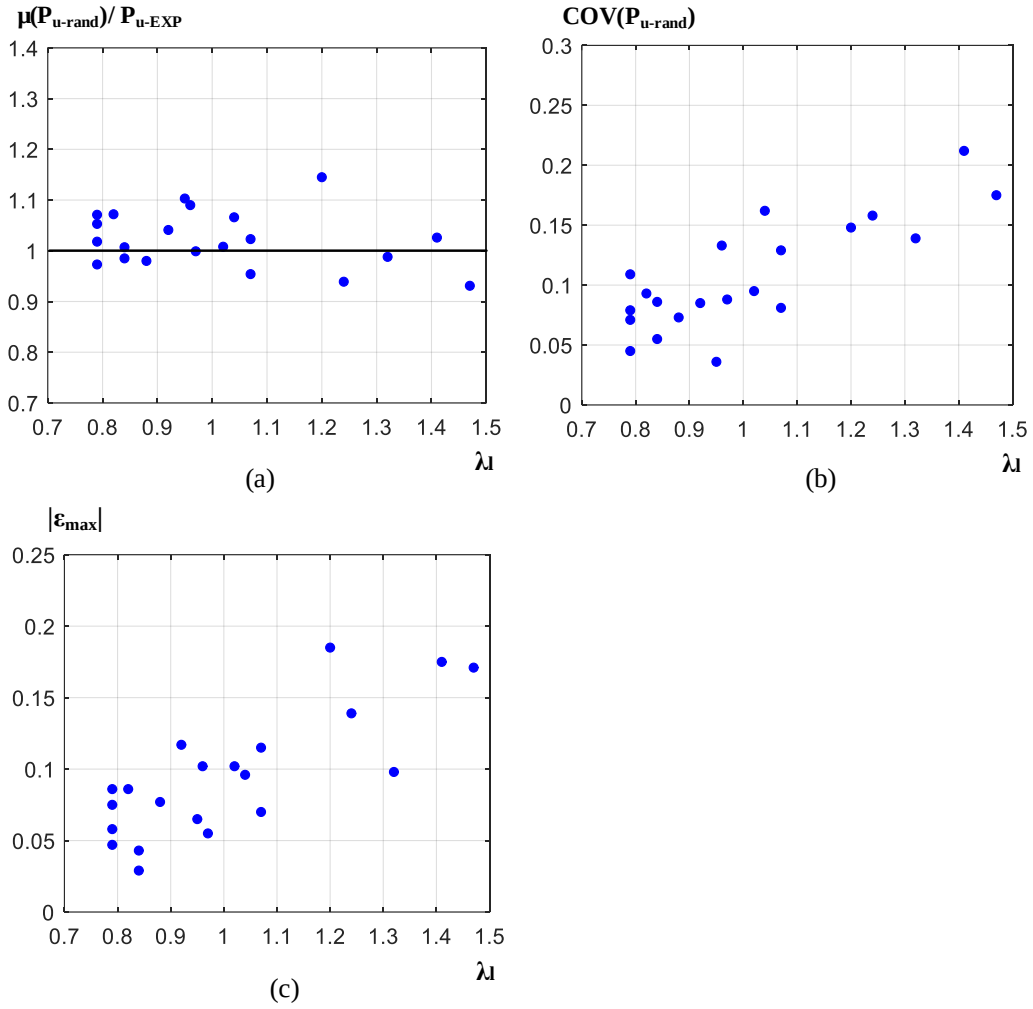

Fig 8.5. Predicted results against cross-sectional slenderness (a) $\mu(P_{u\text{-}rand}) / P_{u\text{-}EXP}$ versus λ_l (b) COV ($P_{u\text{-}rand}$) versus λ_l (c) $|\varepsilon_{max}|$ versus λ_l

On the other hand, both COV ($P_{u\text{-}rand}$) and $|\varepsilon_{max}|$ increase as λ_l increases. One explanation is that, the larger the cross-sectional slenderness is, the more sensitive the column is to initial localized imperfection. Consequently, the change in the value of modelled localized imperfection can result in larger discrepancy in the ultimate compressive strength.

For the columns with relatively lower cross-sectional slenderness ($\lambda_l < 1.0$), the values of COV ($P_{u\text{-}rand}$) and $|\varepsilon_{max}|$ are less than 0.13 and 0.12, respectively. The result indicates that uncertainty in ω has not considerable influence on the ultimate compressive strength of these columns. This may be due to the reason that the columns with relatively lower cross-sectional slenderness are still not sensitive to initial localized imperfection. Besides, the result indicates that ω can statistically be modelled as deterministic for these columns, such as using measured ω in experimental study.

For the columns with $\lambda_l \geq 1.2$, COV ($P_{u\text{-}rand}$) are around 0.139-0.238 and the maximum value of $|\varepsilon_{max}|$ is 17.5%. It demonstrates that random ω results in largely scattered ultimate compressive strength for the columns with larger cross-sectional slenderness, and it is important to consider the effect of uncertainty in ω on these columns. The distribution of $P_{u\text{-}rand}$ for a typical column (R1L1200) is shown in Fig 8.6. In the figure, $P_{u\text{-}rand}$ is normalized by $P_{u\text{-}EXP}$. It is found that the distribution of $P_{u\text{-}rand}$ / $P_{u\text{-}EXP}$ can be fitted by a normal distribution.

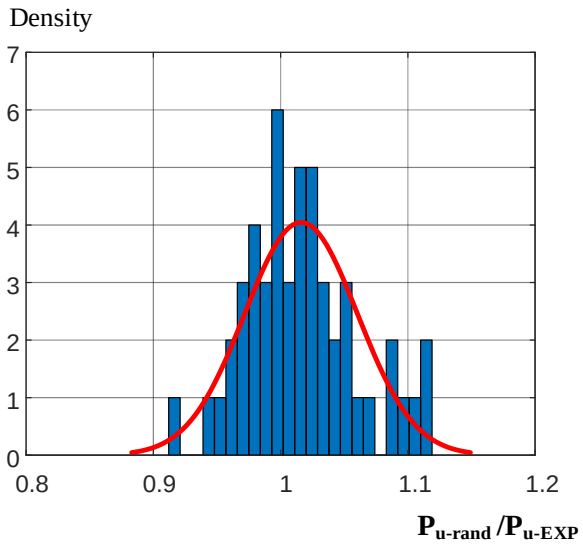

Fig 8.6. Histograms of $P_{u\text{-}rand}$ / $P_{u\text{-}EXP}$ for a typical column (R1L1200)

8.5 Effect of uncertainty in ω on the accuracy of GNA-$\tau_{MN\text{-}\rho}$

8.5.1 Beam-columns for probabilistic studies

The studied beam-columns are the same beam-columns presented in Section 7.4, but only one combined loading case is considered for each beam-column. All the studied beam-columns, shown in Fig. 8.7, are susceptible to local buckling. For all the studied beam-columns, the applied axial load (P) is factored load. For simply supported beam-columns, the applied end moment M_2=e*P; e=50mm (constant). For cantilever beam-columns, the applied horizontal load at the cantilever end is equal to 0.1P. Details of conducted analysis are shown in Table. 8.4.

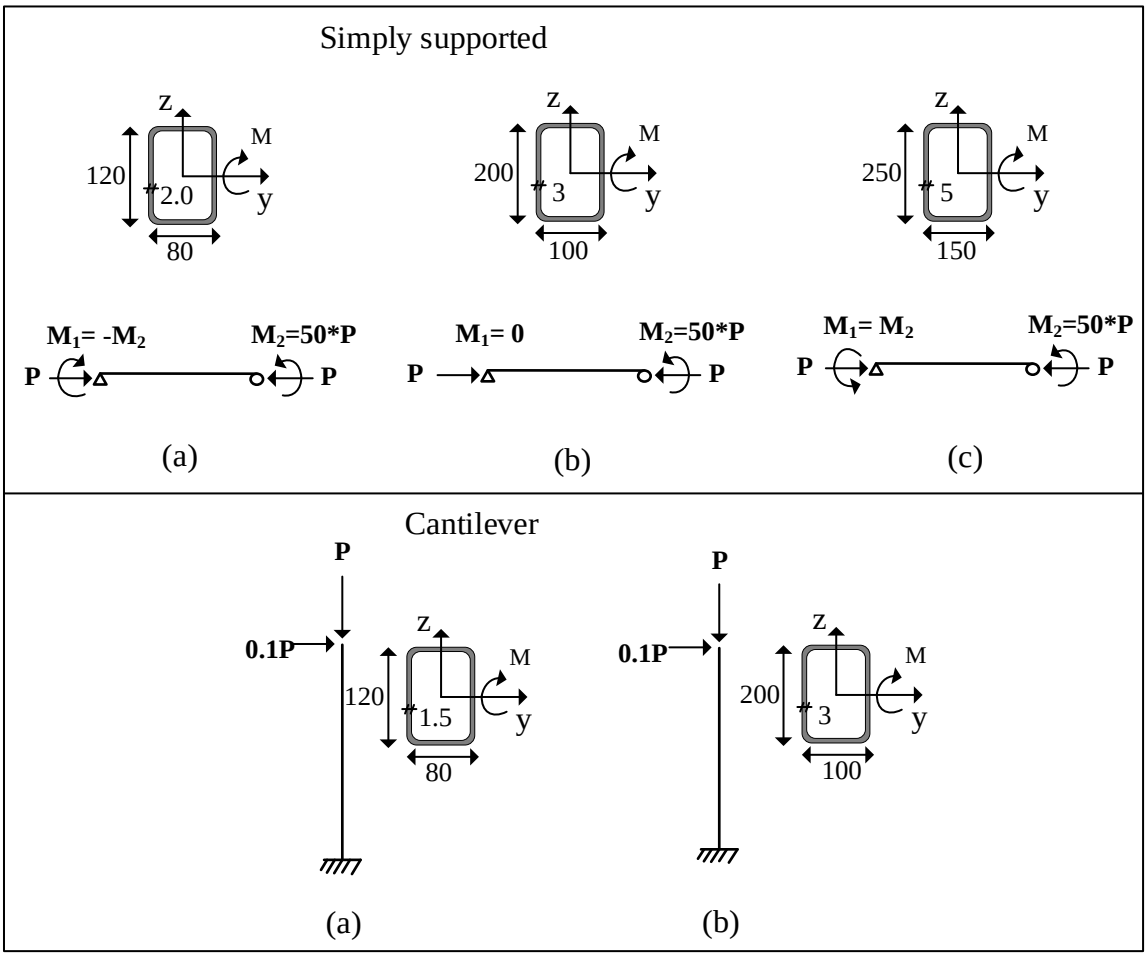

Fig 8.7 The studied beam-columns

For each beam-column, 100 models with random ω are produced. For each model, GMNIA-shell (with random ω) analysis is carried out to determine the ultimate axial load and end moment (referred to as $M_{u\text{-}rand}$). Thus, each beam-column has 100 $M_{u\text{-}rand}$ in all.

Table 8.4. Details of conducted analysis

Method	Element	Localized imperfection (ω)	
		Shape	Amplitude(mm)
GMNIA	Shell	Idealized	ω_{max}=0.185
GNA-$\tau_{MN\text{-}\rho}$	beam	Implicitly considered in $\tau_{MN\text{-}\rho}$	
GMNIA	Shell	Random	$0< \omega_{max} \leq$min {0.008b, 0.5}

8.5.2 Generation of 3D models and FE analysis

The procedure of generating of 3D models with random ω for beam-columns are similar to that for columns.

There is slight difference between simply supported beam-columns and cantilever beam-columns. For simply supported beam-columns, Fourier series expansion of function $f_1(x)$ generated half-sine-waves. For cantilever beam-columns, Fourier series expansion of function $f_1(x)$ generated straight lines, since the effects of out-of-straightness and out-of-plumbness are considered by applying notional loads (equivalent horizontal loads).

Two types of finite elements are employed: one-dimensional beam elements (B21) and three-dimensional shell elements (S4R). In conducting GNA with stiffness reduction, beam elements are employed, while shell element is employed in implementing GMNIA. The cross-section (without rounder corner) is defined as box section for beam element. To make the results determined by beam element and those determined by shell element comparable, the same box section is used for shell element. The stress-strain curves and the longitudinal bending residual stresses were modelled as those presented in Chapter 3

8.5.3. Predicted results of the statistical characteristics of the ultimate external moment

M_u(kN*m)	Simply supported			Cantilever	
	a	b	c	a	b
$M_{u\text{-}GMNIA\text{-}S}$	6.0	21.9	76.8	4.75	30.83
$M_{u\text{-}\tau MN\text{-}\rho}$	5.2	23.5	77	4.03	32.15
$\mu(M_{u\text{-}rand})$	5.9	22.2	79.6	4.66	29.90
$COV(M_{u\text{-}rand})$	0.07	0.05	0.11	0.05	0.13
$\mu(M_{u\text{-}rand})/ M_{u\text{-}GMNIA\text{-}S}$	0.98	1.01	1.04	0.98	0.97
$\mu(M_{u\text{-}ran}) / M_{u\text{-}\tau MN\text{-}\rho}$	1.13	0.94	1.03	1.15	0.93

The predicted results are shown in Table. 8.5. Since the ultimate end moment (M_u) is directly proportional to the ultimate axial load (P_u), where $M_u=e*P_u$ for the simply supported beam-columns and $M_u=0.1P_u*L$ for the cantilever beam-columns, only M_u predicted by different method is shown in the table. In the table, $M_{u\text{-}GMNIA\text{-}S}$ is determined by GMNIA-shell with idealized ω (the lowest local buckling mode), and $M_{u\text{-}\tau MN\text{-}\rho}$ is determined by GNA-$\tau_{MN\text{-}\rho}$. Both of them are already shown in Section 7.4. The mean value of the $M_{u\text{-}rand}$ is denoted $\mu(M_{u\text{-}rand})$.

From the table, COVs (Coefficients of Variation) for the simply supported beam-column of case c is 0.11, and COVs for the cantilever beam-column of case b is 0.13. The two COVs demonstrate a relatively large extent of variability in relation to $\mu(M_{u\text{-}rand})$. One possible explanation is that the localized imperfection (ω)

amplitude of the generated models is largely scattered. The mean-to-nominal ratios, μ ($M_{u\text{-}rand}$)/ $M_{u\text{-}GMNIA\text{-}S}$, for all the beam-columns are about 0.98-1.04, which indicates that for the studied beam-columns, localized imperfection (ω) can be statistically modelled as idealized shape times the deterministic value 0.185 (the mean value of the maximum ω).

The ratios of μ ($M_{u\text{-}rand}$) / $M_{u\text{-}\tau MN\text{-}\rho}$, for all the beam-columns are all about 0.93-1.15. It shows that prediction errors for GNA-$\tau_{MN\text{-}\rho}$ caused by uncertainty in ω are acceptable. This is because the results provided by GNA-$\tau_{MN\text{-}\rho}$ generally close to those provide by GMNIA with idealized ω times the deterministic value of 0.185, where the ultimate external moment of the latter can statistically represent the ultimate external moment of the beam-columns with random ω.

8.6 Concluding remarks

An approach of generating 3D model with random localized imperfection (ω) is presented. The proposed 3D model with random ω is based on superposition of Fourier series expansion of different functions. The effect of uncertainty in ω on the ultimate capacity of cold-formed stainless steel columns and beam-columns that are susceptible to local buckling is studied.

For a series of columns, it is found that both the coefficients of variation and the maximum value of absolute error for the predicted results increases as cross-sectional slenderness increases. This is due to the reason that columns with large cross-sectional slenderness are sensitive to initial localized imperfection, and consequently the change in the value of modelled localized imperfection can lead to much discrepancy in the ultimate compressive strength. Therefore, the effect of uncertainty in ω on the columns with larger cross-sectional slenderness should be considered in practical design.

For the studied beam-columns, the mean value of the ultimate end moment obtained from GMNIA in which ω is modelled randomly, is very close to the ultimate end moment obtained from GMNIA in which ω is modelled as local buckling mode times 0.185. It also shows uncertainty in ω result in prediction errors for GNA-$\tau_{MN\text{-}\rho}$ to some extent, but ignoring uncertainty in ω does not lead to significant errors for GNA-$\tau_{MN\text{-}\rho}$ (prediction errors are within 15%).

9. Conclusions and suggestions for future research

9.1 Conclusions

The following is a summary of the conclusions drawn from this research:

(1) Column flexural stiffness reduction factor (τ_N) and beam flexural stiffness reduction factor (τ_M), applicable to stainless steel members with compact cold-formed RHS and SHS, are developed. The proposed τ_N depends on the maximum internal first order axial force within a member (P_{r1}). The proposed τ_M depends on the maximum internal first order moment within a member (M_{r1}) and material properties (E, f_y, and n). The results of verification study show that GNA coupled with the developed stiffness reduction factor (τ_N and τ_M) reaches the accuracy of GMNIA. The slight discrepancy between the developed stiffness reduction factor (τ_N and τ_M) and the actual stiffness reduction factor will be considered in the development of the approximate expression of stainless steel beam-column stiffness reduction factor (τ_{MN}) expression.

(2) Flexural stiffness reduction factor (τ_{MN}) formulation applicable to the in-plane stability design of stainless steel beam-columns is proposed through analytical and numerical study. The proposed beam-column flexural stiffness reduction factor (τ_{MN}) accounts for deleterious influence of spread of plasticity, residual stresses and member out-of-straightness of 0.001. Two main aspects of developing τ_{MN} are: (1) Develop analytical expression of τ_{MN} through extending formulations that evaluate second order effects of beam-columns. These formulations are extended to determine maximum second order inelastic moment of beam-columns by incorporating τ_{MN} into elastic critical buckling load. (2) Based on numerical study of beam-columns, the approximate expression of τ_{MN} is developed by fitting relevant variables to analytically determined expression.

The soundness and accuracy of τ_{MN} determined by analytical expression are verified through comparison of maximum bending moments within members determined through GNA-τ_{MN} against those obtained from GMNIA. It is observed that predicted results from GNA-τ_{MN} are in very close agreement with those provided by GMNIA. Besides developing flexural stiffness reduction factor (τ_N, τ_M , τ_{MN}) formulations that are applicable to stainless steel members. Moreover, it is worth pointing out that the formulations of evaluating second order elastic effects are extended to determine inelastic maximum second order moment within beam-columns, through incorporating τ_{MN} into elastic critical buckling load. Furthermore, since in

practical design M_{r2} is not known in advance, an approximate expression of τ_{MN}, which is assumed to be a function of relevant variables, is proposed by fitting variables to the analytically determined expression. For the purpose of developing the approximate expression of τ_{MN}, column flexural stiffness reduction factor (τ_N) and beam flexural stiffness reduction factor (τ_M) are derived from stainless steel column strength curves and from the moment-curvature relationship, respectively.

(3) The accuracy of GNA coupled with flexural stiffness reduction factor (determined by the approximate expression) for the in-plane stability design of stainless steel frames is verified. The maximum bending moment and Demand-Capacity ratio within a member determined by GNA-τ_{MN} and GNA-τ_N are compared against those determined by GMNIA. It is found that predicted results of GNA-τ_{MN} are in close agreement with those provided by GMNIA. In some cases, GNA-τ_N gives unsafe predictions for the frames that are very sensitive to second order effects, one possible explanation is the adopted stiffness reduction factor $0.8\tau_N$ underestimates actual reduced stiffness, and therefore underestimates additional second order effects resulted from material non-linearity. Both GNA-τ_{MN} and GNA-τ_N are safe for predicting the ultimate capacity (member-based) of the studied frames that are not sensitive to second order effects. Compared to GNA-τ_N, GNA-τ_{MN} with lower deviation from predicted results of GMNIA, provides improved estimation of internal moments and Demand-Capacity ratios for most members. This is due to the reason that τ_{MN} can accurately capture stiffness reduction caused by spread of plasticity through cross-section and along members. As a consequence, GNA-τ_{MN} produces more reasonable distribution of internal force and moment, and well captures additional second order effects due to material non-linearity.

(4) The stiffness reduction factor formulations, applicable to stainless steel elements and frames with compact sections, are extended to account for local buckling effects and initial localized imperfection (ω). Local buckling effects and influence of initial localized imperfection are accounted for by means of reducing the gross section resistance using a factor ρ. The factor ρ, determined by the Direct Analysis Method, depending on cross-section slenderness, is adopted. The accuracy of GNA with extended stiffness reduction factor for in-plane stability design of stainless steel elements (columns, beams and beam-columns) with non-compact and slender sections is verified. Predicted results by GNA with stiffness reduction (using shell element) are in close agreement with those determined by GMNIA using shell element.

(5) The effect of uncertainty in ω on the ultimate capacity of cold-formed stainless steel columns and beam-columns that are susceptible to local buckling is studied. For a series of columns, it is found that both the

coefficients of variation and the maximum value of absolute error for the predicted results increases as cross-sectional slenderness increases. This is due to the reason that columns with larger cross-sectional slenderness are sensitive to initial localized imperfection, and consequently the change in the value of modelled localized imperfection can lead to much discrepancy in the ultimate compressive strength. Therefore, the effect of uncertainty in ω on the columns with larger cross-sectional slenderness should be considered in practical design. For the studied beam-columns, the mean value of the ultimate end moment obtained from GMNIA in which ω is modelled randomly, is very close to the ultimate end moment obtained from GMNIA in which ω is modelled as local buckling mode times 0.185. It also shows uncertainty in ω result in prediction errors for GNA-$\tau_{MN-\rho}$ to some extent, but ignoring uncertainty in ω won't lead to significant errors for GNA-$\tau_{MN-\rho}$.

9.2 Recommendations for future research

(1) The influence of uncertainty in system strength, member strength, connection strength, and stiffness, should be considered for the stability design of frames. For the GNA coupled with tangent modulus method in this thesis:

(a) Effect of uncertainty in stiffness on member strength is included in member strength formulas with K=1. In the adopted member strength formulations, the resistance factor, 0.9, for both compression and flexure, can ensure reliability index (β) for carbon steel members not fall below 2.6. However, the resistance factor may be lower for stainless steel to ensure similar reliability levels.

(b) Effect of uncertainty in stiffness on overall structural response is thought being included in the stiffness reduction factor. Whether or not reliability requirements are fulfilled should be studied further.

(2) The applicability and accuracy of the GNA coupled with tangent modulus method for frames with non-compact or slender sections should be assessed, and the comparison against system-based design method should be made.

References

Abdel-Ghaffar M., White D.W., Chen W. F. (1991). Simplified second-order inelastic analysis for steel frame design. Special Volume of Session on Approximate Methods and Verification Procedures of Structural Analysis and Design, Proceedings at Structures Congress 91, ASCE, New York, 47-62.

Abaqus v.6.13 Reference Manual. Simulia, Dassault Systemes, 2013.

Afshan S., Gardner L. (2013). Experimental study of cold-formed ferritic stainless steel hollow sections. *Journal of Structural Engineerig ASCE,* 139(5), 717-728.

Afshan S., Rossi B., Gardner L.(2013). Strength enhancements in cold-formed structural sections -Part 1: Material testing, Journal of Constructional Steel Research. 83, 177–188.

Al-Mashary F., Chen W. F. (1991). Simplified second-order inelastic analysis for steel frames. *Journal of Structural Engineering, ASCE*, 69(23), 395-399.

AISC 360-05 (2005): Specification for Structural Steel Buildings, American Institute of Steel Construction, Chicago.

AISC 360-10 (2010): Specification for Structural Steel Buildings, American Institute of Steel Construction, Chicago.

AISC 360-16 (2016): Specification for Structural Steel Buildings, American Institute of Steel Construction, Chicago.

AISC 303-16 (2016), Code of standard practice for steel buildings, American Institute of Steel Construction, Chicago.

AISI (1986): Specifications for the Design of Cold-Formed Steel. American Iron and Steel Institute (AISI), Washington, D.C.

AISI S100-16 (2016): North American Specification for the Design of Cold-Formed Steel Structural Members, American Iron and Steel Institute (AISI), Washington, D.C.

Alvarez R. J., Birnstiel C. (1967). Elasto-plastic analysis of plane rigid frames. Reports of Department of Civil Engineering, School of engineering and science, New York University, New York, USA.

ANSYS v19.0 Reference Manual, ANSYS, Inc. 2019.

Arrayago I., Real E.(2015). Experimental study on ferritic stainless steel RHS and SHS cross-sectional resistance under combined loading. *Structures*, 4, 69–79.

Arrayago I., Real E., Gardner L. (2015). Description of stress-strain curves for stainless steel alloys, *Materials & Design*, 87, 540–552.

Arrayago I. (2016). New approach for efficient design of stainless steel RHS and SHS elements, Doctoral thesis. Universitat Politècnica de Catalunya, Barcelona.

Arrayago I., Real E., Mirambell E.(2016). Experimental study on ferritic stainless steel RHS and SHS beam-columns, *Thin-Walled Structures*, 100, 93–104.

Arrayago I., Rasmussen K.J.R., Real E.(2017a). Full slenderness range DSM approach for stainless steel hollow cross-sections. *Journal of Constructional Steel Research*, 133, 156–166.

Arrayago I., Rasmussen K.J.R., Real E.(2017b). Full slenderness range DSM approach for stainless steel hollow cross-section columns and beam-columns. *Journal of Constructional Steel Research*, 138, 246–263.

Argyris J. H. (1965). Continua and Discontinua. First Conference on Matrix Methods in Structural Mechanics. OH, Wright-Patterson Air Force Base: 11-189.

AS/NZS 4673 (2001): Cold-formed stainless steel structures, Standards Australia/Standards New Zealand.

ASCE/SEI 7-16 (2016). Minimum Design Loads and Associated Criteria for Buildings and Other Structures, American Society of Civil Engineers, Reston.

Austin W.J. (1961). Strength and design of metal beam-columns, *Journal of the Structural Division, ASCE*, 87, 1–32.

Avery P (1998). Advanced Analysis of Steel Frame Structures Comprising Non-Compact Sections. Doctoral Thesis. School of Civil Engineering, Queensland University of Technology, Australia.

Baddoo N (2013). Design Guide 27: Structural Stainless Steel, American Institute of Steel Construction, Chicago.

Baddoo N., Francis P. (2014) Development of design rules in the AISC Design Guide for structural stainless steel, *Thin-Walled Structures*, 83, 200-208.

Batoz J.L., Dhatt G. (1979). Incremental displacement algorithms for nonlinear problems. International Journal for Numerical Methods in Engineering, 14(8), 1262-1267.

Becque J., Rasmussen K.J. R.(2009). Experimental investigation of the interaction of local and overall buckling of stainless steel I-columns. *Journal of Structural Engineering*,135(11), 1340-1348.

Bock M., Arrayago I., Real E.(2015). Experiments on cold-formed ferritic stainless steel slender sections. *Journal of Constructional Steel Research*, 109, 13–23.

Bridge R.Q., Bizzanelli P. (1987). Imperfections in Steel Structures, Proceedings-1987 Annual Technical Session, and Meeting, Structural Stability Research Council, 447-458.

BS 5950-1(2007): Structural use of steelwork in building -Part 1: Code of practice for design-Rolled and welded sections, British Standards Institution.

Chan S.L.(2001). Non-linear behavior and design of steel structures. *Journal of Constructional Steel Research*, 57, 1217–1231.

Chacón R., Vega A., Mirambell E.(2019). Numerical study on stainless steel I-shaped links on eccentrically braced frames. *Journal of Constructional Steel Research*, 159, 67-80.

Chen W. F., Atsuta, T. (1977). Theory of beam-columns, vol. 2, space behavior and design. McGraw-Hill, New York, US.

Chen W.F.(1992). Design of beam-columns in steel frames in the United States, *Thin-Walled Structures*, 13(1–2),1-83.

Chen W.F., Kim S. E.(1997). LRFD steel design using advanced analysis. CRC Press, Boca Raton, Florida, US.

Chen W. F. (2000). Structural Stability: From Theory to Practice. *Engineering Structures*, 22(2): 116-122.

Chen W.F., Lui E.M. (2017). Stability design of steel frames, CRC Press. Boca Raton, Florida, US.

Cheong-Siat-Moy F. (1977). Consideration of secondary effects in frame design, *Journal of the Structural*

Division, ASCE, 103(10), 2005-19.

Clarke M. J., Bridge R. Q., Hancock G. J., Trahair N. S. (1992). Benchmarking and verification of second-order elastic and inelastic frame analysis programs in SSRC TG 29 workshop and monograph on plastic hinge based methods for advanced analysis and design of steel frames, SSRC, Lehigh University, Bethlehem, USA.

Clarke M., Bridge R. Q. (1992). The Inclusion of Imperfections in the Design of Beam-Columns. Proc. 1992 Annu. Tech. Session, SSRC, Lehigh University, Bethelem, 327–346.

Clarke M., Bridge R. Q. (1996). The Design of Steel Frames Using the Notional Load Approach. Proc. 5th Colloq. Stabil. Met. Struct., SSRC, Lehigh University, Bethlehem, 33–42.

COPRA Reference Manual. Data M Sheet Metal Solutions GmbH. Valley. Germany, 2014.

Cruise R.B., Gardner L. (2008). Residual stress analysis of structural stainless steel sections, *Journal of Constructional Steel Research*, 64, 352–366

Davis, J.C. Statistics and Data Analysis in Geology, 3rd Edition.; Wiley & Sons, NewYork, USA, 1973.

Design Manual for Structural Stainless steel-4th Edition. SCI Publication, 2017.

Deierlein G.G., Hajjar J.F., Yura J.A., White D.W., Baker, W.F. (2002). Proposed New Provisions for Frame Stability Using Second-Order Analysis. Proceedings—Annual Stability Conference, SSRC, Seattle, WA.

ECCS (1984). Ultimate Limit State Calculations of Sway Frames with Rigid Joints, Technical Committee 8 - Structural Stability Technical Working Group 8.2 - System, Publication No. 33.

ECCS (1991). Essentials of Eurocode 3 Design Manual for Steel Structures in Buildings, ECCS-Advisory Committee 5, No. 65.

El-Zanaty M., Murray D., Bjorhovde, R. (1980). Inelastic behavior of multistory steel frames. Structural Engineering Report No. 83, University of Alberta, Alberta, Canada.

EN1993-1-1: 2015(E): Eurocode 3: Design of steel structures - Part 1-1: General rules and rules for buildings.

EN 1993-1-1:2005: Eurocode 3: Design of steel structures - Part 1-1: General rules and rules for buildings,

Brussels, Belgium.

EN 1993-1-4:2015: Eurocode 3: Design of steel structures - Part 1.4: General rules -Supplementary rules for stainless steel, Brussels, Belgium.

EN 10219-2(2019): Cold formed welded steel structural hollow sections. Tolerances, dimensions and sectional properties, British Standards Institution.

FCSA-Stainless Steel Hollow Sections Handbook (2008). Finnish Constructional Steelwork Association. Helsinki, Finland.

Gardner L., Nethercot D.A. (2004). Experiments on stainless steel hollow sections—Part 1: Material and cross-sectional behavior. *Journal of Constructional Steel Research*, 60, 1291–1318.

Gardner L., Cruise R. B. (2009). Modeling of residual stresses in structural stainless steel sections, *Journal of Structural Engineering, ASCE*, 135(1), 42-53.

Gardner L.(2019). Stability and design of stainless steel structures – Review and outlook, *Thin-Walled Structures*, 141, 208-216.

Griffis L.G., White D.W. (2013). Design Guide 28: Stability Design of Steel Buildings, American Institute of Steel Construction, Chicago.

Hradil, P. Talja, A. (2013). Investigating the role of gradual yielding in stainless steel columns and beams by virtual testing, in : Proceedings of the 5th International Conference on Structural Engineering, Mechanics and Computation (SEMC 2013). Cape Town, South Africa, 2013, 1459-1464.

Higgins, J.R. Sampling theory in Fourier and signal analysis: foundations, 1st Edition.; Clarendon Press, Oxford, UK, 1996.

Hill H.N. (1944). Determination of stress–strain relations from the offset yield strength values. Technical Note No. 927, National Advisory Committee for Aeronautics. Washington, D.C. 1944.

Huang Y., Young B. (2013). Tests of pin-ended cold-formed lean duplex stainless steel columns. *Journal of Constructional Steel Research*, 82, 203–215.

Jandera M., Gardner L., Machacek J. (2008). Residual stresses in cold-rolled stainless steel hollow sections, *Journal of Constructional Steel Research*, 64, 1255–1263.

Jandera M., Machacek J. (2014). Residual Stress Influence on material properties and behaviour of stainless steel SHS. *Thin-Walled Structures*, 83, 12-18.

JG/T 178-2005 Cold-formed steel hollow sections for building structures; Standards Press of China, Beijing, China.

Johnston B.G (1966). Guide to design criteria for metal compression members. 2nd. John Wiley & Sons, New York.

Johnston B.G. (1976). Guide to Stability Design for Metal Structures, 3rd Ed., SSRC, John Wiley & Sons, Inc., New York.

Kanchanalai T. (1977). The design and behavior of beam-columns in unbraced steel frames. AISI Project No. 189, Report No. 2, Civil Engineering/Structures Research Lab., University of Texas at Austin.

Kanchanalai T., Lu L.W. (1979). Analysis and Design of Framed Columns Under Minor Axis Bending. *Engineering Journal, AISC*, 2, 29–41.

Kavanagh T.C. (1962). Effective Length of Framed Columns. Transactions, Part II, ASCE, 127, 81–101.

Key P.W., Hancock G.J.(1993). A Theoretical investigation of the column behavior of cold-formed square hollow sections, *Thin-Walled structures*, 16, 31-64.

Kim S.E. (1996). Practical advanced analysis for steel frame design. Doctoral thesis, School of Civil Engineering, Purdue University, West Lafayette, US.

Kim S.E., Chen, W.F. (1996a). Practical advanced analysis for braced steel frame design. *Journal of Structural Engineering, ASCE*, 122(11): 1266-1274.

Kim S.E., Chen W.F. (1996b). Practical advanced analysis for unbraced steel frame design. *Journal of Structural Engineering, ASCE*, 122(11): 1259-1265.

Kim S.E., Chen W.F. (1997). Further studies of practical advanced analysis for weak-axis bending. *Engineering Structures*, 19(6): 407-416.

Kim S.E., Chen W.F. (1998). A sensitivity study on number of elements in refined plastic-hinge analysis. *Computers and Structures*, 66(5), 665-673.

Kim S.E., Chen W.F. (1999).Design guide for steel frames using advanced analysis program, *Engineering Structures*, 21, 352–364.

Kim S. E., Park M. H., Choi S. H. (2000). Improved refined plastic-hinge analysis accounting for strain reversal. *Engineering Structures*, 22(1), 15-25.

Kim S.E., Choi S.H. (2001). Practical advanced analysis for semi-rigid space frames. *Solids and Structures*, 38(50-51), 9111-9131.

Kim S.E., Park M.H., Choi S.H. (2001). Direct design of three-dimensional frames using practical advanced analysis, *Engineering Structures*, 23(11), 1491-1502.

Kim S.E., Kim, Y., Choi S.H.(2001). Nonlinear analysis of 3-D steel frames. *Thin-walled Structures*, 39(6), 445-461.

King W. S., White D. W., Chen W. F. (1991). On second-order inelastic methods for steel frame design. *Journal of Structural Engineering, ASCE,* 118(2), 408-428.

Kucukler M., Gardner L., Macorini L.(2014). A stiffness reduction method for the in-plane design of structural steel elements. *Engineering Structures*, 73, 72–84.

Kucukler M., Gardner L., Macorini L. (2015a). Lateral-torsional buckling assessment of steel beams through a stiffness reduction method. *Journal of Constructional Steel Research*, 109, 87-100.

Kucukler M., Gardner L., Macorini L. (2015b). Flexural-torsional buckling assessment of steel beam-columns through a stiffness reduction method. *Engineering Structures*, 101, 662-676.

Kucukler M., Gardner L., Macorini L.(2016). Development and assessment of a practical stiffness reduction method for the in-plane design of steel frames, *Journal of Constructional Steel Research*, 126, 187–200.

Kucukler M., Gardner L.(2018). Design of laterally restrained web-tapered steel structures through a stiffness reduction method. *Journal of Constructional Steel Research*, 141, 63-76.

Kucukler M., Gardner L.(2019a). Design of web-tapered steel beams against lateral-torsional buckling through a stiffness reduction method. *Engineering Structures*, 190, 246-261.

Kucukler M., Gardner L.(2019b). Design of hot-finished tubular steel members using a stiffness reduction method. *Journal of Constructional Steel Research*, 160, 340-358.

LeMessurier W. J. (1977). A Practical Method of Second-Order Analysis: Part 2. Rigid Frames. Engineering Journal, AISC, 14 (2), 49–67.

Liew J. Y. R. (1992). Advanced analysis for frame design. Doctoral thesis, School of Civil Engineering, Purdue University, West Lafayette, US.

Liew J. Y. R., Chen, W. F. (1991). Refining the plastic hinge concept for advanced analysis/design of steel frames. *Journal of Singapore Structural Steel Society, Steel Structure,* 2(1), 13-30.

Liew J. Y. R., White D. W., Chen, W. F.(1991). Beam-column design in steel frameworks-insight on current methods and trends. *Journal of constructional steel research,* 18, 269-308.

Liew J. Y. R., White D. W., Chen W. F. (1993a). Second-order refined plastic hinge analysis for frame design: Part I. *Journal of Structural Engineering, ASCE,* 119 (11), 3196-3216.

Liew J. Y. R., White D. W., Chen W. F. (1993b). Second-order refine plastic hinge analysis for frame design: Part II. *Journal of Structural Engineering, ASCE,* 119 (11), 3217-3237

Liew J.Y.R., Tang, L.K. (1998). Nonlinear refined plastic hinge analysis of space frame structures. Research Report No. CE027/98, Department of Civil Engineering, National University of Singapore, Singapore.

Liu W.Y., Rasmussen K. J.R., Zhang H.(2017). Modelling and probabilistic study of the residual stress of cold-formed hollow steel sections, *Engineering Structures*,150, 986–995.

Li S.H., Zeng G., Ma Y.F., Guo Y.J., Lai X.M. (2009). Residual stresses in roll-formed square hollow sections. *Thin-Walled Structures*, 47(5), 2009, 505-513.

Lui W.M., Ashraf M., Young B.(2014). Tests of cold-formed duplex stainless steel SHS beam–columns. *Engineering Structures*, 74, 111–121.

LS-DYNA SMP R11.0.0 Reference Manual, Livermore Software Technology Corp, 2019.

Matlab 2017(b) Reference Manual. The MathWorks, 2019.

Ma J.L., Chan T.M., Young B.(2015). Material properties and residual stresses of cold-formed high strength steel hollow sections. *Journal of Constructional Steel Research*, 109, 152-165.

McGuire W., Gallagher R.H., Ziemian R.D.(2000). Matrix Structural Analysis, 2nd Edition, John wiley &

Sons, New York, US.

Mirambell E., Real E. (2000). On the calculation of deflections in structural stainless steel beams: an experimental and numerical investigation. *Journal of Constructional Steel Research*, 54, 109–133.

Mintab 18 Reference Manual, Minitab, LLC., 2018.

Nagamachi T., Nakako T., Nakamura D. (2011). Effects of Roll Diameter and Offset on Sectional Shape of Square Steel Pipe Processed by Roll Forming. *Mater. Trans*, 52 (12), 2159-2164.

Orbison J.G. (1982). Nonlinear static analysis of three-dimensional steel frames, Report No. 82-6, Department of Structural Engineering, Cornell University, Ithaca, New York.

Rasmussen K.J.R.(2003). Full range stress–strain curves for stainless steel alloys. *Journal of Constructional Steel Research*, 59, 47–61.

Ramberg W., Osgood W. R. (1943). Description of stress–strain curves by three parameters. Technical Note No. 902, National Advisory Committee for Aeronautics, Washington DC.

Ramm E. (1981). Strategies for Tracing the Nonlinear Response near Limit Points. In: Nonlinear Finite Element Analysis in Structural Mechanics. Springer, New York, 68-89.

Real E., Mirambell E.(2005). Flexural behaviour of stainless steel beams, *Engineering Structures*, 27, 1465–1475.

Riks E. (1972). The application of Newton's method to the problem of elastic stability. Journal of Applied Mechanics, 39:1060-1065.

Riks, E. (1979). An incremental approach to the solution of snapping and buckling problems. *Int. J. Solids Struct*, 15(7), 529–551.

Rossi B.(2014). Discussion on the use of stainless steel in constructions in view of sustainability. *Thin-Walled Structures*, 83,182-189.

Sarawita A.T., Pekőz T. (2006).Notional load method for industrial steel storage racks. *Thin-Walled Structures*, 44(12), 1280-1286.

Sabir B., Lock A. C. (1972). The Application of Finite Elements to the Largedeflection Geometrically

Nonlinear Behavior of Cylindrical Shells. Proceedings of International Conference on Variational Mechanics. Southampton University, Session VII.

Schafer B.W.(2000). Distortional buckling of cold-formed steel columns, Final Report, Sponsored by the American Iron and Steel Institute, Washington, DC.

Schafer B.W. (2019). Advances in the direct strength method of cold-formed steel design, *Thin-Walled Structures*, 140, 533-54.

SEI/ASCE 8-02 (2002): Specification for the design of cold-formed stainless steel structural members, American Society of Civil Engineers (ASCE), Reston, Virginia.

Shen Y.F., Chacón R.(2019). Effect of Uncertainty in Localized Imperfection on the Ultimate Compressive Strength of Cold-Formed Stainless Steel Hollow Sections. *Applied Science*. 9(18), 3827.

Somodi B., Kövesdi B.(2017). Residual stress measurements on cold-formed HSS hollow section columns. *Journal of Constructional Steel Research*, 128, 706-72.

Surovek-Maleck A.E., White D.W.(2004a). Alternative approaches for elastic analysis and design of steel frames. I: Overview. *Journal of Structural Engineering, ASCE*, 130(8), 1186–96.

Surovek-Maleck A.E., White D.W.(2004b). Alternative approaches for elastic analysis and design of steel frames. II: Verification studies. *Journal of Structural Engineering ASCE* 130 (8), 1197–205.

Süli E., Mayers D. (2003). An Introduction to Numerical Analysis. Cambridge University Press. UK.

Theofanous M., Gardner L.(2009).Testing and numerical modelling of lean duplex stainless steel hollow section columns. *Engineering Structures*, 31, 3047-3058.

Tong L.W., Hou G., Chen Y.Y., Zhou F., Shen K., Yang A. (2012). Experimental investigation on longitudinal residual stresses for cold-formed thick-walled square hollow sections. *Journal of Constructional Steel Research*, 73, 105-116.

Von Karman T., Sechler E., Donnell L.H. (1932). The strength of thin plates in compression. *Transactions, ASME*, 54, 53-57.

Vogel U. (1985). Calibrating frames. *Stahlbau*, 10, 1-7.

Wang Y. C. (1988). Ultimate strength analysis of 3-D beam columns and column subassemblages with flexible connections. Doctoral thesis, University of Sheffield, England.

Wang J., Afshan S., Schillo N., Theofanous M., Feldmann M., Gardner L.(2017). Material properties and compressive local buckling response of high strength steel square and rectangular hollow sections. Eng. Struct. 130, 297–315.

Walport F., Gardner L., Real E., Arrayago I., Nethercot D.A. (2019). Effects of material nonlinearity on the global analysis and stability of stainless steel frames. *Journal of Constructional Steel Research*, 152,173–182.

Wempner G. A. (1971). Discrete approximation related to nonlinear theories of solids. International Journal of Solids and Structures 7: 1581-1599.

White D.W., Liew J. Y. R., Chen W. F.(1991). Second-order inelastic analysis for frame design, A report to SSRC Task Group 29 on Recent Research and the Percieved State-of-art, Structural Engineering Report, CE-STR-91-12, Purdue University, West Lafayette, US.

White D. W. (1993). Plastic hinge methods for advanced analysis of steel frames. *Journal of Constructional Steel Research*, 24(2), 121-152.

White D. W., Chen W. F. (1993), *Plastic Hinge Based Methods for Advanced Analysis and Design of Steel Frames*, Structural Stability Research Council, Lehigh University, Bethlehem, US.

White D. W., Clarke M.(1997a). Design of Beam-Columns in Steel Frames: I. A Study of Philosophies and Procedures. *Journal of Structural Engineering, ASCE,* 123 (12), 1556–1564.

White D. W., Clarke M.(1997b). Design of Beam-Columns in Steel Frames. II: Comparison of Standards. *Journal of Structural Engineering, ASCE*, 123 (12), 1565–1575.

White D.W., Hajjar J. G. (1997). Design of Frames without Consideration of Effective Length. *Eng. Struct.*, 19 (10),787–810.

White D.W., Surovek A.E., Alemdar B.N. et al.(2006) Stability analysis and design of steel building frames using the 2005 AISC Specification, *Steel Structures*, 6, 71-91.

White D.W., Jeong W.Y., Toga O.(2016). Comprehensive stability design of planar steel members and

framing systems via inelastic buckling analysis. *International Journal of Steel Structures*, 16(4), 1029-1042.

Wilkinson T., Hancock G.J.(1999). Tests of cold-formed rectangular hollow section portal frames, Research Report No. 783, Centre for Advanced Structural Engineering, The University of Sydney.

White D. W., Nukala P. K. V. (1997). Recent Advances in Methods for Inelastic Frames Analysis: Implications for Design and a Look Toward the Future. Proceedings National Steel Construction Conference, American Institute of Steel Construction, 43, 1-24.

Winter G.(1970). Commentary on the 1968 Edition of the Specification for the Design of Cold-Formed Steel Structural Members. American Iron and Steel Institute, New York, NY.

Wood R.H. (1974). Effective lengths of columns in multi-storey buildings: Part 1- 2 and 3. The Structural Engineer, 52(7,8,9), 235, 295, 341.

Yarimci E. (1966). Incremental inelastic analysis of framed structures and some experimental verification, Doctoral thesis. Department of Civil Engineering, Lehigh University, Bethlehem, US.

Young B., Lui W.M.(2005). Behavior of cold-formed high strength stainless steel sections, *Journal of Structural Engineering, ASCE*, 131(11), 1738-1745.

Zhao O., Gardner L.,Young B.(2016). Experimental study of ferritic stainless steel tubular beam-column members subjected to unequal end moments. *Journal of Structural Engineering, ASCE*, 142(11), 04016091.

Zhao O., Rossi B., Gardner L., Young B.(2015). Behaviour of structural stainless steel cross-sections under combined loading -Part I: Experimental study. *Engineering Structures*, 89, 236–246.

Zheng, B.F., Shu G.P., Xin L.C., Yang, R., Jiang, Q.L. (2016). Study on the Bending Capacity of Cold-formed Stainless Steel Hollow Sections. *Structures*, 8, 63–74.

Ziemian R. D.(1990). Advanced methods of inelastic analysis in the limit states design of steel structures. Doctoral thesis. School of Civil and Environmental Engineering, Cornell University, New York, US.

Ziemian R. D., White D.W., Deierlein G. G., Mcquire W.(1990). One approach to inelastic analysis and design. Proceedings of the 1990 National Steel Conferences. AISC, Chicago, 19.1-19.

Ziemian R. D., McGuire W., Deierlein G. G. (1992a). Inelastic Limit States Design Part I: Planar Frame Studies. *Journal of Structural Engineering, ASCE,*118 (9)9, 2532–2549.

Ziemian R. D., McGuire W., Deierlein G. G. (1992b). Inelastic Limit States Design Part II: Three-Dimensional Frame Study. *Journal of Structural Engineering, ASCE,* 118 (9), 2550–2568.

Ziemian R.D., McGuire W. (2000). Tutorial for MASTAN2. John wiley & Sons, New York, US.

Ziemian R. D., McGuire W. (2002). Modified Tangent Modulus Approach: A Contribution to Plastic Hinge Analysis. *Journal of Structural Engineering, ASCE,* 128(10) 1301–1307.

Ziemian R. D., McGuire W., Seo D. W. (2008). On the Inelastic Strength of Beam-Columns under Biaxial Bending. Proc. SSRC Annual Stability Conference, Nashville, US.

Ziemian R.D (2010). Guide to stability design criteria for metal structures, Engineering and Technology Publishing.

Zienkiewicz O. C. (1971). Incremental Displacement in Non-linear Analysis. Internation Journal for Numerical Methods in Engineering 3: 587-588.

Zubydan A.H.(2010). A simplified model for inelastic second order analysis of planar frames. *Engineering Structures*, 32(10), 3258–68.